CEMENT-BASED COMPOSITES: OPTIMIZATION of BASALT FIBERS-CEMENT MATRICES INTERFACES

by

Morena Iorio

in partial fulfillment of the requirements for the degree of Doctor in

MATERIAL SCIENCE AND ENGINEERING
and
ELECTRICAL, MATERIALS AND NANOTECHNOLOGY ENGINEERING

University Carlos III of Madrid
Sapienza University of Rome

Advisors:

Prof. Francisco Javier González Benito
Prof. Maria Laura Santarelli

March 2019

A toda mi vida… la mia famiglia.

AGRADECIMIENTOS

“Escoge la montaña que deseas subir”...
con estas palabras empecé esta importante etapa de mi vida y hoy solo puedo estar orgullosa y feliz de haber llegado al final de este viaje.

Me gustaría agradecer a todas aquellas personas que, de alguna manera, han contribuido a la realización de todo esto.

En primer lugar, agradecer a mi directora de tesis de la “Università degli Studi di Roma, La Sapienza”, *Maria Laura Santarelli*, por apoyarme cuando decidí realizar una tesis en co-tutela con otra Universidad. Gracias por darme la oportunidad de realizar este objetivo y gracias, además, por haber contribuido a mi formación a lo largo de toda mi carrera universitaria.

Un agradecimiento muy especial a mi director de tesis de la Universidad Carlos III de Madrid, *Francisco Javier González Benito*. Gracias Javier por darme la oportunidad de unirme a tu grupo de investigación y por aceptar dirigir esta tesis doctoral. Gracias por haber sido un gran director de tesis, gracias por tus consejos y, sobre todo, por tu apoyo en cualquier situación. Aprendí mucho de ti en estos tres años... tanto a nivel científico como a nivel personal.

También me gustaría agradecer a todo el grupo de *"Materiales Compuestos Polímericos e Interfaces (GMCPI)"*. En particular, gracias a ti, *Dania*, por estar siempre presente y apoyarme en diferentes situaciones. Gracias por tu valiosa colaboración en este proyecto de tesis.
Gracias a ti, *Jorge* (Giorgio), por compartir cada momento de este etapa juntos... gracias por estar siempre ahí. Gracias también al resto de los chicos del grupo (*Victor, Miguel, José Ernesto, Monire, Danial y Ali*) por animarme en esta parte final.
También me gustaría agradecer a *Gustavo González-Gaitano* de la Universidad de Navarra por su colaboración y disponibilidad.

Agradezco a *Francesco Marra* de la " Università degli Studi di Roma, La Sapienza" por darme la oportunidad de realizar parte de este trabajo en sus laboratorios. Gracias Francesco por tu ayuda y valiosos consejos.

Me gustaría agradecer a *Ida Pettiti* de la " Università degli Studi di Roma, La Sapienza" por la disponibilidad mostrada en la realización e interpretación de algunos de los experimentos relacionados con este proyecto de investigación.

También me gustaría agradecer a todo el *"Departamento de Ciencia e Ingeniería de Materiales e Ingeniería Química de la Universidad Carlos III de Madrid"*. Gracias a todas las personas que me han mostrado su disponibilidad en diferentes momentos y gracias a las personas con quienes tuve la oportunidad de compartir algunos momentos juntos. Un agradecimiento especial a *Juan Carlos, Luis, Cristina, Tere, Mariola, Susana, Carol, Juani y Miguel Ángel.*

Cómo no agradecer a *"DESPACHO 1.1.A01.BIS"*... gracias *Mariu, Belén, Carmen, Gleidys* y *Jorge*. Gracias por todos los buenos momentos que compartimos juntos, gracias por las sonrisas que me habeis regalado. Infinitamente gracias por vuestro apoyo y amistad.

Gracias a todos los chicos del departamento. Gracias *Natalia, María, Alberto, Lucía, Catherine, Edu, Andrés, Nieves, Estela, Raquel, Javi, Pelu, Borja, Marta, Segundo, Andrea G.* por todos los buenos momentos que hemos pasamos juntos... cada uno, a su manera, ayudó a hacer todo este período especial. Gracias a *Amaya* y *Eric* (compañeros de las largas tardes en la universidad) por vuestro apoyo sobre todo en este último período.

Gracias, *Andrea A.* y *Maria F.* por vuestra alegría y gracias a *Pedro* y *Guille* por vuestro cariño en todos momentos. Gracias, finalmente a ti, *Sara*, por estar siempre a mi lado.

Quiero agradecer también a *Valeria*, *Blanca*, *Sandra* y *Lorena* por el cariño, amistad y ánimos durante esta etapa.

Gracias a los *amigos y amigas de siempre*, por el cariño y por haberme apoyado a pesar de la distancia.

Gracias *Silvia* y *Martina*, amigas de siempre y para siempre, por estar siempre presentes en mi vida. Gracias, en particular, Martina por compartir cada momento de esta etapa sobre todo en este ultimo periodo.

Gracias *Francesca* e *Maria*, por todo lo que habéis hecho por mí durante mi estancia en Roma.

Gracias a *ti*... hermana y amiga. Gracias por ser mi punto de referencia y apoyarme siempre en cualquier situación. Gracias por estar siempre presente y haber hecho que la distancia nunca haya sido un problema, tampoco en los momentos más duros.

Gracias *papá* y *mamá*... gracias por vuestro amor incondicional, gracias por apoyar y entender mi decisión de irme fuera de Italia. Gracias por haber sido siempre mi fuerza. Gracias porque, cuando la vida nos puso a prueba, me disteis fuerza para quedarme cuando quería volver. Gracias a ti papá por haber hecho todo lo que yo a distancia no he podido hacer. Y gracias a ti mamá, por regalarme siempre mil sonrisas a pesar de "todo" y a pesar de la distancia.

Gracias también a *quien*, antes de irse, me dijo *"Nunca lo olvides ... siempre estaré ahí para ti"*.

Y finalmente gracias a *quien* me dio la fuerza y el coraje de ir a Madrid y alcanzar mis metas.

Y ahora...
a *"descubrir otra montaña y partir en una nueva adventura".*

RINGRAZIAMENTI

"Scegli la montagna che desideri scalare…
con queste parole ho iniziato questo importante percorso della mia vita ed oggi non posso che essere fiera e felice di essere arrivata al termine di questo cammino.

Desidero ringraziare tutte quelle persone che, in qualche modo, hanno contributo alla realizzazione di tutto questo.

Il mio primo ringraziamento va alla mia relatrice di tesi dell'Università degli Studi di Roma "La Sapienza", *Maria Laura Santarelli*, per avermi appoggiato nel momento in cui ho deciso di intraprendere questo percorso presso l'Università "Carlos III" di Madrid. Grazie Prof. per avermi dato la possibilità di partire e mettermi alla prova. Grazie, inoltre, per aver contribuito alla mia formazione durante tutto il mio percorso universitario.

Un grazie molto speciale va al mio direttore di tesi della "Universidad Carlos III de Madrid", *Francisco Javier Gonzalez Benito*. Grazie Javier per avermi dato la possibilità di entrare a far parte del tuo gruppo di ricerca e per aver accettato di dirigere questa tesi di dottorato. Grazie per essere stato un gran direttore di tesi, grazie per i tuoi consigli e soprattutto grazie il tuo appoggio in qualsiasi situazione. Ho appreso molto da te in questi tre anni…sia a livello scientifico che a livello personale.

Desidero, inoltre ringraziare tutto il gruppo di *"Materiales Compuestos Polimericos e Interfaces (GMCPI)".* In particolare, grazie a te *Dania* per essere sempre stata presente e avermi appoggiata in diverse situazioni. Grazie per la tua preziosa collaborazione in questo progetto di tesi.
Grazie a te *Jorge* (Giorgio), per condividere ogni singolo momento di questo percorso insieme…grazie per esserci stato sempre.
Grazie anche a tutto il resto dei ragazzi del gruppo (*Victor, Miguel, José Ernesto, Monire, Danial* y *Ali*) per avermi sostenuta in questa parte finale.
Desidero inoltre ringraziare *Gustavo González-Gaitano* dell'Università di Navarra per la sua collaborazione e disponibilità.

Ringrazio *Francesco Marra* dell'Universitá degli Studi di Roma Roma "La Sapienza" per avermi dato la possibilitá di realizzare parte di questo lavoro presso i suoi laboratori. Grazie Francesco per il tuo aiuto e i tuoi preziosi consigli.

Desidero ringraziare *Ida Pettiti* dell'Universitá degli Studi di Roma "La Sapienza" per la disponibilitá mostratami nella realizzazione e interpretazione di alcuni degli esperimenti relativi a questo progetto di ricerca.

Ringrazio, inoltre, tutto il *"Departamento de Ciencia e Ingeniería de Materiales e Ingeniería Química de la Universidad Carlos III de Madrid".* Grazie, a tutte le persone che mi hanno mostrato la loro disponibilitá in diversi momenti e grazie alle persone con cui ho avuto modo di condividere qualche momento insieme. Un grazie particolare a *Juan Carlos, Luis, Cristina, Tere, Mariola, Susana, Carol, Juani* e *Miguel Ángel*.

Come non ringraziare il *"DESPACHO 1.1.A01.BIS"* …grazie *Mariu, Belen, Carmen, Gleidys* e *Jorge*. Grazie per tutti i bei momenti che abbiamo condiviso insieme, grazie per i tanti sorrisi che mi avete regalato. Infinitamente grazie per il vostro appoggio e amicizia.

Grazie a tutti i ragazzi del Dipartimento. Grazie *Natalia, Maria, Alberto, Lucia, Caterina, Edu, Andrès, Nieves, Estela, Raquel, Javi, Pelu, Borja, Marta, Segundo, Andrea G.* per tutti i bei momenti trascorsi insieme…ognuno di voi, a modo suo, ha contributo a rendere speciale tutto questo periodo. Grazie ad *Amaya*

e *Eric* (*compañeros* dei lunghi pomeriggi all'universitá) per il vostro appoggio in quest'ultimo periodo. Grazie, *Andrea A.* e *Maria F.* per la vostra allegria e grazie *Pedro* y *Guille* per il vostro affetto in ogni momento. Grazie, infine a te, *Sara* per starmi sempre accanto.

Grazie all'affetto, all'amicizia e appoggio di *Valeria*, *Blanca*, *Sandra* e *Lorena*.

Grazie agli *amici e amiche di sempre* per il loro affetto nonostante la distanza.

Grazie *Silvia* e *Martina*, amiche da sempre e per sempre, per essere sempre presenti nella mia vita. Grazie, in particolare, Martina per condividere con me ogni singolo momento di questo percorso soprattutto in quest'ultimo periodo.

Grazie *Francesca* e *Maria*, per tutto quello che avete fatto per me durante il mio periodo a Roma.

Grazie a *te*… sorella e amica. Grazie per essere il mio punto di rifermento e sostenermi sempre in qualsiasi situazione. Grazie per essere stata sempre presente ed aver fatto sí che la distanza non fosse mai un problema, nemmeno nei momenti piú difficili.

Grazie a te *mamma* e a te *papá*… grazie per il vostro amore incondizionato, grazie per aver appoggiato e aver capito la mia decisione di realizzare questo percorso fuori dall'Italia. Grazie per essere stati la mia forza sempre. Grazie perché quando la vita ci ha messo alla prova, mi avete dato la forza di restare quando volevo tornare. Grazie a te papá, per aver aver fatto quello che io a distanza non sono riuscita a fare. E grazie a te mamma, per avermi regalato sempre mille sorrisi nonostante "tutto" e nonostante la distanza.

Grazie anche a *chi*, prima di andar via mi ha detto *"Non te lo dimenticare mai…Io per te ci saró sempre".*

Ed infine grazie a *chi* mi ha dato la forza e il coraggio di partire per Madrid e poter arrivare oggi fin qui.

Ed ora…
a *"scoprire una nuova montagna e partire per una nuova avventura".*

PUBLISHED AND SUBMITTED CONTENT

Publications and Conference Proceedings

- *M. Iorio, M.L. Santarelli, G. González-Gaitano, J. González-Benito, Surface modification and characterization of basalt fibers as potential reinforcement of concretes, Appl. Surf. Sci. 427 (2018) 1248–1256. doi:10.1016/j.apsusc.2017.08.196.*

  This publication is wholly included as part of the Thesis, in **Chapters 1** and **4**.
  I contributed directly to this publication since I carried out the experiments, participated to discussion of the results and contributed to the final manuscript. The material from this source included in this thesis is not singled out with typographic means and references.

- *M. Iorio, D. Olmos, M.L. Santarelli, J. González-benito, Fluorescence Study of the Hydrolytic Degradation Process of Polysiloxane Modifiers for Basalt Fibers, AIP Conf. Proc. 1981. 020054 (2018). doi:10.1063/1.5045916.*

  This work is wholly included in the Thesis, in **Chapters 3**, **4** and **5**.
  I contributed directly to this work since I carried out the experiments, participated to discussion of the results and contributed to the final manuscript. The material from this source included in this thesis is not singled out with typographic means and references.

- *M. Iorio, D. Olmos, M.L. Santarelli, J. González-Benito, Fluorescence Study of the Hydrolytic Degradation Process of the Polysiloxane Coatings of Basalt Fibers, Applied Surface Science (2018), doi: https://doi.org/10.1016/j.apsusc.2018.12.223*

  This work is the extension of the conference proceeding above mentioned and it is wholly included as part of the Thesis in **Chapters 3** and **5**.
  I contributed directly to this publication since I carried out the experiments, participated to discussion of the results and contributed to the final manuscript. The material from this source included in this thesis is not singled out with typographic means and references.

International Conferences

- XVII CONGRESO INTERNACIONAL DE ADHESIÓN Y ADHESIVOS, *"Modification of Basalt Fibers with Potential Applications as Material for Reinforced Concrete Composites"*, Escuela Técnica Superior de Ingeniería y Diseño Industrial (Universidad Politécnica de Madrid), Madrid, Spain 15^{th}-16^{th} September 2016 (oral presentation).

- 9^{th} INTERNATIONAL CONFERENCE TIMES OF POLYMERS (TOP) AND COMPOSITES, *"Fluorescence Study of the Hydrolytic Degradation Process of Polysiloxane Modifiers for Basalt Fibers"*, Ischia, Italy, 17^{th}-21^{st} June 2018 (oral presentation).

The items related to the International Conferences above mentioned, are included as part of the Thesis in Chapters **3**, **4** and **5**. The material from this source included in this thesis is not singled out with typographic means and references.

OTHER RESEARCH MERITS

Publications and Conference Proceedings

- M. Iorio, J. Teno, M. Nicolás, R. García-González, V.H. Peláez, G. González-Gaitano, J. González-Benito, Conformational changes on PMMA induced by the presence of TiO_2 nanoparticles and the processing by Solution Blow Spinning, Colloid Polym. Sci. doi:10.1007/s00396-018-4268-0.

- D. Olmos, M. Iorio, J. Teno, A. Rodríguez, J. González-Benito, Preparation and Characterization of Submicrometric Fibers of Nanocomposites Based on PVDF filled with CuNp, AIP Conf. Proc. 1981. 020160 (2018) 1–5. doi:10.1063/1.5046022.

International Conferences

- 9th INTERNATIONAL CONFERENCE TIMES OF POLYMERS (TOP) AND COMPOSITES, "Preparation and Characterization of Submicrometric Fibers of Nanocomposites Based on PVDF filled with CuNp", Ischia, Italy, 17th-21st June 2018 (poster).

- 2017 GLOBAL CONFERENCE ON POLYMER AND COMPOSITE MATERIALS (PCM 2017), "Solution Blow Spun PMMA based nanocomposites filled with TiO_2 nanoparticles", Guangzhou, China, 23rd-25th May 2017 (oral presentation).

CONTENTS

ABSTRACT

The main research activity carried out within the frame of the present PhD thesis was focused on the study and development of materials to be used as plasters in the building industry and in the restoration and conservation of Cultural Heritage. In particular, the aim of this PhD thesis was to optimize the fiber-matrix interface in fiber reinforced cement-based composites through specific surface treatments of the natural basalt fibers. Therefore, the compatibility, in terms of adhesion, between chopped basalt fibers (commercial and modified in the present work) and the selected matrices (Portland cement and natural hydraulic lime) was studied to understand and define possible improvements in the final composite materials.

Therefore, different surface treatments were designed on the basalt fibers, to subsequently characterize them and to study the hydrolytic degradation phenomena respectively. With this information, composite materials reinforced with different types of fibers according to their surface nature, were finally designed and characterized.

The first step of the project concerned the design and characterization of chemical coatings of basalt fibers with silane coupling agents.
Surface treatments were carried out after a surface pretreatment through a calcination (elimination of the sizing applied during the production process on the commercial fiber) and an activation (treatment with chlorhydric acid to regenerate silanol groups on the fiber surface) process of the commercial fibers. Subsequently, the fibers were chemically treated with different silane aqueous solutions (aminosilanes): i) γ-aminopropyltriethoxysilane, APTES; ii) γ- aminopropylmethyldiethoxysilane, APDES and iii) mixture 50% by weight of both silanes, APTES + APDES. The commercial and modified fibers were characterized in terms of structure, composition and morphology through different instrumental techniques (DRX, FT-IR, TGA, SEM and AFM). From these initial results, it was observed that the calcination process was effective to remove the commercial sizing present on the fiber surface making the surface smooth. The activation process fully removed possible residues of the initial coatings, making completely smooth the fiber surfaces. In addition, this process regenerated silanol groups allowing the grafting of

aminosilanes on the fibers surface through condensation processes with formation of siloxane bonds. Through the morphological analysis of the silanized fibers, it was found that the silanization process made the surfaces rough, showing higher heterogeneity due to the presence of the organic matter deposited on the fibers. It was found that the higher the amount of triethoxysilane, APTES, used in the composition of the solution, the higher the surface heterogeneity in terms of topography.

In a second phase of the thesis project, the phenomena of hydrolytic degradation of the polysiloxane coatings were studied since the siloxane bonds (-Si-O-Si-) formed with the silanols of the fibers surface and the silanols of the silane molecules, as well as those formed between the silane molecules between them, are hydrolysable bonds dependent on pH. Therefore, it is considered that the study of possible surface degradation phenomena may be useful to understand similar phenomena that could occur at the fiber-matrix interface. These studies are considered of crucial importance since, during the preparation of cement-based composite materials (matrix characterized by alkaline pH), it is necessary to mix the components with water. The hydrolytic degradation processes of the siloxane coatings were studied by monitoring the pH of the aqueous solution where the silanized fibers were immersed, by steady-state fluorescence spectroscopy. After modification with silane coupling agents, the silanized fibers were chemically labeled with a fluorescent label (fluorescein isothiocyanate, FITC) to be immersed afterwards in different aqueous solutions (pH=7 and pH=10). The study was carried out at different temperatures to study the kinetics of the process. The kinetic study allowed to obtain information about the activation energy of the three studied systems (APTES, APTES+APDES, APDES) and to evaluate the equilibrium degradation times for the different silanes. The results indicated that the hydrolytic rate of the three coatings increased in the order: APDES < APTES+APDES < APTES. It was found that the mechanism of the hydrolytic process is the same for the three studied systems and it was concluded that the rate of the hydrolytic degradation process is related to the initial concentration of siloxane bonds (-Si-O-Si-) able to be hydrolyzed. In addition, this study suggests that, in cement-based fiber-reinforced composites, the use of a polyorganosiloxane with a lower crosslinking degree, such as the APDES coating, could be the most effective strategy to resist a possible attack of water, especially in the alkaline environment characteristic of the cement matrix.

Finally, composite materials reinforced with different types of fibers according to their surface nature were prepared. Mortar samples based on Portland cement and chopped basalt fibers (commercial and modified) were prepared. On the other hand, mortar samples based on natural hydraulic lime and chopped basalt fibers (commercial and modified) were also prepared. Mechanical performances of the composite materials were evaluated by three-point flexural test and compressive strength test. An analysis and subsequent discussion on the interactions and compatibility between the reinforcing agent and the matrix were done. Different characteristics of the fiber surface were considered in order to find the best conditions, in terms of preparation of materials, to obtain interfaces whose special characteristics contribute to improve the performance of the final composite materials. Therefore, a fractographic analysis on the images obtained by scanning electron microscopy (SEM) and laser and optical profilometry were performed to study the compatibility between fiber and matrix. To evaluate other possible interactions between fiber and matrix and to understand possible contributions in terms of mechanical adhesion between them, a study on the fiber surface roughness at nanoscopic scale by atomic force microscopy (AFM) was carried out. In addition, the possible contribution to the final mechanical behavior related to the porous structure of the samples was also studied through BET-BJH analysis by N_2 adsorption-desorption. From these studies it was found, that, in general, the simple presence of basalt fibers as well as specific variations of the fibers surface nature, increased the mechanical performance of the materials under study compared to the reference mortars that is the materials without fibers. Finally, it was possible to conclude that, independently of the used matrix, better mechanical performances are mainly associated to the best adhesion at the fiber-matrix interface, which, in particular, is achieved in the case of mortars reinforced with basalt fibers treated with the mixture of two silanes (APTES + APDES).

RESUMEN

El siguiente proyecto de tesis doctoral se ha centrado en el estudio y desarrollo de materiales con potencial uso como revestimientos en el sector de la construcción y en la restauración de edificios históricos de gran interés cultural. En particular, como objetivo principal de la investigación se pretendió optimizar la interfase fibra-matriz de materiales compuestos reforzados con fibra de matriz cerámica (cementosa) a través de tratamientos superficiales de fibras naturales de basalto. Para ello, se estudió, en términos de adhesión, la compatibilidad existente entre las fibras cortas de basalto (comerciales y modificadas en el presente trabajo) y las matrices seleccionadas (cemento Portland y cal hidráulica natural) con el fin de comprender y definir posibles mejoras en las prestaciones o comportamiento en servicio final del material compuesto.

Por ello, se diseñaron diferentes tratamientos superficiales sobre las fibras de basalto, para posteriormente caracterizarlos y estudiar fenómenos de degradación hidrolítica respectivamente. Con esta información finalmente se diseñaron y caracterizaron los materiales compuestos reforzados con los diferentes tipos de fibras según su naturaleza superficial.

La primera fase del proyecto consistió en el diseño y caracterización de recubrimientos químicos de fibras de basalto con agentes de acomplamiento silano. Los tratamientos superficiales se realizaron después de un tratamiento previo por medio de un proceso de calcinación (eliminación del ensimaje superficial aplicado durante la fase producción en las fibras comerciales) y activación (tratamiento con ácido clorhídrico para promover la regeneración de grupos silanol de la superficie) de las fibras comerciales. Posteriormente, las fibras se trataron químicamente con diferentes disoluciones acuosas de agentes de acoplamiento silano (aminosilanos): i) γ-aminopropiltrietoxisilano, APTES; ii) γ-aminopropilmetildietoxisilano, APDES y iii) mezcla al 50% en peso de ambos silanos, APTES + APDES. Las fibras comerciales y modificadas se caracterizaron en términos de su estructura, composición y morfología a través de diferentes técnicas instrumentales (DRX, FT-IR, TGA, SEM y AFM). A partir de estos resultados iniciales, se observó que el proceso de calcinación fue eficaz para eliminar el ensimaje presente en la fibra

comercial y suavizar su superficie. El siguiente proceso de activación eliminaba completamente los posibles residuos de recubrimientos iniciales, consiguiéndose así superficies de fibras completamente lisas. Además, este proceso favoreció la regeneración de grupos silanol que fueron fundamentales para el injerto de los aminosilanos en la superficie de las fibras a través de procesos de condensación con formación de enlaces siloxano. Gracias al análisis morfológico de las fibras silanizadas se encontró que el proceso de silanización generaba superficies en las fibras más rugosas mostrando mayor heterogeneidad debida a la presencia de la sustancia organica depositada sobre las fibras. Se encontró que cuanto mayor era la cantidad de trietoxisilano, APTES, utilizado en la composición de la solución, mayor era la heterogenidad superficial en términos topográficos.

En una segunda fase del proyecto de tesis, se estudiaron los fenómenos de degradación hidrolítica de los recubrimientos de base organosiloxánica ya que los enlaces de siloxano (-Si-O-Si-) que se forman entre los silanoles de la superficie de las fibras y los silanoles de las moléculas de silano, así como los formados entre las propias moléculas de silano son enlaces hydrolizables dependientes del pH. Por lo tanto, el estudio de posibles fenómenos de degradación superficiales se piensa que podrían extrapolarse a fenómenos similares que pudieran ocurrir en la interfase fibra-matriz. Este tipo de estudios se considera que son de fundamental importancia pues durante la preparación de los materiales compuestos de matriz de cemento (matriz de pH alcalino) se necesita la mezcla de los componentes con agua. Mediante la utilización de espectroscopía de fluorescencia de estado estacionario se estudiaron los procesos de degradación hidrolítica de los recubrimientos siloxánicos controlando el pH de la disolución acuosa en la que se sumergieron las fibras silanizadas. Para ello, las fibras después de haber sido modificadas con los agentes de acoplamiento de silano, se marcaron químicamente con una especie fluorescente (isotiocianato de fluoresceína, FITC) y posteriormente se sumergieron en disoluciones acuosas a pH controlado (pH=7 y pH=10). El estudio se llevó a cabo a diferentes temperaturas para estudiar la cinética del proceso. El estudio cinético permitió obtener información sobre la energía de activación de los tres sistemas estudiados (APTES, APTES+APDES, APDES) y estimar los tiempos de degradación hidrolítica en el equilibrio para los diferentes silanos. Los resultados obtenidos indicaron que la velocidades de degradación de los tres recubrimientos aumenta según el orden: APDES < APTES+APDES <APTES. Se ha

encontrado que el mecanismo del proceso de degradación es el mismo para los tres sistemas estudiados, por lo que se concluye que la velocidad de hidrólisis depende de la concentración inicial de los enlaces de siloxano (-Si-O-Si-) capaces de ser hidrolizados. Además, este estudio sugiere que, en compuestos a base cementosa reforzada con fibras, el uso de un poliórganosiloxano con un bajo grado de reticulación, como el correspondiente a un recubrimiento realizado con APDES, podría ser la estrategia más eficaz para resistir un posible ataque de agua, especialmente en el ambiente alcalino característico de la matriz de cemento.

Finalmente, se prepararon los materiales compuestos reforzados con los distintos tipos de fibras según su naturaleza superficial. Por un lado, se prepararon morteros a base de cemento Portland y fibras cortas de basalto (comerciales y modificadas). Por otro lado, se prepararon morteros a base de cal hidráulica natural y fibras cortas de basalto (comerciales y modificadas). Se investigaron las propiedades mecánicas de los materiales compuestos a través de ensayos de flexión en tres puntos y de compresión. Los resultados obtenidos permitieron realizar un análisis y posterior discusión en función de las interacciones y compatibilidad entre el agente de refuerzo y la matriz considerando diferentes características de las superficie de las fibras intentando encontrar las mejores condiciones, en términos de preparación de materiales, para conseguir interfases cuyas características especiales contribuyan a mejorar las prestaciones de los materiales compuestos finales. En este sentido, además, se llevó a cabo un análisis fractográfico de imágenes obtenidas por microscopía electrónica de barrido (SEM) y perfilometrías láser y óptica respectivamente para estudiar la compatibilidad entre la fibra y la matriz. Para evaluar otras posibles interacciones entre la fibra y la matriz, se realizó un estudio de rugosidad de las superficies de las fibras a escala nanosópica por microscopía de fuerza atómica (AFM) y así entender la posible contribución de adhesión mecánica entre las fibras y la matriz. Además, también se estudió la posible contribución al comportamiento mecánico final de la estructura porosa de las muestras, utilizando para ello análisis BET-BJH por adsorción-desorción de N_2.
De estos estudios se encontró que la simple presencia de fibras de basalto junto con variaciones específicas de la naturaleza superficial de las mismas en general aumentan las prestaciones mecánicas de los materiales bajo estudio en comparación con los morteros de referencia, es decir, materiales sin fibras.

Finalmente, se pudo concluir, independientemente de la matriz utilizada, que las mejores prestaciones mecánicas se asocian fundamentalmente a mejor adhesión en la interfase fibra-matriz que en particular se consigue en el caso de morteros reforzados con fibras de basalto tratadas con la mezcla de los dos silanos (APTES+APDES).

RIASSUNTO

Il seguente progetto di tesi di dottorato di ricerca si è incentrato sullo studio e sviluppo di materiali da utilizzare come intonaci nel settore dell'edilizia e per il ripristino di edifici storici di grande interesse culturale. In particolare, lo scopo principale del progetto di ricerca è stato quello di ottimizzare l'interfase fibra-matrice all'interno dei materiali compositi fibrorinforzati a matrice cementizia attraverso trattamenti superficiali delle fibre naturali di basalto. Pertanto, è stata studiata, in termini di adesione, la compatibilità esistente tra le fibre corte di basalto (commerciali e modificate nel presente lavoro) e le matrici selezionate (cemento Portland e calce idraulica naturale) con lo scopo di comprendere e definire possibili miglioramenti delle prestazioni e del comportamento finale dei materiali compositi.

Pertanto, sono stati preparati diversi trattamenti superficiali sulle fibre di basalto, per essere successivamente caratterizzati e poter studiare rispettivamente i fenomeni di degradazione idrolitica. Con queste informazioni sono stati infine preparati e caratterizzati i materiali compositi rinforzati con le fibre con diversi trattamenti superficiali.

La prima fase del progetto ha riguardato la preparazione e caratterizzazione di rivestimenti chimici delle fibre di basalto con agenti di accoppiamento silano. I trattamenti superficiali sono stati eseguiti dopo aver effettuato un pretrattamento mediante un processo di calcinazione (rimozione del rivestimento superficiale applicato in fase di produzione sulla fibra commerciale) e di attivazione (trattamento con acido cloridrico per favorire la rigenerazione dei gruppi silanoli superficiali) delle fibre commerciali. Successivamente le fibre sono state chimicamente trattate con soluzione acquose di agenti di accoppiamento silano (amminosilani): i) *γ-amminopropiltrietossisilano*, APTES ii) *γ-amminopropilmetildietossisilano*, APDES ii) miscela al 50% in peso di entrambi i silani, APTES+APDES. Le fibre commerciali e modificate sono state caratterizzate in termini di struttura, composizione e morfologia mediante diverse tecniche strumentali (XRD, FT-IR, TGA, SEM e AFM). Da questi primi risultati si è osservato che il processo di calcinazione era efficace per rimuovere il rivestimento presente sulla fibra commerciale e rendeva la superficie liscia. Il successivo processo di attivazione rimuoveva completamente possibili residui di rivestimento iniziale rendendo la superficie del tutto liscia. Inoltre, questo

processo ha favorito la rigenerazione di gruppi silanoli fondamentali per l'innesto degli amminosilani sulla superficie delle fibre attraverso processi di condensazione con formazione di legami silossanici. Attraverso l'analisi morfologica delle fibre silanizzate, è stato osservato che il processo di silanizzazione generava superfici più rugose evidenziando una maggiore eterogeneità dovuta alla presenza della sostanza organica depositata sulle fibre. Si è constatato che quanto maggiore fosse la quantità di trietossisilano, APTES, utilizzata nella composizione della soluzione, maggiore era l'eterogeneità superficiale in termini topografici.

In una seconda fase del progetto di tesi, sono stati studiati i fenomeni di degradazione idrolitica dei rivestimenti a base di organosilossani in quanto, i legami silossanici (-Si-O-Si-) che si formano tra i silanoli della superficie delle fibre e i silanoli delle molecole di silano, così come quelli formati tra le proprie molecole di silano, sono legami idrolizzabili dipendenti dal pH. Pertanto, si ritiene che lo studio di possibili fenomeni di degradazione superficiale possa essere utile per comprendere fenomeni simili che potrebbero verificarsi all'interfaccia fibra-matrice. Questi studi sono considerati di fondamentale importanza dal momento che, durante la preparazione dei materiali compositi a matrice cementizia (matrice a pH alcalino), è necessario miscelare i componenti con acqua. Attraverso l'uso della spettroscopia di fluorescenza a stato stazionario, sono stati studiati i processi di degradazione idrolitica dei rivestimenti silossanici controllando il pH della soluzione acquosa in cui le fibre silanizzate erano immerse. Per realizzare questo, le fibre dopo essere state trattate con gli agenti di accoppiamento silano, sono state chimicamente etichettate con una molecola fluorescente (isotiocianato di fluoresceina, FITC) e successivamente immerse in diverse soluzioni acquose a pH standard (pH=7 e pH=10). Lo studio è stato realizzato a diverse temperature per poter studiare la cinetica del processo. Lo studio cinetico ha permesso di ottenere informazioni circa l'energia di attivazione dei tre sistemi studiati (APTES, APDES, APTES+APDES) e di stimare i tempi di degradazione idrolitica all'equilibrio per i diversi silani. I risultati ottenuti hanno rilevato che la velocità di degradazione per i tre rivestimenti aumenta secondo il seguente ordine: APDES < APTES+APDES < APTES. Si è visto che il meccanismo del processo di degradazione è lo stesso per i tre sistemi studiati, pertanto si è concluso la velocità di idrolisi dipende dalla concentrazione iniziale dei legami silossanici (-Si-O-Si-) in grado di essere idrolizzati. Inoltre, da questo studio è emerso che probabilmente nei compositi fibrorinforzati a matrice cementizia, l'uso di un poliorganosilossano con un basso grado di reticolazione

come quello corrispondente ad un rivestimento realizzato con APDES, potrebbe essere la strategia più efficace per resistere ad un possibile attacco dell'acqua, specialmente nell'ambiente alcalino caratteristico della matrice cementizia.

Successivamente, sono stati realizzati i materiali compositi con le fibre con i diversi trattamenti superficiali. Sono stati preparati, rispettivamente, campioni di malta a base di cemento Portland e fibre corte di basalto (commerciali e modificate) e campioni di malta a base di calce idraulica naturale e fibre corte di basalto (commerciali e modificate). Sono state studiate le proprietà meccaniche dei materiali compositi attraverso il test di resistenza a flessione a tre punti e il test di resistenza a compressione. I risultati ottenuti hanno permesso di realizzare un'analisi e successiva discussione basata sulle interazioni e la compatibilità tra l'agente di rinforzo e la matrice considerando le diverse caratteristiche della superficie della fibra e cercando di trovare le migliori condizioni, in termini di preparazione dei materiali, per ottenere interfacce le cui caratteristiche specifiche possono contribuire a migliorare le prestazioni dei materiali compositi finali. Pertanto, è stata condotta, inoltre, un'analisi frattografica delle immagini ottenute mediante microscopia a scansione elettronica (SEM) e misure di profilometria laser e ottica rispettivamente, per studiare la compatibilità tra fibra e matrice. Per valutare ulteriori possibili interazioni fibra-matrice, è stato realizzato uno studio di rugosità superficiale a scala nanosopica attraverso microscopia di forza atomica (AFM) in modo da poter comprendere il possibile contributo dell'adesione meccanica tra le fibre e la matrice. Inoltre, è stato studiato anche il possibile contributo al comportamento meccanico finale relativo alla struttura porosa dei campioni, utilizzando l'analisi BET-BJH per adsorbimento-desorbimento di N_2.

Da questi studi è emerso che la semplice presenza di fibre di basalto insieme a specifiche variazioni della natura superficiale delle fibre stesse, in generale aumentano le prestazioni meccaniche dei materiali in studio rispetto alle malte di riferimento, cioè materiali senza fibre.

Infine, è stato possibile concludere che, indipendentemente dalla matrice utilizzata, le migliori prestazioni meccaniche sono principalmente associate ad una migliore adesione all'interfaccia fibra-matrice, che si ottiene, in particolare, nel caso di malte rinforzate con fibre di basalto trattate con la miscela di due silani (APTES + APDES).

CHAPTER 1

INTRODUCTION AND OBJECTIVES

CHAPTER 1
INTRODUCTION AND OBJECTIVES

1.1 Introduction

In the present moment, several industrial and technological applications require the use of new low cost and environmentally friendly materials, offering other properties that are not present in traditional materials. Due to this, special efforts should be addressed in the material science and engineering areas, trying to design and develop innovative composite materials.

In this contest, the design of fiber-reinforced composite materials is especially interesting because they are widely used in different sectors such as aerospace, aeronautical, automotive, construction, sporting goods industries, among others. When fibers are incorporated to different matrices, they usually increase mechanical resistance and stiffness without compromising other characteristics as the low weight [1–5].

Different types of fibers are available to reinforce polymeric, metallic and ceramic matrices. Nevertheless, the necessity of reducing risk for human health and environment impact, suggests using new materials that can be directly obtained from natural sources without reducing materials performances in certain applications.

In the last decade, natural basalt fiber extruded from naturally fire-resistant basalt has emerged as a contender between the most used fiber reinforcements in composites [6–8]. Basalt fibers are classified as natural fibers of mineral origin characterized by high performance and a great range of good mechanical (high-tensile strength and high E-modulus), thermal (high temperature resistance) and chemical properties [9]. Furthermore, one of the great advantages of these fibers is the high availability of the raw material overworld and their low cost [10,11]. Moreover, basalt fibers can be easily processed using conventional methods and equipments and they do not need any other additional step in the single producing process, making them to have an additional advantage in terms of costs. Finally, it is interesting to highlight that basalt fibers are safe for health because their diameters are larger than 9 micrometers and they are not subjected to longitudinal fracture,

so they cannot be considered as inhalable materials. Due to the last characteristics mentioned basalt fibers have been recently classified as *"The green industrial material for the twenty-first century".* This definition reveals the sustainability, point of growing interest in new worldwide productions. In many cases basalt fibers might be an extraordinary candidate to replace synthetic fibers in composite materials. Nowadays, the fiber market is mainly oriented to the use of glass and carbon fibers. Basalt fibers might be an extraordinary candidate to replace the last ones since they have better tensile strength than E-glass fibers, greater failure strain than carbon fibers as well as good resistance to chemical attack [9]. Moreover, due to the high resistance against the action of fungi and microorganisms and their high mechanical properties, basalt fibers can be used for many applications as alternative to the other type of natural fibers of vegetable origin [11–13] .

The use of high-performance and eco-friendly materials is currently in high demand in different engineering and industrial fields. In the last years, a great interest of this type of materials is growing in the building industry where the concept of sustainability is becoming important. Moreover, special attention to fiber-reinforced materials is being developed in many countries where special climatic conditions and catastrophic events such as floods and earthquakes are becoming more frequent [11,14–16]. These events, sometimes, contribute to the deterioration of the modern and ancient buildings. In Italy for example, the most important historical centres have been damaged as a consequence of these catastrophic events. In this way, the identification and use of new materials for the preservation and conservation of cultural heritage are very important issues that generate considerable interest. The necessity of maintaining the characteristics of ancient materials implies finding out innovative materials for restoring masonry and plasters, guaranteeing their properties especially in terms of mechanical performance. Moreover, a very important issue to be considered in a restoration intervention is compatibility with the original structure; therefore, an especial care should be taken into account when selecting materials. Sometimes, the use of non-compatible materials could enhance building deterioration processes leading to the necessity of continuous structure reparations.

To satisfy the growing need of innovative and eco-friendly materials in modern building industry and in the restoration field, the main research activity carried out within the frame of the present PhD thesis was focused on the study of basalt fiber reinforced cement matrices.

Among the large variety of cement materials, Portland cement is one of the most used. It was developed in the mid nineteenth century and was rapidly become the main choice in the building industry. It is a hydraulic binder primarily used in mortar and concrete. It is largely used as construction and repair material in the modern building industry although in certain cases it was used to restore ancient masonry structures or buildings [17–19].
Restoration interventions that have employed cement-based mortars have shown several incompatibilities (high mechanical strength, efflorescence phenomena owing to the formation of large amounts of soluble salts by migrations of alkaline ions, low permeability with excessive water retention) causing extensive damage to the ancient masonry structures. Due to these problems, in the last years lime-based mortars have received special attention for restoration activities, looking for higher compatibility (physical, chemical and mechanical) with the original components [9].
In this contest, special attention is dedicated to the Natural Hydraulic Lime (NHL). This is a hydraulic binder highly compatible with structures of great cultural interest since lime based-mortar have been used as construction material since ancient time. In addition, the interest of using NHL for new construction is recently growing because it is responsible of reduction of CO_2 emission in comparison with the common Portland cement since less energy is required in the production process. Nevertheless, due to its lower mechanical properties NHL is not being widely used in comparison with Portland cement[16,20–25].

On the other hand, considering the potential applications of these materials it is important to take into account some disadvantages. First of all, it should be point out that cement materials are classified as brittle materials and great problems might be due to shrinkage cracking phenomenon [18,26,27]. In general, random dispersion of short fibers within the cement-based matrices might contribute to reduce this problem since they should lead to more isotropic reinforcement limiting crack opening [28]. Up to the present moment, several studies refer on the use of commercial short basalt fibers to reinforce cement-based materials [6,29,30]. Among other interesting conclusions, experimental results pointed out that better performance of cement based materials could be obtained by the optimization of fiber-matrix interface through surface treatments [31–33].

In fact, it is well known that properties of composite materials are strongly dependent on the type of adhesion between the reinforcement and the matrix [34,35]. One of the methods to improve the interface in composite materials is through especial surface treatments of

the fibers. Among others, silane coupling agents are the most commonly used modifiers of fibers surfaces [35,36]. However, most of the studies concerning the modification of fibers surface are mainly oriented to improve specific interactions with polymeric matrices [37–42]. In the present work, it is proposed to perform chemical coatings and study the particular interaction with cement matrices since the research is currently less widespread.

Besides, other important issue that deserve especial attention is related to the effect of external agents or small molecules such as water since it may lead to materials failure by interphase hydrolytic degradation. When silane coupling agents are used to modify the fibers the siloxane bonds formed with fibers surface and/or with other silane molecules can be more or less easily hydrolyzed depending on pH [43–45]. Therefore, taking into account that manufacturing of cement-based composite needs mixing with water, the study of possible hydrolytic degradation processes that might occur at the interface in these materials is very important to conveniently design these materials to improve their final performance. In addition, cement matrices are characterized by alkaline pH [46]. Therefore, considering a possible application of these polyorganosiloxanes coatings in cement materials, the study of their behavior in alkaline environment is particularly important.

1.2. Objectives

The aim of this PhD thesis is to optimize the fiber-matrix interface in fiber reinforced cement based-composites through specific surface treatments of the fibers.

The compatibility between as-received and modified natural basalt fibers and cement-based matrices will be studied to finally understand possible improvements of final performance of the composites. These materials have potential use as plasters in the building industry and in the restoration and conservation of Cultural Heritage as alternative to traditional materials.

In order to achieve this goal, several specific objectives have been set during this research project:

- To design and carry out controlled surface treatments on the basalt fibers

  In order to improve fiber-matrix interface different surfaces treatments based on chemical attachment of silane coupling agents are proposed. However, before silane coating, ideal surfaces of the fibers must be achieved by appropriate surface pre-treatments of the as-received fibers.

- To characterize the surface of the as-received and modified fibers

  A proper characterization with several analytical techniques is necessary to evaluate the effectiveness of the surface treatments. Information about their structure, composition and morphology/topography will be useful to finally understand possible improvements of the resulting interphases in the composites and consequently their final performance.

- To study degradation phenomena of the surface treatments

  Hydrolysis of the silane-based coatings will be studied by pH measurements and monitoring the fluorescence arising from fluorescent molecules chemically attached to the coatings.

- To evaluate the influence of the presence of fibers and their modifications on mechanical performance of the cement-based composite materials

  Three-point flexural test and compressive strength test will be carried out to study the mechanical behavior of all the materials under study.

- To study compatibility between the fibers and the matrix and the influence of the presence of fibers on the matrix.

  This objective is focused to understand the influence of the presence of the fibers and in particular, the interphases generated between the fibers and the cement-based matrices on the mechanical performance. Topographic analysis of the surface fractured materials will be carried out to study basalt fibers-cement based matrices adhesion and fracture mechanisms. Porosity and microstructure of the matrices, as

important factors influencing the mechanical properties, were evaluated under the presence or not of basalt fibers.

A schematic representation of the working plan of the present PhD thesis is shown in Figure 1.

To reach the goals above mentioned, the research activity has been developed in three main parts:

1. DESIGN AND CHARACTERIZATION OF BASALT FIBERS SURFACES.
2. HYDROLITIC DEGRADATION STUDY OF SILANE BASED COATINGS.
3. CHARACTERIZATION OF FIBER-REINFORCED COMPOSITES.

After this introduction, in Chapter 2 some concepts and basis necessary to help understanding the rest of the manuscript will be given. Then, in Chapter 3 a description of the materials and the experimental techniques and methods used to achieve the objectives above considered will be done. Next, Chapter 4 presents the topics related to the design and characterization of the fiber surface, and Chapter 5 discusses the hydrolytic degradation phenomena appearing in the polyorganosiloxanes coatings. Finally, Chapters 6 and 7 are focused on the study of fiber-reinforced composite performance when Portland cement and Natural Hydraulic Lime, NHL, are used as matrices respectively.

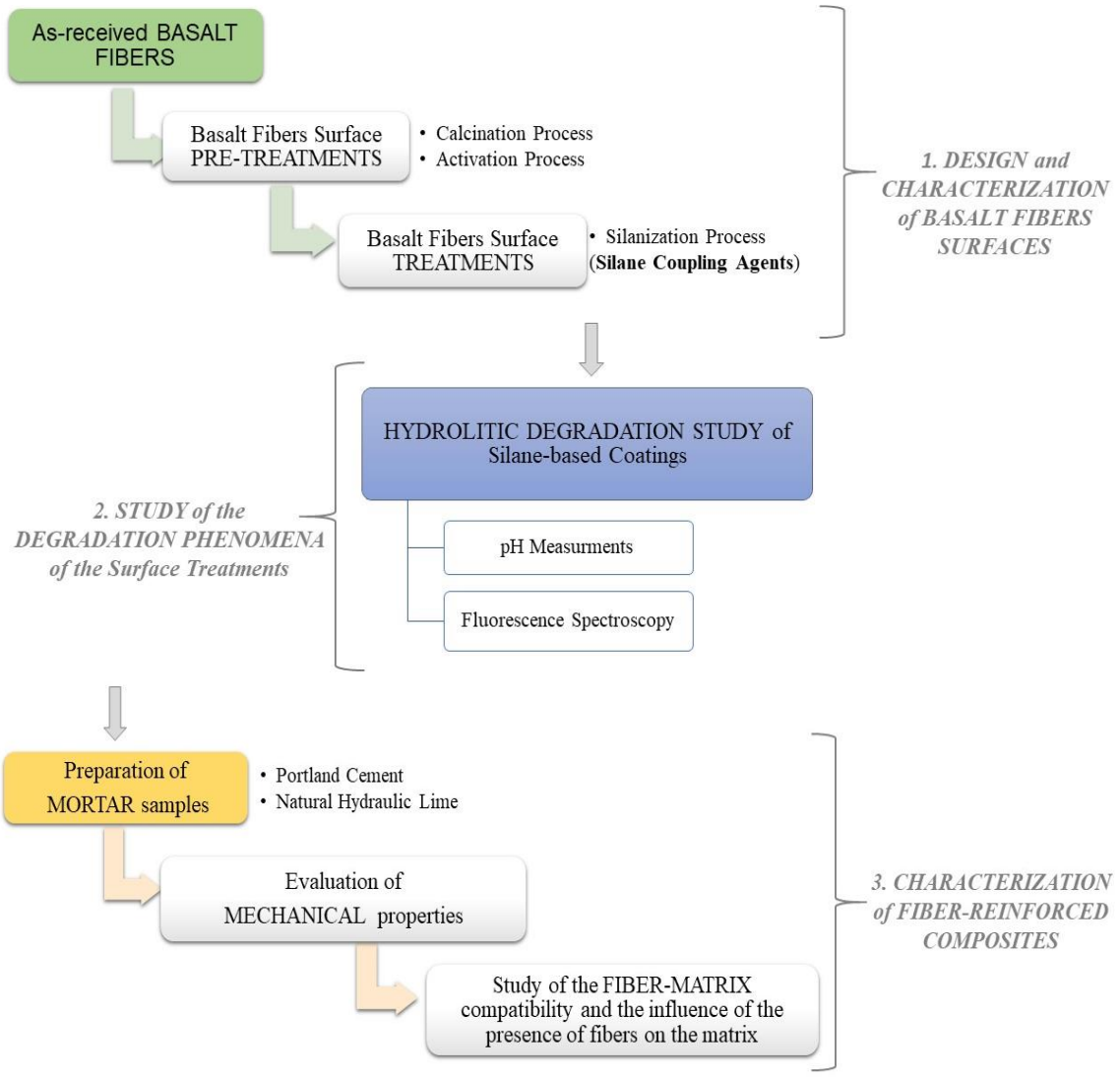

Figure 1. Scheme of the working plan of PhD Thesis.

References

[1] P.K. Mallik, Fiber-Reiforced Composites. Materials, Manufacturing, and Design, Third Edit, CRC Press Taylor & Francis Group, 2007. doi:13:978-1-4200-0598.

[2] William D. Callister Jr., D.G. Rethwisch, Materials Science and Engineering An Introduction, Eight Edit, John Wiley & Sons, Inc, 2010. doi:10.1016/0261-3069(91)90101-9.

[3] S. Chandra Das, E. Haque Nizam, Applications of Fiber Reinforced Polymer Composites (FRP) in Civil Engineering, Int. J. Adv. Struct. Geotech. Eng. 03 (2014) 2319–5347.

[4] A. Bentur, S. Mindess, Fibre Reinforced Cementitious Composites, Second edi, Taylor & Francis Group, 2006. doi:https://doi.org/10.1201/9781482267747.

[5] B. Clauß, Fibers for Ceramic Matrix Composites, Ceram. Matrix Compos. Fiber Reinf. Ceram. Their Appl. (2008) 1–20. doi:10.1002/9783527622412.ch1.

[6] V. Fiore, T. Scalici, G. Di Bella, A. Valenza, A review on basalt fibre and its composites, Compos. Part B Eng. 74 (2015) 74–94. doi:10.1016/j.compositesb.2014.12.034.

[7] K. Singha, A Short Review on Basalt Fiber, Int. J. Text. Sci. 1 (2012) 19–28. doi:10.5923/j.textile.20120104.02.

[8] V. Dhand, G. Mittal, K.Y. Rhee, S.J. Park, D. Hui, A short review on basalt fiber reinforced polymer composites, Compos. Part B. 73 (2015) 166–180. doi:10.1016/j.compositesb.2014.12.011.

[9] M. Iorio, M.L. Santarelli, G. González-Gaitano, J. González-Benito, Surface modification and characterization of basalt fibers as potential reinforcement of concretes, Appl. Surf. Sci. 427 (2018) 1248–1256. doi:10.1016/j.apsusc.2017.08.196.

[10] S. Parmar, Basalt Fiber: Newer Fiber for FRP Composites, Int. J. Emerg. Technol. Eng. Res. 4 (2016) 43–45.

[11] D. Saravanan, Spinning the rocks - Basalt fibres, J. Inst. Eng. (India), Part TX Text. Eng. Div. 86 (2006) 39–45.

[12] A. Greco, A. Maffezzoli, G. Casciaro, F. Caretto, Mechanical properties of basalt fibers and their adhesion to polypropylene matrices, Compos. Part B Eng. 67 (2014) 233–238. doi:10.1016/j.compositesb.2014.07.020.

[13] R.D. Tolêdo Filho, K. Ghavami, G.L. England, K. Scrivener, Development of vegetable fibre-mortar composites of improved durability, Cem. Concr. Compos. 25 (2003) 185–196. doi:10.1016/S0958-9465(02)00018-5.

[14] M. Lal Regar, A. Islam Amjad, Basalt Fibre–Ancient Mineral Fibre for Green and Sustainable Development, Tekstilec. 59 (2016) 321–334. doi:10.14502/Tekstilec2016.59.321-334.

[15] G.J. Parra-Montesinos, H.W. Reinhardt, A.E. Naaman, High Performance Fiber Reinfroced Cement Composites 6 HPFRCC 6, in: RILEM BOOKSERIES, Springer, 2012. doi:10.1017/CBO9781107415324.004.

[16] F. Iucolano, B. Liguori, C. Colella, Fibre-reinforced lime-based mortars: A possible resource for ancient masonry restoration, Constr. Build. Mater. 38 (2013) 785–789. doi:10.1016/j.conbuildmat.2012.09.050.

[17] P.-C. Aïtcin, Portland cement, in: P.-C. Aïtcin, R.J. Flatt (Eds.), Sci. Technol. Concr. Admixtures, Woodhead Publishing, 2016: pp. 27–51. doi:10.1016/B978-0-08-100693-1.00003-5.

[18] A.M. Brandt, Fibre reinforced cement-based (FRC) composites after over 40 years of development in building and civil engineering, Compos. Struct. 86 (2008) 3–9. doi:10.1016/j.compstruct.2008.03.006.

[19] K. Callebaut, J. Elsen, K. Van Balen, W. Viaene, Nineteenth century hydraulic restoration mortars in the Saint Michael's Church (Leuven, Belgium): Natural hydraulic lime or cement?, Cem. Concr. Res. 31 (2001) 397–403. doi:10.1016/S0008-8846(00)00499-3.

[20] J. Lanas, J.I. Alvarez, Masonry repair lime-based mortars: Factors affecting the mechanical behavior, Cem. Concr. Res. 33 (2003) 1867–1876. doi:10.1016/S0008-8846(03)00210-2.

[21] J. Lanas, R. Sirera, J.I. Alvarez, Study of the mechanical behavior of masonry repair lime-based mortars cured and exposed under different conditions, Cem. Concr. Res. 36 (2006) 961–970. doi:10.1016/j.cemconres.2005.12.003.

[22] S. Amziane, L. Arnaud, Bio-aggregate-based Building Materials: Applications to Hemp Concretes, John Wiley & Sons, Inc, 2013. doi:DOI: 10.1002/9781118576809.

[23] R. Maddalena, J.J. Roberts, A. Hamilton, Can Portland cement be replaced by low-carbon alternative materials? A study on the thermal properties and carbon emissions of innovative cements, J. Clean. Prod. 186 (2018) 933–942. doi:10.1016/j.jclepro.2018.02.138.

[24] R.M. Andrew, Global CO_2 emissions from cement production, Earth Syst. Sci. Data. 10 (2018) 195–217. doi:10.5194/essd-10-195-2018.

[25] M. Arandigoyen, J.I. Alvarez, Pore structure and mechanical properties of cement-lime mortars, Cem. Concr. Res. 37 (2007) 767–775. doi:10.1016/j.cemconres.2007.02.023.

[26] N. Banthia, C. Zanotti, M. Sappakittipakorn, Sustainable fiber reinforced concrete for repair applications, Constr. Build. Mater. 67 (2014) 405–412. doi:10.1016/j.conbuildmat.2013.12.073.

[27] D.W. Fowler, Repair materials for concrete structures, in: N. Delatte (Ed.), Fail. Distress Repair Concr. Struct., Woodhead Publishing Limited, 2009: pp. 194–207. doi:10.1533/9781845697037.2.194.

[28] K. Raoufi, J. Weiss, The role of fiber reinforcement in mitigating shrinkage cracks in concrete, in: R. Fangueiro (Ed.), Fibrous Compos. Mater. Civ. Eng. Appl., Woodhead Publishing Limited, 2011: pp. 168–188. doi:10.1016/B978-1-84569-558-3.50006-5.

[29] R. Ralegaonkar, H. Gavali, P. Aswath, S. Abolmaali, Application of chopped basalt fibers in reinforced mortar: A review, Constr. Build. Mater. 164 (2018) 589–602. doi:10.1016/j.conbuildmat.2017.12.245.

[30] L. Jian-jun, M. Ying, L. Yan-chun, The Performance of Green Basalt Fiber and its Application in the Civil Engineering Field, Appl. Mech. Mater. 193–194 (2012) 548–552. doi:10.4028/www.scientific.net/AMM.193-194.548.

[31] M.L. Santarelli, F. Sbardella, M. Zuena, J. Tirillò, F. Sarasini, Basalt fiber reinforced natural hydraulic lime mortars: A potential bio-based material for restoration, Mater. Des. 63 (2014) 398–406. doi:10.1016/j.matdes.2014.06.041.

[32] M.L. Santarelli, F. Sbardella, M. Zuena, M. Albé, G. Quattrociocchi, J. Tirilló, M. Valente, F. Sarasini, Malte più performanti con le fibre di basalto, Compos. Mag. 33 (2014) 7–16. http://hdl.handle.net/10278/44412.

[33] Z.C. Girgin, M.T. Yıldırım, Usability of basalt fibres in fibre reinforced cement composites, Mater. Struct. Constr. 49 (2016) 3309–3319. doi:10.1617/s11527-015-0721-4.

[34] N. Suzuki, H. Ishida, A Review on the Structure and Characterization Techniques of Silane/Matrix Interphases, Macromol. Symp. 108 (1996) 19–53. doi:https://doi.org/10.1002/masy.19961080105.

[35] A.T. DiBenedetto, Evaluation of fiber surface treatments in composite materials, Pure Appl. Chem. 57 (1985) 1659–1665. doi:10.1351/pac198557111659.

[36] S.-J. Park, J.-S. Jin, J.-R. Lee, Influence of silane coupling agents on the surface energetics of glass fibers and mechanical interfacial properties of glass fiber-reinforced composites, J. Adhes. Sci. Technol. 14 (2000) 1677–1689. doi:10.1163/156856100742483.

[37] D. Olmos, J. Gonzalez-Benito, Composites formed by glass fibers and PS-modified epoxy matrix. Influence of the glass fibers surface on the morphologies and mechanical properties of the interphases generated, Polym. Compos. 31 (2010) 946–955. doi:10.1002/pc.20879.

[38] J.G. Iglesias, J. González-Benito, A.J. Aznar, J. Bravo, J. Baselga, Effect of Glass Fiber Surface Treatments on Mechanical Strength of Epoxy Based Composite Materials, J. Colloid Interface Sci. 250 (2002) 251–260. doi:10.1006.

[39] T. Deák, T. Czigány, P. Tamás, C. Németh, Enhancement of interfacial properties of basalt fiber reinforced nylon 6 matrix composites with silane coupling agents, Express Polym. Lett. 4 (2010) 590–598. doi:10.3144/expresspolymlett.2010.74.

[40] R. Balart, J.M. España, M.D. Samper, E. Fages, L. Sanchez-Nacher, Investigation of the Effect of Different Silane Coupling Agents on Mechanical Performance of

Basalt Fiber Composite Laminates with Biobased Epoxy Matrices J.M., Polym. Compos. 34 (2013) 376–381. doi:10.1002/pc.

[41] Y. Xie, C.A.S. Hill, Z. Xiao, H. Militz, C. Mai, Silane coupling agents used for natural fiber/polymer composites: A review, Compos. Part A Appl. Sci. Manuf. 41 (2010) 806–819. doi:10.1016/j.compositesa.2010.03.005.

[42] J. González-Benito, A. Aznar, J. Baselga, Solvent and Temperature Effects on Polymer-Coated Glass Fibers . Fluorescence of the Dansyl Moiety, J. Fluoresc. 11 (2001).

[43] H. Ishida, J.L. Koenig, The reinforcement mechanism of fiber-glass reinforced plastics under wet conditions: A review, Polym. Eng. Sci. 18 (1978) 128–145. doi:10.1002/pen.760180211.

[44] H. Ishida, J.L. Koenig, Effect of Hydrolysis and Drying on the Siloxane Bonds of a Silane Coupling Agent Deposited on E-Glass Fibers, J. Polym. Sci. Polym. Phys. Ed. 18 (1980) 233–237.

[45] D. Olmos, A.J. Aznar, J. Baselga, Hydrolytic damage study of the silane coupling region in coated silica microfibres : pH and coating type effects, J. Mater. Process. Technol. 144 (2003) 82–86. doi:10.1016/S0924-0136(03)00325-X.

[46] A. Hakamy, F.U.A. Shaikh, I.M. Low, High-performance natural fiber-reinforced cement composites, Adv. Ceram. Matrix Compos. Second Ed. (2018) 277–305. doi:10.1016/B978-0-08-102166-8.00012-8.

CHAPTER 2

BASIS ABOUT BASALT-FIBERS REINFORCED COMPOSITE MATERIALS

CHAPTER 2
BASIS ABOUT BASALT FIBER-REINFORCED COMPOSITE MATERIALS

In this Chapter an overview about the basalt fiber-reinforced composite materials will be done. In particular, general notions concerning production process, composition, properties and some problems related to this kind of materials will be discussed. Here it is important to highlight that specific problems and solutions proposed to solve them, will be later considered in the corresponding Chapters 4, 5, 6 and 7.

2.1. Fiber-reinforced Composite Materials

Many modern technologies require the use of materials that offer unique combinations of different properties that cannot be present simultaneously in traditional materials such as conventional metal alloys, ceramics and polymers. The possibility of combining different properties into a single material and extending the validity ranges (synergy) has been achieved and is continuously improved with the preparation of composite materials.

In general, a composite material is defined as a material system composed of a mixture or combination of two different constituents which differ in their chemical form and composition leading, in addition, to clear phase separation [1,2].

The two constituents or phases are the matrix, which is continuous and surrounds the other phase, known as dispersed phase or reinforcement. The latter represent the discontinuous phase, and usually is harder and tougher than the continuous phase.

Composite materials are usually classified according to the scheme shown in Figure 1. This is a classification based on the type of reinforcement [2]. In fact, depending on the type of reinforcement used, it can be distinguished:

- *PARTICLE-REINFORCED COMPOSITES.*
- *FIBER-REINFORCED COMPOSITES.*
- *STRUCTURAL COMPOSITES.*

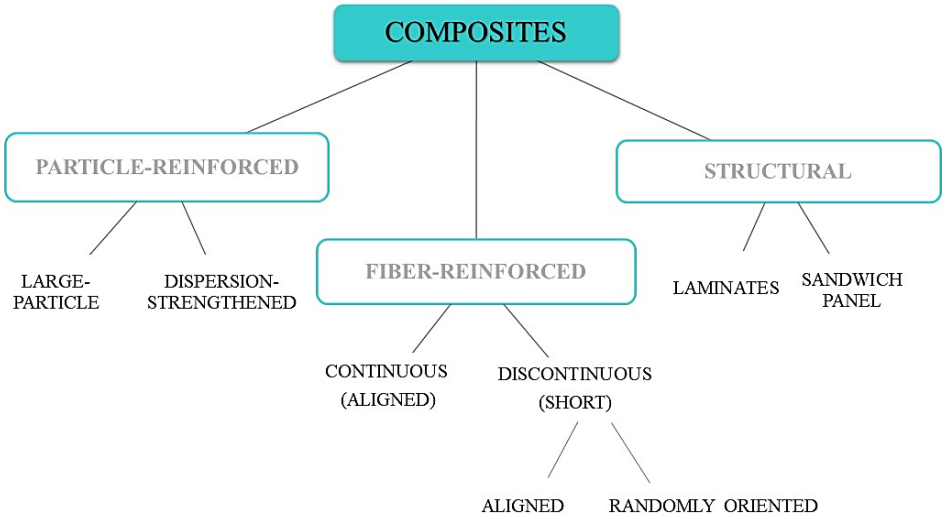

Figure 1. General classification of composite materials.

In this PhD thesis, attention is paid to fiber-reinforced composites. Among others, the main applications of these materials are found in several industrial fields (such as aeronautical, automotive, sporting goods, aerospace, marine, electronics, medical industry etc.). However, in the last decades the use of these materials in the building industry is receiving especial attention. In particular, in this work, fiber-reinforced materials focused to the construction sector and restoration are considered.

A fiber-reinforced composite material consists of fibers of high strength and modulus embedded in a matrix. The synergy between these two constituents, fiber and matrix, confers to the whole material a large variety of good properties that cannot be achieved with either of the constituents acting alone. In general, the main goal of this type of materials is to achieve high resistance and/or stiffness with low weights [1,2].

In a fiber-reinforced composite material, the fiber and the matrix have specific roles. The fiber provides reinforcement to the matrix acting as the principle load transmitter. In general, fibers improve the total mechanical properties of the composites. On the other hand, the roles of the matrix are: i) to place and orient the fibers, ii) to transfer stresses to the fibers and iii) to protect the fibers form adverse environment (such as chemicals and moisture) and from mechanical degradation (e.g. by abrasion) [3].
Usually, the fibers can be incorporated to the matrix in continuous or discontinues forms (see Figure 1) and the matrix material can be a polymer, a metal or a ceramic.

In this project short randomly oriented fibers (basalt fibers) within ceramic matrices (cement-based matrices), are considered. Cement-based matrices are brittle materials and possess low resistance to crack propagation, which is manifested in their low fracture toughness. Therefore, the primary reason for the incorporation of basalt fibers to the ceramic matrices is to increase its mechanical performance mainly in terms of fracture toughness [2].

It should be point out that the final performance of a composite material mainly depends or is influenced by fiber length, fiber orientation, mechanical properties of the fiber and fiber content. However, it is well known that the final performance of fiber-reinforced materials not only depends on the properties of the main constituents (fiber and matrix) but also on other aspects such as the nature of fiber-matrix interface [2]. The term interface refers a two-dimensional border separating distinct phases (e.g., fiber, matrix, interphase, silane coating, etc.). This term sometimes should be confused with the term interphase that is a region in which the fiber and matrix phases are chemically and/or mechanically combined. The interphase may be a diffusion zone, a nucleation zone, a chemical reaction zone, etc., or any combination of the above [4,5].

Specifically, this thesis project is mainly focused on the optimization of the fiber-matrix interface in fiber-reinforced materials through special surface treatments of the fibers (see section 2.1.3). Therefore, in this work the term interface will be used to refer a well definite region between fiber and matrix, while the term interphase will be used to describe the region between the matrix and the fiber, in which the fiber surface treatments are also included.

2.1.1. Reinforcing Agents

Nowadays, a large variety of synthetic and natural fibers is available in the market. This work is mainly focused on the use of natural fibers. The latter are obtainable from an animal, vegetal or mineral source [6,7]. In this project, basalt fibers classified as natural fibers of mineral origin are studied. Some peculiarities and characteristics concerning this type of fibers will be discussed below.

Basalt Fibers

In the last decade, basalt fibers extruded from naturally fire-resistant basalt has emerged as reinforcing agents in fiber reinforced composite materials. They are natural fiber directly obtained from the melting of the basalt. Basalt is a solid, compact igneous rock which is formed when volcanic lava cools adequately to solidify, widespread worldwide [8]. As an example, in Figure 2 basalt columns present around the world are shown.

Figure 2. Basalt Columns at Litlanesfoss-Iceland.

The chemical structure of the basalt is similar to the conventional glass (Figure 3), in fact, it is mainly characterized by SiO_2, Al_2O_3, CaO, MgO, Fe_2O_3 and FeO (Table 1) [8]. Depending on SiO_2 content, basalts are classified as alkaline basalts (up to 42% of SiO_2), slightly acidic basalts (43-46% of SiO_2), acidic basalts (over 46% of SiO_2). Moreover, depending on the chemical composition the color of the basalt could change from brown and gray to dull green [9].

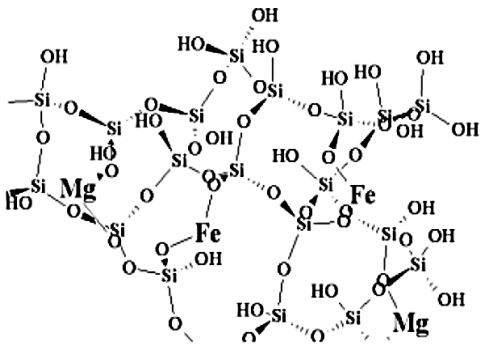

Figure 3. Network structure of basalt [10]

Table 1. Chemical composition of basalt [8].

Chemical compound	%
SiO_2	48.8-52.8
Al_2O_3	14-17.5
Fe_2O_3	7.3-13.3
MgO	6.2-16
CaO	8.59
Na_2O	3.34
K_2O	1.46
TiO_2	0.9-1.6
P_2O	0.28
MnO	0.1-0.16
Cr_2O_3	0.06

Due to its great abundance in the world, basalt can be used for many applications and, among others, for fiber manufacturing. However, it is important to highlight that for fiber manufacturing not all type of basalt can be used for making continuous filaments with a diameter range from 9 to 24 microns. Basalt rocks with SiO_2 content above 46% (the so named acidic basalt) are suitable for fiber production. Moreover, other criteria must be satisfied: ability to melt without solid residue, appropriate melt viscosity for fiber formation and ability to solidify in a glassy phase without noticeable crystallization [9,11].

Production process of basalt fiber

Usually, basalt continuous filaments are made from the basalt rocks by spinneret method like glass fibers. However, the basalt fibers production is simpler than glass fibers due to a less complex chemical composition. In fact, basalt fibers are obtained directly from melted basalt rock without additional additives [10,12]. A scheme of the process is shown in Figure 4.

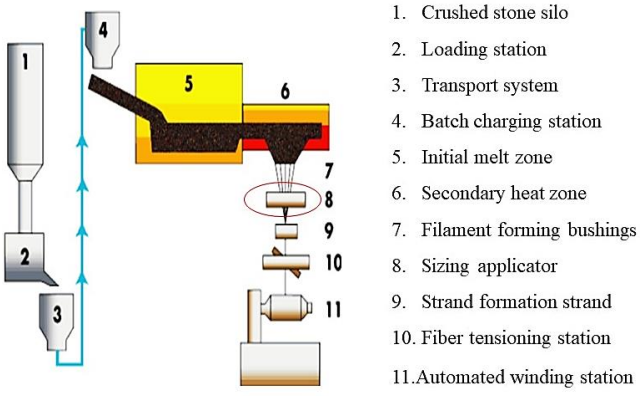

Figure 4. Scheme of basalt fibers production [12].

Crushed basalt rocks are charged into bath-type melting furnace by a dozing charger. They are converted into melt under 1460-1500 °C. Molten basalt flows from furnace through feeder channel through the platinum-rhodium bushing with minimum 200 holes. The fibers are drawn from the melt under hydrostatic pressure and subsequently cooled to get hardened filaments. In the next step, a silane based sizing liquid is applied on the fiber surface hereby the sizing components impart standard integrity, lubricity and resin compatibility [11–13].

Moreover, the application of the sizing is necessary to avoid a decrease in the fiber strength values since it help to stops the development of micro-cracks on the filament surface. In addition, the sizing improve the adhesive properties of the fibers [8].
In the frame of this research project the attention is focused especially on this step of the process (step 8 of Figure 4). Until now, most of the commercial sizing are produced for polimeric matrices. The developing of a sizing compatible with cement matrices is less widespread. One of the main goals of this thesis is the study of a new chemical coating to be applied on the fiber surface in this part of the production process. Therefore, the preparation of new surface treatments compatible with cement matrices is proposed.

After sizing is applied, the filaments are collected together to form “strand” and forwarded to be wound on take up devices [11–13].

Different fiber morphologies can be obtained: continuous basalt fibers, chopped strands (by cutting continuous strands into short lengths), milled (produced by grinding continuous strands), fabrics, bars/rod. Chopped strands is the fiber morphology choose for the development of this research project.

Properties of basalt fibers

Basalt fiber present a large variety of good properties, due to this up to now they can be considered an interesting alternative to other types of fibers currently present in the fiber market. The main properties of basalt fibers are:

- High tensile strength.
- High E-Modulus.
- High abrasion resistance since they are extremely hard (from 5 to 9 on Mohs scale).

- High temperature resistance.
- Strong resistance to the action of fungi and microorganisms.
- Good resistance to UV-light.
- Anti-corrosion properties.
- Excellent thermal and sound insulation.
- Good chemical stability (they have good resistance against alkaline environment - pH up to 13-14 - but relatively less stability in strong acids) [8–14].

Safety and Toxicity of Basalt Fibers

Safety and toxicity are two important parameters to be considered when handling fibers. Therefore, it is important to point out that basalt fiber arising from natural raw material (the basalt rock) does not cause any damage to the health since, in the production process, filaments are spun with a diameter between 9 and 13 µm. Moreover, they cannot split longitudinally and consequently they are characterized as no-respirable [8,11]. Studies about problems related to the fibers, indicate that only fibers having diameters smaller than 3 µm are considerable inhalable, having no problems of inhalation fibers with length greater than 5 µm and length/diameter ratios greater than 3 [15]. Moreover, it should be point out that, the US and European occupational safety guidelines have labeled continuous basalt fibers and fabrics as safe materials [8,11]. In addition, it is important to mention that they have no toxic reaction with air or water, and they are non-combustible. When in contact with other chemicals they produce no chemical reactions that may damage health or environment. Moreover, they are easy to process (no additives are added to the melt) and to recycle. Therefore, basalts fibers are classified as ecological friendly material [7,10] .

Comparison with other fibers and applications

Most of the industrial applications are focused especially on the use of the common glass and carbon fibers. Because of the good range of excellent properties above mentioned, basalt fiber sometime can replace synthetic fibers. Table 2 describes some of the properties of the basalt fibers compared with E-Glass, S-Glass and carbon fibers, currently more widely used as reinforcement in composite materials.

Table 2. Comparison of basalt and some synthetic fibers [12].

PROPERTIES	**CONTINUOUS BASALT**	**E-GLASS**	**S-GLASS**	**CARBON**
Tensile Strength (MPa)	3000 – 4840	3100 – 3800	4020 – 4650	3500 – 6000
Elastic Modulus (GPa)	79.3-93.1	72.5 – 75.5	83 – 86	230 – 600
Elongation at break	3.1	4.7	5.3	1.5 ~ 2.0
Temperature Withstand °C	-260 +700	-50 +380	-50 +300	-50 +700

From Table 2, it is possible to observe that basalt fibers could be an optimal alternative especially to E-glass fibers because of its higher tensile strength and elastic modulus values. Moreover, basalt fibers have excellent thermal properties compared to glass fibers. This make basalt fibers very attractive for several applications in composite materials with respect the common glass fibers. On the other hand, due to high tensile strength and low elongation at break sometimes could replace carbon fibers. Finally, another aspect to be considered is the lower price of basalt fibers with respect the glass and carbon fibers [12].

Owing to the large variety of good advantages discussed above, basalt fibers have attracted attention for different industrial applications (such as in the automotive, electricity and electronics, chemical and petrochemical, aircraft, sporting goods etc.). Moreover, they also found application in the building industry as reinforcement in concrete [7,8,11,12,14]. About this issue and in particular, about the use of the basalt fibers as reinforcing agent for cement matrices, a more extended discussion will be given in the Chapters 6 and 7.

2.1.2. Matrices

In this research project two different ceramic matrices are considered: Portland cement and natural hydraulic lime. A brief description about the production process and their main properties and problems will be done.

- *Portland Cement*

Cement was discovered in 1824 by J. Aspin, but only from 1835 with L.C. Johnson, Portland cement becomes the dominant binder in the building industry, being the most common type of cement used around the world [16].

This building material is obtained by mixing two raw materials largely diffused: limestone ($CaCO_3$) and clay (silica SiO_2, alumina, Al_2O_3, and iron oxide Fe_2O_3). Through a complex production process the so-called *clinker*, that represent the base material of the cements currently available in the market, is obtained. In detail, the clinker is obtained by grounding and mixing limestone and clay in precise proportions and by heating the mixture to a temperature of about 1450°C in a rotary kiln. This process leads to the formation of the four principal compounds forming the *clinker*:

- Tricalcium silicate *($SiO_2 \cdot 3CaO$).*
- Dicalcium silicate *($SiO_2 \cdot 2CaO$).*
- Tricalcium aluminate *($Al_2O_3 \cdot 3CaO$).*
- Tetracalcicium ferroaluminate *($4CaO \cdot Al_2O_3 \cdot Fe_2O_3$).*

Usually, these substances are also known as C_3S, C_2S, C_3A and C_4AF [1] respectively.

C_3S and C_2S represent the silicate phase of the Portland cement, whereas C_3A and C_4AF the aluminous phase. The silicate phases are the most abundant.

However, to make Portland cement, the clinker should be ground and mixed with a certain amount of calcium sulphate (usually gypsum up to 5%). It is important to grind the cement particles finely because, depending on this, its reactivity can change. The finer the cement, the more reactive it is.

The process of setting and hardening the cement is the result of the reactions that take place between the water and the clinker. In this regard, it is important to point out that the principal four components of Portland cement, when mixed with water, shown different hydration kinetics and different hydration products. The most reactive compound is C_3A. To reduce the rapid hydration of C_3A that could lead to the "*flash set*" phenomenon (so-called in the concrete industry) and to allow a certain period of workability before setting,

[1] Pseudo-chemical notations: C=CaO; S=SiO_2; A=Al_2O_3; F=Fe_2O_3.

the gypsum should be added. Gypsum is added to retard the setting process. In fact, in contact with water, the gypsum reacts with C_3A leading to the formation of ettringite, which precipitates on the C_3A granules avoiding the penetration of water and therefore strongly delaying, the process of hydration of C_3A and the formation of calcium aluminate hydrated (also known as C-A-H). The hydration of C_4AF is similar to that of C_3A, but much slower. However, although the C_3A is the most reactive, the hydration process of Portland cement is dominated by the silicate phases. The C_3S is the most important phase since it is the main component of cement (50-70%). The hydration of C_3S is largely responsible for the beginning of the set and early strength development while the hydration of C_2S is significant in terms of the final strength of the hardened cement. In fact, C_2S hydrates much more slowly than C_3S. However, the hydration products for both phases are the silicate calcium hydrate (better known as C-S-H) and portlandite ($Ca(OH)_2$).

The C-S-H is the main responsible of the mechanical properties and durability of the cement materials. The $Ca(OH)_2$ production does not affect the mechanical properties. Its importance is due to the fact that it maintains high the pH of the cement.

The hydration reactions, transform the hydrated cement paste more or less rapidly into a hardened material that continues to gain strength with time as long as there is enough water to hydrate all the cement particles [17–20]. The hardening of the mass is a long process that may continue for several years [2].

Another process important to be mentioned is the carbonatation process. During this process, the atmospheric CO_2 can penetrate the porous structure of these materials and a carbonation reaction takes place. Thus, CO_2 reacts with portlandite and the others cement hydration products, with a consequent pH lowering [21]. Generally, this process does not negatively affect the cement materials. Sometimes it reduces porosity and lead to a formation of a protective layer on the surface of the material [22,23]. In contrast, when steel is present in these materials, low values of pH contribute to their degradation [17].

Some considerations might be made on the different types of cement commercially available. All type of cement currently used, are regulated by the European Standard EN 197-1 [24]. The latter provides 5 main classes of cements (***CEM I*** *Portland Cement,* ***CEM II*** *Portland-composite cement,* ***CEM III*** *Blastfurnace cement,* ***CEM IV*** *Pozzolanic*

*cement, **CEM V** Composite cement),* 27 sub-types and 6 resistance class. In this study a CEM II/A- L 42.5 R is used. It corresponds to a Portland cement with a content of between 6% and 20% by mass of limestone, with strength class 42.5 and high initial strength (R).

- *Natural Hydraulic Lime (NHL)*

Hydraulic lime are traditional building materials and represent a fundamental step in the history of the binders used in architecture before the advent of Portland cement. The use of the lime starts with the Greek civilization. However, the systematic use of lime is due to Romans who used this material for the preparation of mortars and concrete to build large buildings and exceptional size constructions or structures. However, Romans obtained hydraulic compounds by mixing air lime and hydraulic products (a volcanic sand know as pozzolan) and not directly with hydraulic lime [25,26].
In fact, the hydraulic lime was developed staring from 1793 when J. Smeaton discovered that heating limestone containing impurities of clays produced a type of lime (the hydraulic lime) with characteristics like those of the lime-pozzolan mixture.

Natural hydraulic lime is produced by calcination of more or less argillaceous or siliceous limestones at the temperature between 1100 °C and 1250 °C. During the calcination process, the reaction between lime ($CaCO_3$) and aluminosilicates (SiO_2+Al_2O_3) takes place leading to the formation of calcium oxide and calcium silicates and aluminates. They are subsequently reduced to a powder by the addition of controlled amount of water (*slaking*) with or without the need for further grinding.
However, it is important to highlight some difference with the hydraulic phases of cement since they have important influence on the final properties of the binder. As described previously, cement is produced at higher temperature than natural hydraulic lime. This leads to the formation of different compounds. In fact, in natural hydraulic lime the mayor hydraulic phase is represented by the C_2S whereas in cement the most abundant phases are C_3S. Sometimes C_3S is present because of local *"hot spot"* in the lime kiln. Moreover, in cement all the calcium oxide (CaO) is combined in calcium silicates (mainly C_3S) and calcium aluminates (C_3A and C_4AF). In contrast in natural hydraulic lime a certain amount of free CaO remains that will convert to free $Ca(OH)_2$ after slaking.

However, as in the case of cement, the hydraulic reaction takes place. By chemically reaction with water, stable hydrates and insoluble compounds are formed (hydrated

calcium silicate, C-S-H, and aluminate, C-A-H). Besides, portlandite ($Ca(OH)_2$) is also developed.

These compounds allow the material to be to set and harden and remain stable even under water (hydraulic action). In this case, the hardening process takes place also by reaction with the atmospheric CO_2. During this process part of CO_2 is reabsorbed with the reconstitution of $CaCO_3$ or limestone [16,26–29].

The different types of limes used as construction materials currently available in the market are regulated by the European Standard EN 459-1 [29]. In accordance with their chemical composition, two important class are considered: air limes (they have no hydraulic properties and are not able to harden underwater) and limes with hydraulic properties. Related to the latter the standard distinguishes between *artificial hydraulic limes* **(HL)**, *formulated limes* **(FL)** and the above discussed *natural hydraulic limes* **(NHL)** in which the hydraulic properties derive from the natural raw material without any other additions.

Natural hydraulic limes (NHL) are classified in accordance with their minimum compressive strength at 28 days as NHL 2, NHL 3.5, and NHL 5. In this PhD thesis the last one, NHL 5, is the class used.

Cement and natural hydraulic lime are primarily used as hydraulic binders in mortar and concrete to bind aggregates of inert particles (sand and/or gravel) into a cohesive mass. These are considered to be composite materials [2].

The term *mortar* generically indicates a mixture of several components that come appropriately mixed together in certain proportions, in order to give the mixture, in the fresh state, an appropriate workability and, in the hardened state, adequate physical-mechanical, aesthetic and durability properties. In the most common sense, mortar is obtained by intimately mixing an aggregate (such as sand) with a binder (such as cement or lime) and adding water until a perfectly blended and homogeneous mixture is obtained, of the desired consistency, in relation to the use that must be made of it: substrates, plasters, decorations, etc. The same mixture, but with larger aggregates (such as gravel and crushed stone) takes the name of concrete [30].

Depending on the binder used, cement-based mortars and natural hydraulic lime-based mortars are distinguished. In this study cement matrices are mixed with sand and chopped basalt fibers to form the so-called fiber reinforced mortars.

Shrinkage cracking phenomenon

The main problem affecting mortar and concrete is the shrinkage cracking phenomenon. It represents a great problem in this type of materials. Therefore, it was found appropriate to consider this aspect more in detail.

Shrinkage cracking phenomenon is due to volume changes in the materials and it is strongly depending of the properties of the cement matrix (such as composition and hydration reactions) and external factors related to the changes in moisture ambient. Due to these changes in the volume, tensile stress develops and consequently concrete and mortar cracking take place. It is responsible of the weakness and durability of the whole structure. In fact, these cracks can increase the penetration of water and other aggressive agents (such as chlorides) resulting in a faster degradation of the material. In addition, it is responsible of aesthetics damage since some cracks could appear on the construction surfaces. However, it should be pointed out that usually this phenomenon is more common in mortar than in concrete since the latter contain coarse aggregate which limit the shrinkage amount [31–33].

Usually, four types of shrinkage cracking can be distinguished:

- *Autogenous shrinkage*

  This type of shrinkage, also known as chemical shrinkage, takes place when cement products are mixed with water just at early stages of the cement hydration. The hydration reaction provokes a reduction in the volume of the mixture since the reaction products formed during the hydration of cement and lime occupy less space than the corresponding reactants. This is not due to external phenomena arising from environment.

- *Plastic shrinkage*

  It occurs immediately the material is setting, when it is still in the plastic stage and it is due to the external factors (humidity, temperature, wind rate). It is associated to

the rapid evaporation of the water from the surface of mortars and concretes. Usually, the loss of water from the fresh paste due to external conditions, generate negative capillary pressures that cause the volume of the paste to contract and consequently cracks are developed.

- *Carbonation shrinkage*

  It is associated to the carbonation process occurring in mortar and concrete when in contact with the atmospheric CO_2. The chemical reaction between the latter and calcium hydroxide in the hardened matrix leads to a reduction in volume. This type of shrinkage is limited to the surface of mortar and concrete.

- *Drying shrinkage*

  It is related to the drying of hardened cement-based materials due to the loss of capillary water. This is mainly caused from external factors (temperature and humidity) [31,34,35]

However, these effects must be evaluated together as a total shrinkage phenomenon occurring in mortars and concrete leading to appearance of cracks that have a negative effect on the whole material. A solution to solve this problem is by introducing short fibers. This topic will be discussed more in detail in Chapter 6.

2.1.3. Surface Treatments

Surface treatments of the fibers surfaces is a way to improve the bonding across fiber-matrix interface in composite materials. The methods that could be employed to modify the fiber surface are different. Among others, the modification of fiber surface with silane coupling agents is receiving each time more attention [3,36–42].

Silane Coupling Agents

A coupling agent is a chemical usually with double functionality used to create a chemical bridge between the reinforcement and the matrix in composite materials. Their primary function is to confer a good adhesion between the reinforcement/filler (in the present case fiber) and the matrix. Moreover, as previously discussed in the section 2.1.1 of this Chapter, the application of a sizing based on silanes, during the manufacturing process, is

very important to enhance the fiber strength since it can reduce some defects present on the fiber surface. In addition, the sizing contributes to avoid damage during handling [42–44].

The use of silane coupling agents presents several advantages. First of all, they are commercially available in a large scale. Moreover, they can improve the adhesion between the reinforcement and the matrix through favorable interactions. Generally silane coupling agents have hydrolizable groups (alkoxy in the present work) capable of reacting with silanols of the reinforcement surface (such as in the case of basalt fibers), and other functional groups more compatible or that can favorably interact with the matrix [45,46]. In addition, they can be used at room temperature, even under conditions of extreme humidity, and without losing effectiveness [40].

Among those silane, difunctional organosilicon compounds of general formula **Y-Si(X)$_3$**, or **R-(CH$_2$)$_n$-SiX$_3$** are the most commonly used. **Y** or **R** represents a non-hydrolysable organo-functional group (such amino, mercapto or epoxy) physically or chemically compatible with the matrix. On the other hand, **X** represents a hydrolysable group (such as methoxy *–OCH$_3$*, ethoxy *–OCH$_2$CH$_3$* or chlorine *–Cl*). These groups, after hydrolyzing to silanol can react with other silanol groups present on the surface of the silicic material to form siloxane linkages.

The main steps of the interaction between silane coupling agents and fibers can be described as follows:

a) **Hydrolysis:** silane monomers are hydrolyzed in presence of water yielding to reactive silanol groups.

$$R\text{-}SiX_3 + 3H_2O \rightarrow R\text{-}Si(OH)_3 + 3HX$$

b) **Self-condensation:** in concomitance the condensation reaction of silanols starts taking place with the formation of Si-O-Si bonds (Figure 5).

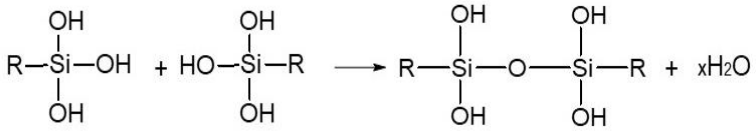

Figure 5. Self-condensation process.

c) **Hydrogen bond formation between fiber surface and silane:** when fibers are added to the silane aqueous solution, the free reactive silanol groups of silanes can react with the hydroxyl groups of the silicic fiber's surfaces (like basalt fibers) forming hydrogen bonds (Figure 6).

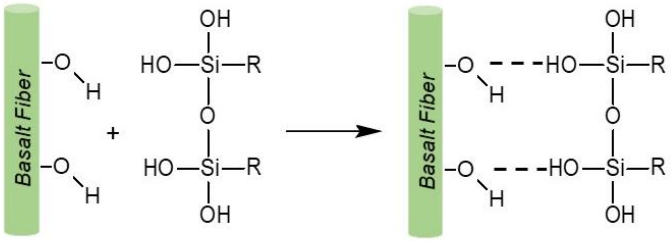

Figure 6. Hydrogen bond formation between fiber surface and silane coupling agents.

d) **Chemical grafting:** in general, at temperatures slightly higher than 100 ºC condensation between silanols of the silane and the silanols of the fibers takes place to yield siloxanes bonds with dehydration. Depending on the silane, the continuous condensation between silanol groups of the silane can generate a more or less crosslinked siloxanic structure of the coating (Figure 7) [37,41,42,47–51].

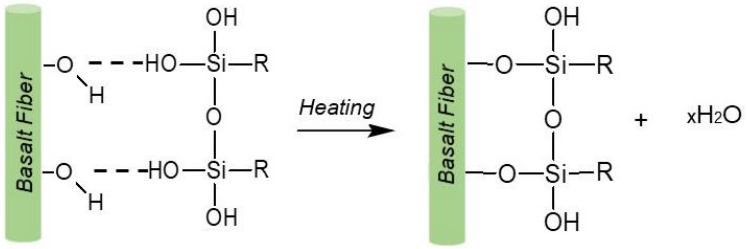

Figure 7. Chemical grafting and polyorganosiloxane structure formation.

The role of the interface, the fibers and the silane coupling agents specifically in cement matrices and the use of these materials in the building industry and in the restoration and conservation, will be discussed more in detail in the following Chapters 4, 5, 6 and 7.

References

[1] W.F. Smith, Scienza e tecnologia dei materiali, 1a edizion, McGraw- Hill Libri, 1995.

[2] William D. Callister Jr., D.G. Rethwisch, Materials Science and Engineering An Introduction, Eight Edit, John Wiley & Sons, Inc, 2010. doi:10.1016/0261-3069(91)90101-9.

[3] P.K. Mallik, Fiber-Reinforced Composite Materials, Manufacturing, and Design, Third Edit, 2007.

[4] K.E. Geckeler, F. Rupp, J. Geis-Gerstorfer, Interfaces and interphases of (bio)materials: Definitions, structures, and dynamics, Adv. Mater. 9 (1997) 513–518. doi:10.1002/adma.19970090614.

[5] R.E. Swain, K.L. Reifsnider, K. Jayaraman, M. el-Zein, Interface/Interphase Concepts in Composite Material Systems, J. Thermoplast. Compos. Mater. 3 (1990) 13–23. doi:10.1177/089270579000300102.

[6] D. Chandramohan, K. Marimuthu, A review on Natural Fibers, Int. J. Recent Res. Appl. Stud. 8 (2011). doi:10.5923/j.textile.20120104.02.

[7] V. Fiore, T. Scalici, G. Di Bella, A. Valenza, A review on basalt fibre and its composites, Compos. Part B Eng. 74 (2015) 74–94. doi:10.1016/j.compositesb.2014.12.034.

[8] M. Lal Regar, A. Islam Amjad, Basalt Fibre–Ancient Mineral Fibre for Green and Sustainable Development, Tekstilec. 59 (2016) 321–334. doi:10.14502/Tekstilec2016.59.321-334.

[9] T. Deák, T. Czigány, Chemical Composition and Mechanical Properties of Basalt and Glass Fibers: A Comparison, Text. Res. J. 79 (2009) 645–651. doi:10.1177/0040517508095597.

[10] J. Militký, R. Mishra, H. Jamshaid, Basalt fibers, in: A.R. Bunsell (Ed.), Handb. Prop. Text. Tech. Fibres, 2nd Editio, 2018: pp. 805–840. doi:10.1016/B978-0-08-101272-7.00020-1.

[11] D. Saravanan, Spinning the rocks - Basalt fibres, J. Inst. Eng. (India), Part TX Text. Eng. Div. 86 (2006) 39–45.

[12] K. Singha, A Short Review on Basalt Fiber, Int. J. Text. Sci. 1 (2012) 19–28. doi:10.5923/j.textile.20120104.02.

[13] S. Parmar, Basalt Fiber: Newer Fiber for FRP Composites, Int. J. Emerg. Technol. Eng. Res. 4 (2016) 43–45.

[14] V. Dhand, G. Mittal, K.Y. Rhee, S.J. Park, D. Hui, A short review on basalt fiber reinforced polymer composites, Compos. Part B. 73 (2015) 166–180. doi:10.1016/j.compositesb.2014.12.011.

[15] R. Costa, R. Orriols, Man-Made Mineral Fibers and The Respiratory Tract, Arch. Bronconeumol. 48 (2012) 460–468. doi:10.1016/j.arbr.2012.04.004.

[16] K. Callebaut, J. Elsen, K. Van Balen, W. Viaene, Nineteenth century hydraulic restoration mortars in the Saint Michael's Church (Leuven, Belgium): Natural hydraulic lime or cement?, Cem. Concr. Res. 31 (2001) 397–403. doi:10.1016/S0008-8846(00)00499-3.

[17] P.-C. Aïtcin, Portland cement, in: P.-C. Aïtcin, R.J. Flatt (Eds.), Sci. Technol. Concr. Admixtures, Woodhead Publishing, 2016: pp. 27–51. doi:10.1016/B978-0-08-100693-1.00003-5.

[18] M. Michaux, E.B. Nelson, B. Vidick, Chemistry and Characterization of Portland Cement, Dev. Pet. Sci. 28 (1990) 2-1-2–17. doi:10.1016/S0376-7361(09)70300-0.

[19] P.K. Mehta, P.J.M. Monteiro, CONCRETE Microstructure, Properties, and Materials, Third Ed., McGraw-Hill, 2006. doi:10.1036/0071462899.

[20] D. Marchon, R.J. Flatt, Mechanisms of cement hydration, in: P.-C. Aïtcin, R.J. Flatt (Eds.), Sci. Technol. Concr. Admixtures, Woodhead Publishing, 2016: pp. 129–145. doi:10.1016/B978-0-08-100693-1.00008-4.

[21] C. Pade, M. Guimaraes, The CO2 uptake of concrete in a 100 year perspective, Cem. Concr. Res. 37 (2007) 1348–1356. doi:10.1016/j.cemconres.2007.06.009.

[22] F.P. Glasser, J. Marchand, E. Samson, Durability of concrete - Degradation phenomena involving detrimental chemical reactions, Cem. Concr. Res. 38 (2008) 226–246. doi:10.1016/j.cemconres.2007.09.015.

[23] V.D. Pizzol, L.M. Mendes, H. Savastano, M. Frías, F.J. Davila, M.A. Cincotto, V.M. John, G.H.D. Tonoli, Mineralogical and microstructural changes promoted by accelerated carbonation and ageing cycles of hybrid fiber-cement composites, Constr. Build. Mater. 68 (2014) 750–756. doi:10.1016/j.conbuildmat.2014.06.055.

[24] E. Standard, EN 197-1 Cement. Part 1: Composition, specifications and conformity criteria for common cements, (2011).

[25] J.P. Adam, L'arte di costruire presso i Romani, materiali e tecniche, 9 Ed., Longanesi, Milano, 2008.

[26] J. Lanas, J.L. Perez Bernal, M.A. Bello, J.I. Alvarez Galindo, Mechanical properties of natural hydraulic lime-based mortars, Cem. Concr. Res. 34 (2004) 2191–2201. doi:10.1016/j.cemconres.2004.02.005.

[27] A. Battaglia, A. Rattazzi, V. Kafetsi, Terra, Fuoco, Acqua, Aria: LA CALCE, ERMES, 2011.

[28] C. Figueiredo, R.J. Ball, M. Lawrence, Is BS EN 459-1:2015 fit for purpose in the context of conservation?, J. Build. Limes Forum. 23 (2016) 46–52. doi:10.2966/scrip.

[29] E. Standard, EN 459-1 Building lime. Part 1: Definitions, specifications and

conformity criteria, (2011).

[30] A. Rattazzi, Conosci il grassello di calce? Origine, produzione e impiego del grassello di calce in architettura, nell'arte e nel restauro, Edicom Edizioni, 2007.

[31] M. Lenart, Assessment of mortar shrinkage in aspect of organic and inorganic modifiers use, Procedia Eng. 108 (2015) 309–315. doi:10.1016/j.proeng.2015.06.152.

[32] C.J. Larosche, Types and causes of cracking in concrete structures, in: Fail. Distress Repair Concr. Struct., Woodhead Publishing Limited, 2009: pp. 57–83. doi:10.1533/9781845697037.1.57.

[33] T. Aly, J.G. Sanjayan, F. Collins, Effect of polypropylene fibers on shrinkage and cracking of concretes, Mater. Struct. 41 (2008) 1741–1753. doi:10.1617/s11527-008-9361-2.

[34] D.P. Bentz, O.M. Jensen, Mitigation strategies for autogenous shrinkage cracking, Cem. Concr. Compos. 26 (2004) 677–685. doi:10.1016/S0958-9465(03)00045-3.

[35] T.R. Naik, R.N. Kraus, Y. Chun, A. Science, Effect of Different Types of Aggregates on Autogenous and Drying Shrinkage of Concrete, 1st Int. Conf. Adv. Constr. Mater. (n.d.) 147–160.

[36] S.J. Park, J.S. Jin, J.R. Lee, Influence of silane coupling agents on the surface energetics of glass fibers and mechanical interfacial properties of glass fiber-reinforced composites, J. Adhes. Sci. Technol. 14 (2000) 1677–1689. doi:10.1163/156856100742483.

[37] Y. Xie, C.A.S. Hill, Z. Xiao, H. Militz, C. Mai, Silane coupling agents used for natural fiber/polymer composites: A review, Compos. Part A Appl. Sci. Manuf. 41 (2010) 806–819. doi:10.1016/j.compositesa.2010.03.005.

[38] D. Olmos, J. Gonzalez-Benito, Composites formed by glass fibers and PS-modified epoxy matrix. Influence of the glass fibers surface on the morphologies and mechanical properties of the interphases generated, Polym. Compos. 31 (2010) 946–955. doi:10.1002/pc.20879.

[39] J.G. Iglesias, J. González-Benito, A.J. Aznar, J. Bravo, J. Baselga, Effect of Glass Fiber Surface Treatments on Mechanical Strength of Epoxy Based Composite Materials, J. Colloid Interface Sci. 250 (2002) 251–260. doi:10.1006.

[40] R. Balart, J.M. España, M.D. Samper, E. Fages, L. Sanchez-Nacher, Investigation of the Effect of Different Silane Coupling Agents on Mechanical Performance of Basalt Fiber Composite Laminates with Biobased Epoxy Matrices J.M., Polym. Compos. 34 (2013) 376–381. doi:10.1002/pc.

[41] J. González-Benito, J.C. Cabanelas, A.J. Aznar, M.R. Vigil, J. Bravo, J. Baselga, Surface characterization of silanized glass fibers by labeling with environmental sensitive fluorophores, Appl. Polym. Sci. 62 (1996) 375–384.

[42] A.T. DiBenedetto, Evaluation of fiber surface treatments in composite materials,

Pure Appl. Chem. 57 (1985) 1659–1665. doi:10.1351/pac198557111659.

[43] B. Wei, S. Song, H. Cao, Strengthening of basalt fibers with nano-SiO2-epoxy composite coating, Mater. Des. 32 (2011) 4180–4186. doi:10.1016/j.matdes.2011.04.041.

[44] B. Wei, H. Cao, S. Song, Surface modification and characterization of basalt fibers with hybrid sizings, Compos. Part A Appl. Sci. Manuf. 42 (2011) 22–29. doi:10.1016/j.compositesa.2010.09.010.

[45] M. Abdelmouleh, S. Boufi, M.N. Belgacem, A. Dufresne, Short natural-fibre reinforced polyethylene and natural rubber composites: Effect of silane coupling agents and fibres loading, Compos. Sci. Technol. 67 (2007) 1627–1639. doi:10.1016/j.compscitech.2006.07.003.

[46] S. Shokoohi, A. Arefazar, R. Khosrokhavar, Silane coupling agents in polymer-based reinforced composites: A review, J. Reinf. Plast. Compos. 27 (2008) 473–485. doi:10.1177/0731684407081391.

[47] N. Suzuki, H. Ishida, A Review on the Structure and Characterization Techniques of Silane/Matrix Interphases, Macromol. Symp. 108 (1996) 19–53. doi:https://doi.org/10.1002/masy.19961080105.

[48] N.R. Paluvai, S. Mohanty, S.K. Nayak, Mechanical and thermal properties of sisal fiber reinforced acrylated epoxidized castor oil toughened diglycidyl ether of bisphenol A epoxy nanocomposites, J. Reinf. Plast. Compos. 93 (2015) 2107–2116. doi:10.1177/0731684415595126.

[49] E. Metwalli, D. Haines, O. Becker, S. Conzone, C.G. Pantano, Surface characterizations of mono-, di-, and tri-aminosilane treated glass substrates, J. Colloid Interface Sci. 298 (2006) 825–831. doi:10.1016/j.jcis.2006.03.045.

[50] J.-K. Kim, Y.-W. Mai, Surface treatments of fibers and effects on composite properties, in: Eng. Interfaces Fiber Reinf. Compos., Ltd, Elsev, 1998: pp. 171–237. doi:http://dx.doi.org/10.1016/B978-008042695-2/50006-3.

[51] M.C. Brochier Salon, M.N. Belgacem, Competition between hydrolysis and condensation reactions of trialkoxysilanes, as a function of the amount of water and the nature of the organic group, Colloids Surfaces A Physicochem. Eng. Asp. 366 (2010) 147–154. doi:10.1016/j.colsurfa.2010.06.002.

CHAPTER 3

EXPERIMENTAL PART

CHAPTER 3
EXPERIMENTAL PART

In this Chapter a description of the most relevant characteristics of the materials employed in this work is done. Moreover, the preliminary characterization of the raw materials used will be shown. Besides, a brief description of the instrumental techniques and methods used to carry out the experiments proposed in this PhD thesis is also presented. In order to avoid repeating information and improve the manuscript clarity, description of samples preparation will be carried out in the corresponding Chapters 4, 5, 6 and 7.

3.1. Materials

3.1.1. Basalt Fibers

In this work, basalt fibers were chosen as potential reinforcing agent to be modified with different surface treatments and, after that, to be used in cement-based materials. As-received chopped basalt fibers with a commercial sizing compatible with cement matrices were used (Figure 1).

Figure 1. Chopped Basalt Fibers.

The main properties provided by the supplier are summarized in Table 1.

Table 1. Properties of Basalt Fibers.

CHOPPED BASALT FIBERS	
Filament diameter	17 µm
Length	6.4 mm
Specific weight (without sizing)	2.67 g/cm^3
Type of sizing	Silane
Sizing content	0.4-0.8 wt%

Scanning Electron Microscopy, *SEM*, with energy dispersive X-ray microanalysis, *EDX*, (see section 3.2.1) was used to obtain morphological and compositional information about the commercial basalt fibers.

A field emission scanning electron Microscopy (FE-SEM), Zeiss AURIGA SEM was used. The fibers were sputter coated with chrome prior to examination. As an example, a SEM image of the as-received basalt fibers is shown in the Figure 2. Some heterogeneities (indicate by the arrows) due to the presence of commercial sizing are observed.

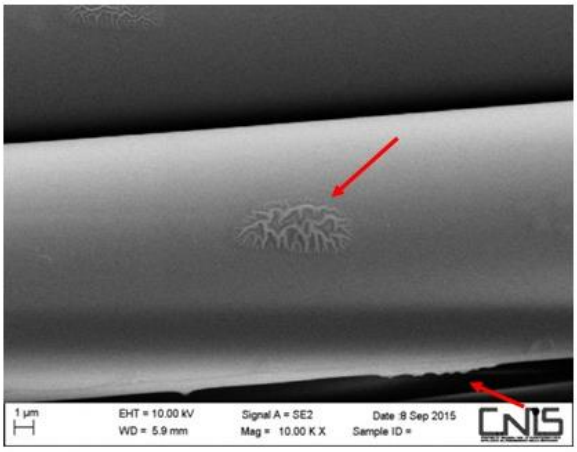

Figure 2. SEM images of the as-received basalt fiber.

Energy dispersive X-ray spectroscopy, *EDX*, allow identifying the elements expected taking into account the typical composition of a common basalt fiber (SiO_2, Al_2O_3, CaO, MgO, K_2O, Na_2O, Fe_2O_3) shown in section 2.1.1 of Chapter 2. Moreover, Carbon (*C*) and Nitrogen (*N*) elements are also revealed. Their presence could be ascribed to the sizing applied on the fiber surface during the production process.

Table 2. Data obtained from EDX elemental analysis of as-received basalt fiber.

Element	**O**	**Si**	**C**	**Al**	**Ca**	**Mg**	**Fe**	**Na**	**K**	**N**
wt%	52.30	21.61	7.78	6.11	4.06	1.51	3.28	1.04	1.06	1.25

A more detailed characterization of the as-received basalt fibers will be shown in the Chapter 4 were a comparison with pretreated and amino-silane modified fibers is also considered.

3.1.2. Silane Coupling Agents

The surface modification of as-received basalt fibers was carried out using silane coupling agents, commonly used as surface modifying agents of fibers [1–9]. In order to obtain different molecular structure at the fiber-matrix interface three aminosilanes aqueous solutions were prepared using two different aminosilanes:

a) *γ-aminopropiltriethoxysilane* (APTES)

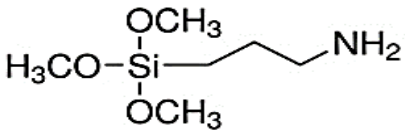

Molecular Weight	221.37 g·mol^{-1}
Density	0.946 g/ml

Figure 3. APTES chemical structure and their properties.

b) γ-aminopropilmethyldiethoxysilane (APDES)

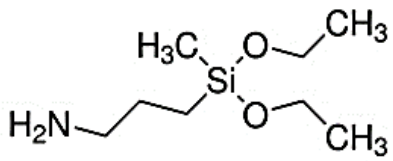

Molecular Weight	191.34 g·mol^{-1}
Density	0.916 g/ml

Figure 4. APDES chemical structure and their properties.

c) Mixture 50% by weight of the two silanes (APTES + APDES).

3.1.3. Fluorescent Label

To study the hydrolytic degradation of the polyorganosiloxane coatings of the basalt fibers, the fluorescence arising from fluorescent labels was used. In particular, steady state fluorescence spectroscopy was performed to characterize the silane modified fibers and to monitor fluorescent intensity of the aqueous solution causing hydrolytic degradation.

The silanized fibers were chemically labelled with a fluorescent molecule. The latter contains a group or fluorophore that can absorb electromagnetic radiation at specific wavelength and subsequently emit electromagnetic radiation at a higher wavelength (fluorescence). The fluorophore is chemically attached to the functional groups (amino groups) of the coating to be studied, providing very sensitive way of detecting its presence. Among others, fluorescein and its derivatives represent one of the most employed fluorescent labeling agents [10]. Fluorescein isothiocyanate (FITC) was selected for this study. The high molar absorptivity at the wavelength of the argon laser (488 nm), the large fluorescence quantum yield and high photostability of the fluorescein dyes points it as a good choice, expecting it to be a very sensitive fluorescent label [11]. The chemical structure and their properties are shown in Figure 5.

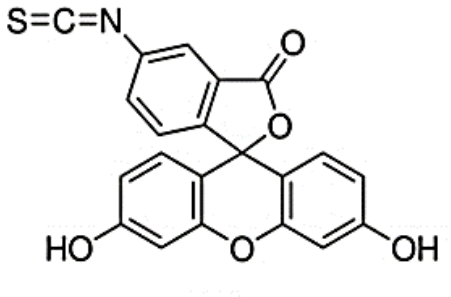

Molecular Formula	$C_{21}H_{11}NO_5S$
Molecular Weight	389.4 $g \cdot mol^{-1}$
Excitation	λ_{max} = 495 nm
Emission	[1]λ_{max} = 525 nm

Figure 5. FITC chemical structure and properties.

The isothiocyanate group (–N=C=S) of the FITC easily reacts with the amino group (–NH_2) of the silane coupling agents to form a thiourea bond (Figure 6) [10,12]. Therefore,

[1] At ph= 9 λmax = 520 nm

the FITC can be covalently attached to the silane coating through a stable thiourea bond [13].

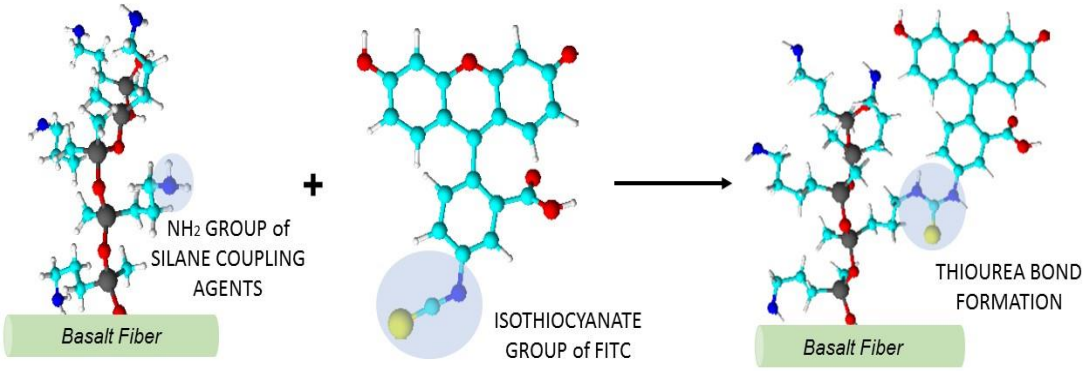

Figure 6. Aminosilanes coupling agents and their expected reaction with fluorescein isothiocyanate.

Here it is important to highlight, for future interpretations and discussions, that fluorescein in aqueous solution may appear in its cationic, neutral, and dianonic forms what makes its absorption and fluorescence properties strongly dependent on the pH [11]. For this reason, the experiments of hydrolytic degradation in this work were carried out at controlled pH using buffer solutions.

3.1.4. Cement Matrices

Mortars samples were prepared using two different hydraulic binders as matrix:

a) Portland Cement

A common Portland cement was chosen as a matrix to study the interaction with the basalt fibers. In particular, Portland cement type PII/A-L 42.5 R according European Standard EN 197-1 was chosen as binder to prepare cement-based mortars [14]. This is a common cement largely used in the building industry for several applications. The specifications of the cement employed, provided by the supplier, are summarized in Table 3.

Table 3. Properties of commercial PII/A-L 42.5 R cement.

		Standard Specification	***Usual***
Composition	Clinker	88 %	80-94 %
	Limestone (L)	12 %	6-20 %
	Calcium Sulfate	--	5 %
Chemical Properties	Sulfates (SO_3)	3.3 %	< 4.0 %
	Chlorides	0.02 %	< 0.10 %
Mechanical Properties	Compressive Strength at 7 days	--	43 MPa
	Compressive Strength at 28 days	42.5-62.5 MPa	55 MPa

Compositional and structural information of the commercial Portland cement used were obtained by Thermogravimetric Analysis, *TGA*, and X-Ray Diffraction, *XRD* (see section 3.2.1).

TGA analysis was performed using a Mettler Toledo TGA/SDTA 851e analyzer equipped with a TSO800GC1 flow gas controller and a TSO801RO universal samples robot. The analysis was carried out using a platinum crucible at 10 °C/min heating rate under inert atmosphere from 30°C to 1000°C.

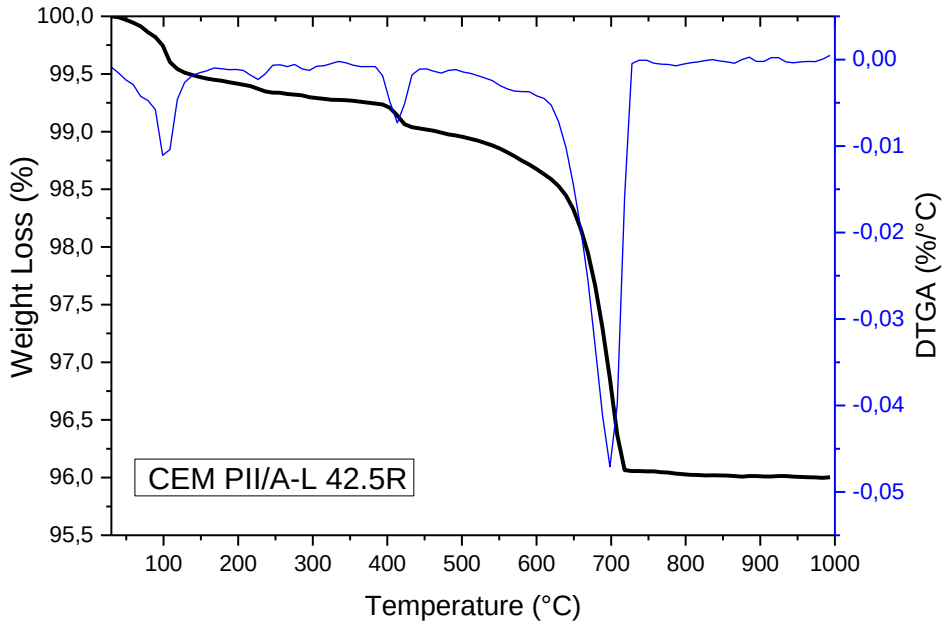

Figure 7. TGA and its derivative, DTGA, for PII/A-L 42.5 R Portland cement.

Figure 7 shows the presence of three endothermic processes: i) the first one at about 100 °C is ascribed to the calcium sulfate ($CaSO_4 \cdot 2H_2O$) dehydration; ii) the second one corresponds to a weight loss around 400 °C which is usually associated to the calcium hydroxide ($Ca(OH)_2$) dehydration and iii) third one, at about 700 °C corresponds to the weight loss due to the $CaCO_3$ decarbonation. From the weight loss data and considering the corresponding molar weight for each compound, the associated weight percentages of $CaSO_4 \cdot 2H_2O$, $Ca(OH)_2$ and $CaCO_3$ were calculated. The results are given in the Table 4.

Table 4. TGA results of PII/A-L 42.5 R cement.

Temperature (°C)	*Weight Loss (%)*	*$CaSO_4 \cdot 2H_2O$ (%)*	*$Ca(OH)_2$ (%)*	*$CaCO_3$ (%)*
~ 100	0.5	2.4	-	-
~ 400	0.3	-	1.2	-
~ 700	3	-	-	7

X-Ray powder diffraction, XRD, was performed using a Philips X'Pert-MPD diffractometer, with Cu-k_α radiation, step size of 0.020°, time per step of 2s from 5° to 80°. XRD difractogram (Figure 8) revealed the main crystalline phases typical of a Portland cement: dicalcium silicate, *C_2S*, tricalcium silicate, *C_3S*, tricalcium aluminate, *C_3A*, tricalcium aluminate, *C_4AF*, tetracalcium aluminoferrite and gypsum phases are also detected [15–17]. It is observed that the most abundant phase is C_3S.

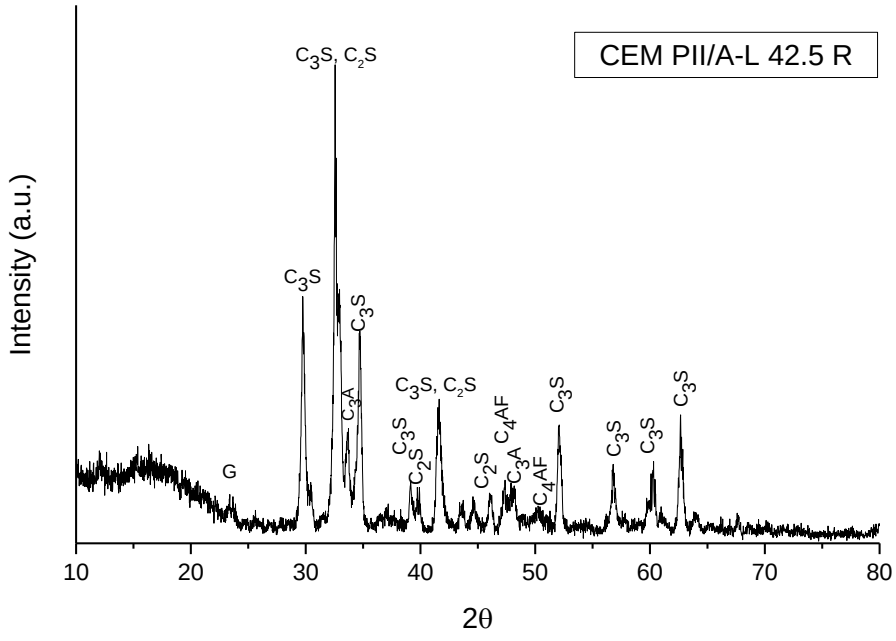

Figure 8. XRD pattern of PII/A-L 42.5 R Portland cement. *G* = Gypsum, *C_3S* = tricalcium silicate, *C_2S* = dicalcium silicate, *C_3A* = tricalcium aluminate, *C_4AF* = tetracalcium aluminoferrite.

b) Natural Hydraulic Lime

A Natural Hydraulic Lime, NHL 5 according the European Standard EN 459-1, was chosen as the binder to realize lime-based mortars [18]. In Table 5 the main properties of NHL 5 according EN 459-1 provided by the supplier are shown.

Table 5. Properties of Natural Hydraulic Lime, NHL 5.

		Natural Hydraulic Lime, NHL 5
Physical-Chemical Properties	Sulfates (SO_3)	≤ 2%
	$Ca(OH)_2$	≥ 15 %
	H_2O	≤ 2%
Mechanical Properties	Compressive Strength at 7 days	≥ 2 MPa
	Compressive Strength at 28 days	5-15 MPa

Commercial natural hydraulic lime was characterized by TGA and XRD analysis as was done for the commercial cement.

From TGA and DTGA curves (Figure 9) the $Ca(OH)_2$ dehydration and $CaCO_3$ decarbonation respectively at temperatures around 400 °C and 700 °C can be clearly seen. As in for the case of cement, the corresponding weight percentage for each component was calculated. The results are shown in Table 6.

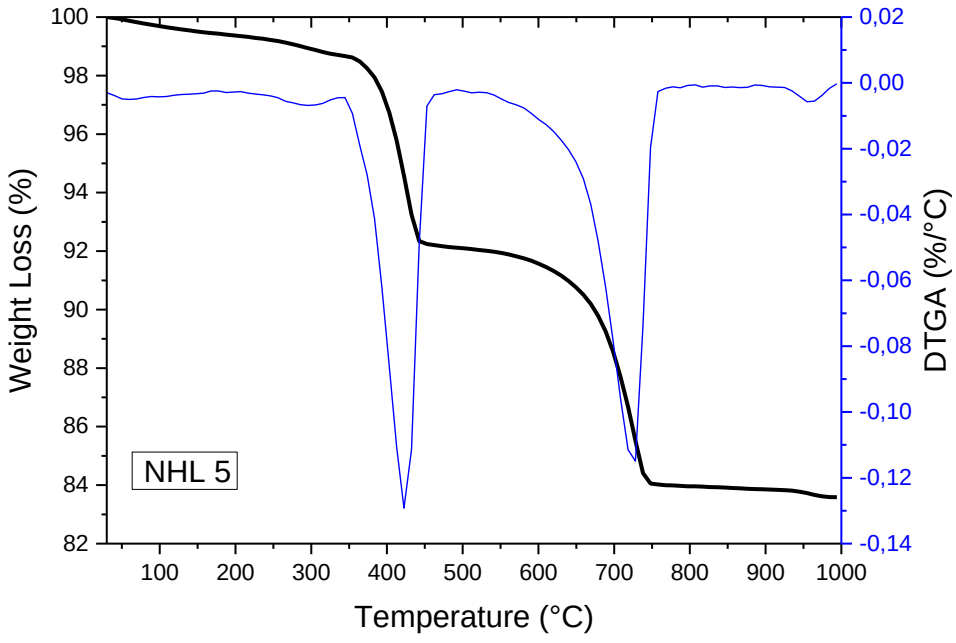

Figure 9. TGA and its derivative, DTGA, for Natural Hydraulic Lime, *NHL 5*.

Table 6. TGA results of Natural Hydraulic Lime, *NHL 5*.

Temperature (°C)	*Weight Loss (%)*	*$Ca(OH)_2$ (%)*	*$CaCO_3$ (%)*
~ 400	6.6	27.1	-
~ 700	8.1	-	18.6

In the XRD pattern of NHL 5 (Figure 10), as expected, the dominant phases observed are: dicalcium silicate, C_2S, calcite and portlandite [19,20].

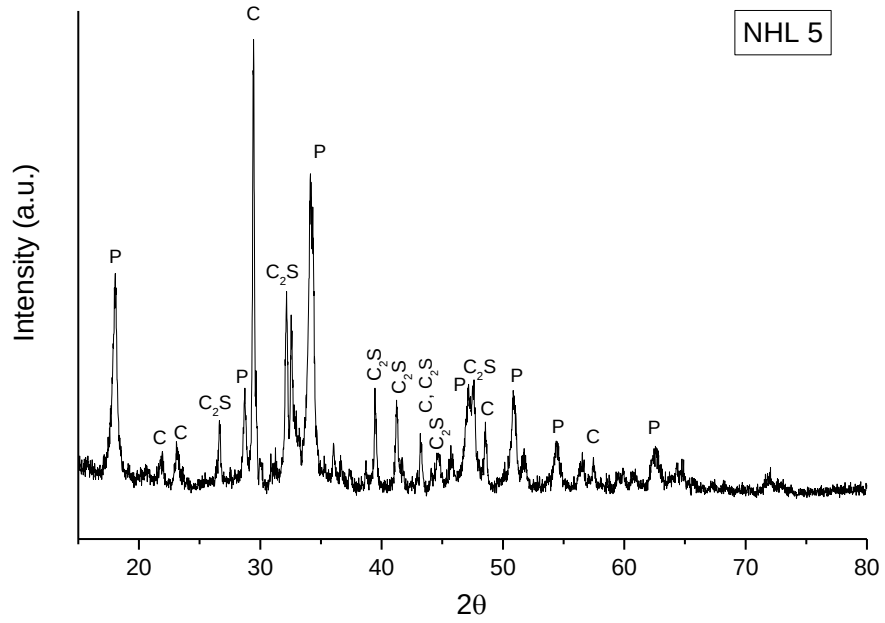

Figure 10. XRD pattern for natural hydraulic lime, *NHL 5*. *C* = Calcite, C_2S = dicalcium silicate, *P* = portlandite.

3.1.5. Aggregate

To prepare cement and natural hydraulic based mortars, a commercial sand was used as aggregate. In detail, a siliceous sand with a grain size between 0.2-0.5 mm was chosen. The corresponding granulometric curve and the physico-chemical properties provided by the supplier are given in Figure 11 and Table 7 respectively.

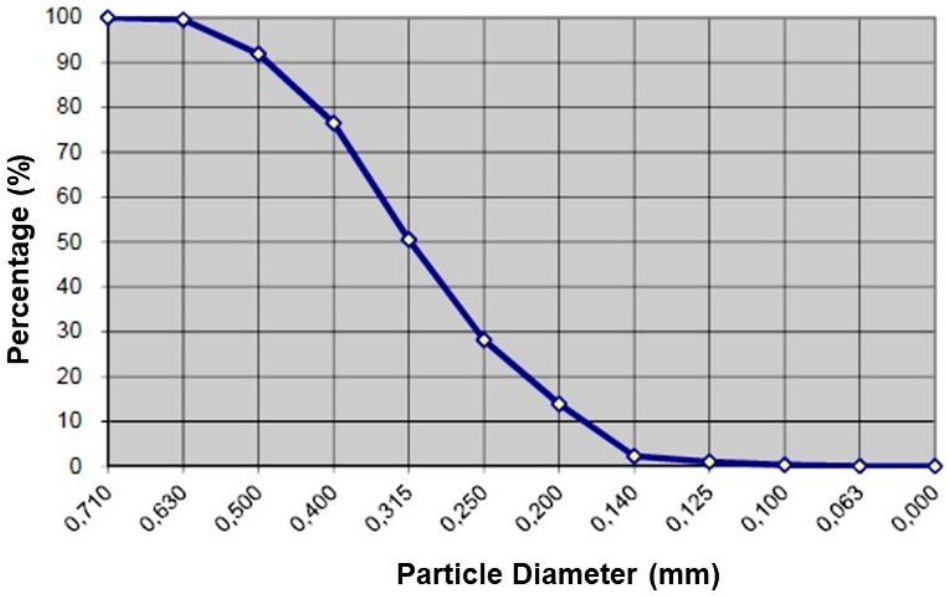

Figure 11. Granulometric curve for siliceous sand.

Table 7. Physical-chemical properties of the siliceous sand.

Siliceous Sand	
SiO_2 ***> 98.0 %***	MgO < 0.05 %
Al_2O_3 < 0.80 %	Na_2O < 0.06 %
Fe_2O_3 < 0.05 %	K_2O < 0.40 %
CaO < 0.10 %	TiO_2 < 0.02 %
Hardness: 7 Mohs	
Apparent Density: 1.4-1.7 Kg/m^3	

The aggregate was also characterized by XRD diffraction. The analysis was performed in the same conditions used for cement and natural hydraulic lime.

Figure 12 shows the XRD pattern of the aggregate were the dominant phase is quartz. The analysis confirms the siliceous character of the aggregate in accordance to the data provided by the supplier.

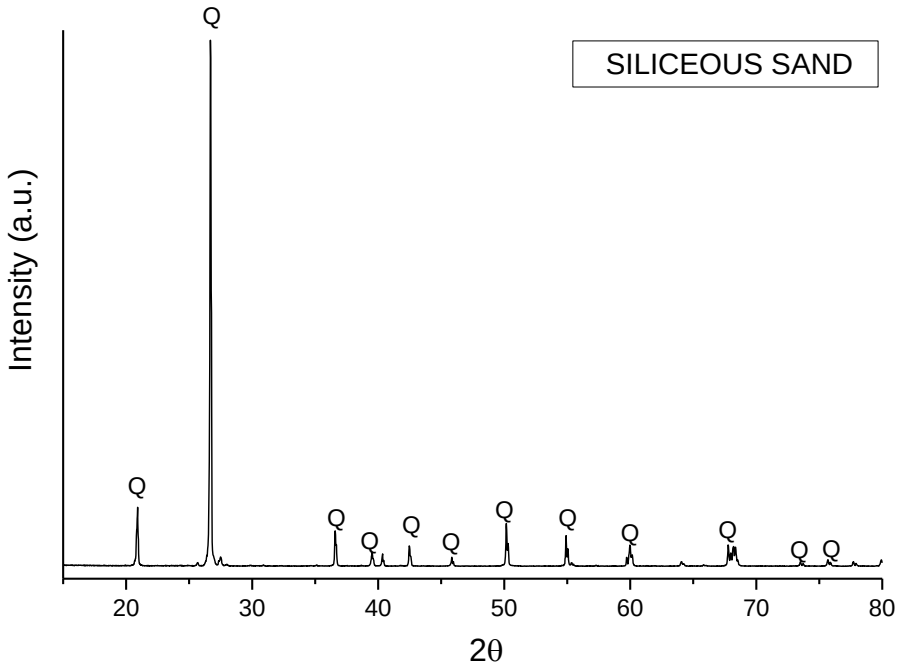

Figure 12. XRD pattern for siliceous sand.

3.1.6. Materials for molds preparation

A commercial silicon was employed to prepare the molds to cast the mortar samples. Generally, European Standards recommend using steel molds of size 16 x 4 x 4 cm to cast the mortars before mechanical test. For this project of thesis, silicone molds of size 8 x 2 x 2 cm, smaller than those suggested by the standard because of the difficulty of obtaining large amounts of modified fibers, were prepared. Figure 13 shows the steps for molds preparation.

An aluminum mold of size 8 x 2 x 2 cm (Figure13 a) was previously designed, put in a box and filled up with the silicon (Figure13 b). Finally, the silicone mold is obtained (Figure 13 c).

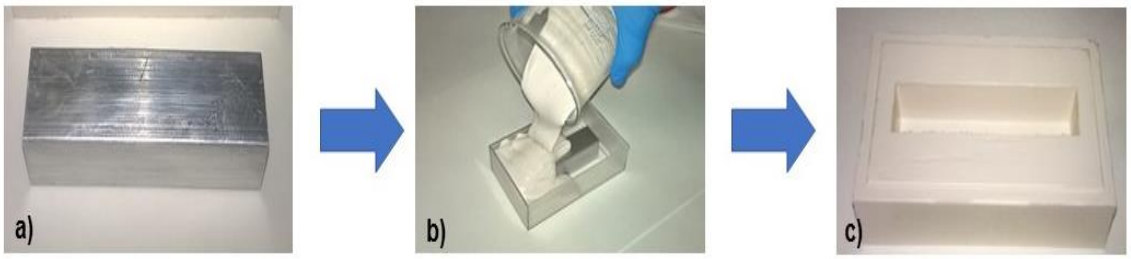

Figure 13. Silicone molds preparation.

3.2. Instrumental Techniques and Methods

In this section a brief description of the instrumental techniques and methods used in this thesis will be done. When necessary, an extended version of the description of a particular technique or method will be given in the corresponding Chapters 4, 5, 6 and 7.

3.2.1. Characterization of the As-received and Modified Basalt Fibers Surfaces

Structure, composition and morphology of the as-received and modified basalt fibers were studied using the instrumental techniques showed below.

X-Ray diffraction (XRD)

Structural characteristics of the as-received, calcinated and activated basalt fibers were studied by X-Ray Diffraction (XRD) to evaluate possible changes induced by surface pre-treatments of fiber surface (calcination and the activation processes) respect to the structure of the commercial basalt fibers.

XRD is a powerful technique used for the identification of crystalline phases of the materials. X-ray diffraction peaks arise from constructive interferences of a monochromatic beam of X-rays scattered at specific angles from the lattice planes characterizing the sample investigated. The result is a diffractogram that shows the X-ray diffracted intensity as a function of the radiation/sample incidence angle or directly the distance between the planes of the crystal structure of the sample. This distance is characteristic of each crystalline phase present in the sample [21].

Fourier transformed infrared spectroscopy (FT-IR)

FT-IR spectroscopy is a widespread and powerful tool for the identification and characterization of a different range of materials allowing qualitative and the quantitative analysis of them. It is a vibrational spectroscopy that allows the identification of the functional groups that characterize organic and inorganic compounds. When IR radiation beam is sent through a sample, the beam passes through it and the sample absorbs radiation as a function of the wavelength. The absorption of the light at different wavenumbers corresponds to stimulation of the vibrational energy levels of a molecule or a group of

atoms covalently bonded. A FT-IR spectrum consists of absorption bands characteristics of the examined substance that appear at specific frequencies or wavenumbers [22,23].

In this work, FTIR analysis of as-received and modified basalt fibers were performed in transmission mode. To do this the fibers were grounded and mix with KBr to prepare easy to handle discs necessary to perform the analysis. This method of analysis was very useful to obtain information about the initial structure of the as-received basalt fibers and to evaluate structural variations of them in the modified fiber surfaces. Moreover, it allowed estimating the amount of polyorganosiloxanes grafted on the fiber surfaces.
Besides, FT-IR analysis was always used to check the surface treatments given on the fiber surfaces before dispersing them in the cement matrices.

Thermogravimetric analysis (TGA)

In thermogravimetric analysis the mass of a sample under a controlled atmosphere is continuously recorded as a function of temperature or time while the sample is heated usually with constant ramp of temperatures. A diagram that shows the mass or the mass percentage as a function of temperature or time, known as thermogram or thermal decomposition curve, is obtained. The thermogram usually allows evaluating the thermal stability, the thermodegradation rate, the kind of reaction associated to the mass loss and the sample composition [24]. TGA analysis was performed on the as-received and modified basalt fibers to ensure the removal of the organic matter applied during the manufacturing process and the grafting of the silane coupling agents.

Scanning electron microscopy (SEM-EDS)

Morphological studies of the as-received and treated basalt fibers were carried out by scanning electron microscopy (SEM). This technique uses a focused beam of electrons that interact with the sample studied, producing various signals that can be used to obtain information about the surface topography/morphology and composition of the sample. Among all the signals that could be obtained, backscattered electrons (BSE) were chosen to obtain the SEM images of this work. Backscattered electrons provide topographic and compositional information. In fact, they allow to obtain general information on the differences in the average atomic number of the phases present in the sample under examination. The higher the atomic number of the observed phase, the greater the emission

of BSE electrons will be and therefore the brighter the phase will appear in the corresponding image. Moreover, characteristic X-rays produced by the interaction of electrons with the sample may also be detected in an SEM equipped with an energy dispersive X-ray detector (EDX). Through them it is possible to identify and even quantify elemental composition of sample [25].

Atomic force microscopy (AFM)

Atomic force microscopy (AFM), which is one of the so-called scanning probe microscopy techniques (SPM), is a technique widely used in the field of materials science. This technique allows a characterization of materials in terms of topography/morphology at micro- and nanoscale.

Using atomic force microscopy (AFM), a tip attached to a flexible cantilever is moved across the sample surface to scan the surface to obtain topographical and morphological information at nanoscale. The forces between the tip and the sample are measured during scanning by monitoring the deflection of the cantilever. Three operating mode are known: i) non-contact mode, ii) contact mode and iii) tapping mode. The latter is the operating mode used in this work to study the basalt fibers surfaces. In tapping mode, the cantilever is oscillated at or near its resonant frequency. It allows to obtain high resolution topographic images of surface samples avoiding problems arising from friction, adhesion, electrostatic forces and other difficulties [26,27]. The analysis was performed on single basalt fibers as it is shown in the Figure 14.

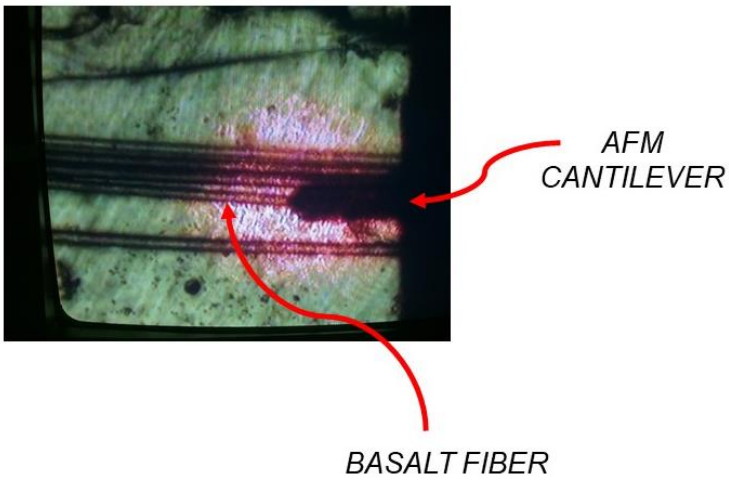

Figure 14. AFM cantilever with tip scanning single basal fiber.

3.2.2. Hydrolytic Degradation Study of Surface Coatings

The hydrolytic degradation of the silane coatings was monitored by pH measurements and steady state fluorescence spectroscopy.

pH measurements

To follow the processes occurring during the immersion of the silanized basalt fibers in pure water, the pH of the aqueous solution was measured as a function of the immersion time. In order to do this, silanized basalt fibers were introduced in a cellulose paper bag hanged by the use of a nylon thread and immersed in a beaker with distilled and deionized water. The aqueous solution was continuously stirred. In Figure 15 a representation of the experiment set-up is shown.

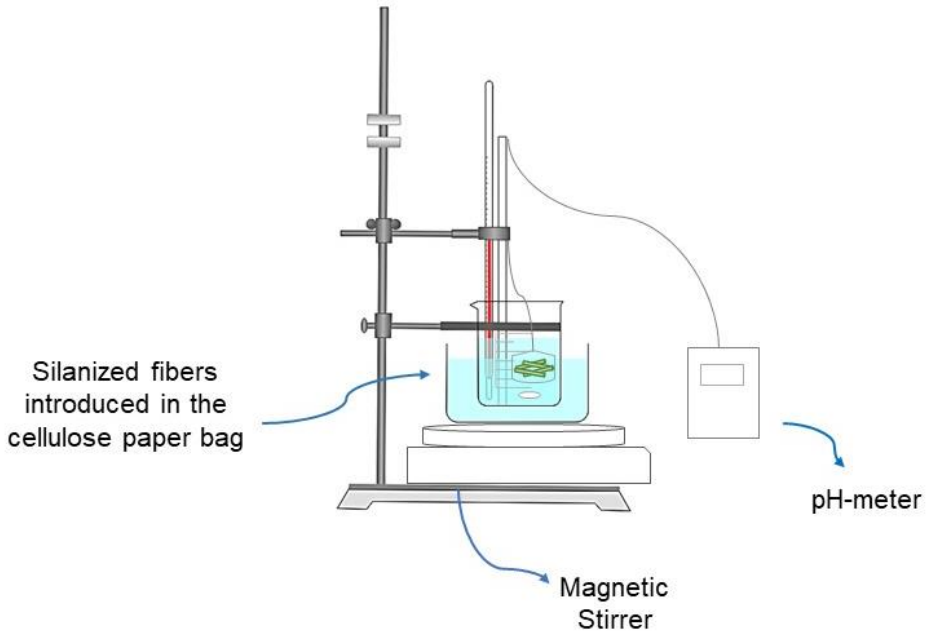

Figure 15. Scheme of set-up based on pH measurements used to monitor hydrolysis degradation of the silanized basalt fibers.

Fluorescence Spectroscopy

Fluorescence spectroscopy is a technique of analysis where a beam of light excites the electrons of the molecules of certain compounds at a certain wavelength and causes them to emit radiation of longer wavelengths. Fluorescence measurements can be classified into two types of measurements: steady-state and time-resolved. The first one, used in this

work, is the most common type and is performed with constant illumination and emission detection. The sample is illuminated with a continuous beam of light at a certain excitation wavelength, and the intensity of light emitted is recorded as a function of the wavenumber. The result is a fluorescence spectrum generally presented as emission spectrum that is a representation of the fluorescence intensity versus the wavelength (nanometers) or the wavenumber (cm^{-1}) measured at a constant excitation wavelength. On the other hand, excitation spectra can be also recorded; in this case the emission intensity is registered as a function of the excitation wavelength [28].

In order to monitor the hydrolytic degradation of the polyorganosiloxane coatings, a thermostated cell holder was used, where a quartz cuvette with the buffer solution is placed. The FITC labeled fibers were introduced in a very small cellulose paper bag, hanged using a nylon thread and immersed in the aqueous solution continuously stirred with a magnetic bar. As the hydrolytic degradation is occurring, fragments of the labelled coating are released in the aqueous solution leading to fluorescence which is recorded as a function of time. In Figure 16 a scheme of the hydrolytic degradation experiment using fluorescence spectroscopy is shown.

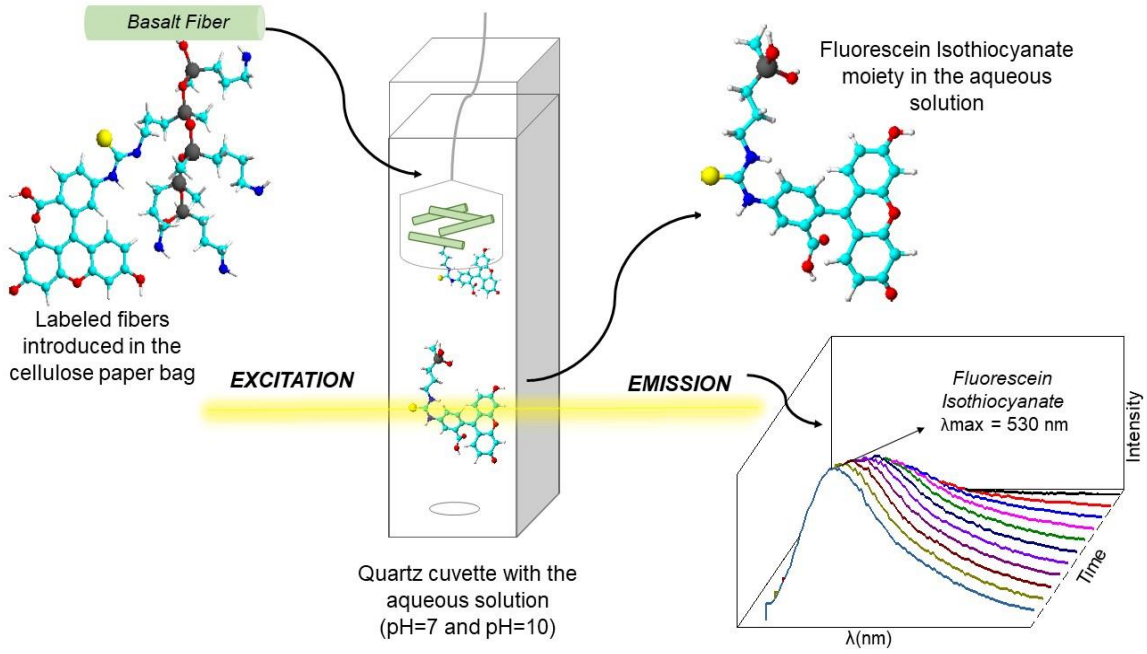

Figure 16. Scheme of the hydrolytic degradation experiment using fluorescence spectroscopy.

3.2.3. Characterization of Composite Materials

Mechanical Tests

As it is known, the stress-strain behavior of brittle materials (such as ceramic materials) is usually evaluated using three-point flexural test and compressive strength test [29,30].

In this study, these two tests were used to obtain information about the mechanical properties of the composite materials prepared. Due to the great heterogeneity characterizing ceramics materials, six specimens for each group of samples prepared were tested. Tests were performed on cement and natural hydraulic-based mortars without basalt fibers to evaluate possible change due to the contribution of the addition of the fibers. Moreover, specimens containing as-received and modified basalt fiber were tested to study the different mechanical behavior due to the different surface treatments.

a) Three-point flexural test

The three-point flexural test was conducted to test neat and fiber-reinforced mortars as shown in Figure 17. During these tests, a force is applied perpendicular to the longitudinal axis of the sample. The top surface of the specimen is placed in a state of compression, while the bottom surface is in tension. Stress is obtained from the load applied, the specimen thickness, the bending moment, and the moment of inertia of the cross-section. The maximum tensile stress exists at the bottom specimen surface directly below the point of load application. The stress at fracture using this test is known as flexural strength and it represent an important mechanical parameter in this type of materials.

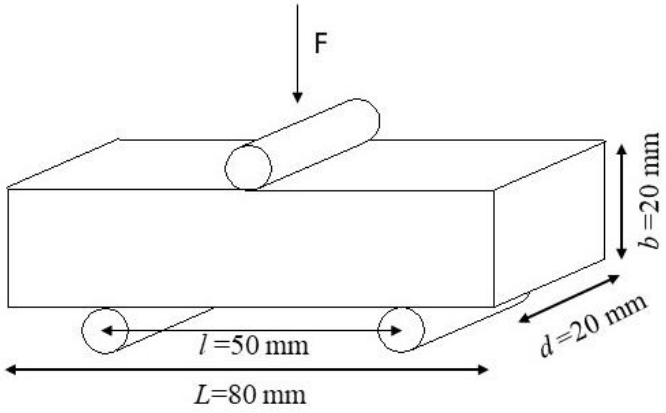

Figure 17. Three-point flexural strength test.

The flexural strength is obtained from the equation (1) (when a rectangular cross section is used) while the strain is obtained by the use of equation (2):

$$\textit{Flexural Strength} \qquad \sigma_f = \frac{3}{2}\frac{Fl}{bd^2} \tag{1}$$

where F is the maximum load applied (N), l is the support span (mm), b is the width of test beam (mm) and d is the depth or thickness of tested beam (mm).

$$\textit{Flexural Strain} \qquad \varepsilon = \frac{6\,\Delta l\,d}{l^2} \cdot 100 \tag{2}$$

where Δl is the displacement (mm), d is the depth or thickness of tested beam (mm) and l is the support span (mm).

Flexural Modulus, E, was also estimated according equation (3):

$$\textit{Flexural Modulus} \qquad E = \frac{1}{4}\frac{l^3\,s}{b\,d^3} \tag{3}$$

where l is the support span (mm), b is the width of test beam (mm), d is the depth or thickness of tested beam (mm) and s is the slope of the initial straight-line portion of the load (N) – deflection (mm) curve [30–33].

b) Compressive Strength test

It is known that an important property of ceramic materials is their capacity to resist compressive stresses. Therefore, cubic portions arising from three-point flexural test were prepared and compressive strength tests were carried out. During the tests, a cube is placed between the platens of the testing machine and it is compressed between them by a gradually applied load. The maximum amount of compressive load a material can bear before fracturing is revealed.

Below the equations used to calculate compressive strength (4) and strain (5) are given:

$$\textit{Compressive Strength} \qquad \sigma_c = \frac{F}{A} \tag{4}$$

where F is the maximum load applied (N) and A is the specimen area (mm).

$$\textit{Compressive Strain} \quad \varepsilon = \frac{\Delta l}{l_0} \cdot 100 \tag{5}$$

where Δl is the displacement (mm) and l_0 is the initial specimen length (mm) [30,32].

BET-BJH textural analysis

In order to evaluate the textural properties of the composite materials prepared with cement matrix and basalt fibers with different surface treatments, BET-BJH analysis of data obtained from N_2 adsorption/desorption measurements was carried out. This technique is based on the physisorption of a gaseous adsorbate (in this case nitrogen) on solid adsorbent (the mortar sample) [34,35].

The adsorption/desorption isotherms given by the analysis are plotted in a graph where the y-axis represents the adsorbed volume given in cubic centimeters of nitrogen (at STP conditions) per gram of adsorbent and the x-axis the relative pressure p/p^o, where p is the measured equilibrium pressure, and p^o is the vapor pressure of nitrogen at the temperature of the measurement.

When the obtained desorption and adsorption curves do not coincide with each other, different hysteresis loops are generated. Besides, the hysteresis loop varies from one system to another and at each one corresponds a typical pore structure. It is influenced by many factors such as amount, geometry and size distribution of pores.

According the International Union of Pure and Applied Chemistry, IUPAC, classification, the main gas physisorption isotherms can be grouped in six types and the hysteresis loops in four types (Figure 18) [36–38].

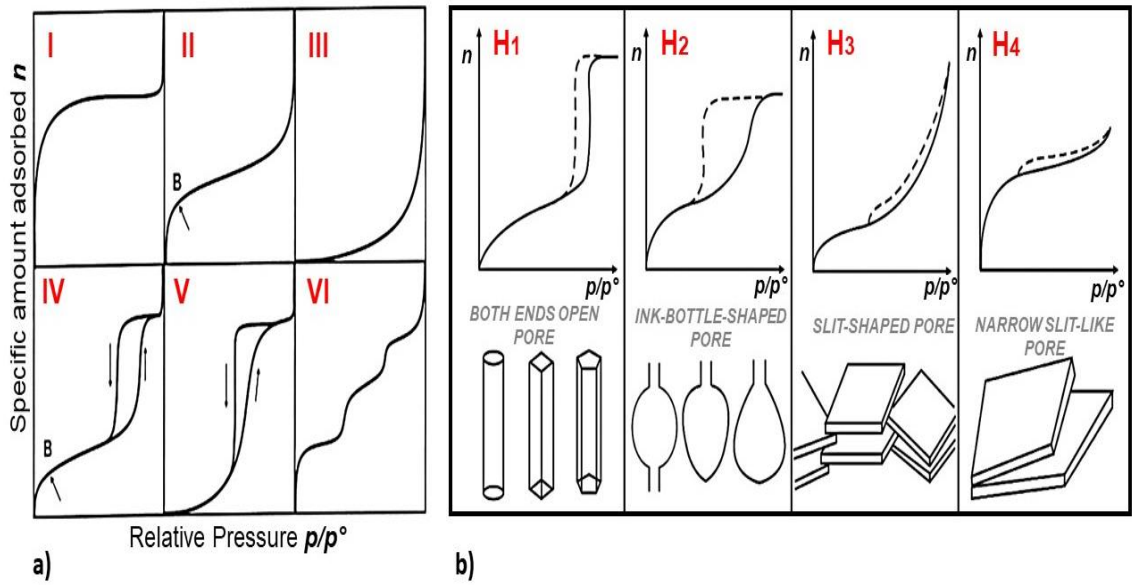

Figure 18. IUPAC classification of the six main types of gas physisorption isotherms a) and the hysteresis loops and their corresponding pore shape b) [36,39].

Through the adsorption curve, by different mathematical models, information about surface area, total pore volume and pore size distribution can be obtained. In particular, the specific surface area is calculated according to Brunauer–Emmett–Teller (BET) multipoint method, while the total pore volume and the pore size distribution are determined from the adsorption curve by the Gurvitsch rule and the Barret–Joyner–Halenda (BJH) method [40–42].

Surface profilometry measurements

A fractographic analysis of mortar samples from the inspection of the fracture surfaces obtained after the three-point flexural tests was performed. In order to study differences in failure mechanism at different scale, two different no-contact profilometers were employed: laser and optical profilometers.

a) Laser Profilometer

Laser Profilometer is a non-contact, non-destructive testing instrument used to scan and map the surface of a sample. 3D topographical images and surface parameters can be obtained. The instrument used in this work uses a laser source and a triangulation detection system (the sensor, the emitted laser and the reflected light form a triangle). It operates on

the basic principle wherein a laser beam is projected on the surface of sample under measurement and a part of this beam is then reflected via focusing optics onto a detector. The laser moves on the detector according to the sample shift [43–45].

In this work the whole profile of fracture surface of mortars was investigated as shown in Figure 19.

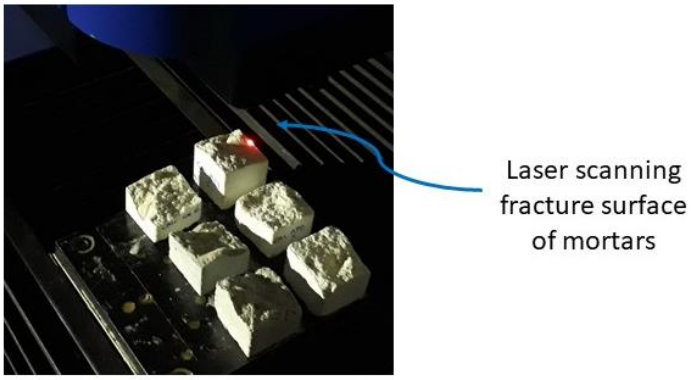

Figure 19. Laser Profilometry measurements on fracture surface of mortars.

3D topographical images and surface parameters can be obtained. In this work, primary profile parameters, P_a and P_q where computed.

According to EN ISO 4287:1997 [46], P_a and P_q are amplitude parameters calculated on the primary profile being the primary profile directly generate by the raw profile.
In particular, P_a represents the arithmetical mean of the absolute ordinate values Z(x) within the sampling length (6):

$$P_a = \frac{1}{l}\int_0^1 |Z(x)|\, dx \tag{6}$$

Whereas, P_q is the root mean square value of the ordinate values Z(x) within the sampling length (7):

$$P_q = \sqrt{\frac{1}{l}\int_0^1 Z^2(x)\, dx} \tag{7}$$

b) Optical Profilometer

Optical profilometry is a rapid, nondestructive, and non-contact surface technique. It utilizes optical light interference principles to scan the surface of the samples. It allows to obtain morphological and topographical 3D images and information of the surface profiles without damaging the actual surface features [45,47–49]. In this work, 3D topographical images were obtained and primary profile parameters, P_a and P_q, discussed above, were evaluated.

Fractographic analysis was carried out also by SEM analysis to study the dispersion, the adhesion and the interface between fibers and cement matrices.

Moreover, to evaluate possible changes due to the different surface treatments in the cement matrices, an estimation of the roughness at nanoscopic scale by AFM was also done. Especially, R_a and R_q roughness parameters were evaluated by AFM. According to EN ISO 4287:1997, R_a and R_q are amplitude parameters calculated on the roughness profile.

In particular, R_a represents the arithmetical mean of the absolute ordinate values Z(x) within the sampling length (8):

$$R_a = \frac{1}{l}\int_0^1 |Z(x)|\, dx \tag{8}$$

Whereas, R_q represents the root mean square value of the ordinate values Z(x) within the sampling length (9):

$$R_q = \sqrt{\frac{1}{l}\int_0^1 Z^2(x)\, dx} \tag{9}$$

Depending on the type of study performed, different conditions were used. Therefore, the latter will be reported in the corresponding Chapters 4, 5, 6 and 7.

References

[1] D. Olmos, J. Gonzalez-Benito, Composites formed by glass fibers and PS-modified epoxy matrix. Influence of the glass fibers surface on the morphologies and mechanical properties of the interphases generated, Polym. Compos. 31 (2010) 946–955. doi:10.1002/pc.20879.

[2] J.G. Iglesias, J. González-Benito, A.J. Aznar, J. Bravo, J. Baselga, Effect of Glass Fiber Surface Treatments on Mechanical Strength of Epoxy Based Composite Materials, J. Colloid Interface Sci. 250 (2002) 251–260. doi:10.1006.

[3] T. Deák, T. Czigány, P. Tamás, C. Németh, Enhancement of interfacial properties of basalt fiber reinforced nylon 6 matrix composites with silane coupling agents, Express Polym. Lett. 4 (2010) 590–598. doi:10.3144/expresspolymlett.2010.74.

[4] S.-J. Park, J.-S. Jin, J.-R. Lee, Influence of silane coupling agents on the surface energetics of glass fibers and mechanical interfacial properties of glass fiber-reinforced composites, J. Adhes. Sci. Technol. 14 (2000) 1677–1689. doi:10.1163/156856100742483.

[5] R. Balart, J.M. España, M.D. Samper, E. Fages, L. Sanchez-Nacher, Investigation of the Effect of Different Silane Coupling Agents on Mechanical Performance of Basalt Fiber Composite Laminates with Biobased Epoxy Matrices J.M., Polym. Compos. 34 (2013) 376–381. doi:10.1002/pc.

[6] J. González-Benito, J. Baselga, A.J. Aznar, Microstructural and wettability study of surface pretreated glass fibres, J. Mater. Process. Technol. 92–93 (1999) 129–134. doi:10.1016/S0924-0136(99)00212-5.

[7] Y. Xie, C.A.S. Hill, Z. Xiao, H. Militz, C. Mai, Silane coupling agents used for natural fiber/polymer composites: A review, Compos. Part A Appl. Sci. Manuf. 41 (2010) 806–819. doi:10.1016/j.compositesa.2010.03.005.

[8] J. González-Benito, The nature of the structural gradient in epoxy curing at a glass fiber/epoxy matrix interface using FTIR imaging, J. Colloid Interface Sci. 267 (2003) 326–332. doi:10.1016/S0021-9797(03)00550-2.

[9] D. Olmos, J. González-Benito, Visualization of the morphology at the interphase of glass fibre reinforced epoxy-thermoplastic polymer composites, Eur. Polym. J. 43 (2007) 1487–1500. doi:10.1016/j.eurpolymj.2007.01.004.

[10] G.T. Hermanson, Fluorescent Probes, in: Bioconjugate Tech., Third Ed., 2013: pp. 395–463. doi:https://doi.org/10.1016/B978-0-12-382239-0.00010-8.

[11] R. Sjback, J. Nygren, M. Kubista, Absorption and fluorescence properties of fluorescein, Spectrochim. Acta Part A. 51 (1995) L7–L21. doi:https://doi.org/10.1016/0584-8539(95)01421-P.

[12] A. Imhof, M. Megens, J.J. Engelberts, D.T.N. de Lang, R. Sprik, W.L. Vos, Spectroscopy of Fluorescein (FITC) Dyed Colloidal Silica Spheres, J. Phys. Chem. B. 103 (1999) 1408–1415. doi:10.1021/jp983241q.

[13] P.D. Castrillo Sánchez, Preparación, caracterización y análisis de materiales nanocompuestos basados en sistemas epoxi-caolín, Carlos III University of Madrid, 2010. http://e-archivo.uc3m.es/handle/10016/9183.

[14] E. Standard, EN 197-1 Cement. Part 1: Composition, specifications and conformity criteria for common cements, (2011).

[15] I. Galobardes, Compressive Strenght Development of Wet Mix Sprayed Concretes with Cement Type II and Alkali-free Accelerators, (2011). doi:10.13140/2.1.3711.1680.

[16] E. Jumate, D.L. Manea, X-Ray Diffraction Study of Hydratation Processes in the Portland Cement, in: Civ. Eng. Install., 2011: pp. 79–86. doi:10.1093/gerona/55.6.B274.

[17] Q. Ye, K. Yu, Z. Zhang, Expansion of ordinary Portland cement paste varied with nano-MgO, Constr. Build. Mater. 78 (2015) 189–193. doi:10.1016/j.conbuildmat.2014.12.113.

[18] E. Standard, EN 459-1 Building lime. Part 1: Definitions, specifications and conformity criteria, (2011).

[19] F. Iucolano, B. Liguori, C. Colella, Fibre-reinforced lime-based mortars: A possible resource for ancient masonry restoration, Constr. Build. Mater. 38 (2013) 785–789. doi:10.1016/j.conbuildmat.2012.09.050.

[20] M.L. Santarelli, F. Sbardella, M. Zuena, J. Tirillò, F. Sarasini, Basalt fiber reinforced natural hydraulic lime mortars: A potential bio-based material for restoration, Mater. Des. 63 (2014) 398–406. doi:10.1016/j.matdes.2014.06.041.

[21] A.A. Bunaciu, E.G. Udriştioiu, H.Y. Aboul-Enein, X-Ray Diffraction: Instrumentation and Applications, Crit. Rev. Anal. Chem. 45 (2015) 289–299. doi:10.1080/10408347.2014.949616.

[22] I. Adrover Gracia, Applicazioni della Spettrofotometria IR allo Studio dei Beni Culturali, il prato, 2001.

[23] P.J. Larkin, Infrared and Raman Spectroscopy: Principles and Spectral Interpretation, Second Ed., 2018. doi:https://doi.org/10.1016/C2015-0-00806-1.

[24] G.R. Heal, Thermogravimetry and Derivative Thermogravimetry, in: P.J. Haines (Ed.), Princ. Therm. Anal. Calorim., Royal Society of Chemistry, 2002: pp. 10–53.

[25] Ludwig Reimer, Scanning Electron Microscopy: Physics of Image Formation and Microanalysis, Second Ed., 1998. doi:10.1007/978-3-540-38967-5.

[26] U. Maver, T. Maver, Z. Persin, M. Mozetic, A. Vesel, M. Gaberscek, K. Stana-Kleinschek, Polymer Characterization with the Atomic Force Microscope, Polym. Sci. (2013). doi:10.5772/51060.

[27] N. Jalili, K. Laxminarayana, A review of atomic force microscopy imaging systems: Application to molecular metrology and biological sciences, Mechatronics. 14

(2004) 907–945. doi:10.1016/j.mechatronics.2004.04.005.

[28] J.R. Lakowicz, Principles of Fluorescence Spectroscopy, Third Edit, 2006. doi:10.1007/978-0-387-46312-4.

[29] A.M. Neville, J.J. Brooks, Concrete Technology, Second Ed., Pearson, 2010.

[30] William D. Callister Jr., D.G. Rethwisch, Materials Science and Engineering An Introduction, Eight Edit, John Wiley & Sons, Inc, 2010. doi:10.1016/0261-3069(91)90101-9.

[31] D. Olmos, S.G. Prolongo, J. González-Benito, Thermo-mechanical properties of polysulfone based nanocomposites with well dispersed silica nanoparticles, Compos. Part B Eng. 61 (2014) 307–314. doi:10.1016/j.compositesb.2014.01.054.

[32] E. Standard, EN 1015-11 Methods of test for mortar for masonry. Part 11: Determination of flexural and compressive strength of hardened mortar., (2000).

[33] D.R. Askeland, P.P. Fulay, W.J. Wright, The Science and Engineering of Materials, Sixth Edit, CL-Engineering, 2011.

[34] L.M. Anovitz, D.R. Cole, Characterization and Analysis of Porosity and Pore Structures, Rev. Mineral. Geochemistry. 80 (2015) 61–164. doi:10.2138/rmg.2015.80.04.

[35] S. Maria, Methods for porosity measurement in lime-based mortars, Constr. Build. Mater. 24 (2010) 2572–2578. doi:10.1016/j.conbuildmat.2010.05.019.

[36] F. Rouquerol, J. Rouquerol, K. Sing, Adsorption by Powders & Porous Solids. Principles, Methodology and Applications, Academic Press, 1999. doi:https://doi.org/10.1016/B978-0-12-598920-6.X5000-3.

[37] R.S.H. Mikhail, L.E. Copeland, Pore structures and surface Areas of hardened Portland Cement Pastes By Nitrogen Adsorption, Can. J. Chemisrty. 42 (1964) 426–438.

[38] K.S.W. Sing, International Union of Pure And Applied Chemistry, Reporting Physisorption data for Gas / Solid Systems with Special Reference to the Determination of Surface Area and Porosity, Pure Appl. Chem. 54 (1982) 2201–2218. doi:10.1351/pac198557040603.

[39] T. Li, Z. Jiang, C. Xu, et al., Effect of pore structure on shale oil accumulation in the lower third member of the Shahejie formation, Zhanhua Sag, eastern China: Evidence from gas adsorption and nuclear magnetic resonance, Mar. Pet. Geol. 88 (2017) 932–949. doi:10.1016/j.marpetgeo.2017.09.030.

[40] A. Pacella, C. Cremisini, E. Nardi, M.R. Montereali, I. Pettiti, M. Giordani, M. Mattioli, P. Ballirano, Different erionite species bind iron into the structure: A potential explanation for fibrous erionite toxicity, Minerals. 8 (2018) 1–16. doi:10.3390/min8020036.

[41] L. Chronopoulou, C. Palocci, F. Valentino, I. Pettiti, S. Wacławek, M. Černík, M.

Petrangeli Papini, Stabilization of Iron (Micro)Particles with Polyhydroxybutyrate for In Situ Remediation Applications, Appl. Sci. 6 (2016) 417. doi:10.3390/app6120417.

[42] E.P. Barrett, L.G. Joyner, P.P. Halenda, The Determination of Pore Volume and Area Distributions in Porous Substances. I. Computations from Nitrogen Isotherms, J. Am. Chem. Soc. 73 (1951) 373–380. doi:10.1021/ja01145a126.

[43] T. Giesko, A. Zbrowski, P. Czajka, Laser profilometers for surface inspection and profile measurement, Probl. Eksploat. (2007) 97–108.

[44] K.R. Wu, A. Yan, J.Y. Liu, D. Zhang, W. Yao, Reconstruction and analysis of 3-D profile of fracture surface of concrete, Cem. Concr. Res. 30 (2000) 981–987. doi:10.1016/S0008-8846(00)00249-0.

[45] L. Courard, A. Garbacz, B. Bissonnette, Topography evaluation methods for concrete substrates: Parametric study, in: M.G. Alexander, H.-D. Beushausen, F. Dehn, P. Moyo (Eds.), Concr. Repair, Rehabil. Retrofit. III-Proc.3rd ICCRR, CRC Press Taylor & Francis Group, 2012.

[46] EN ISO 4287:1997 Geometrical Product Specifications (GPS) - Surface texture: Profile method - Terms, definitions and surface texture parameters, (1999).

[47] P.M.D. Santos, E.N.B.S. Júlio, A state-of-the-art review on roughness quantification methods for concrete surfaces, Constr. Build. Mater. 38 (2013) 912–923. doi:10.1016/j.conbuildmat.2012.09.045.

[48] A. Garbacz, L. Courard, B. Bissonnette, A surface engineering approach applicable to concrete repair engineering, Bull. Polish Acad. Sci. Tech. Sci. 61 (2013) 73–84. doi:10.2478/bpasts-2013-0006.

[49] A. Garbacz, L. Courard, K. Kostana, Characterization of concrete surface roughness and its relation to adhesion in repair systems, Mater. Charact. 56 (2006) 281–289. doi:10.1016/j.matchar.2005.10.014.

CHAPTER 4

SURFACE MODIFICATION AND CHARACTERIZATION OF BASALT FIBERS AS POTENTIAL REINFORCEMENT OF MORTARS

CHAPTER 4.
SURFACE MODIFICATION AND CHARACTERIZATION OF BASALT FIBERS AS POTENTIAL REINFORCEMENT OF MORTARS

Abstract

Basalt fibers were surface treated with silane coupling agents as a method to enhance the adhesion and durability of fiber-matrix interfaces in cement- based composite materials. In particular, this work has been focused on the study of basalt fibers chemical coatings with aminosilanes and their subsequent characterization. Surface treatments were carried out after removing the original sizing applied by manufacturer and pretreating them with an activation process of surface silanol regeneration. Different samples were considered to make convenient comparisons: as received fibers (commercial), calcinated fibers (without commercial sizing), activated samples (calcinated fibers subjected to an acid process for hydroxyl regeneration), and silanized fibers with *γ-aminopropiltriethoxysilane, γ-aminopropilmethyldiethoxysilane* and a mixture of 50% by weight of both silanes. A deep characterization was carried out in terms of structure using X-ray diffraction, XRD, and Fourier transform infrared spectroscopy, FTIR, thermal properties by thermogravimetric analysis, TGA, coupled with single differential thermal analysis, SDTA, and morphology by scanning electron microscopy, SEM, and atomic force microscopy, AFM.

4.1. Introduction

Nowadays, the growing need to design materials able to enhance performance of traditional materials to be used in several industrial applications, is generating great interest. In this context, the use of basalt fiber-reinforced materials represents a promising and innovative alternative to traditional materials.
The choice of basalt fibers lies in the fact that they are characterized from a large variety of excellent properties. A detailed description of basalt fibers has been previously presented in Chapters 1 and 2.

One of the final use of fibers is as reinforcement of concrete or mortar in structural or non-structural materials to reduce the adverse effects of shrinkage cracking of cement and natural hydraulic lime (NHL) mortars used in many historical structures and buildings which have significant cultural interest.

Sarasini et al. in 2014 [1,2] investigated the effect of commercial basalt fibers in this type of matrices studying the mechanical properties in terms of fracture and damage mechanism highlighting the role played by the interface between the fiber and the cement matrices. However, they pointed out the necessity of carrying out more investigation focused on this issue trying to find out how inducing a better balance between two usually opposing needs, strength and toughness enhancement.

It is well known that properties of composite materials are strongly influenced by the type of adhesion between the reinforcement and the matrix [3,4]. Depending on the characteristics of the fiber-matrix interfacial region, the composite subjected to different sorts of loads can be either brittle or damage-tolerant under the effect of several factors or even combination of them (temperature, radiation, humidity). Thus, in order to obtain composites with good mechanical properties it is important, among other things, to tailor a proper fiber-matrix interface to improve final performance of the composites avoiding, for instance, several failure mechanisms that could start at the interface such as fiber debonding and pull-out, fiber sliding and crack bridging [5].

The surface modification of reinforcements through special treatments is one of the most common strategies to overcome the later. Probably the most successful method to carry out

this lies on the creation or increment of particular functional groups to facilitate physical interactions or even chemical bonding between the constituents [6]. Therefore, it is reasonable to think that also, in the case of basalt fibers, one of the challenges must be optimizing the fiber-matrix interface through surface treatments of the fibers to finally increase the attractive interactions, reduce imperfections and, protect the fibers from the aggressive environment given by the matrix. The usual way to fulfill the latter is by generating: i) an adequate roughness, for instance, to increase the specific surface and ii) a surface with particular chemical functionalities.

It is well known that coupling agents have a great effect on the interface structure and properties of composite materials [4,7]. Among them, the most commonly used are the silane coupling agents consisting on difunctional organosilicon compounds with general formula $Y\text{-}Si(X)_3$ and previously described in Chapter 2 (section 2.1.3) [6]. In particular, aminosilanes are commonly used as surface modifying agents in fibers [6,8–21]. Besides, several studies shown that they can improve the composite performance in several matrices (as cement matrix) [22,23]. When modifying with this kind of silanes special attention must be paid on the interphase structure since it is quite well known that, because of the chemical and structural differences of this coupling agent interface layer can greatly influence in the mechanical properties of composite materials [6]. Thus, a good characterization of fibers surface along the whole process of their modification is a prerequisite to finally understand the last properties of the composites.

The aim of this work is to modify basalt fibers surface under well controlled conditions using different model surface treatments and characterize them in such a way that the data collected (structure, morphology, etc.) were enough to finally understand possible improvements of the properties of cement based composite materials. The surface treatments will be based on chemical coatings of the basalt fiber with aminosilanes having different functionally order (triethoxysilane, 3, diethoxysilane, 2, and a mixture of them 50% by weight). These choices were made looking for obtaining different molecular structure at the fiber surface and consequently at the interface of composites.

4.2. Experimental

4.2.1. Materials

Basalt continuous filament (mean diameter 17 μm) chopped to a length of about 6.4 mm with a sizing compatible with cement and natural hydraulic lime (NHL) matrices was supplied by Incothelogy GmbH. A chlorydric acid aqueous solution (37% wt), Sharlab, was used to prepare pretreated basalt fibers. Two silanes, γ-aminopropiltriethoxysilane (APTES) and γ-aminopropilmethyldiethoxysilane (APDES), supplied by ABCR GmbH & Co.KG, were used in order to obtain different surface coatings of the basalt fibers.

4.2.2. Samples Preparation

Neat basalt fibers were obtained by a surface pretreatment of the as-received fibers following several steps:

- ***Disgregation:*** Commercial basalt fibers were initially stirred within destilled and deionized water at room temperature to attain maximum separation between them.

- ***Calcination:*** Disgregated fibers were heat treated at 120°C for 30 min to remove water and after that at 505°C for 1h to remove any organic substance, such as sizing or impurities. A thermocouple placed near the sample was used to control the temperature.

- ***Activation:*** The calcinated fibers were subjected to an activation process with commercial chlorhydric acid aqueous solution (37% wt) for 1h to regenerate silanol groups, Si-OH, on the fiber surface. After that, all samples were washed with destilled and deionized water and finally dried at 110°C for 1 h and stored in a dessicator until silanization.

- ***Silanization:*** The fibers were then chemically coated with the aminosilane coupling agents. 1g of basalt fibers was inmersed in 50 ml of silane 2% wt aqueous solution for 1h at room temperature. In order to obtain different molecular structures different silane aqueous solutions were used: i) γ-aminopropiltriethoxysilane

(APTES); ii) γ-aminopropilmethyldiethoxysilane (APDES) and iii) a mixture of them wirh a composition of 50% by weight (APTES+APDES).

After squeezing the fibers, the adsorbed silane was cured at 110 °C for 1h to accelerate condensation reaction and to remove water. In order to eliminate some unreacted silane monomers or oligomers that could remain physisorbed on the basalt fibers surface the fibers were subjected to a Soxhlet extraction with dry toluene for 3 h. Finally, fibers were put in an oven at 110°C for 1h to remove adsorbed toluene [6,8,15,20,24].

As an aproximation the structures expected for the basalt fibers surfaces using the different silane solutions would be those shown in Figure 1 [20]: i) smooth surfaces with low concentration of silanol groups for calcinated basalt fibers; ii) smooth surfaces with increased concentration of surface silanols groups for activated fibers; iii) surfaces with lineal or bowed siloxane coating when APDES is used and iv) crosslinked siloxane structures when APTES solutions are used being higher the crosslinking degree the higher the APTES concentration. Therfore when a mixture of silanes (APTES+APDES) is used a more open crosslinked structure is expected.

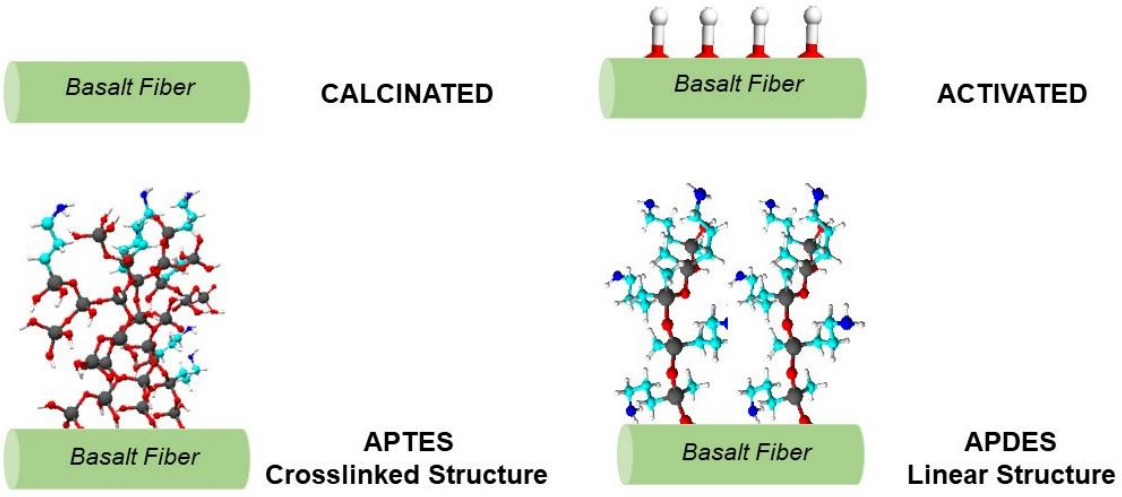

Figure 1. Scheme of the expected basalt fiber surface structures expected for the different treatments considered.

4.2.3. Experimental Techniques

4.2.3.1. X-Ray Diffraction (XRD)

Structural characteristics of as-received, calcinated and activated basalt fibers were studied by X-Ray Diffraction (XRD) using a Bruker AXS D8 ADVANCE diffractometer with a CuKα1 radiation, step size of 0.020°, time per step of 1 s from 5° to 65°.

4.2.3.2. Thermal Analysis

Thermogravimetric analysis was carried out using a Mettler Toledo TGA/SDTA 851e analyzer equipped with a TSO800GC1 flow gas controller and a TSO801RO universal samples robot. The analysis of the as-received and treated basalt fibers were performed using a platinum crucible at 10°C/min heating rate under inert atmosphere from 30°C to 800°C.

4.2.3.3. Fourier Transform Infrared Spectroscopy (FT-IR)

FT-IR spectra of as-received and modified basalt fibers were recorded with a FT-IR Spectrum GX (Perkin-Elmer). Basalt fibers (as-received and treated) was ground, mixed with KBr powder and pressed using a Specac Press to make discs of 1 cm of diameter to perform the FTIR studies in the transmission mode. In particular, discs with 1% and 5% by weight of fibers were considered to better visualized absorption bands in the low and high energy regions of the spectra respectively. As background, a pure KBr disc was used. Every spectrum was recorded from 400 to 4000 cm^{-1} using 2 cm^{-1} of resolution and 20 scans for the corresponding interferogram averaging. Finally, taking into account the proportionality between absorbance and the amount of the absorbing species, to represent the spectra all of them were normalized respect to the well weighted amount of fibers used to prepare the KBr discs.

4.2.3.4. Scanning Electron Microscopy (SEM)

As-received and treated basalt fibers were inspected by scanning electron microscopy using a TENEO field emission scanning electron microscope, FESEM (FEI). The acceleration voltage was 2.0 kV and the T1 detector was used taking the signal coming

from backscattered electrons. As the samples are not conductive, prior to examination, they were sputter coated with gold using a low vacuum coater Leica EM ACE200.

4.2.3.5 Atomic Force Microscopy (AFM)

Atomic force microscopy, AFM, was used to inspect topographical characteristics of the basalt fibers. A microscope Multi-Mode Nanoscope IVA (Digital Instruments/Veeco Metrology Group) was used. All measurements were conducted at ambient conditions in tapping mode with antimony doped silicon probe (k = 1-5 N/m). The frequency was adjusted to the resonant frequency of the probe close to the surface of the sample to be analyzed. The initial amplitude of the probe oscillation and set-point amplitude applied for imaging were chosen to maximize the image contrast among the different constituents of the samples.

4.3. Results and Discussion

4.3.1. Characterization of As-Received Basalt Fibers

In the Figure 2 XRD patterns of the as-received (a), calcinated (b) and activated (c) basalt fibers are shown. XRD analysis of the commercial basalt fibers reflects only an amorphous structure without any evidence of crystalline phases being in accordance with bibliography [25,26]. Besides, either the calcination or the activation processes do not seem to change the structure of the basalt fibers at least in terms of crystallinity.

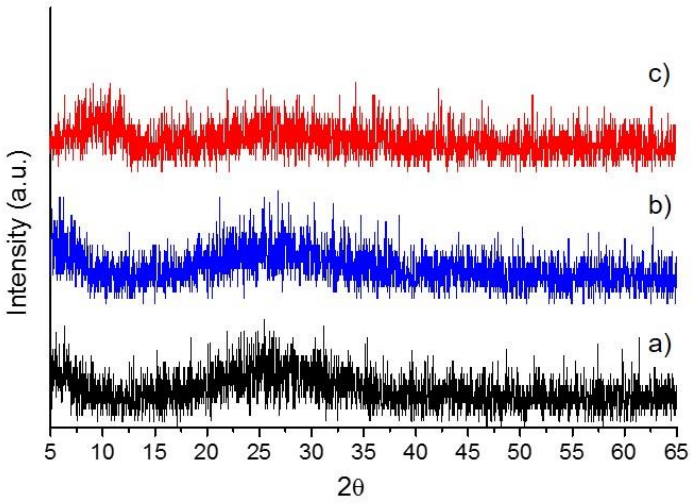

Figure 2. XRD patterns of as-received (a), calcinated (b) and activated (c) basalt fibers.

In Figure 3 TGA curves (top) and its corresponding derivatives DTGA (bottom) are shown for all the basalt fibers considered in the present work. In particular, for the as-received fibers, represented by the black curves, two clear observations can be made: the weight loss at about 100 ºC due to the adsorbed water on the fiber and a thermal degradation process in the range going from 200 to 550 °C with a weight loss of 0.4% by weight (Table 1). This degradation can be ascribed to the presence of the organic coating associated to the sizing of the commercial fibers. It is important to point out that around the temperature of 450 ºC the dehydroxilation process of silica occurs which involves the condensation of surface hydroxyl groups to form siloxane bonds releasing water molecules [21,27]. Therefore, the weight loss calculated in this range might include part of the water associated to this process. Nevertheless, this result points out that the conditions selected for the calcination process 505 ºC for 1 h should be enough to fully remove the commercial sizing avoiding simultaneously an excessive dehydroxilation of the surface.

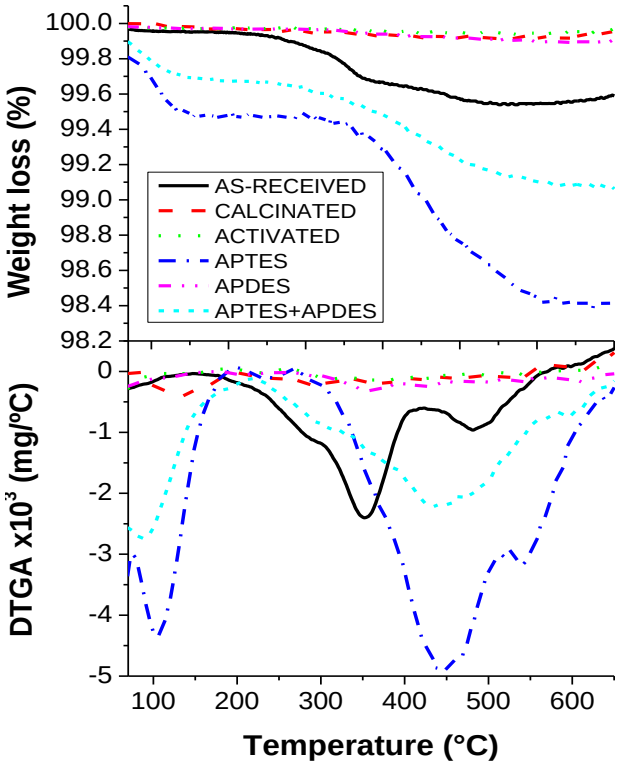

Figure 3. TGA curves (top) and their derivatives, DTGAs (bottom) for the fibers under study.

The FT-IR spectrum of as-received basalt fiber is shown in the Figure 4. In the region of high energy the FTIR spectrum of the commercial basalt fibers (Figure 4a) shows a broad band from 3600-3200 cm^{-1} that usually is assigned to the hydrogen bonded O-H stretching

that can come either from water adsorbed on the fiber surface or from the silanol groups, -Si-OH [24,28].

In the range from 3000 to 2800 cm^{-1} the characteristic CH stretching bands coming from the methylene, CH_2, and methyl, CH_3, groups can be observed. These bands ensured the organic character which is typical of the most common sizings used in the production process of glass and basalt fibers. In the low energy region of the spectrum (Figure 4b) the absorption bands at 1000 and 740 cm^{-1} corresponding to the Si-O vibrations typical of silane sizings and basalt fibers (they are mainly composed by SiO_2) are detected.

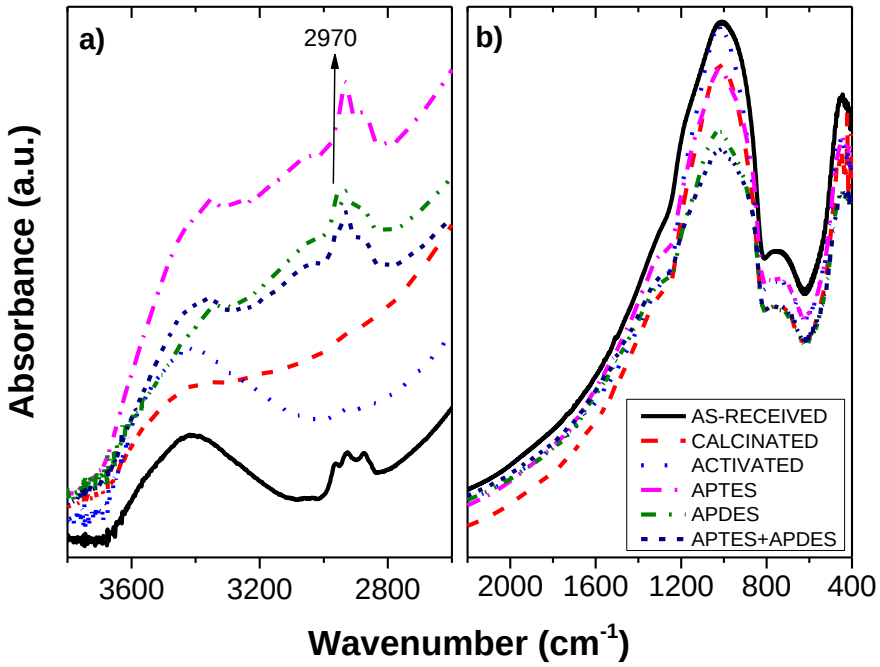

Figure 4. High (a) and low (b) energy regions of FTIR Spectrum of all fibers under study.

The morphology and topography of the as-received basalt fibers were studied by SEM and AFM (Fig. 5a and 5b). Dark grey in the SEM and light yellow "islands" in the AFM height images reflect a heterogeneous surface of the fibers due to the presence of the sizing. Moreover, some regions in the SEM image (pointed by an arrow) suggest that the shape of the fibers is not perfectly cylindrical but it presents some imperfections. These imperfections, similar to a valley on the fiber surface are also clearly visible in the 3D AFM images (Figure 5c) of treated basalt fibers.

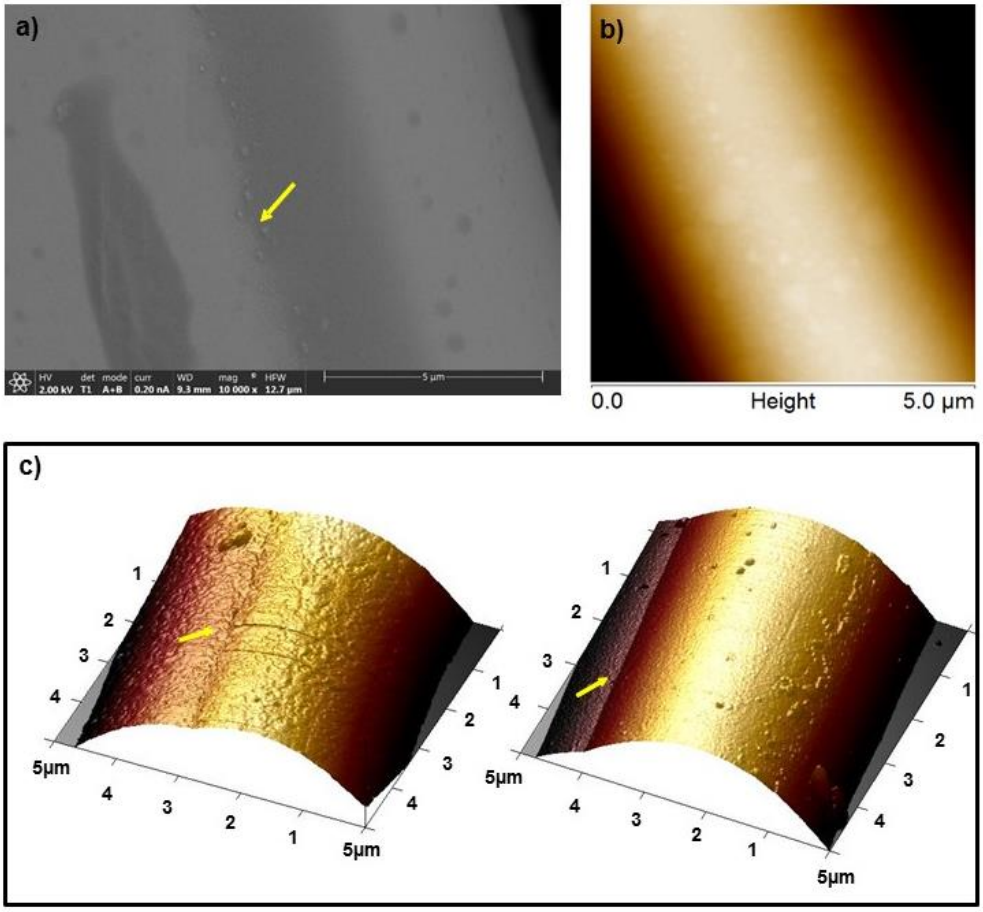

Figure 5. SEM (a), AFM Heigh (b) images of as-received basalt fiber and 3D AFM (c) images of APDES (left) and APTES+APDES (right) coated basalt fibers.

4.3.2. Characterization of Modified Basalt Fibers

XRD Analysis, Fig, 2b and 2c, shows that calcinated and activated basalt fibers are characterized by the same structure of as-received basalt fibers (Fig.2a). The amorphous structure of the as-received basalt fibers without any evidence of crystalline phases is preserved. It is possible to confirm that calcination and activation processes carried out in order to obtain an ideal surface necessary to apply the new chemical coatings based on aminosilanes, do not modify the structure of the original basalt fibers.

From the TGA and DTGA curves (Figure 3) the thermodegradation process associated to the organic matter was analyzed within the range 200°C - 400°C in order to be sure that only organic coating is analyzed avoiding to count for the water release due to the deshydroxylation phenomenon. The weight loss in every case was calculated and gathered in the Table 1.

As can be seen and attending the accuracy of the thermobalance the data in the Table 1 suggest that a treatment at 505 °C for 1 h is enough to remove the whole sizing of the commercial fibers. As it is shown, activation process helps to completely remove the original sizing. On the other hand, DTGA curves show (Figure 3) that the maximum rate of thermodegradation for the aminosilane coatings are shifted to higher temperatures respect to that observed for the sizing of the as-received basalt fibers indicating, as expected, different structures. Usually commercial sizings are formed by a mixture of several components, silanes, plasticizers, lubricants, etc. In Table 1 it can be seen that the order in terms of degree of coating is: APTES > APTES+APDES > APDES, as expected if higher functionality implies higher reactivity with higher amount of monomer incorporation. It is observed that the silane with a crosslinked structure is grafted in more amount on the fiber surface than the silane with a linear structure.

Table 1. TGA results of as-received and treated basalt fibers.

Sample	***Temperature Range (ºC)***	***Weight loss (%)***
AS-RECEIVED	200 – 550	0.40
AS-RECEIVED	200 – 400	0.28
CALCINATED	200 – 400	0.04
ACTIVATED	200 – 400	0.02
APTES	200 – 400	0.21
APTES+APDES	200 – 400	0.19
APDES	200 – 400	0.03

FTIR was also used to study structural variation of the basalt fiber surface with the different treatments considered. In the Figure 4 FTIR the spectra of all the modified or unmodified basalt fibers are represented. Paying attention to the high energy region (Figure 4a) some clear observations can be made: a) after calcination there is a reduction of the broad band centered at about 3400 cm^{-1} that can be mainly associated to a decrease in the adsorbed water since no clear evidence of deshydroxilation at 505 ºC was observed by TGA (Figure 3). Besides, b) the absorption bands due to CH (CH_2, CH_3) stretching vibrations of the sizing disappear. c) When the activation process is carried out an increase of the band at about 3400 cm^{-1} occurs evidencing the existence of higher number of hydrogen bonded OH probably coming from more adsorbed water induced by a more hydrophilic surface with higher silanol groups content. In fact, the reason why the HCl

treatment was called activation is because a more reactive surface is created by means of a silanol groups regeneration as it was explained elsewhere [24,29]. Taking into account several reported assignations of absorption bands (see Table 2) [30], an easier analysis of the silane coated fibers FTIR spectra can be done.

Table 2. Absorption Bands of Aminosilanes [30].

ν (cm^{-1})	***Absorption bands of Aminosilane***
3400	ν (O-H)
3400-3300	ν_{as} (N-H)
2970-2960	ν_{as} (C-H) (CH_3)
2930-2920	ν_{as} (C-H) (CH_2)
1600	δ (N-H)
1450	δ (CH_2)
1440	δ (CH_3)
1410	δ (Si- CH_2)
1380	δ (CH_3)
1260	ν (Si-C)
1160	ρ (CH_3)
1100	ν_{as} (Si-OSi)
1100	ν_{as} (Si-OC)
1000	ν_{as} (Si-OSi)
950	δ (Si-OH)

It is clear therefore that the presence of aminosilanes can be identified with absorption bands at 3400-3300 cm^{-1} due to N-H stretching modes. On the other hand, in the range of 3000-2800 cm^{-1} the C-H stretching bands arising from the methylene, CH_2, and methyl, CH_3, groups are observed. In fact, as expected from the chemical structures of the hydrolyzed silanes used (Figure 6), only for the APTES coating the band at 2970 cm^{-1} does not appear which indicates the absence of methyl groups.

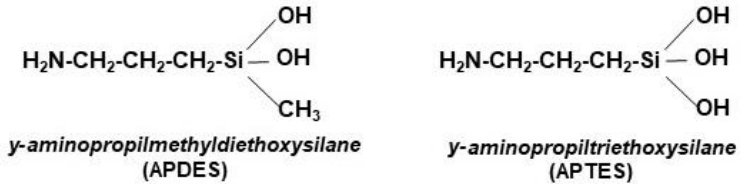

Figure 6. Molecular structures of hydrolyzed APDES and APTES silane coupling agents.

Moreover, paying attention to the above-mentioned O-H stretching band at about 3400 cm^{-1} for the unmodified and modified basalt fibers, some considerations in relation to the hydrophilicity/hydrophobicity of the fiber surface may be done.

In fact, it can be inferred some reasoning in relation to hydrophobicity since, the stronger the band corresponding to the O-H stretching the higher the amount of hydroxyl groups or even adsorbed water which should point out lower hydrophobicity for the fiber surfaces.

It can be clearly observed how the incorporation of aminosilanes highly reduces the relative absorbance of the O-H stretching bands respect to both the fibers with commercial sizing and the activated fibers, evidencing higher hydrophobicity. Finally, comparing between the three aminosilane coatings it can be seen that the order in terms of relative absorbance for the O-H stretching bands is the following: APTES > APTES + APDES > APDES. In other words, one would expect the same order in terms of hydrophilicity for the three aminosilane coatings. Besides, these observations are in agreement with contact angle data reported in a previous study about the wettability of surface treated glass fibers [24].

Finally, from the FTIR results an estimation of the amount of silane grafted on the fibers surface was carried out. The amount of silane showing in the Table 3 was calculate from the measurement of absorbance of the band at 2930 cm^{-1} corresponding to the CH stretching band of the CH_2 group using the following equation:

$$c = A_{2930}/3Kb \quad (1)$$

where **c** is the silane concentration in mol/cm^3, $\boldsymbol{A_{2930}}$ is the absorbance corresponding to the CH absorption band of the CH_2 group, $\boldsymbol{K}$ is the specific absorptivity for the silane (1.7 x 10^4 cm^2/mol) and $\boldsymbol{b}$ is the optical path. Division by 3 is performed to take into account the three methyl groups contribution of each molecule hydrolyzed silane [30,31]. An estimation of the amount of silane in terms of percentage was at the same time carried out. Taking into account the volume of discs and the silane concentration in mol/cm^3 previously calculated according the equation mentioned above, the moles number of the CH_2 group present in each disc and thus the moles number of each silane were calculated.

In this way considering the molecular weight of each silane used, the silane weight in the disc was obtained. In the case of the mixture of the two silanes, an average of the molecular weight was considered. Finally, knowing the initial weight of the discs (including fiber and silane weights), the percentage respectively of each silane was obtained.

The results are shown in the Table 3.

Table 3. Estimation of the concentration of silane on the fiber surface by FTIR.

Sample	A_{2930}	***b (cm)***	***c (mol/cm^3)***	***% weight by FTIR***	***% weight by TGA****
APTES	0.029	0.0451	1.26×10^{-5}	0.30	0.21
APTES+APDES	0.023	0.0453	9.95×10^{-6}	0.23	0.19
APDES	0.017	0.0512	6.51×10^{-6}	0.17	0.03

* Table 1

According to TGA results, it is observed that the silane content seems to follow the order: APTES > APTES+APTES > APDES. The small differences found between the results provided by the two techniques could be ascribed to the associated error to the measuring instruments.

Although relevant results are obtained from the high energy region of the spectra, not significant observations can be drawn from the low energy region of FTIR spectra.

In Figure 7, the SEM images of treated basalt fibers compared to as-received basalt fibers are shown. Calcinated (b) and activated (c) basalt fibers look very similar each other; nevertheless, some differences due to the processes are better observed by AFM analysis (Figure 8). However, as a consequence of these two treatments a smoother surface due to the removal of original sizing can be observed.

Finally, the images (d, e, f) of Figure 7, corresponds to the silanized basalt fibers after the heat cleaning and activation processes. As a result of the incorporation of the aminosilanes, some heterogeneities are observed on the fibers surfaces. In particular, these heterogeneities are more clear when the APTES, the aminosilane with a crosslinked structure, is applied.

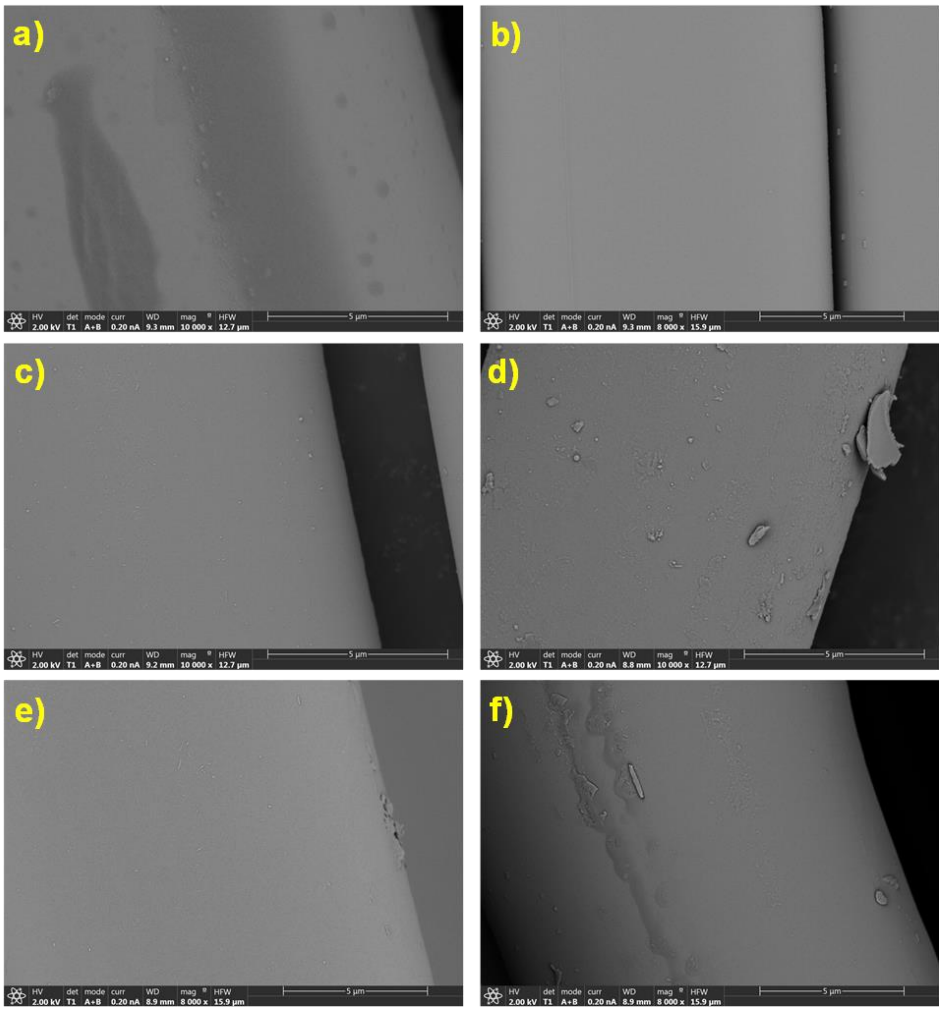

Figure 7. SEM Images of as-received (a), calcinated (b), activated (c), APTES coated (d), APDES coated (e), APTES+APDES coated (f) basalt fibers.

Changes on the fibers surface are better studied by AFM because the preliminary preparation of the sample to be analyzed is quite easy. Besides, the gold coating used to observe samples by SEM might hide some small superficial characteristics. In the Figure 8, 3D AFM images of the as-received and treated basalt fibers are shown. A kind of "islands" are better observed on the commercial fiber surface arising from the sizing (Figure 8a). The images corresponding to the calcinated basalt fibers (Figure 8b) shows sometimes a kind of scratches which might reflect locations where fibers could be joined by the action of the sizing. However, the amount of remaining sizing is almost zero because no evidence of organic coating was detected by FTIR spectroscopy and only a small amount of organic substance (weight loss of 0.04%) was detected by TGA that might be considered negligible. On the other hand, according to TGA results shown in the Table 1 and the observations of 3D AFM images like in Figure 8c it is evidenced that the activation

process ensures total removal of those possible amounts of remaining sizing making the fiber surface clearly smoother.

In comparison with the SEM images, the 3D AFM images of the silanized basalt fibers (Figures 8d and 5c) better show the heterogeneous topography given by the coating. It can be observed that the distribution of the coupling agents on the fibers is in the form of droplets; i.e. there is formation of islands on the fiber being in accordance with other results the scientific literature observed for E-glass fibers treated with aminosilanes [19]. Furthermore, it is interesting to highlight that the way of coating depends on the kind of silane used. The islands of sizing seem to be homogeneously distributed on the basalt fiber surface when they are treated with *γ-aminopropilmethyldiethoxysilane* (APDES) whereas "mountains-like" of sizing are better observed when the *γ-aminopropiltriethoxysilane* (APTES) is used. These observations suggest that topography due to the heterogeneities arising from the sizing deposition could be controlled and therefore parameters as the roughness which are essential to finally attain good adherence or interface properties when the fibers are used as reinforcements in composites.

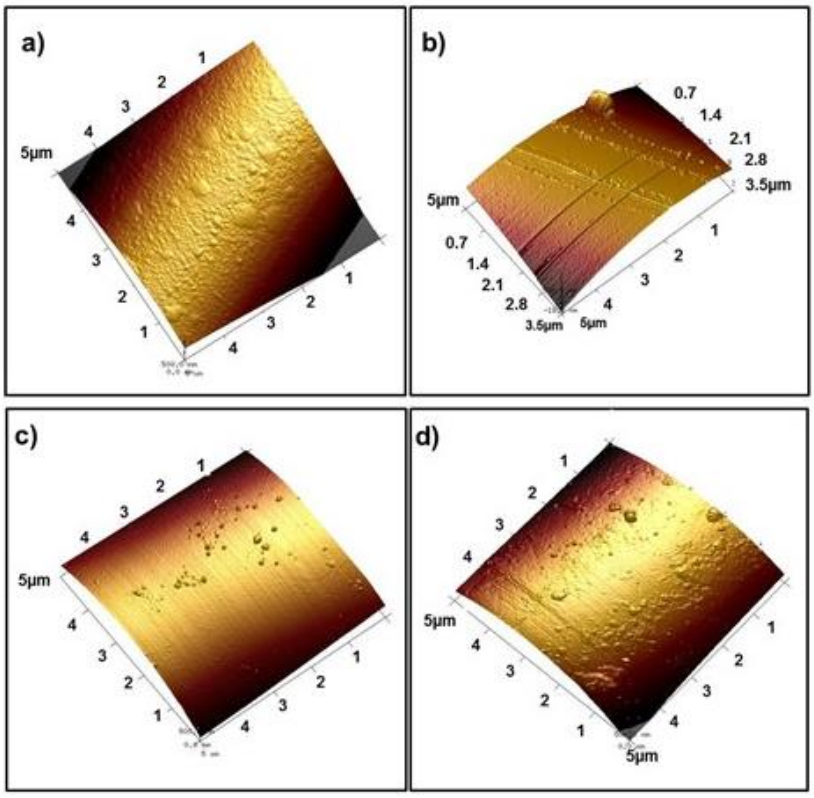

Figure 8. 3D AFM Images of as-received (a), calcinated (b), activated (c), APTES coated (d) basalt fibers.

4.4. Conclusions

The modification of basalt fibers surface in a controlled way using model coatings or surface preparation was carried out in this work. In particular, a careful and detailed characterization of them, necessary to collect data in order to, subsequently, understand specific interactions with cement- based matrices, was done.

The preliminary study about the structure, composition and morphology/topography of as-received basalt fibers by several analytical techniques (XRD, TGA, FT-IR, FE-SEM and AFM) confirmed that commercial fibers are characterized by an amorphous structure and a heterogeneous sizing of organic nature applied on the fiber surface during the production process.
Depending on the treatment given changes in the structure, composition and topography are observed. In particular, the calcination process removes the most of commercial sizing present on the fiber surface making the surface smooth.

The activation process fully removes all residues of sizing that could remain on the calcinated fiber surface and makes the topography smoother than calcination process. Moreover, this process regenerates silanol groups on the fiber surface allowing the grafting of aminosilanes.

The three chemical coatings based on aminosilane (APTES, APDES and APTES+APDES) make the surface rough. It was concluded that the higher the amount of triethoxysilane in the composition of the coating solution, the more organic matter deposited on the fibers, so as the topographical heterogeneity. This heterogeneity could be responsible of a most adhesion between the matrix and the fiber.

References

[1] M.L. Santarelli, F. Sbardella, M. Zuena, M. Albé, G. Quattrociocchi, J. Tirilló, M. Valente, F. Sarasini, Malte più performanti con le fibre di basalto, Compos. Mag. 33 (2014) 7–16. http://hdl.handle.net/10278/44412.

[2] M.L. Santarelli, F. Sbardella, M. Zuena, J. Tirillò, F. Sarasini, Basalt fiber reinforced natural hydraulic lime mortars: A potential bio-based material for restoration, Mater. Des. 63 (2014) 398–406. doi:10.1016/j.matdes.2014.06.041.

[3] N. Suzuki, H. Ishida, A Review on the Structure and Characterization Techniques of Silane/Matrix Interphases, 108 (1096) 19–53. doi:https://doi.org/10.1002/masy.19961080105.

[4] A.T. DiBenedetto, Evaluation of fiber surface treatments in composite materials, Pure Appl. Chem. 57 (1985) 1659–1665. doi:10.1351/pac198557111659.

[5] V.A. Rybin, A. V. Utkin, N.I. Baklanova, Alkali resistance, microstructural and mechanical performance of zirconia-coated basalt fibers, Cem. Concr. Res. 53 (2013) 1–8. doi:10.1016/j.cemconres.2013.06.002.

[6] J.G. Iglesias, J. González-Benito, A.J. Aznar, J. Bravo, J. Baselga, Effect of Glass Fiber Surface Treatments on Mechanical Strength of Epoxy Based Composite Materials, J. Colloid Interface Sci. 250 (2002) 251–260. doi:10.1006.

[7] S.-J. Park, J.-S. Jin, J.-R. Lee, Influence of silane coupling agents on the surface energetics of glass fibers and mechanical interfacial properties of glass fiber-reinforced composites, J. Adhes. Sci. Technol. 14 (2000) 1677–1689. doi:10.1163/156856100742483.

[8] D. Olmos, J. González-Benito, Visualization of the morphology at the interphase of glass fibre reinforced epoxy-thermoplastic polymer composites, Eur. Polym. J. 43 (2007) 1487–1500. doi:10.1016/j.eurpolymj.2007.01.004.

[9] R. Balart, L.S.-N. J.M. España, M.D. Samper, E. Fages, Investigation of the Effect of Different Silane Coupling Agents on Mechanical Performance of Basalt Fiber Composite Laminates with Biobased Epoxy Matrices J.M., Polym. Compos. 34 (2013) 376–381. doi:10.1002/pc.

[10] T. Deák, T. Czigány, P. Tamás, C. Németh, Enhancement of interfacial properties of basalt fiber reinforced nylon 6 matrix composites with silane coupling agents, Express Polym. Lett. 4 (2010) 590–598. doi:10.3144/expresspolymlett.2010.74.

[11] Y. Xie, C.A.S. Hill, Z. Xiao, H. Militz, C. Mai, Silane coupling agents used for natural fiber/polymer composites: A review, Compos. Part A Appl. Sci. Manuf. 41 (2010) 806–819. doi:10.1016/j.compositesa.2010.03.005.

[12] E. Feresenbet, D. Raghavan, G.A. Holmes, The influence of silane coupling agent composition on the surface characterization of fiber and on fiber-matrix interfacial shear strength, J. Adhes. 79 (2003) 643–665. doi:10.1080/00218460309580.

[13] B. Wei, H. Cao, S. Song, Surface modification and characterization of basalt fibers

with hybrid sizings, Compos. Part A Appl. Sci. Manuf. 42 (2011) 22–29. doi:10.1016/j.compositesa.2010.09.010.

[14] D. Olmos, R. López-Morón, J. González-Benito, The nature of the glass fibre surface and its effect in the water absorption of glass fibre/epoxy composites. The use of fluorescence to obtain information at the interface, Compos. Sci. Technol. 66 (2006) 2758–2768. doi:10.1016/j.compscitech.2006.03.004.

[15] J. González-Benito, A. Aznar, J. Baselga, Solvent and Temperature Effects on Polymer-Coated Glass Fibers . Fluorescence of the Dansyl Moiety, J. Fluoresc. 11 (2001).

[16] S.G. Turrión, D. Olmos, J. González-Benito, Complementary characterization by fluorescence and AFM of polyaminosiloxane glass fibers coatings, Polym. Test. 24 (2005) 301–308. doi:10.1016/j.polymertesting.2004.11.006.

[17] J. González-Benito, The nature of the structural gradient in epoxy curing at a glass fiber/epoxy matrix interface using FTIR imaging, J. Colloid Interface Sci. 267 (2003) 326–332. doi:10.1016/S0021-9797(03)00550-2.

[18] D. Olmos, A.J. Aznar, J. Baselga, J. González-Benito, Kinetic study of epoxy curing in the glass fiber/epoxy interface using dansyl fluorescence, J. Colloid Interface Sci. 267 (2003) 117–126. doi:10.1016/S0021-9797(03)00620-9.

[19] E. Metwalli, D. Haines, O. Becker, S. Conzone, C.G. Pantano, Surface characterizations of mono-, di-, and tri-aminosilane treated glass substrates, J. Colloid Interface Sci. 298 (2006) 825–831. doi:10.1016/j.jcis.2006.03.045.

[20] D. Olmos, J. Gonzalez-Benito, Composites formed by glass fibers and PS-modified epoxy matrix. Influence of the glass fibers surface on the morphologies and mechanical properties of the interphases generated, Polym. Compos. 31 (2010) 946–955. doi:10.1002/pc.20879.

[21] M. Jiménez, J. González-Benito, A.J. Aznar, J. Baselga, Degradación hidrolítica de recubrimientos polisiloxánicos de fibras de vidrio, 39 [4] (2000) 425–430.

[22] P. Hosseini, R. Hosseinpourpia, A. Pajum, M.M. Khodavirdi, H. Izadi, A. Vaezi, Effect of nano-particles and aminosilane interaction on the performances of cement-based composites: An experimental study, Constr. Build. Mater. 66 (2014) 113–124. doi:10.1016/j.conbuildmat.2014.05.047.

[23] F. Švegl, J. Šuput-Strupi, L. Škrlep, K. Kalcher, The influence of aminosilanes on macroscopic properties of cement paste, Cem. Concr. Res. 38 (2008) 945–954. doi:10.1016/j.cemconres.2008.02.006.

[24] J. González-Benito, J. Baselga, A.J. Aznar, Microstructural and wettability study of surface pretreated glass fibres, J. Mater. Process. Technol. 92–93 (1999) 129–134. doi:10.1016/S0924-0136(99)00212-5.

[25] M. Welter, M. Schmücker, K.J.D. MacKenzie, Evolution of the fibre-matrix interactions in basalt-fibre-reinforced geopolymer-matrix composites after heating,

J. Ceram. Sci. Technol. 6 (2015) 17–24. doi:10.4416/JCST2014-00034.

[26] S.I. Gutnikov, M.S. Manylov, Y. V. Lipatov, B.I. Lazoryak, K. V. Pokholok, Effect of the reduction treatment on the basalt continuous fiber crystallization properties, J. Non. Cryst. Solids. 368 (2013) 45–50. doi:10.1016/j.jnoncrysol.2013.03.007.

[27] L.T. Zhuravlev, The surface chemistry of amorphous silica. Zhuravlev model, Colloids Surfaces A Physicochem. Eng. Asp. 173 (2000) 1–38. doi:10.1016/S0927-7757(00)00556-2.

[28] J. Gonzalez-Benito, J.C. Cabanelas, A.J. Aznar, M.R. Vigil, J. Bravo, J. Baselga, Surface characterization of silanized glass fibers by labeling with environmentally sensitive fluorophores, J. Appl. Polym. Sci. 62 (1996) 375–384. doi:10.1002/(SICI)1097-4628(19961010)62:2<375::AID-APP12>3.3.CO;2-V.

[29] A.Larena, J.Martínez Urreaga, M.U. de la Orden, Effects of previous leaching with hydrochloric acid of E-glass short fibre on the fibre reaction with chlorosilanes, Mater. Lett. 12 (1992) 415–418.

[30] D. Olmos Díaz, Materiales compuestos epoxi-sílice: estudio de interfases, (2003) 247. http://hdl.handle.net/10016/11351.

[31] C.-H. Chiang, H. Ishida, J.L. Koenig, The structure of γ-aminopropyltriethoxysilane on glass surfaces, J. Colloid Interface Sci. 74 (1980) 396–404. doi:10.1016/0021-9797(80)90209-X.

CHAPTER 5

STUDY OF THE HYDROLYTIC DEGRADATION PROCESS OF THE POLYSILOXANE COATING OF BASALT FIBERS

CHAPTER 5
STUDY OF THE HYDROLYTIC DEGRADATION PROCESS OF THE POLYSILOXANE COATINGS OF BASALT FIBERS

Abstract

Basalt fiber surfaces were modified using different silane aqueous solutions to generate a variety of polyorganosiloxane coatings. After removing the commercial coating of the fibers by calcination and subsequent activation processes, polysiloxanes were grafted on the fiber surfaces. Three aqueous solutions were used for the silanization: i) γ-aminopropyltriethoxysilane, APTES; ii) γ -aminopropylmethyldiethoxysilane, APDES, and iii) a mixture of 50% by weight of both APTES+APDES. The silanized fibers were chemically labeled with fluorescein isothiocyanate to be immersed afterwards in different aqueous solutions (pH=7 and pH=10) to study the hydrolytic degradation of the polysiloxane coatings. The hydrolysis phenomena were monitored by steady state fluorescence at different temperatures to subsequently study the kinetics of the process. The hydrolysis process was also studied by monitoring the pH of the solution in which the silanized fibers were immersed as a function of time. The data obtained from fluorimetry were fitted to an integrated expression arising from a first order kinetic process, which allowed estimation of the activation energies of the hydrolytic degradations. The results indicated that although the hydrolytic rate of the polysiloxane coatings increased in the order APDES < APTES+APDES < APTES, differences in the mechanism were not the cause of that order; the initial concentration of siloxane bonds able to be hydrolyzed was responsible.

5.1. Introduction

It is well known that the performance of composite materials is greatly dependent on the interphases formed between the materials used as reinforcements and matrices [1,2]. In fact, the properties of composite materials are strongly influenced by the type of adhesion between the reinforcement and the matrix. Therefore, the surface modification of reinforcements through special treatments represents one of the most common strategies to improve the adhesion or interphase properties in composites [3,4]. In particular, when silicic materials are used to reinforce other materials such as plastics and cement-based materials, their surface treatments mainly consist of the application of silane coupling agents [5–7]. Among those, as was previously described in Chapters 2 and 4, difunctional organosilicon silane compounds of general formula $Y\text{-}Si(X)_3$ are the most commonly used.

Silane coupling agents are usually very effective in improving the interfacial region generated in the type of composites mentioned above [8–10]. In fact, a chemical bond between the constituents of the composite is usually formed, creating an interphase with intermediate properties between the reinforcement and the matrix, which may favor the load transfer from the matrix to the reinforcement through the interphase. In addition, it is generally stated that silane surface treatments of reinforcements provide a relatively water resistant bond [4,11,12].

However, the siloxane bond is a hydrolyzable bond which is highly dependent on pH [13,14]. To obtain information about possible hydrolytic degradation processes occurring at the interphases of these composites, a thorough study would be necessary to fully understand the final performance of the materials. One of the agents that might cause an interface failure is water: through a simple hydrolytic process, water may lead to a weaker interaction between the reinforcement and the matrix, poorer transmission of loads between them and, consequently, higher probability of a catastrophic mechanical failure.

In previous works, studies of the water effect on glass fiber/silane coupling agent interfaces were conducted [11,15]. It was stated that when glass fibers are treated with hydrolyzed silane solution, multilayers of the silane coupling agent (in particular when a trifunctional silane is used) are deposited on the fiber surface: the first is a chemically reacted layer, the second a chemisorbed layer and the third a physisorbed layer. It was shown that the

chemically reacted layer was characterized by a higher stability against hot water extraction, which conferred the silanized substrate with a high resistance to hygrothermal attack. The chemisorbed layer mainly consisted of oligomers with higher functionality in terms of siloxane bond formation. This three-dimensional or cross-linked layer possesses better resistance to hydrolysis. Generally, it could be extracted by boiling water after prolonged immersion. The outer part of the coating, the physisorbed layer, consisted of oligomers that did not form part of the siloxane network and that were easily hydrolyzed, able to be extracted with water even at room temperature [11,15,16].

Taking into account the abovementioned characteristics, it is reasonable to think that the behavior under the effect of water and temperature could be different depending on the chemical structures. Therefore, controlling the structure of the coating by the use of different silane systems grafted on the fibers may be a way of controlling hydrolysis phenomena. Consequently, a deep knowledge and a good understanding of the chemical mechanism of the hydrolytic degradation of silane-based coatings are crucial to advance materials design and processing technologies to improve the performance of materials against hydrothermal failure. All of these aspects are especially important in the case of fiber reinforced cement-based composites, since their manufacture implies the mixture of their components with water.

Since cement matrices are characterized by alkaline pH [17,18] to evaluate the polysiloxane coatings degradation under the effect of water, understanding their behavior in alkaline environments should be also of primary importance.

Due to the growing interest in understanding structural changes of the silane coupling agent on silicic surfaces - to consequently study the molecular mechanism of the hydrolytic degradation process - several studies regarding these questions were previously conducted. In particular, different techniques (such as radioisotope techniques, laser Raman spectroscopy, ion scattering spectroscopy (*ISS)*, secondary ion mass spectrometry (*SIMS)*, and Fourier transform infrared spectroscopy (*FTIR*) were employed for that purpose [11].

D. Olmos et al. [19] monitored the hydrolytic degradation of different polyorganosiloxane coatings of silica microfibers by using fluorimetry. The method consisted of labeling the

siloxane-based coatings with a fluorescent dye and then monitoring the fluorescence emission of an aqueous solution in which the microfibers were immersed. Compared to others, this experiment is a simple and especially sensitive method because fluorimetry allows detection of very small concentrations of the hydrolysis products.

In the present work, basalt fibers (potential reinforcements of cement-based materials) were modified with different aminosilanes to generate a variety of polyorganosiloxane coatings. After that, they were labeled with fluorescein isothiocyanate (FITC). Once the fibers were labeled with fluorescein groups, the hydrolytic degradation of the polysiloxane coatings was monitored by fluorimetry. The influences of pH and temperature on the kinetics of the hydrolytic process were also studied.

5.2. Experimental

5.2.1. Materials

Basalt continuous filaments with 17 µm mean diameter (Incothelogy GmbH) were used after being chopped to a length of approximately 6.4 mm. They were supplied with a commercial coating compatible with cement and natural hydraulic lime (NHL) matrices. Two silanes, γ-aminopropyltriethoxysilane and γ-aminopropylmethyldiethoxysilane supplied by ABCR GmbH & Co. KG, were used to silanize the basalt fibers to obtain different surface coatings. Fluorescein isothiocyanate isomer I supplied by Sigma-Aldrich, was used as fluorescent label. To prepare solutions of FITC, *N,N-dimethylformamide* (DMF) (Sigma-Aldrich) was used as solvent. It is important to remember that fluorescein in aqueous solution occurs in cationic, neutral, anionic and dianionic forms that makes its absorption and fluorescence properties strongly pH-dependent [20] . For this reason, the experiments were carried out at controlled pH by using buffer solutions of neutral pH (potassium dihydrogen phosphate, pH= 7.0 ± 0.02 at 20 ºC, Scharlau) and pH 10 (pH=10.0 ± 0.05 at 20 ºC, Panreac Química, S.A., Barcelona, Spain).

5.2.2. Samples Preparation

Considering that the commercial fibers are already commercially coated, a cleaning of their surface is necessary before applying a new coating in a controlled way. Indeed, a surface pretreatment (calcination and activation processes) of the received basalt fibers and

a silanization process were carried out according to the methods described in section 4.2.2 of Chapter 4. After the silanization with aqueous solutions of i) APTES, ii) APDES and iii) a mixture of 50% by weight of both APTES and APDES, the coated fibers were labeled as follows: 0.4 g of each sample was immersed in 25 mL of FITC (10^{-4} M) solution in DMF and stirred for 20 min at room temperature.

Finally, the labeled samples were washed with dimethylformamide (DMF) to remove all of the physisorbed or nonreacted FITC and then vacuum dried for at least 3 h at 40 ºC [19,21,22]. The surface characterization of the modified basalt fibers was already carried out in Chapter 4 (see section 4.3.2).

5.2.3. Instrumental Techniques

Degradation of the silane coatings was monitored by pH measurements at room temperature by using a Lab 745 pH-meter (SI Analytics) as described in Chapter 3 (section 3.2.2). In particular, 0.35 g of silanized basalt fibers were introduced in a cellulose paper bag and hung using a nylon thread to be immersed in a beaker containing 30 mL of distilled and deionized water. The aqueous solution was continuously stirred while pH values were measured as a function of time for 23 hours.

After the experiments, the water was evaporated from the remaining solutions and the residues were analyzed by Fourier transform infrared spectroscopy (FTIR) in the transmission mode using an FTIR Spectrum GX (Perkin-Elmer). FTIR spectra were recorded in the range of 400-4000 cm^{-1} from the average of 20 scans with a resolution of 4 cm^{-1}.

On the other hand, the hydrolysis degradation was studied by steady state fluorescence spectroscopy using an Edinburgh Instruments Co. fluorimeter. However, before monitoring the coating hydrolyses, spectra of the FITC labeled fibers and activated fibers (without coating) were obtained via front face excitation using a solid sample holder placed at an angle of 15º with respect to the excitation beam. Every spectrum was recorded between 500–700 nm, setting the excitation wavelength at 483 nm, with a dwell time of 0.1 s and excitation and emission slits at 10 and 7 nm.

The hydrolytic degradation experiment of the polyorganosiloxane coatings, was described in detail in Chapter 3 (see section 3.2.2). The experiments were carried out at different

temperatures (25 ºC, 35 ºC, 40 ºC and 45 ºC) and pH (7 and 10). It must be pointed out that the experiments at pH=10 were performed only at temperature of 40 °C.

Fluorescence spectra were recorded for 10 h between 490–700 nm, setting the excitation wavelength at 483 nm, the dwell time at 0.1 s and excitation and emission slits at 4 nm. Finally, the hydrolysis was studied from the representations of the integrated fluorescence intensity (area of the fluorescence spectra) as a function of the immersion time.

5.3. Results and Discussion

5.3.1. pH Measurments

To monitor the processes occurring during the immersion of the modified basalt fibers in pure water, the pH of the aqueous solution was measured as a function of the immersion time (Fig. 1).

The three plots showed similar profiles, although with slope changes occurring at different immersion times depending on the type of aminosilane grafted on the fibers. In general, the plots can be divided into two regions: in the first one, the pH increases due to the protonation of amino groups, and in the second one, the pH decreases due to the siloxane hydrolysis and subsequent silanol generation. Taking into account that both phenomena might occur simultaneously and that they have opposite tendencies in terms of pH, the appearance of a maximum should indicate the point when the pH variation begins to be controlled by the hydrolytic process.

By considering the immersion times at the maxima of the pH plots in Figure 1, an order for the hydrolytic degradation rate may be inferred for the coatings under study: APTES > APTES+APDES > APDES.

Here, it was considered that the faster the hydrolytic process, the sooner it will control the pH variation of the solution.

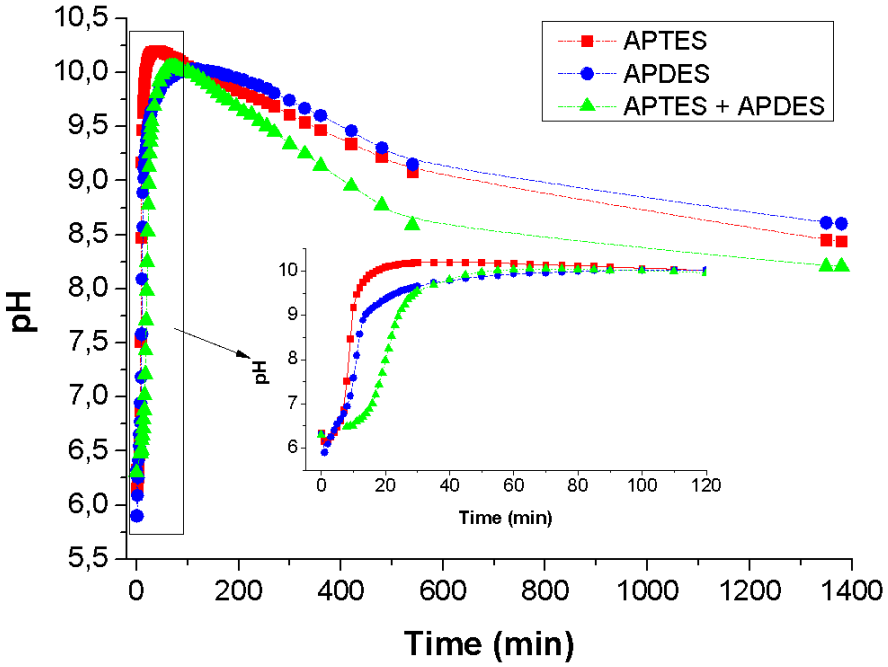

Figure 1. pH measurements of the silanized basalt fibers immersed in distilled and deionized water.

To prove that the coatings were removed from the basalt fiber surfaces due to the hydrolytic fragmentation, FTIR spectra were recorded from the three residues remaining after evaporating the water (Fig. 2). The FTIR spectra showed the characteristic absorption bands (Table 1) attributed to the polyorganosiloxane generated on the fiber surfaces. In particular, in the high-energy region of the FTIR spectra (3800-2800 cm^{-1}), some characteristic bands of the different aminosilanes are present: the N-H stretching of the amino groups and the C-H stretching bands of the methylene, CH_2 and methyl CH_3 groups. These results are in agreement with the FTIR spectra obtained for the three coatings on the fibers and reported in the section 4.3.2 of Chapter 4, indicating that fragments of the polyorganosiloxane coatings were incorporated in the solution due to hydrolysis during the water immersion of the fibers.

However, this method allows only a qualitative analysis of the hydrolytic process to be considered since this phenomenon is expected to be dependent on the pH of the solution which, as it was shown, is continuously changing. For this reason, an additional hydrolytic phenomena study method should be considered.

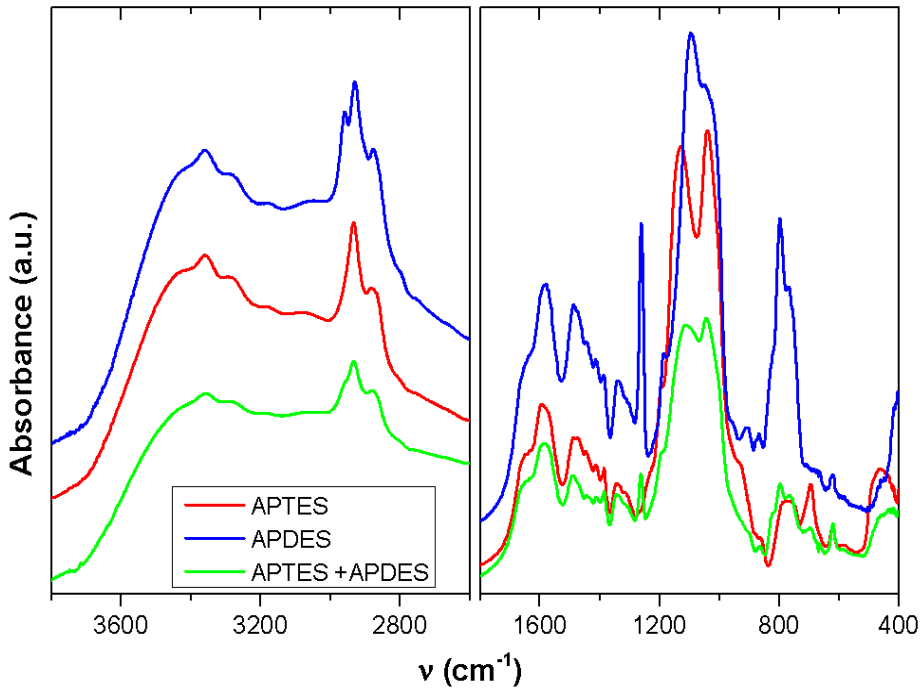

Figure 2. FTIR spectra of the residues obtained from the pH experiment.

Table 1. Absorption Bands of Aminosilanes [23,24].

ν (cm^{-1})	***Absorption bands of Aminosilane***
3400	ν (O-H)
3400-3300	ν_{as} (N-H)
2970-2960	ν_{as} (C-H) (CH_3)
2930-2920	ν_{as} (C-H) (CH_2)
1600	δ (N-H)
1483	δ (CH_2)
1450	δ (CH_2)
1440	δ (CH_3)
1410	δ (Si-CH_2)
1380	δ (CH_3)
1260	ν (Si-C)
1160	ρ (CH_3)
1100	ν_{as} (Si-OSi)
1100	ν_{as} (Si-OC)
1000	ν_{as} (Si-OSi)
950	δ (Si-OH)

5.3.2. Fluorescence Experiments

Figure 3 displays the normalized fluorescence spectra of the FITC when chemically bonded to the silanized basalt fibers.

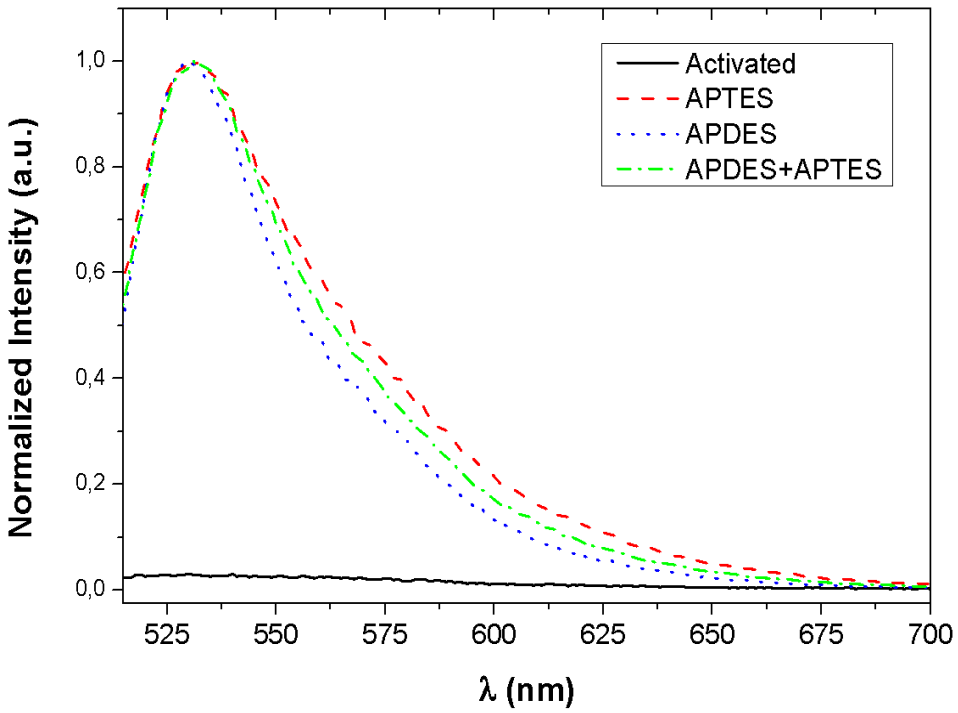

Figure 3. Normalized fluorescence spectra of activated and labeled silanized basalt fibers

In all cases, a broad band centered at approximately 530 nm is observed - in accordance with the fluorescence emission characteristics of FTIC provided by the supplier of the dye --with a fluorescence maximum at a wavelength of λ_{max} = 520 nm and pH = 9. However, slight variations can be observed throughout the entire profile of the fluorescence spectrum depending on the nature of the coating. It is observed that higher silane functionality (functionality order: APTES > APTES+APDES > APDES) corresponds to broader fluorescence bands. This result may be explained by considering the more heterogeneous surroundings for the fluorophore when using a silane with higher functionality. In principle, different crosslinking degrees can be obtained in a silane with high functionality regions, leading to different environments for the FITC fluorescent label or more heterogeneity at a molecular scale. In Figure 3, the emission spectrum of the activated fibers is also added as a control, evidencing an emission that can be considered negligible with respect to the fluorescence emission from the silanized fibers modified with FITC.

5.3.3. Hydrolysis Monitoring by Fluorimetry

In Figure 4, the integrated fluorescence intensity of the aqueous solutions (pH = 7) in which the fibers were immersed is represented as a function of the immersion time for all the studied samples and at different temperatures.

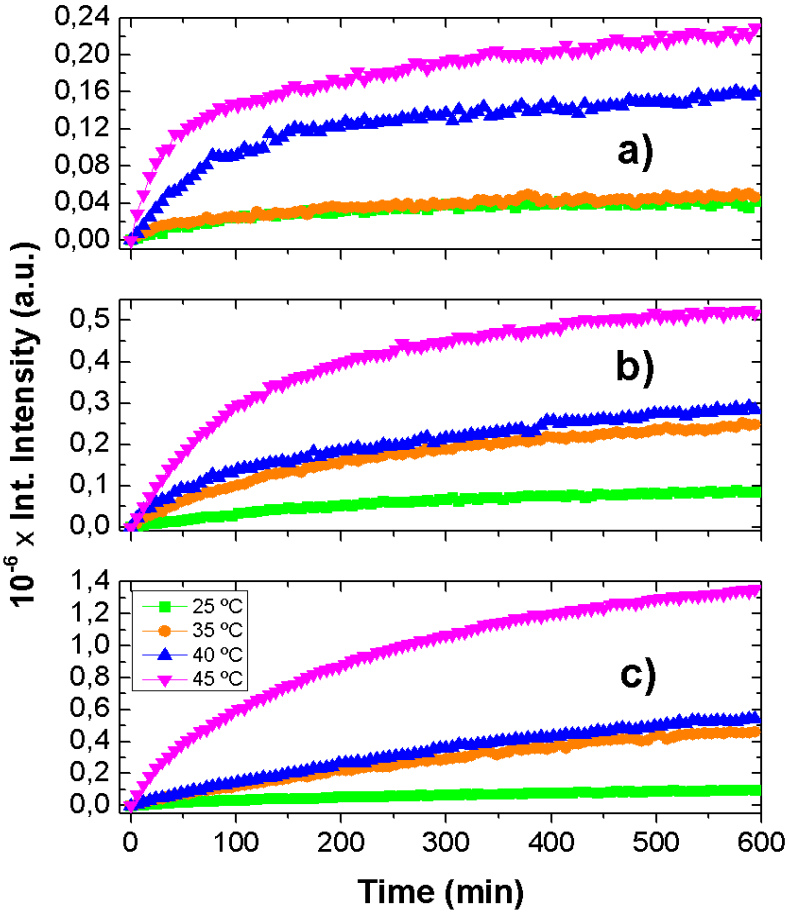

Figure 4. Integrated fluorescence intensity as a function of immersion time of the aqueous solution (pH = 7) in which the modified fibers were immersed: a) APTES, b) APTES+APDES and c) APDES.

In all cases, the fluorescence intensity quickly increases and then stabilizes, reaching a plateau. It is observed that at the beginning of the process, the slopes of the curves are different depending on the nature of the polyorganosiloxanes and the temperature. In terms of the coating natures, the slopes increase in the following order: APDES < APDES+APTES < APTES. If a higher slope is associated with a faster hydrolytic process, the fluorescence results are in accordance with the results obtained from the pH measurements. However, in this case the measurements are obtained at constant pH

because a buffer solution was used. In addition, a higher temperature is translated into a higher hydrolytic rate, as expected. The effect of the increase of the temperature, in fact, promotes the breakage of a higher number of siloxane bonds.

Considering that more amino groups are susceptible to reaction with the FITC moiety in the case of the APTES coating, one would expect increased fluorescence intensity in the aqueous solution after hydrolysis during the fluorescence experiments. However, the opposite result was observed. Apart from considering that total fluorescence can be dependent on several external factors such as lamp intensity, another possible explanation may be found in the consideration of lower yield of thiourea formation due to steric hindrance. A high crosslinking degree in the polysiloxane coating may lead to reduced accessibility to the amino groups and concomitant decreased FITC attachment. In fact, this is the expected situation for the γ-aminopropyltriethoxysilane chemical structure proposed by Wang et al. after being reacted on silica-based surfaces [16,25]. As those authors described, the structure of the γ-aminopropyltriethoxysilane is characterized by three different layers with different functionality in terms of the cross-linking degree. The outer part, which consists of a small molecular oligomer, is presumably the most accessible to allow the reaction between the amino groups and the isothiocyanate group of the fluorescent moiety. In contrast, a more linear and open chemical structure expected for the difunctional silane, APDES, should allow easier reaction with the fluorescent moiety. Therefore, the results in terms of total intensity may be interpreted simply according to the FITC concentration. Higher amounts of FITC fluorophores should yield higher fluorescence intensity after hydrolysis without influencing the hydrolysis mechanism, which should only depend on the nature of the siloxane coating and pH.

5.3.4. Kinetic Study of the Hydrolytic Degradation Process

To perform a kinetic study of the hydrolytic degradation process of the coatings of the basalt fibers, the following equilibrium reaction is assumed for the hydrolysis of the siloxane bonds in the polyorganosiloxanes:

$$\text{Si-O-Si} + H_2O \rightleftharpoons 2\ \text{Si-OH} \qquad (1)$$

where Si-O-Si is the hydrolyzable siloxane bond, and Si-OH is the silanol group formed after the hydrolysis.

Furthermore, another assumption is to consider that the direct and the reversed reactions of the equilibrium represented by the equation (1) are first order reactions. On the other hand, if the initial concentration of the reactant is named "a" or $[Si\text{-}O\text{-}Si]_0$ = "a", and the amount of siloxane reacted "x", then the concentration of the siloxane groups at a given reaction time will be $[Si\text{-}O\text{-}Si]_t = (a - x)$ and the concentration of silanol groups generated will be $[Si\text{-}OH]_t = 2x$.

Consequently, for a first order reaction, the direct reaction rate could be expressed by $v_1 = k_1 [Si\text{-}O\text{-}Si]_t = k_1(a - x)$ while the reversed reaction rate would be $v_2 = k_2[Si\text{-}OH]_t = k_2\ 2x$ and, therefore, the hydrolysis rate should be described by the difference between the direct reaction rate and the reversed reaction rate, $v_1 - v_2$. If that hydrolysis rate is expressed as the variation of the silanol production as a function of time, $d[SiOH]_t/dt$, the expression for the hydrolysis rate would be described by the equation (2):

$$v = \frac{1}{2}\frac{d[Si-OH]_t}{dt} = v_1 - v_2 = k_1\,(a - x) - 2k_2x \qquad (2)$$

Taking into account that there is no change in the silanol production when the equilibrium is reached, $d[SiOH]_t/dt = 0$ and that the siloxane reacted is named as x_e, the equation (2) could be written as:

$$\frac{1}{2}\frac{d[Si-OH]_t}{dt} = 0 = k_1(a - x_e) - 2k_2x_e \qquad (3)$$

By rearranging equation (3), an equilibrium constant, K_c, could be obtained as the ratio between the direct reaction rate and the reversed reaction rate, k_1/k_2:

$$\frac{k_1}{k_2} = \frac{2x_e}{a - x_e} = K_c \qquad (4)$$

Furthermore, by solving k_2 from (4) and replacing it in (2), it can be written:

$$\frac{d[Si-OH]_t}{dt} = k_1 \frac{a}{x_e} (x_e - x) \quad (5)$$

and, after variables separation in equation (5) and the corresponding integration, equation (6) is obtained:

$$k_1 \cdot t = \frac{x_e}{a} \ln \frac{x_e}{x_e - x} \quad (6)$$

If the fluorescence intensity, *I*, is proportional to the number of fragments released from the coating by the hydrolysis, and these fragments are proportional to the concentration of siloxane groups that have been reacted at a certain time, x, then fluorescence intensity, *I*, should be proportional to x.

$$x = D \cdot I \quad (7)$$

where "D" is a constant. Introducing this relation into the expression (6), it can be obtained:

$$k_1 \cdot t = \frac{x_e}{a} \ln \frac{x_e}{x_e - D \cdot I} \quad (8)$$

After taking exponentials in Eq. (8) and rearranging an expression for fluorescent intensity as a function of reaction time is obtained:

$$I = \frac{x_e}{D} - \frac{x_e}{D} e^{-\frac{aK_1 t}{x_e}} \quad (9)$$

Since for every sample x_e is a constant, eq. (9) can be simplified by

$$I = I_e - I_e e^{-ct} \quad (10)$$

where I_e and c are constants that only depend on temperature:

$$I_e = \frac{x_e}{D} \text{ and } c = \frac{aK_1}{x_e} \quad (11)$$

To test the effectiveness of the mechanism proposed, the data of the fluorescence intensity as a function of reaction or immersion time were fitted by the use of equation (10). Regardless of the sample and temperature, the fitting was quite close as seen in Figure 5, where as an example, the fits for the samples at 25 ºC are shown. Therefore, as a first approximation, in the presence of water the degradation process of the three coatings studied can be described by a hydrolytic equilibrium reaction where both the direct and reversed reactions are first order reactions.

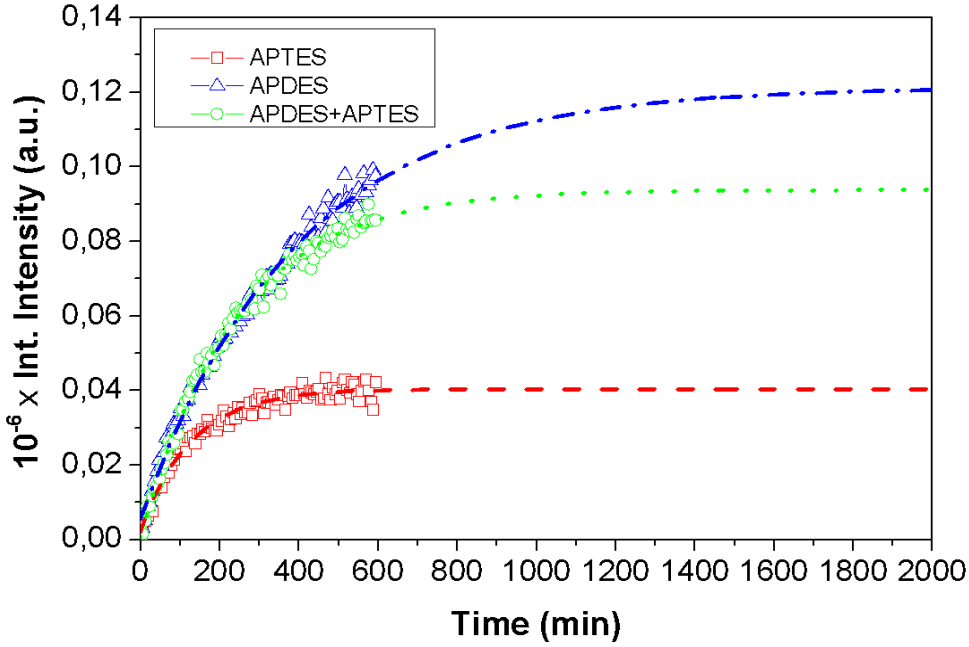

Figure 5. Examples of fluorescence data fitting by the integrated rate equation (9).

Considering this and accepting the mechanism proposed for the hydrolytic degradation, an estimation of the required time to reach equilibrium can be made. The criterion chosen might be the time for which the fluorescence intensity of the fitted curve does not change by more than 1%. Using this criterion, for different temperatures, the degradation times when the equilibrium was reached for all the samples were obtained (Table 2).

Table 2. Estimated hydrolytic degradation times at pH = 7 when equilibrium is reached.

Temperature	t_{APTES} *(min)*	$t_{APTES+APDES}$ *(min)*	t_{APDES} *(min)*
25 ºC	115	144	156
35 ºC	117	140	170
40 ºC	113	125	166
45 ºC	103	122	137

If faster hydrolytic degradation is translated to shorter time to reach the equilibrium, the hydrolytic degradation rates of the coatings could be ordered as follows: APTES > APDES+APTES > APDES. In principle, this result might have two possible explanations: i) different mechanism of the hydrolytic process as a function of the polyorganosiloxane structure and ii) differences in the initial concentration of the hydrolyzable Si-O-Si bonds. The last explanation is based on the consideration that the concentration of Si-O-Si bonds is expected to be dependent on the amount of attached silane and, especially, the crosslinking degree which, in fact, will be favored with the functionality of the silane. Therefore, more material quantity and greater crosslinking degree is expected when APTES is used to coat the fibers (Figure 6). Alternatively, when APDES (with a linear structure) solution is applied to the basalt fibers, reduced amounts of attached material and siloxane bonds are expected (Figure 6). The results from a deep characterization of the basalt fibers modified with APTES and APDES are in good agreement with the abovementioned conclusions (see section 4.3.2 of Chapter 4).

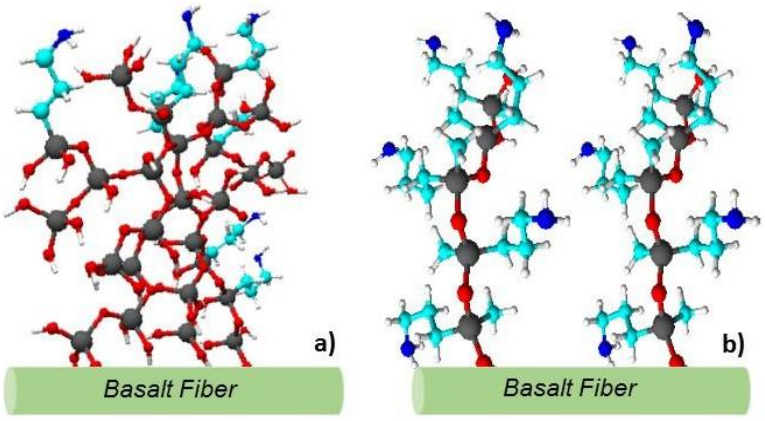

Figure 6. Expected chemical structures of the basalt fiber coatings after the treatments with a) APTES and b) APDES aqueous solutions.

To evaluate whether a change of the mechanism is the main contribution to the variation in the hydrolytic degradation rate, the activation energy (Ea) values were estimated from the curve fittings as follows. From equation (7) it can be written that:

$$x_e = D \cdot I_e \tag{12}$$

where I_e is the fluorescence intensity at equilibrium that depends on temperature, $I_e(T)$. On the other hand, the k_1 was assumed as an Arrhenius-like kinetic constant

$$k_1 = Ae^{\frac{-E_a}{RT}} \tag{13}$$

where A is the pre-exponential factor, R the general gas constant, T the absolute temperature and E_a the activation energy of the process. Combining the equations (11), (12) and (13), it can be written:

$$c(T) = \left(\frac{a}{D}\right)\frac{1}{I_e(T)}Ae^{-\frac{E_a}{RT}} \tag{14}$$

Since c(T) and $I_e(T)$ values can be obtained as fitting parameters by using the fitting function (10), activation energies can be obtained from the ratios between expressions such as the equation (14) at two different temperatures, T_i and T_j, respectively:

$$\frac{c(T_i)}{c(T_j)} = \frac{I_e(T_j)}{I_e(T_i)}e^{-\frac{E_a}{R}\left(\frac{1}{T_i}-\frac{1}{T_j}\right)} \tag{15}$$

$$E_a = \frac{R}{\left(\frac{1}{T_i}-\frac{1}{T_j}\right)}Ln\left[\frac{I_e(T_j)}{I_e(T_i)}\cdot\frac{c(T_j)}{c(T_i)}\right] \tag{16}$$

Considering that four temperatures were studied for each sample, six combinations of pairs of temperatures in expression (16) can be used to obtain six activation energies. Therefore, an apparent activation energy should be obtained from the average of those six values. Table 3 gathers the average values of the average activation energies obtained for the hydrolytic degradation of the three coatings under study.

Table 3. Averaged activation energy *(Ea)* values for the hydrolytic degradation of the three coatings under study.

Coating	Ea *(kcal/mol)*
APTES	24 ± 15
APDES	29 ± 17
APTES + APDES	22 ± 5

In principle, all of the results are in agreement with others reported in previous studies where an activation energy of 23.6 kcal/mol was obtained for the hydrolysis of siloxane bonds.

Taking into account the error in the values of Table 3, it can be concluded that the activation energy of the hydrolytic process is the same for the three coatings, therefore suggesting that the corresponding chemical mechanism is the same. It follows that another reason exists for the different hydrolytic degradation rates observed for the three coatings.

In general, regardless of the reaction order, the rate increases with the initial concentration of the reactants; therefore, it is reasonable to assume that the rate of the hydrolytic process was dependent on the initial concentration of siloxane bonds. From the results obtained by thermogravimetric analysis (TGA) for the same studied systems and showed in section 4.3.2 of Chapter 4, it was possible to use the weight loss and molecular weight of the silane to estimate the number of moles of siloxane bonds, n_{SioSi}, susceptible to being hydrolyzed (in the case of the APTES + APDES mixture, a mean value between the molecular weights of the two silanes was used) (Table 4). The estimated values of the number of moles are shown in Table 4.

Table 4. Estimated values for the number of moles of Si-O-Si hydrolyzed bonds.

Coating	$n^o_{Si\text{-}O\text{-}Si}$ *(mol)*
APTES	4.7×10^{-5}
APTES+APDES	3.5×10^{-5}
APDES	4.5×10^{-6}

Assuming a first order reaction for the direct reaction of the hydrolytic process, at a hydrolytic reaction time, t = 0, the initial reaction rate, v_o, must be directly proportional to the initial concentration of siloxane bonds or the initial number of moles at constant volume:

$$v_o = \left(\frac{dI}{dt}\right)_{t=0} = Constant \cdot [SiOSi]_o \quad (17)$$

where the values of v_o can be obtained from the initial slope of the curves of integrated fluorescence intensity as a function of immersion time, while the values of the initial number of moles of siloxane bonds can be taken from Table 4. If there were a clear dependence between the initial concentration of siloxane bonds and the hydrolytic rate, one would expect the same values for the ratios between the initial reaction rates for two coatings and the ratios between the corresponding initial numbers of moles of siloxane bonds.

$$\frac{v_o(APTES)}{v_o(APDES)} = \frac{n^o_{SiOSi}(APTES)}{n^o_{SiOSi}(APDES)} \quad (18)$$

where $n^o_{SiOSi}(coating)$ represents the initial number of moles of siloxane bonds of a particular polysiloxane coating.

For a better comparison, the ratios between initial reaction rates and the ratios between initial numbers of moles are compiled in Table 5. Their behaviors are coincident, suggesting that the initial concentration of siloxane bonds is the primary reason for the different hydrolytic degradation rates observed for the coatings under study.

Table 5. Relationship between the concentration Si-O-Si bonds and the hydrolytic degradation rate.

Coating	$n^o_{Si\text{-}O\text{-}Si} / n^o_{Si\text{-}O\text{-}Si}$	$(dI/dt)_{Coating\ i} / (dI/dt)_{Coating\ j}$
APTES/APDES	10.4	9.2
APTES+APDES/APDES	7.8	4.2
APTES/APTES+APDES	1.3	1.9

5.3.5. Polysiloxane Coatings Degradation in Alkaline Environment (pH =10)

In Figure 7 it is possible to observe the influence of the pH on the polysiloxane coatings degradation at 40 °C. It is found that, in all cases the fluorescence intensity rapidly increases, then stabilizes and finally seems to reach a plateau regardless the pH.

Paying attention to the slopes of the first linear region of the curves in Figure 7, it could be said that, as a first approximation, the order in terms of coatings degradation rate is:

APDES < APTES+APDES < APTES. These results agree with the order observed when the hydrolysis experiments were carried out at pH = 7 (see Figure 4).

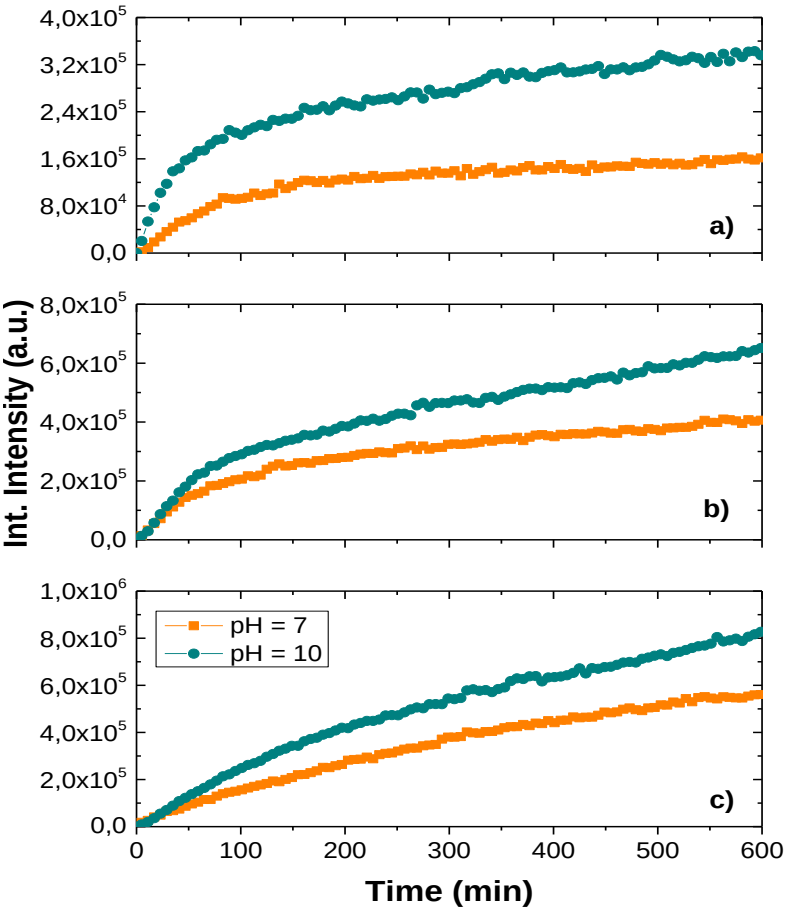

Figure 7. Influence of the pH on the polysiloxane coatings degradation at 40 °C: a) APTES, b) APTES+APDES and c) APDES.

Additionally, considering the integrated rate equation (9), it was possible to make an exponential fit for each curve when the pH was set at 10. These results suggest that the kinetics model proposed is useful to describe the hydrolytic degradation process independently on the pH.

Consequently, the hydrolytic degradation times, when the equilibrium was reached at pH = 10, were also estimated as described in section 5.3.4. Results are shown in Table 6.

Table 6. Estimated hydrolytic degradation times at pH = 10 when equilibrium is reached.

	t_{APTES} *(min)*	$t_{APTES+APDES}$ *(min)*	t_{APDES} *(min)*
pH = 10	110	138	160
**** pH = 7***	113	125	166

* Table 2.

Considering that a faster hydrolytic degradation should lead to a shorter time to reach the equilibrium, the results obtained point out that the hydrolytic degradation rates of the coatings studied at pH=10 follow the order: APTES > APTES+APDES >APDES. The same order was observed when modified fibers were immersed in the aqueous solution at pH=7 (see Table 2). Finally, it can be observed (Table 6) that there are not significant differences in terms of hydrolysis rates as a function of the pH's studied.

5.4. Conclusions

The use of fluorescein isothiocyanate fluorescence is an appropriate method to evaluate the hydrolytic degradation of exceedingly small concentrations of polyorganosiloxane coatings grafted on the basalt fibers. The kinetic mechanism of the hydrolysis process was proposed in this work, which allowed information about the activation energy of the three systems studied to be obtained. Furthermore, an evaluation of the equilibrium degradation times for the different polyorganosiloxanes is determined. It must be pointed out the goodness of the kinetic model proposed for the hydrolytic degradation process independently on the pH used. The results obtained with different systems and different measurements are in good agreement.

These results demonstrate that the mechanism of the hydrolytic process is very similar for the three systems studied. Nevertheless, some differences in the rate of the hydrolytic degradation process are observed. Indeed, the hydrolytic degradation rate is related to the initial concentration of the Si-O-Si bonds and, consequently, to the number of the hydrolyzed siloxane bonds. This number is higher when a silane with a cross-linked structure is used. Furthermore, the hydrolytic degradation of the silane coupling agents quickens depending on the increase of the siloxane crosslinking degree.

It could be assumed that one method to reduce the rate of hydrolytic degradation at the interface in the fiber reinforced cement-based composites would be to minimize the degree

of coating. A polyorganosiloxane with a lower crosslinking degree and correspondingly reduced amount of Si-O-Si bonds, such as the APDES coating, could be the most effective strategy to resist possible water attack mainly in the alkaline environment characteristic of the cement matrix.

References

[1] J.-K. Kim, Y.-W. Mai, Engineered Interfaces in Fiber Reinforced Composites, 1st Editio, 1998. doi:https://doi.org/10.1016/B978-008042695-2/50000-2.

[2] M.J. Salkind, The Role of Interfaces in Fiber Composites, in: Surfaces Interfaces II, 1968: pp. 417–445. doi:10.1007/978-1-4757-0178-4_14.

[3] A.T. DiBenedetto, Evaluation of fiber surface treatments in composite materials, Pure Appl. Chem. 57 (1985) 1659–1665. doi:10.1351/pac198557111659.

[4] N. Suzuki, H. Ishida, A Review on the Structure and Characterization Techniques of Silane/Matrix Interphases, Macromol. Symp. 108 (1996) 19–53. doi:https://doi.org/10.1002/masy.19961080105.

[5] Y. Xie, C.A.S. Hill, Z. Xiao, H. Militz, C. Mai, Composites : Part A Silane coupling agents used for natural fiber / polymer composites : A review, Compos. Part A. 41 (2010) 806–819. doi:10.1016/j.compositesa.2010.03.005.

[6] S.J. Park, J.S. Jin, J.R. Lee, Influence of silane coupling agents on the surface energetics of glass fibers and mechanical interfacial properties of glass fiber-reinforced composites, J. Adhes. Sci. Technol. 14 (2000) 1677–1689. doi:10.1163/156856100742483.

[7] S. Shokoohi, A. Arefazar, R. Khosrokhavar, Silane coupling agents in polymer-based reinforced composites: A review, J. Reinf. Plast. Compos. 27 (2008) 473–485. doi:10.1177/0731684407081391.

[8] J.G. Iglesias, J. González-Benito, A.J. Aznar, J. Bravo, J. Baselga, Effect of Glass Fiber Surface Treatments on Mechanical Strength of Epoxy Based Composite Materials, J. Colloid Interface Sci. 250 (2002) 251–260. doi:10.1006.

[9] D. Olmos, J. González-Benito, Visualization of the morphology at the interphase of glass fibre reinforced epoxy-thermoplastic polymer composites, Eur. Polym. J. 43 (2007) 1487–1500. doi:10.1016/j.eurpolymj.2007.01.004.

[10] M. Afroz, I. Patnaikuni, S. Venkatesan, Chemical durability and performance of modified basalt fiber in concrete medium, Constr. Build. Mater. 154 (2017) 191–203. doi:10.1016/j.conbuildmat.2017.07.153.

[11] H. Ishida, J.L. Koenig, A Fourier-Transform Infrared Spectroscopic Study of the Hydrolytic Stability of Silane Coupling Agents on E-Glass Fibers, J. Polym. Sci. Polym. Phys. Ed. 18 (1980) 1931–1943. doi:https://doi.org/10.1002/pol.1980.180180906.

[12] C.C. Le-Huy, L.G. Britcher, J.G. Matisons, The effect of silane concentration on the adsorption of poly (vinyl acetate-co-maleate) and γ -methacryloxypropyl-trimethoxysilane onto E-glass fibers, Silicon Chem. 3 (2002) 195–205.

[13] H. Ishida, J.L. Koenig, The Reinforcement Mechanism of Fiber-Glass Reinforced Plastics Under Wet Conditions: A review, Polym. Eng. Sci. 18 (1978) 128–145. doi:10.1002/pen.760180211.

[14] H. Ishida, J.L. Koenig, Effect of Hydrolysis and Drying on the Siloxane Bonds of a Silane Coupling Agent Deposited on E-Glass Fibers, J. Polym. Sci. Polym. Phys. Ed. 18 (1980) 233–237. doi:https://doi.org/10.1002/pol.1980.180180206.

[15] J.-K. Kim, Y.-W. Mai, Surface treatments of fibers and effects on composite properties, in: Eng. Interfaces Fiber Reinf. Compos., Ltd, Elsev, 1998: pp. 171–237. doi:http://dx.doi.org/10.1016/B978-008042695-2/50006-3.

[16] D. Wang, F.R. Jones, Surface analytical study of the interaction between y-amino propyl trethoxysilane and E-glass surface-Part II X-ray photoelectron spectroscopy, J. Mater. Sci. 28 (1993) 2481–2488. doi:https://doi.org/10.1007/BF01151683.

[17] V.D. Pizzol, L.M. Mendes, H. Savastano, M. Frías, F.J. Davila, M.A. Cincotto, V.M. John, G.H.D. Tonoli, Mineralogical and microstructural changes promoted by accelerated carbonation and ageing cycles of hybrid fiber-cement composites, Constr. Build. Mater. 68 (2014) 750–756. doi:10.1016/j.conbuildmat.2014.06.055.

[18] A. Hakamy, F.U.A. Shaikh, I.M. Low, High-performance natural fiber-reinforced cement composites, Adv. Ceram. Matrix Compos. Second Ed. (2018) 277–305. doi:10.1016/B978-0-08-102166-8.00012-8.

[19] D. Olmos, A.J. Aznar, J. Baselga, Hydrolytic damage study of the silane coupling region in coated silica microfibres : pH and coating type effects, J. Mater. Process. Technol. 144 (2003) 82–86. doi:10.1016/S0924-0136(03)00325-X.

[20] R. Sjback, J. Nygren, M. Kubista, Absorption and fluorescence properties of fluorescein, Spectrochim. Acta Part A. 51 (1995) L7–L21. doi:https://doi.org/10.1016/0584-8539(95)01421-P.

[21] D. Olmos, A.J. Aznar, J. Baselga, J. González-Benito, Kinetic study of epoxy curing in the glass fiber/epoxy interface using dansyl fluorescence, J. Colloid Interface Sci. 267 (2003) 117–126. doi:10.1016/S0021-9797(03)00620-9.

[22] J. González-Benito, A. Aznar, J. Baselga, Solvent and Temperature Effects on Polymer-Coated Glass Fibers . Fluorescence of the Dansyl Moiety, J. Fluoresc. 11 (2001). doi:https://doi.org/10.1023/A:1013974907580.

[23] M. Iorio, M.L. Santarelli, G. González-Gaitano, J. González-Benito, Surface modification and characterization of basalt fibers as potential reinforcement of concretes, Appl. Surf. Sci. 427 (2018) 1248–1256. doi:10.1016/j.apsusc.2017.08.196.

[24] C.-H. Chiang, H. Ishida, J.L. Koenig, The structure of γ-aminopropyltriethoxysilane on glass surfaces, J. Colloid Interface Sci. 74 (1980) 396–404. doi:https://doi.org/10.1016/0021-9797(80)90209-X.

[25] D. Wang, F.R. Jones, P. Denison, Surface analytical study of the interaction between y-amino propyl trethoxysilane and E-glass surface Part I Time-of-flight secondary ion mass spectrometry, J. Mater. Sci. 27 (1992) 36–48. doi:https://doi.org/10.1007/BF00553834.

CHAPTER 6

STUDY OF THE INTERACTIONS BETWEEN BASALT FIBERS AND CEMENT MATRIX

CHAPTER 6
STUDY OF THE INTERACTIONS BETWEEN BASALT FIBERS AND CEMENT MATRIX

Abstract

Basalt fibers-reinforced cement-based mortars with potential use as plasters for modern buildings were prepared. To optimize compatibility between reinforcement and matrix, interactions between basalt fibers and cement matrix were studied. Different characteristics of the reinforcement surface were considered looking for the best interphase respect to the final performance of the composite materials. As-received, calcinated, activated and silanized (by three different silane aqueous solutions: i) γ-aminopropyltriethoxysilane, APTES; ii) γ-aminopropylmethyldiethoxysilane, APDES and iii) a mixture APTES+APDES 50 % by weight) basalt fibers were dispersed in Portland cement matrix. Mechanical behavior of the resulting composites were evaluated by three-point flexural tests and compressive strength tests. Final correlation between the fiber surface characteristics and mechanical performance was carried out taking into account possible induced microstructural changes and adhesion at the interface. In the first case, porosity studies by BET-BJH textural analysis were carried out, while in the second case fractographic analysis by SEM analysis and laser and optical profilometry were performed. A clear improvement in mechanical properties was obtained when basalt fibers were dispersed in cement matrix. In general, results from the analysis performed suggest that better behavior is achieved when APTES+APDES silanized basalt fibers are dispersed in cement matrix (APTAPD+CEM sample).

6.1. Introduction

Portland cement, developed in the mid nineteenth century, has rapidly become the preferred material for building and architectonical restoration. Portland cement-based materials have the advantages of being widely available, relatively inexpensive compared to many other materials and usually have stiffness and thermal expansion compatible with the material to be repaired, being relatively easy to apply and cure. However, its brittleness is a great problem so as its relatively high modulus and low tensile strength. Moreover, other disadvantages come from the effect of reactions with some aggregates or chemical agents in the environment and the poor resistance to crack propagation. However, as it was previously discussed in the Chapter 2, most of the problems related to this type of materials, are due to shrinkage cracking phenomena [1,2].

To reduce this problem the use of short and randomly dispersed fibers may be a solution since they have an important function transmitting properly stresses to the matrix and limiting crack openings. In addition, fibers may act as attachment points crossing cracks, making difficult their propagation. Therefore, it is expected fiber reinforcement limit the extent of shrinkage cracking by decreasing the width of the cracks.

The presence of the fibers can improve properties such as tensile, flexural, impact, fatigue and abrasion strength, elongation at break and toughness in composite materials. In particular, one of the major roles of the fibers in concretes and mortars is to increase the fracture energy, which is directly related to cracks formation and propagation. The effectiveness of fibers to improve the fracture energy depends on the mass, aspect ratio and nature of the fibers, the nature of the matrix and the adhesion between fibers and the matrix among other factors [3,4]. In general, the mass of fibers used in these materials is limited to 1–3% by volume. When this so low mass of fibers is used, there is only an improvement in terms of fracture toughness of concretes and mortars in most of the practical cases. Mechanical strength of the whole material can be increased when higher mass of fibers is used [3,5–7]. On the other hand, since the size and aspect ratio of fibers influences the crack formation and propagation, some important issues should be considered. Indeed, in a cementitious material the matrix cracking occurs first at the micro level, consequently the presence of short and relatively closer fibers acts on the microcracks avoiding the coalescence in macrocracks. Although large fibers (up to 50 or 80 mm) may stop macrocracks propagation, they only contribute to increase the toughness

with a relatively small improvement in the strength of the composite. Furthermore, short fibers could enhance the strength of the resulting material providing a little improvement in post-peak toughness because they have to be pulled out after that macrocracks are being propagated (Figure 1) [2,8].

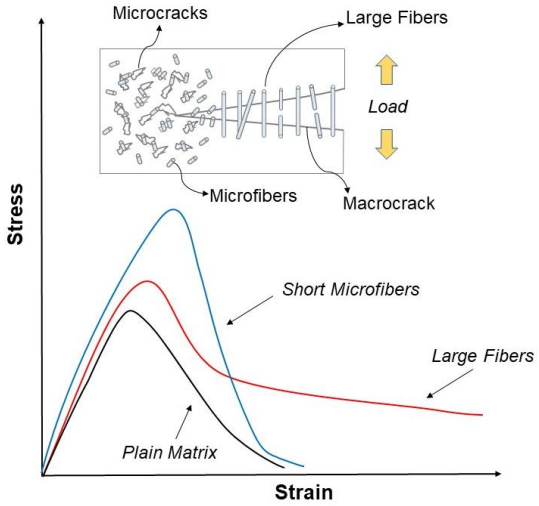

Figure 1. Effect of short and large fibers on the crack propagation [2,8].

The fiber-matrix interactions have a great influence on the mechanical properties in this type of materials since the fiber-matrix interface is crucial in the ability of fibers to transfer loads to the matrix and stabilize cracks propagation. If fiber-matrix interactions are too low there is not continuity along the composite material, being responsible for its weakness [9]. For these reasons, a good adhesion between fiber and matrix should be achieved in order to avoid failure mechanisms that could occur at the interface such as debonding, pull-out, fiber sliding and crack bridging phenomena (Figure 2). These phenomena have a significant influence on the total energy consummation during crack propagation [5,10,11].

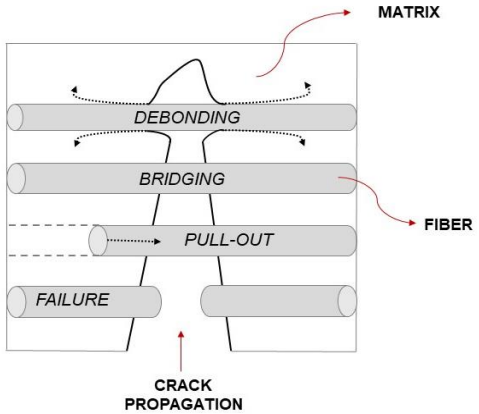

Figure 2. Mechanism occurring at the fiber-matrix interface [11].

In order to enhance the fiber-matrix interfacial adhesion, several methods have been proposed. Among them, modification of fiber surfaces through chemical treatments is one of the most used [11,12].

Various types of fibers have been used to reinforce mortars and concretes. The first example well known of an inorganic fiber reinforced building material was cement mixed with asbestos fibers. However, since 1970 its use decreased due to the risk to human health associated to fiber breathing [6]. Other types of fibers used as reinforcement are: steel, glass and carbon fibers, synthetic polymeric fibers (such as polypropylene, polyethylene and polyolefin, polyvinyl alcohol (PVA) etc.) and natural vegetable fibers (applied only in ordinary concretes and not in high performance structural concrete [2]). Vegetable fibers have disadvantages under humid and alkaline environments leading to reduction in strength and toughness of the cement matrix [13].

Currently, a great interest is in the use of basalt fibers that for their good mechanical and chemical properties could be applied as reinforcements in cement materials. As previously described in Chapter 2, they represent an economic and sustainable alternative to the other type of fibers. In fact, their surface properties and morphology avoid any harmful or carcinogenic impacts and cause no hazard to people [14]. Moreover, basalt fibers offer performance similar to glass fibers at lower price and may be less-expensive alternative to carbon fibers. They can replace steel and carbon fibers due to its high rigidity and low elongation or extension at break [12].

Furthermore, the higher resistance to corrosion make basalt fibers more effectiveness than steel in concrete structure. In fact, the use of basalt fibers is optimal for marine environments for example. Studies refers also on the highest chemical stability of the basalt fibers respect to the common glass fibers in cement materials [7].

In recent years, the use of basalt fibers in concrete engineering has been developing increasingly. Due to this, several studies were carried out about commercial basalt fibers reinforced cement-based materials. The presence of basalt fibers in concrete and mortar can control non-structural concrete cracks and reduce the early dry shrinkage, improving the early crack resistance of the concrete; furthermore, they can enhance the elongation at break and impact and frost resistance.

Most of the studies are focused on the influence of different amount, length and diameter of chopped basalt fibers in cement matrix. In general, when adding fibers an increase in

the mechanical properties and a reduction of the shrinkage phenomenon could be achieved [7,14]. Moreover, Branston et al. [15] have found that the presence of basalt fibers only clearly increases pre-cracking strength.

Jiang et al. [16] showed that after adding chopped basalt fibers to a cement matrix tensile strength, flexural strength and toughness index were improved while, compressive strength did not increase significantly. High et al. [17], studying the use of chopped basalt fibers for concrete structures, have found that the fibers enhanced the flexural modulus but they had only a little effect on the compressive strength. However, it is also important to mention that previous studies stated that better performance of basalt fiber-reinforced cement composites can be achieved by improving the fiber-matrix interface through surface treatments of the fibers [18,19].

Limited research about new surface treatments of basalt fibers to finally improve matrix-reinforcement adhesion in cement-based materials is available. In this regard, the aim of the present work is to improve the performance of cement-based materials by optimization of fiber-matrix interface through fibers surface treatments.

Fiber-reinforced cement-based mortars formed by chopped basalt fibers and a common Portland cement were prepared looking for their potential use as materials for plaster in modern buildings. In particular, commercial basalt fibers were modified by several surface treatments as described in Chapter 4. Different composite materials were prepared by dispersing the different fibers (as-received, calcinated, activated and silanized with different aminosilanes) within the cement matrix. Mechanical performances of the resulting composites materials were evaluated by mechanical tests (three-point flexural tests and compressive strength tests) and finally a correlation between possible microstructural changes and adhesion at the interface was considered.

It is well agreed that the role of porosity of a mortar is important in terms of moisture transport, mechanical properties, durability and compatibility of the mortar to the masonry where it will be applied. Due to this, porosity measurements were carried out. Although different techniques can be used to determine porosity in this type of materials, in the present work BET analysis by N_2 adsorption/desorption measurements was used. In particular, the determination of the surface area by nitrogen adsorption-desorption give more information than the most commonly used mercury intrusion porosity (MIP) because greater range of porosity (from micro to macro porosity) can be studied [20–22].

On the other hand, studies about the adhesion were carried out by fractographic analysis using scanning electron microscopy (SEM) and laser and optical profilometry trying to understand the interaction existing between the fibers and matrix so as the failure mechanism. Besides, the evaluation of the fiber surface roughness at nanoscopic scale by atomic force microscopy (AFM) was also used to interpret fiber-matrix adhesion in terms of a mechanical join.

6.2. Experimental

6.2.1. Materials

In this study, the binder used to prepare mortar samples was a Portland cement PII/A-L 42.5 R according to European Standard EN-197 [23]. It was provided by Cementos Portland Valderrivas (Madrid, Spain). As aggregate, a siliceous sand, with a grain size between 0.2-0.5 mm, provided by Arenas Silíceas Gómez Vallejo (Segovia, Spain) was used. Basalt continuous filament (mean diameter 17 μm) chopped to a length of about 6.4 mm with a sizing compatible with cement matrix was supplied by Incothelogy GmbH. A chlorhydric acid aqueous solution (37% wt), Sharlab, and two silanes, γ-aminopropiltriethoxysilane (APTES) and γ-aminopropilmethyldiethoxysilane (APDES), supplied by ABCR GmbH & Co.KG, were used to prepare pre-treated and silane coated basalt fibers.

A commercial silicone (Silastic 3481 Base +Curing Agent S81, Feroca, S.A.) was used to prepare the molds for the mortar samples.

6.2.2. Samples Preparation

Mortar samples were prepared with a binder/aggregate ratio of 1:2. Distilled and deionized water was used in a water/binder ratio of 0.45. To obtain the composites, as-received or modified basalt fibers were added to the reactive mixture at 1% by weight. The methods used to modify basalt fibers are described in Chapter 4.

To ensure the effectiveness of the surface treatments given to the fibers their incorporation to the reactive mixture, the structure of the coatings was checked by Fourier transformed infrared spectroscopy, FT-IR.

The standard UNI EN 196-1:2005 [24] was used as a guide for the preparation of mortar samples. The mixing was done in a standard mixer (IIC S.A., *Amasadora Automàtica Multinorma*). The process started mixing the cement and water for 30 s at low agitation speed. After that, the aggregate was added, blending the system for 30 s at high speed (when fibers are added, firstly they must be manually mixed with the aggregate to ensure a better dispersion in the cement paste). Then, the mixer stops for 90 s to subsequently continue rotating for other 60 s.

Finally, fresh mixtures were cast in 20 × 20 × 80 mm silicon molds (Figure 3). Molds were half filled and compacted to avoid voids formation. Afterward, a second layer of mixture was poured, and the sample was compacted again.

Samples were cured and tested according to the standard UNI EN 1015-11:2007 [25]. Specimens are prepared by subjecting the mixture at temperature 25 ºC and RH 95±5% for 7 days in the polyethylene bags (Fig.4b) and finally, they were stored in a climatic chamber for 21 days at 25 °C and RH 65±5% (Fig.4c) before performing the mechanical tests. Therefore, the specimens were tested 28 days after their preparation and immediately after they have been removed from the curing conditions as the UNI EN 1015-11:2007 states.

In the Table 1 are gathered the samples codes and the components of the corresponding mixtures (six specimens were prepared for each mixture).

Table 1. Sample codes of the cement-based mortars prepared and components of the mixtures.

Code	Components of Mixtures
REF CEM	cement + sand
ASR + CEM	cement + sand + as-received basalt fibers
CAL + CEM	cement + sand + calcinated basalt fibers
ACT + CEM	cement + sand + activated basalt fibers
APT + CEM	cement + sand + silanized APTES basalt fibers
APD + CEM	cement + sand + silanized APDES basalt fibers
APTAPD + CEM	cement + sand + silanized APTES+APDES basalt fibers

Figure 3. 20×20×80 mm silicon molds.

Figure 4. Mixing (a) and curing (b-c) of cement-based mortar samples.

6.2.3. Instrumental Techniques

6.2.3.1. Mechanical Tests

Mechanical tests were performed according to standard UNI EN 1015-11:2007 using a MICROTEST EM2/200/FR (Madrid, Spain) universal testing machine. Three-point flexural tests and compressive tests were carried out on six specimens for each type of sample.

For three-point flexural test a 5 kN load cell was used. The support span was set at 50 mm and the load was applied with a rate of 2 mm/min. Cubic portions (20×20×20 mm) of each specimen resulting from the fractured specimens were mechanical tested by compression using a 20 kN load cell and applying the load at rate of 2 mm/min.

Finally, the flexural and compressive strength data were statistically treated using Weibull distribution that is one of the most widely used distributions functions to describe the fracture strength of ceramics [26,27].

The statistical theory of brittle fracture proposed by Weibull is represented by the equation (1):

$$P_f = 1 - e^{\left[-\left(\frac{\sigma}{\sigma_0}\right)^m\right]} \quad (1)$$

where P_f is the probability of failure of the material, σ is the strength applied on the material, σ_0 is the scale parameter or the characteristic strength for which the P_f is 63.2% (it is analogous to the median strength) and m is the shape parameter or Weibull modulus or a measure of the data scatter (the higher this value, the narrower the distribution).

The parameter m and σ_0 are calculated from the linear regression of Eq. (1) when linearized by means of logarithms:

$$\ln\ln\left[\frac{1}{(1-P_f)}\right] = m\ln(\sigma) - m\ln(\sigma_0) \quad (2)$$

where P_f is:

$$P_f = \frac{(i-0.5)}{n} \quad (3)$$

where i is the i-th datum and n is the total number of data points (for this study n=6) [26–30].

The way of obtaining the Weibull strength distribution plots for each group of samples can be found in Appendix A.

6.2.3.2. BET-BJH Textural Analysis

To evaluate mortar microstructural changes due to the presence of the fibers in the matrix so as their surface treatments, BET-BJH analysis by N_2 adsorption/desorption measurements was carried out. In particular, the specific surface area was calculated according to Brunauer–Emmett–Teller (BET) multipoint method while the total pore

volume and the pore size distribution were determined from the adsorption curve by the Gurvitsch rule and the Barret–Joyner–Halenda (BJH) method respectively [31–33].

In this study BET-BJH textural analysis were carried out by N_2 adsorption/desorption measurements at the liquid nitrogen temperature (-196 °C) using a 3-Flex 3500 analyzer (Micromeritics, Norcross, GA, USA). The analysis was performed on small pieces arisen from the samples previously three-point flexural tested. Only one representative sample for each batch was investigated. Before performing the analysis, the samples were vacuum dried at 110 °C for 3 h to remove from the pores water and other adsorbed contaminants.

6.2.3.3. Scanning Electron Microscopy (SEM)

To investigate the interaction between as-received and modified fibers with cement matrix, the fracture surfaces of specimens were inspected by scanning electron microscopy using a TENEO field emission scanning electron microscope, FESEM (FEI). The acceleration voltage was 4.0 kV and 5.0 kV and the T1 detector was used taking the signal coming from backscattered electrons. As the samples are not conductive, prior to examination, they were sputter coated with gold using a low vacuum coater Leica EM ACE200. Before SEM inspections, samples were vacuum dried at 40 °C for 48h. SEM images were collected at different magnifications to obtain information about the dispersion of the fibers in the matrix (120×), the adhesion of the matrix to the fiber surface and to study the fiber-matrix interface (2000× and 3500×). SEM observations were carried out on small regions of only one of the facture surfaces of the specimens taking a representative one according mechanical tests results.

6.2.3.4. Surface Profilometry Measurements

Another fractographic analysis of the of composite materials was carried out by laser and optical profilometry. In principle, these two methods should give fracture mechanism information at different scale.

- Laser Profilometry

  Laser profilometry was carried out using a Talyscan 150 (Taylor-Hobson) instrument. The 3D surface profile and the corresponding surface parameters (P_a and P_q) of the

composite materials were evaluated. P_a and P_q, primary profile parameters, were chosen to know the whole heterogeneity and irregularities of the fractured surfaces (e.g voids due to the pull-out of the fibers, cracks, height differences on fracture relief).

The surface inspection was carried out on only one surface of fracture of the specimens. Three surfaces for each sample were analyzed in order to obtain averaged data. An area of about 20 mm × 20 mm was scanned at 2500 µm/s taking horizontal profiles each 5 µm and vertical profiles each 20 µm.

- Optical Profilometry

Optical profilometry was performed using an OLYMPUS DSX 500 instrument. Only one surface of fracture of each specimen was inspected. Three surfaces for each sample were analyzed in order to obtain averaged data. The investigated area (1994 µm × 1994 µm) was chosen in five different regions of each fractured surface (one in the center and four near the corners as it is shown in Figure 5 a).

P_a and P_q parameters were also obtained to evaluate heterogeneities and irregularities at higher magnification (10× magnification). Ten profiles were taken from each of the five areas (five vertical and five horizontal, Figure 5 b).

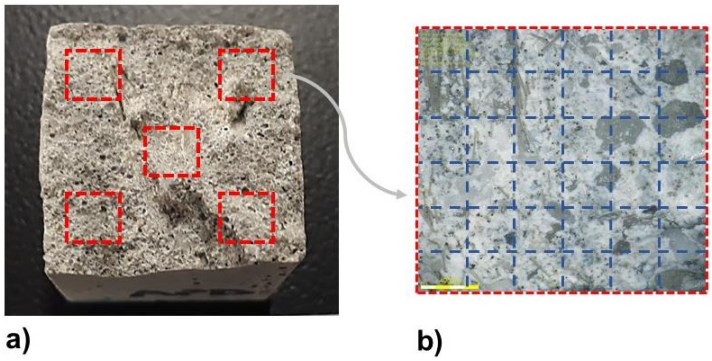

Figure 5. Inspected regions by optical profilometry a) and profiles taken b) to carry out the surface analysis.

6.2.3.5. Atomic Force Microscopy (AFM)

An evaluation of the roughness of as-received and modified fibers surface was performed by atomic force microscopy, AFM, using a microscope Multi-Mode Nanoscope IVA

(Digital Instruments/Veeco Metrology Group). The measurements were conducted at ambient conditions in tapping mode with antimony doped silicon probe (k = 1-5 N/m). The frequency was adjusted to the resonant frequency of the probe close to the surface of the sample to be analysed. The initial amplitude of the probe oscillation and set-point amplitude applied for imaging were chosen to maximize the image contrast among the different constituents of the samples.

R_a and R_q roughness parameters were obtained to study the topography at nanoscale. Due to the heterogeneity of the fiber surface, the roughness was calculated in several representative regions of the fiber surface: in smooth areas and in the areas with a high amount of sizing (Figure 6). The red squares show the representative areas where roughness measurements were done. A 2nd order flatten[1] was used before estimate surface roughness parameters.

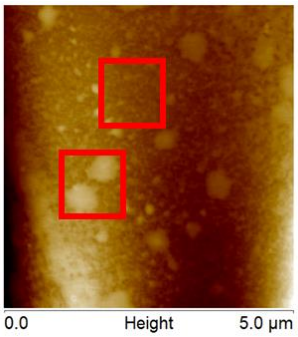

Figure 6. AFM Height Image of as-received basalt fibers.

6.3. Results and Discussion

6.3.1. Mechanical Tests

➢ *Three-point flexural strength test*

Figures (7-11) show the *stress-strain* curves and representative images of fractured specimens of each group of tested samples. The curves were modified since the original

[1] The flatten is a filter useful prior to roughness analysis. It eliminates unwanted features from scan lines (e.g. noise, bow and tilt) from the image. Each line is fit individually to center data (0th order) and remove tilt (1st order), or (2nd or 3rd) order bow.

curves displayed some artifacts arising from the testing machine (the method employed to modify curves is described in the Appendix B).

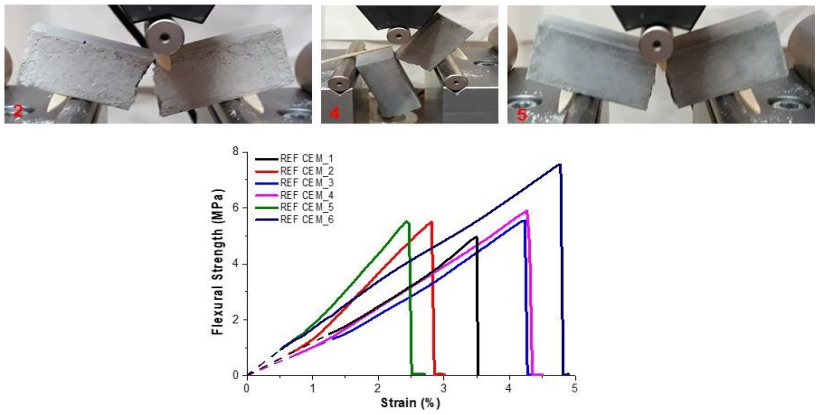

Figure 7. *Stress-strain* curves and representative images of fractured specimens of REF CEM samples.

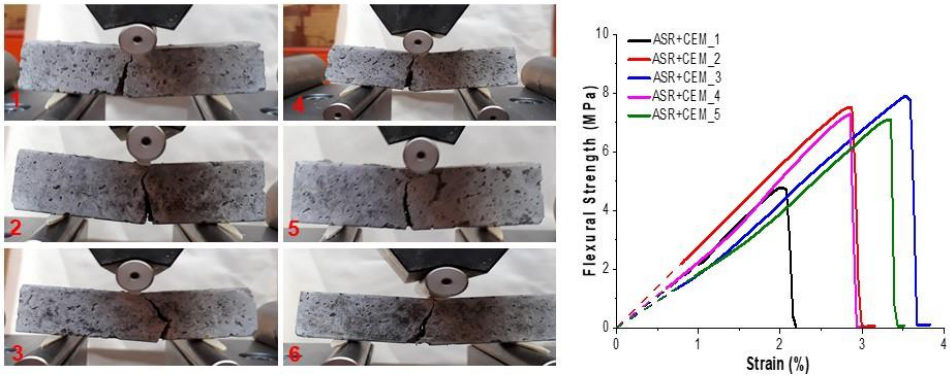

Figure 8. *Stress-strain* curves and representative images of the fractured specimens of the ASR+CEM samples.

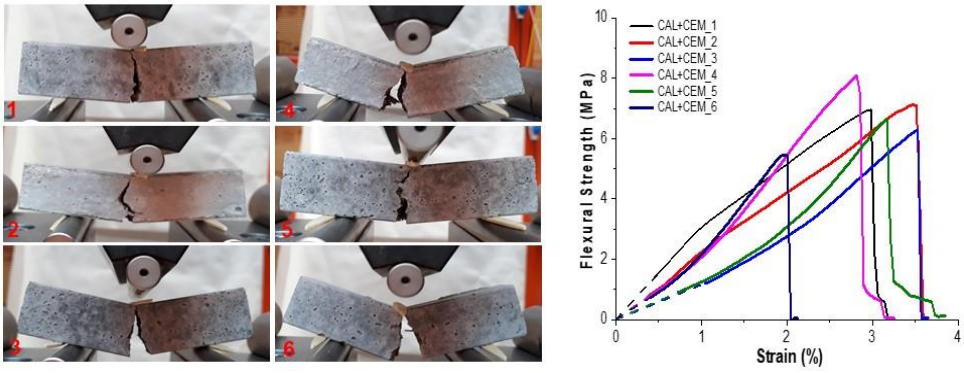

Figure 9. *Stress-strain* curves and representative images of the fractured specimens of the CAL+CEM samples.

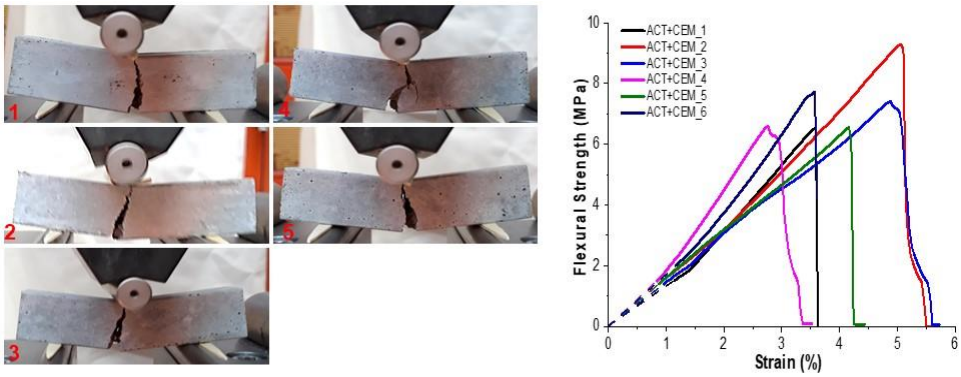

Figure 10. *Stress-strain* curves and representative images of the fractured specimens of the ACT+CEM samples.

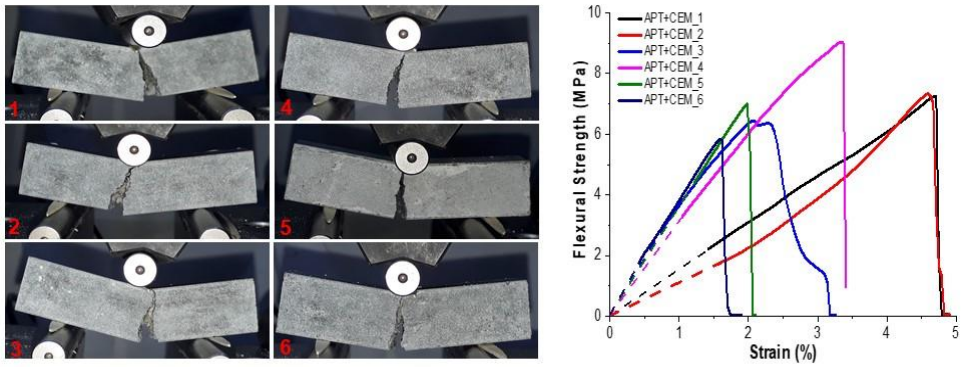

Figure 11. *Stress-strain* curves and representative images of fractured specimens of the APT+CEM samples.

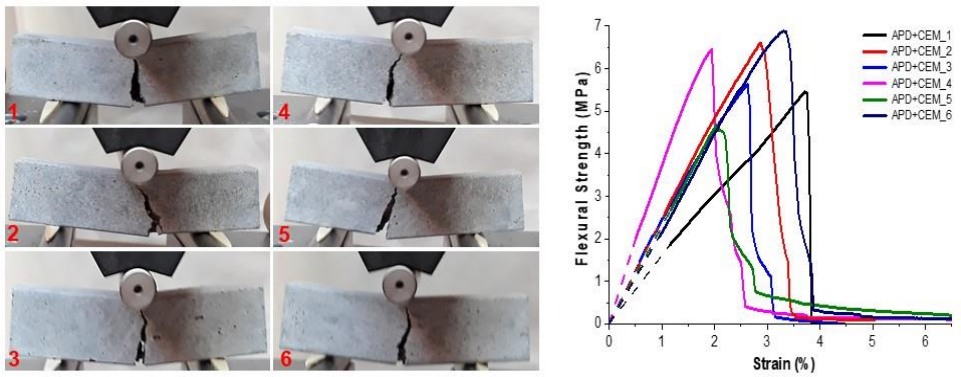

Figure 12. *Stress-strain* curves and representative images of fractured specimens of the APD+CEM samples.

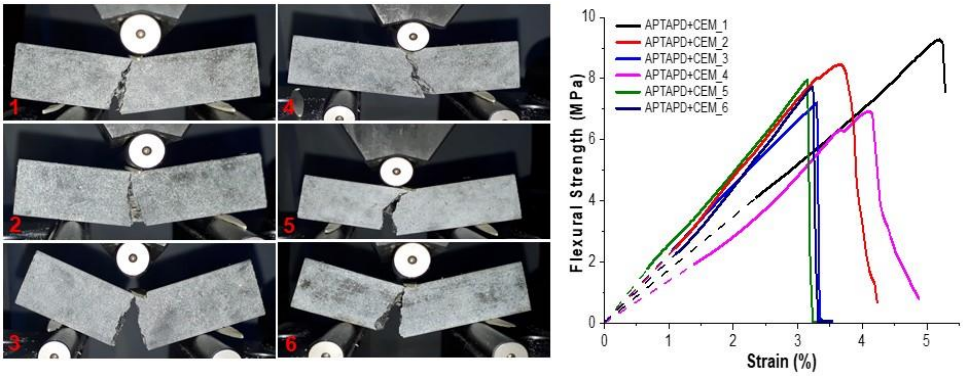

Figure 13. S*tress-strain* curves and representative images of fractured specimens of the APTAPD+CEM samples.

Considering the fracture behavior of the samples tested (Fig. 7-13), for the neat mortar more homogeneous fracture is observed leading to complete separation between the two pieces resulting from the fracture. On the other hand, the region of fracture for the samples reinforced with the fibers point out more tortuous crack development and the pieces resulting from the tests after the corresponding fracture, are not completely separated each other.

However, flexural strength plots suggest that specimens containing fibers failed in the same brittle manner as the neat mortar (REF CEM). Only slight differences are observed for samples containing modified fibers (Fig.9-13).

In order to study possible changes between each group of samples, a deeper analysis of the three-point flexural test data was done. For instance, the flexural strength (σ_f) values obtained for each batch were discussed according Weibull distribution (when necessary and after applying the Grubbs method [34] some datum was not considered for the statistical analysis). In the Figure 14 the Weibull probability plots for the flexural strength for all the samples studied are shown.

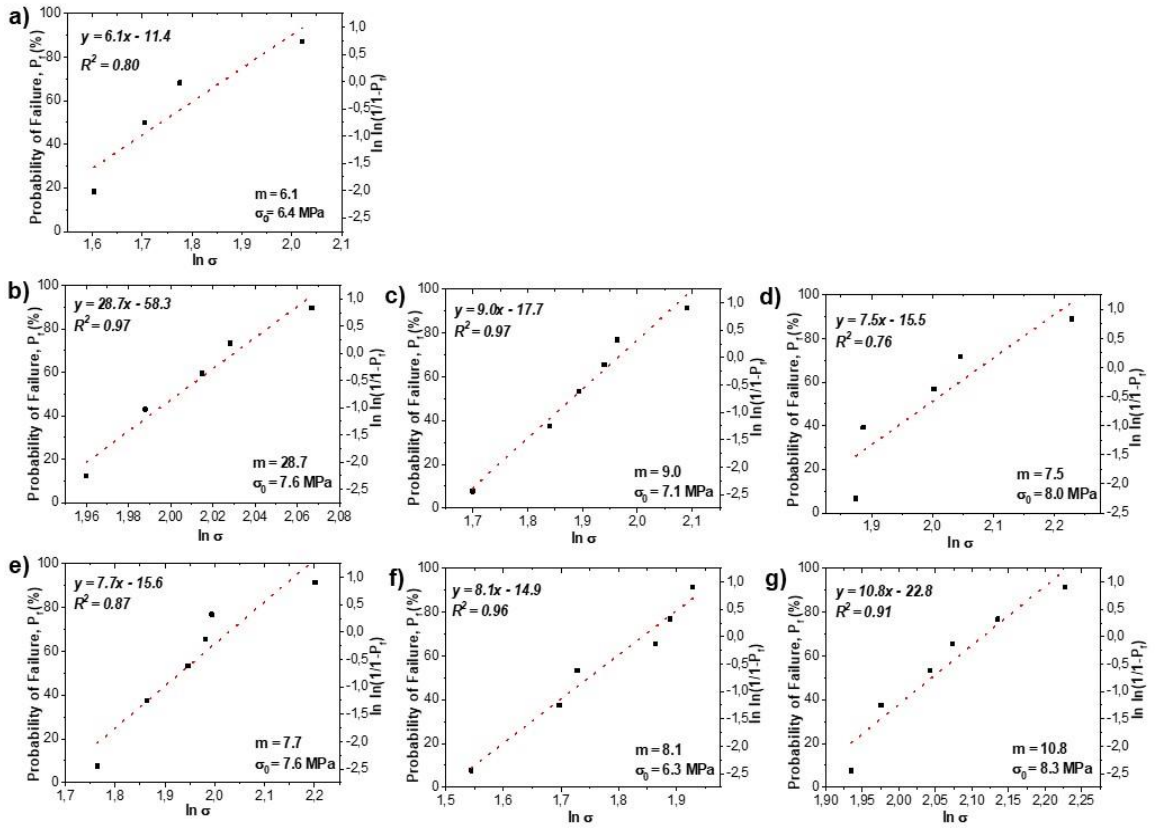

Figure 14. Weibull probability plots for the flexural strength of every sample under study: a) REF CEM, b) ASR+CEM, c) CAL+CEM, d) ACT+CEM, e) APT+CEM, f) APD+CEM and g) APTAPD+CEM.

The statistical properties of the averaged flexural strength values for the different composites applying Weibull statistics are summarized in the Table 2.

Table 2. Parameters obtained after the Weibull fitting of the data obtained from the three-point flexural tests.

Samples	Averaged Flexural Strength, σ_f (MPa)	Weibull Characteristic Strength, σ_0 (MPa)	Weibull Modulus, m	Correlation, (r)
REF CEM	5.8 ± 0.9	6.4	6.1	0.80
ASR+CEM	7.5 ± 0.3	7.6	28.7	0.97
CAL CEM	6.8 ± 0.9	7.1	9.0	0.97
ACT+CEM	7.3 ± 1.1	8.0	7.5	0.76
APT+CEM	7.2 ± 1.1	7.6	7.7	0.87
APD+CEM	6.0 ± 0.8	6.3	8.1	0.96
APTAPD+CEM	7.9 ± 0.9	8.3	10.8	0.91

Considering the low number of data (n = 6) used to carry out Weibull analysis, a quite good linear relationships between lnln [1/(1−P)] and lnσ, in the most of cases are observed.

Therefore, it can be considered that the σ_f values obtained are statistically significant and the Weibull distribution fit is reliable. Poorer fits observed might be ascribed to the presence of pores and microcracks with various orientations. Besides, the Weibull moduli obtained are within the range of values found for other similar ceramic materials [29]. On the other hand, it is important to remember that a high Weibull modulus is associated to narrow strength distributions. This is usually desirable, because a material with high Weibull modulus is more predictable in terms of its mechanical failure, being less likely to break at a stress much lower than a mean value. Moreover, the Weibull characteristic strength values, σ_0, obtained are comparable to the mean flexural strength values obtained experimentally for each sample.

Toughness (in terms of fracture energy) was evaluated by integrating the total area under the flexural stress-strain curve to evaluate a possible effect of the fibers. In this work, the post-cracking behavior was also considered for the toughness determination. Moreover, the flexural modulus, *E* (calculated considering the elastic part of the curve, Equation (3) of the Chapter 3) and the elongation at break, ε (deflection at the maximum stress) were determined in order to have an idea of the rigidity and brittleness of the materials respectively.

Averaged values of the results obtained for each sample are given in the Table 3 and plotted in Fig. 15.

Table 3. Flexural parameters of the studied cement-based mortar samples.

Samples	**Flexural Strength, σ_f (MPa)**	**Flexural Modulus, E (MPa)**	**Toughness (MPa)**	**Elongation at Break, ε (%)**
REF CEM	5.8 ± 0.9	180 ± 45	1041 ± 456	3.7 ± 0.9
ASR+CEM	7.5 ± 0.3	257 ± 20	1210 ± 150	3.1 ± 0.3
CAL CEM	6.8 ± 0.9	252 ± 54	997 ± 294	3 ± 0.6
ACT+CEM	7.3 ± 1.1	206 ± 50	1535 ± 542	4 ± 0.9
APT+CEM	7.2 ± 1.1	263 ± 82	1224 ± 503	3 ± 1.4
APD+CEM	6.0 ± 0.8	222 ± 59	1066 ± 239	2.7 ± 0.7
APTAPD+CEM	7.9 ± 0.9	228 ± 34	1592 ± 487	3.8 ± 0.8

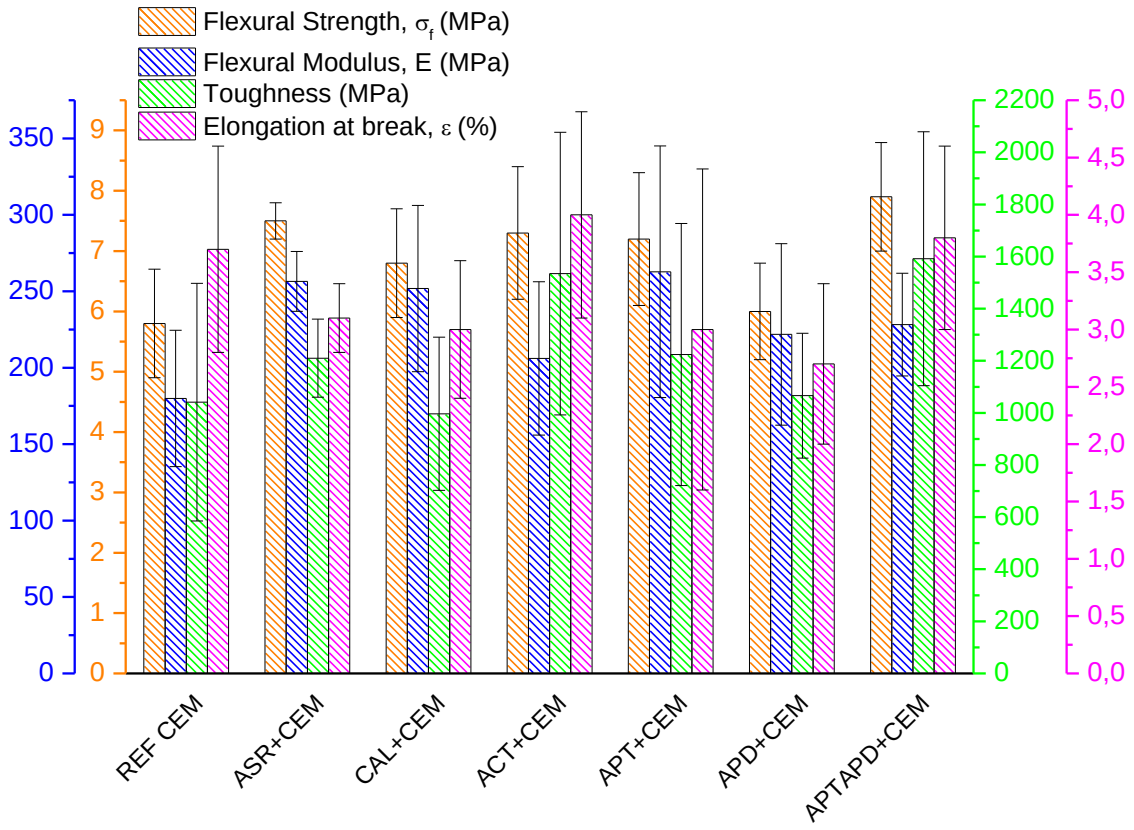

Figure 15. Comparison of flexural behavior from the values of different parameters for all the samples under study.

It can be observed that the standard deviation obtained in every parameter for this type of materials is in general very high. However, it seems that there is a tendency to increase the flexural strength (σ_f), when fibers are added to the mortar. The APD+CEM sample shows a flexural strength value similar to that obtained for the neat mortar while, the samples containing as-received, activated and silanized with APTES or the mixture APTES+APDES basalt fibers present the highest values of σ_f. Here again it is confirmed that a surface treatment seems to be responsible of a better adhesion with the matrix enhancing the resistance of the whole material. However, regarding our results only when a trifunctional silane is used the mechanical performance is enhanced, being even improved if a more opened structure is generated at the interface with the addition of the difunctional silane. In fact, the APTAPD+CEM sample showed a highest value of the flexural strength.

APTAPD+CEM and ACT+CEM samples showed the highest flexural toughness values. In these cases, higher toughness is related to higher resistance to crack propagation. Probably, in the case of ACT+CEM and APTAPD+CEM samples, the presence of high number of

OH groups and/or easier accessibility to those OH on the fibers, might be responsible of better interaction with the cement matrix preventing fiber sliding respect to the matrix during mechanical test and even after material facture has occurred. For the other samples, the toughness values are not significantly different than the neat mortar.

Considering the flexural modulus, *E*, it can be said that it increases when adding fibers to the cement matrix, which it has sense taking into account the higher modulus of the basalt fibers respect to the cement matrix.

On the other hand, considering the values of elongation at break, ε one could conclude that the samples APTAPD+CEM and ACT+CEM are less brittle than the others pointing out another possible contribution to their higher toughness.

As a main conclusion extracted from the flexural results it seems that a better compatibility (in terms of adhesion) exists between the APTES+APDES basalt fibers and the cement matrix.

- *Compressive strength test*

The *stress-strain* curves corresponding to the compressive tests for all the samples under study are shown in Figure 16. As previously described for the three-point flexural strength tests plots, in this case, a modification of the original curves was carried out using the data treatment described in appendix B.

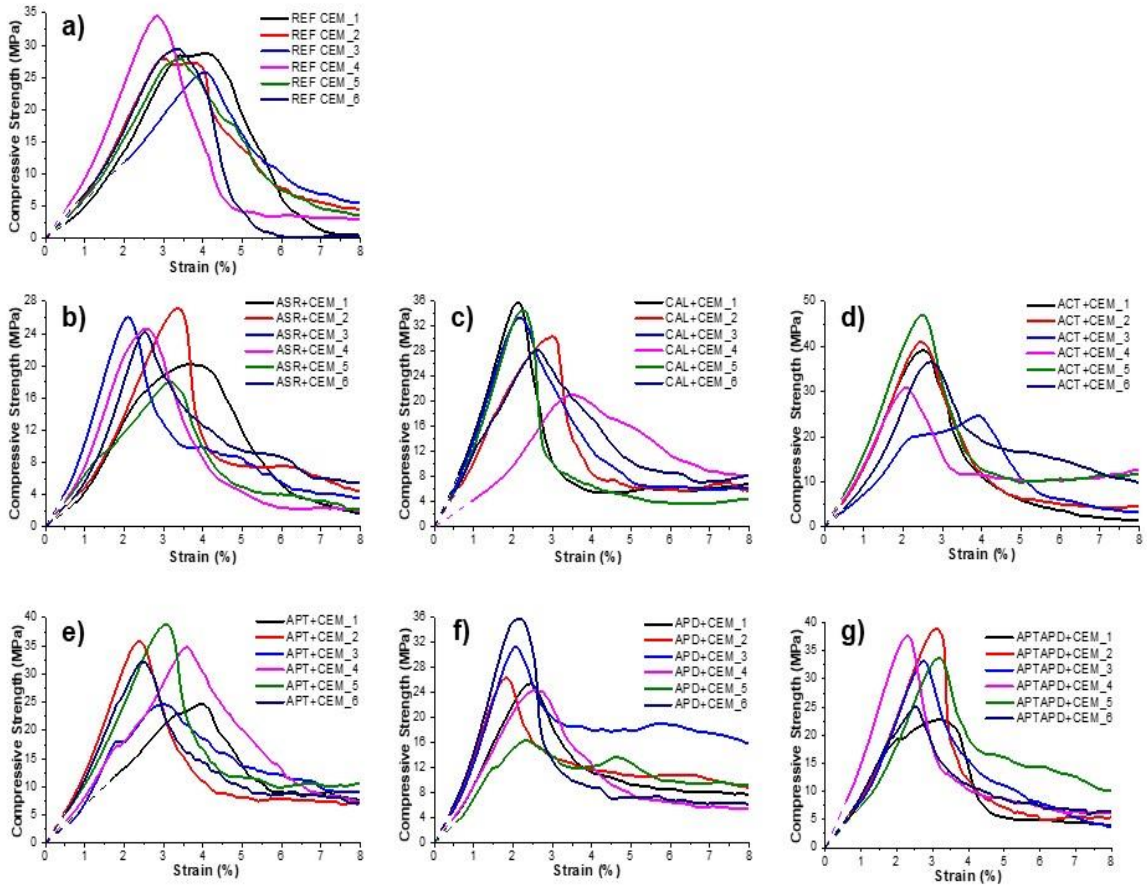

Figure 16. *Stress-strain* curves for all the samples under study: a) REF CEM, b) ASR+CEM, c) CAL+CEM, d) ACT+CEM, e) APT+CEM, f) APD+CEM and g) APTAPD+CEM.

Here, Weibull statistical analysis was also performed. The Weibull probability plots for the compressive strength results are given in the Figure 17 and the corresponding statistical properties are summarized in the Table 4.

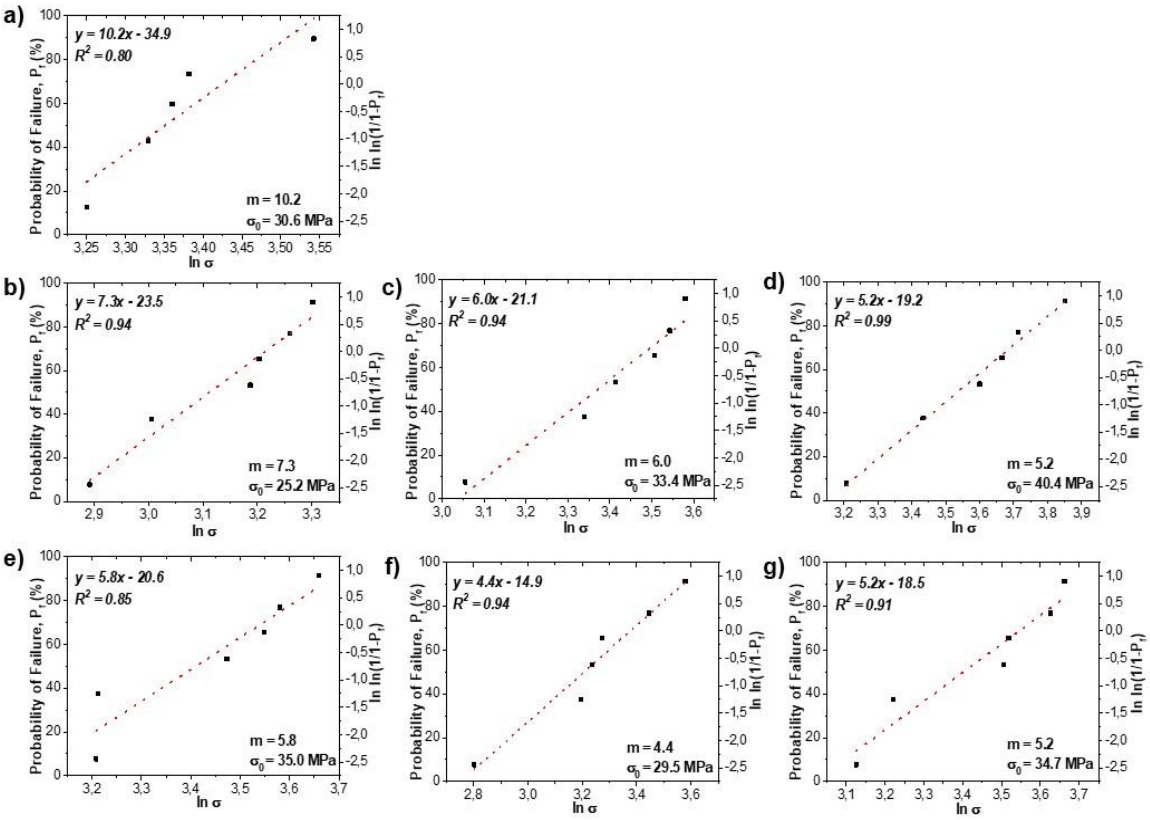

Figure 17. Weibull probability plots for the compressive strength of every sample under study: a) REF CEM, b) ASR+CEM, c) CAL+CEM, d) ACT+CEM, e) APT+CEM, f) APD+CEM and g) APTAPD+CEM.

Table 4. Parameters obtained after the Weibull fitting of the compressive strength tests data.

Samples	Averaged Compressive Strength, σ_c (MPa)	Weibull characteristic strength, σ_0 (MPa)	Weibull modulus, m	Correlation (r)
REF CEM	29.1 ± 3.0	30.6	10.2	0.80
ASR+CEM	23.4 ± 3.5	25.2	7.3	0.94
CAL+CEM	30.6 ± 5.4	33.4	6.0	0.94
ACT+CEM	36.6 ± 7.8	40.4	5.2	0.99
APT+CEM	31.9 ± 5.9	35.0	5.8	0.85
APD+CEM	26.6 ± 6.6	29.5	4.4	0.94
APTAPD+CEM	31.9 ± 6.6	34.7	5.2	0.91

As in the case flexural strength results, a good linear fit was also observed for the compressive strength results. Consequently, the compressive strength experimental data can be also described with the Weibull distribution function, being the compressive strength values statistically significant.

The Weibull compressive modulus values are slightly lower compared to the values of Weibull modulus obtained from the flexural strength tests. In general, an increase in the Weibull modulus is related to a decrease in the standard deviation or data dispersion [29]. For the compressive strength values, higher dispersions were observed; however, taking into account the values of the averaged compressive strength, compressive experiments seem to be subjected to a similar relative error than flexural experiments (Table 4).

To better understand the compressive behavior of the studied mortars, other important mechanical parameters were considered as well.

Compressive strength, σ_c, Modulus, E, toughness and elongation at break, ε, were estimated from maximum compressive stress, the slope of the elastic part of the stress-strain curves, the area below the compressive curves until the maximum compressive strength value and the specimens deformation at break (deflection at the maximum stress), respectively.

The results are summarized in Table 5 and the corresponding trends are shown in Figure 18.

Table 5. Compressive behavior of the cement-based mortar samples studied.

Samples	Compressive Strength, σ_c (MPa)	Compressive Modulus, E (MPa)	Toughness (MPa)	Elongation at Break, ε (%)
REF CEM	29.1 ± 3.0	1062 ± 216	5683 ± 1902	3.4 ± 0.5
ASR+CEM	23.4 ± 3.5	1091 ± 306	3420 ± 769	2.9 ± 0.6
CAL CEM	30.6 ± 5.4	1482 ± 495	3885 ± 617	2.6 ± 0.5
ACT+CEM	36.6 ± 7.8	1755 ± 432	4822 ± 971	2.7 ± 0.6
APT+CEM	31.9 ± 5.9	1308 ± 361	4852 ± 954	3.1 ± 0.6
APD+CEM	26.6 ± 6.6	1500 ± 436	2985 ± 650	2.2 ± 0.3
APTAPD+CEM	31.9 ± 6.6	1445 ± 285	4407 ± 801	2.8 ± 0.4

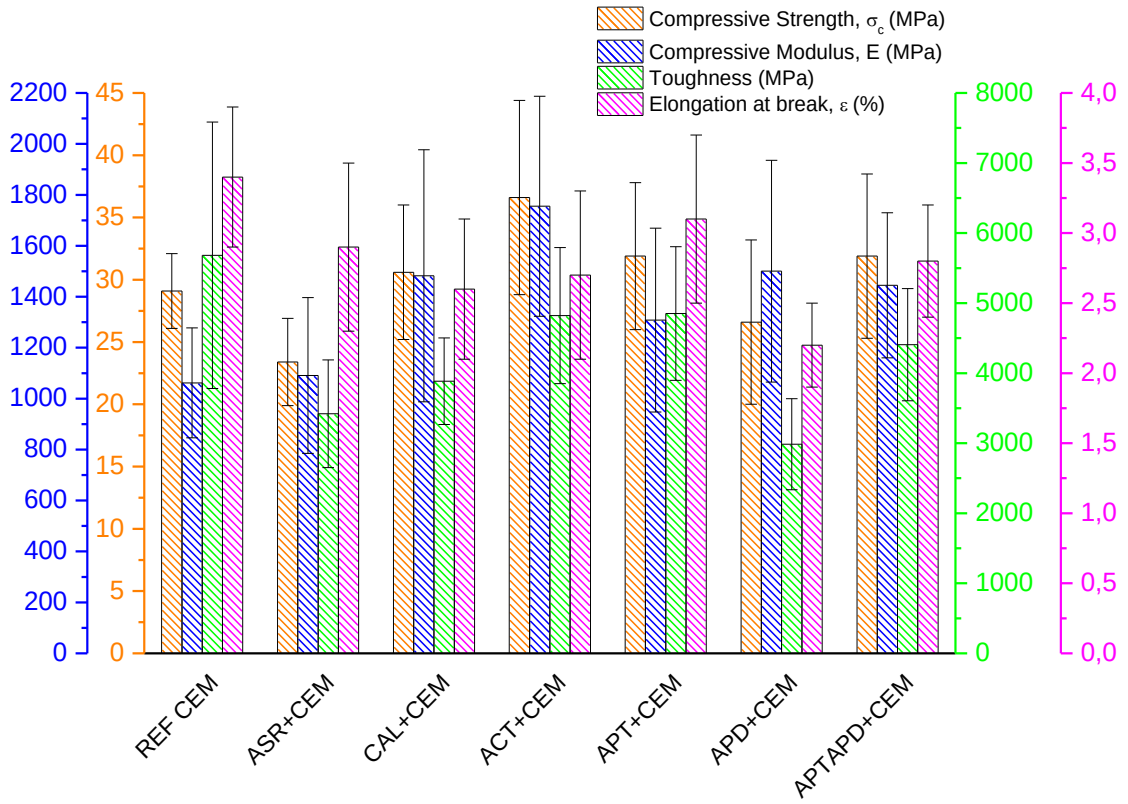

Figure 18. Comparison of compressive behavior from the values of different parameters for all the samples under study.

In the case of the compressive strength, it is observed how slightly higher values were obtained for samples containing activated (ACT+CEM) and silanized APTES (APT+CEM) and APTES+APDES (APTAPD+CEM) basalt fibers. In terms of strength these results are in accordance with those obtained from the flexural tests. Here again it might be said that the higher accessibility to the OH groups generated by the activation process seems to induce a better compatibility with the cement matrix.

Considering the trend of the other mechanical parameters it can be said that, the compressive modulus, *E*, increases for all samples containing fibers, except when commercial fibers are used, respect to REF CEM, and the elongation at break, *ε*, decreases. This result is in accordance with the consideration of an increase in the modulus of any material when another with higher modulus is added.

The unexpected value of the modulus when as-received fibers (ASR+CEM sample) are used might be due to a different disposition of the fibers when they are mixed with the cement reactive components. The sizing of the commercial basalt fibers makes them very

flexible which might cause their collapse in the form of random coil that could not confer the opportune resistance in terms of rigidity to the whole material. On the contrary, the surface treatments proposed in this work make the fibers less flexible. This could suggest that when they are mixed with the components of the mortars, they remain in their more extended form, being more separated each other and consequently leading to more effective reinforcement.

A representation of the explanation of this different behavior between commercial fibers and treated fibers is done in Figure 19.

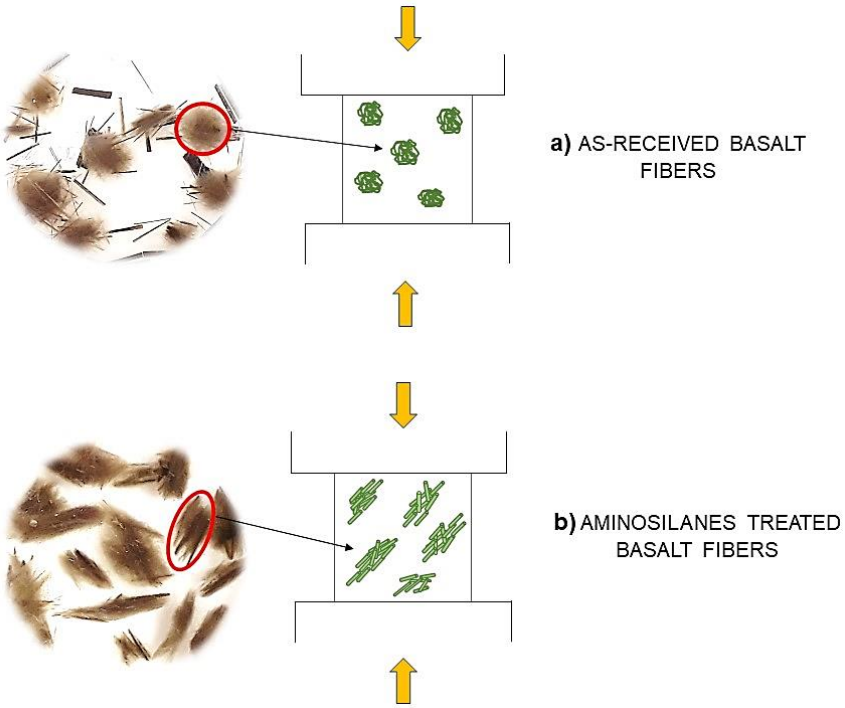

Figure 19. As-received a) and aminosilanes treated b) basalt fibers after stirring with water and expected compressive behavior.

In addition to the above discussed, it should be pointed out that in general the sample containing as-received fibers (ASR+CEM) shows slightly lower values than the neat mortar. These results are in accordance with other studies, showing that commercial fibers does not increase significantly the compressive strength [16,17].

On the other hand, in general, toughness decreases for all samples with fibers respect to the neat mortar (REF CEM).

Here, it is expected to be less effective the reinforcement due to the load transmission form the matrix to the fibers and therefore only the small contribution due to the modulus increase associated to the incorporation of fibers should account.

6.3.2. BET-BJH Textural Analysis

According to IUPAC, pores can be classified as micro-pores (≤ 20 Å), meso-pores (20–500 Å), macro-pores (> 500 Å) [35]. Pores studied at different scales give different information. Indeed, in a cement paste, usually capillary pores (larger than 100 Å) and gel pores (smaller than 100 Å) are present. The first ones mostly influence the strength and permeability while gel pores influence the shrinkage phenomena and creep [36,37]. In this work, the investigation of pores by BET analysis is mainly focused on mesopores since they, among others, determine the durability of the whole material [38].

Fig. 20 shows the N_2 adsorption-desorption isotherms for all the samples prepared. According to the *IUPAC* classification (see section 3.2.3 of Chapter 3) the adsorption curves obtained could be classified as *Type IV* with an hysteresis loop that is usually associated with the filling and emptying of the mesopores by capillary condensation [39]. Furthermore, the shape of the hysteresis loops can be assigned to the *Type H3*, that refers to aggregates of plate-like particles giving rise to slit-shaped pores [35,39].

Mikhail et al. [40] refers that tobermorite gel (C-S-H), which is largely responsible for the pore structure of the hardened cement paste, consists of very thin sheets that may well produce plate-like or slit-shaped pores. Regarding to this, even though the pore distribution calculated by BJH method refers to a pore system with cylindrical pore, the validity of a pore analysis can be extended also to solid materials containing different pore shapes.

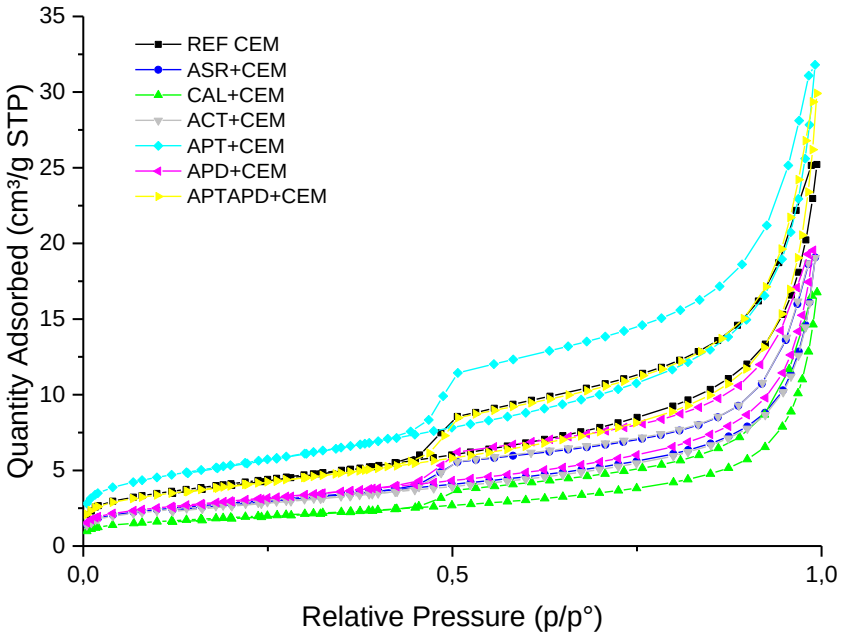

Figure 20. Nitrogen adsorption-desorption isotherms of cement-based mortars.

Starting from the adsorption curves, specific surface area (SA) and pore volume values were obtained. The results are shown in the Table 6. The standard deviation obtained in every case was smaller than the instrumental error, therefore, the standard deviation assigned to SA (BET) values was the instrumental error.

Table 6. SA and Pore Volume results of cement-based mortars.

	SA (BET) (m^2*g^{-1})	**Total Pore Volume (cm^3*g^{-1})**
REF CEM	14.7 ± 0.5	0.0391
ASR+CEM	10.1 ± 0.5	0.0296
CAL+CEM	6.6 ± 0.5	0.0260
ACT CEM	9.7 ± 0.5	0.0295
APT+CEM	19.1 ± 0.5	0.0493
APD+CEM	10.6 ± 0.5	0.0303
APTAPD+CEM	14.1 ± 0.5	0.0464

The REF CEM sample showed a pore volume value of 0.0391 $cm^3 \cdot g^{-1}$ according to the value found in bibliography [16]. Considering the obtained values, except for the sample APT+CEM, there is a decrease in the SA (BET) results for the fiber-reinforced materials and as a consequence, in general it seems that the presence of fibers induces a decrease in the total pore volume of the materials under consideration except for APT+CEM and APTAPD+CEM samples

On the other hand, an estimation of the distributions of pore diameters of the samples analyzed was carried out which results are represented in the Figure 21.

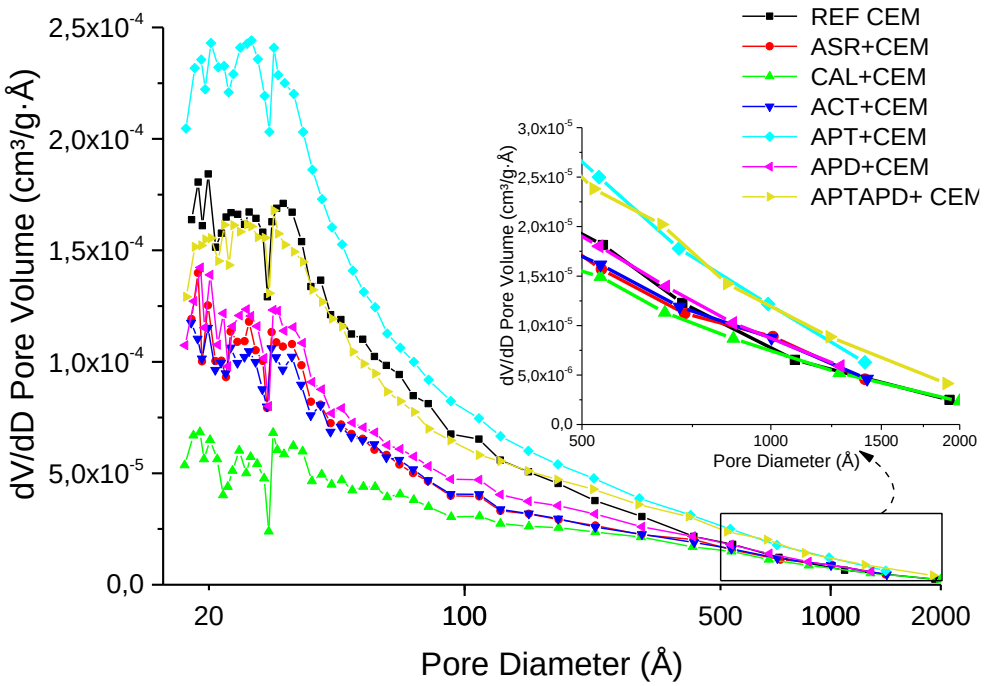

Figure 21. Pore diameter distributions of cement-based mortars.

The samples are characterized by similar porous structure with substantial presence of mesopores (with a diameter between 20-500 Å) and macropores (with a diameter greater than 500 Å). Regardless the sample, the pores distribution curves show maxima at around 20 Å.

Considering the micro-mesopores range (~17-500 Å), a decrease in the amount of pores is observed for the samples with fibers except in the case APT-CEM, being in accordance with the results shown in Table 6. The decrease of the number of pores is quite modest until 200 Å for the sample realized with silanized APTES+APDES basalt fibers (APTAPD+CEM sample) compared to the REF CEM. On the contrary, starting from about 200 Å in diameter, higher pore amounts are observed.

When the range of macrospores (500-2000 Å) is considered, an increase of porosity is observed (see inset of Figure 21) for the samples with fibers silanized with APTES

(APTAPD+CEM and APT+CEM). Finally, if the whole range of pore sizes is considered, it is observed that the porosity shows the following trend for the materials reinforced with silanized fibers: APTES > APTES + APDES > APDES. This trend suggests that the higher the crosslinking degree of the fiber coating the higher the porosity in the whole composite material.

Several studies referred that the presence of fibers in cement increased the porosity of the materials in terms of large pores. Jiang et al. [16] studied the microstructure of chopped basalt fiber-reinforced concrete by MIP analysis showing an increase in the porosity for the samples prepared with fibers. According to our results, it is clear therefore that it is not only important the presence of fibers but also the nature of their surfaces. Variations in the total pore volume of cement-based materials depending on the surface treatment of the fibers used as reinforcement were observed (Table 6 and Figure 21). However, slight differences were actually found in the results, therefore, the presence of fibers so as their surface treatments do not seem to change significantly the meso and micro structure of the neat mortar.

In order to show the reproducibility of the porosity measurements, the analysis was performed on two different specimens arising from the same mixture (APTAPD + CEM). The results obtained (Fig.22) are indicative of the goodness of the measurements and, in addition, of sample preparation.

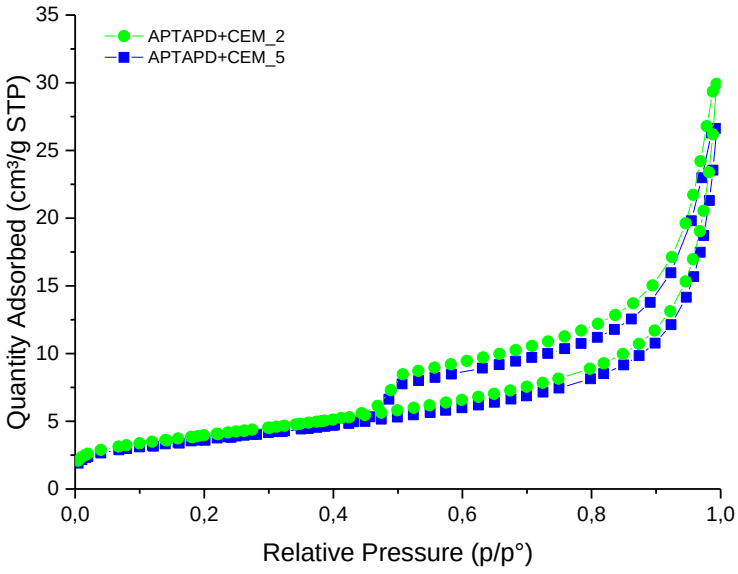

Figure 22. Nitrogen adsorption-desorption isotherms.

6.3.3. Fractographic Analysis

6.3.3.1. Scanning Electron Microscopy (SEM)

Fracture surfaces were observed by scanning electron microscopy to study the failure mechanism of the composites when they are subjected to the three-point flexural strength tests.

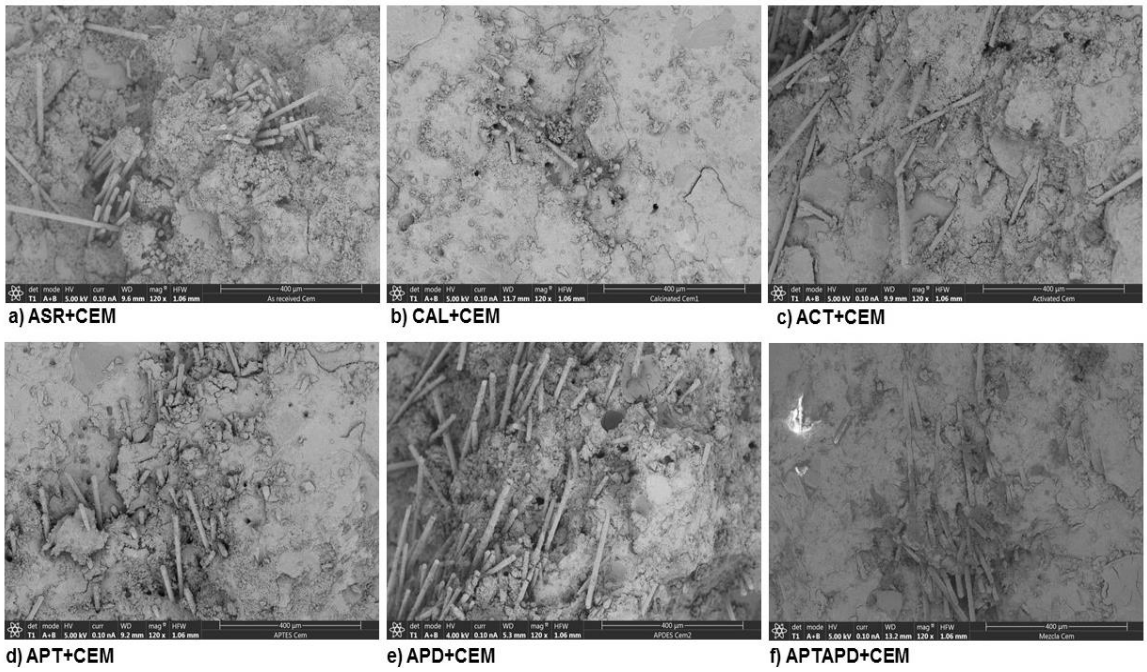

Figure 23. SEM images for all fiber reinforced mortar samples at 120× magnification.

In Figure 23 the fracture surfaces of the fiber reinforced mortar samples at 120× magnification are showed. From these SEM images, information about the dispersion of the fiber in the matrix is obtained. A heterogeneous dispersion of the fibers in the matrix and evidences of pull-out phenomena are observed for all samples.

The chopped fibers are mixed with the reactive components of the mortar in the form of bundles. It seems therefore that the process of mixing did not allow separating the fibers each other in the bundle leading to the corresponding not uniform dispersion within the cement matrix.

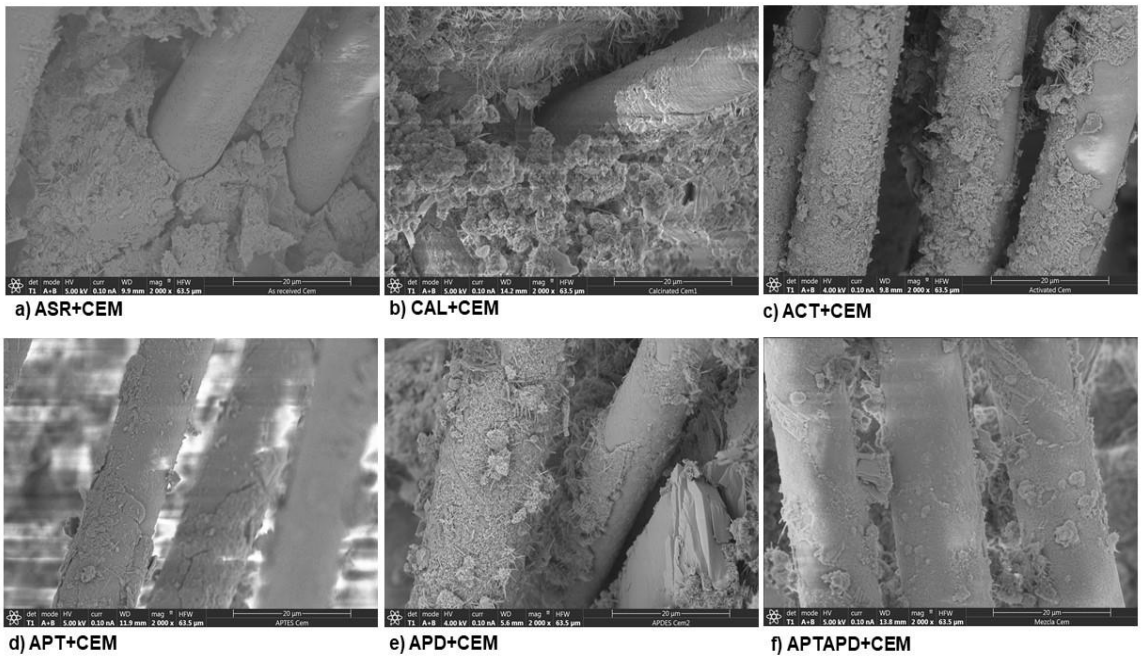

Figure 24. SEM images for all fiber reinforced mortar samples at 2000× magnification.

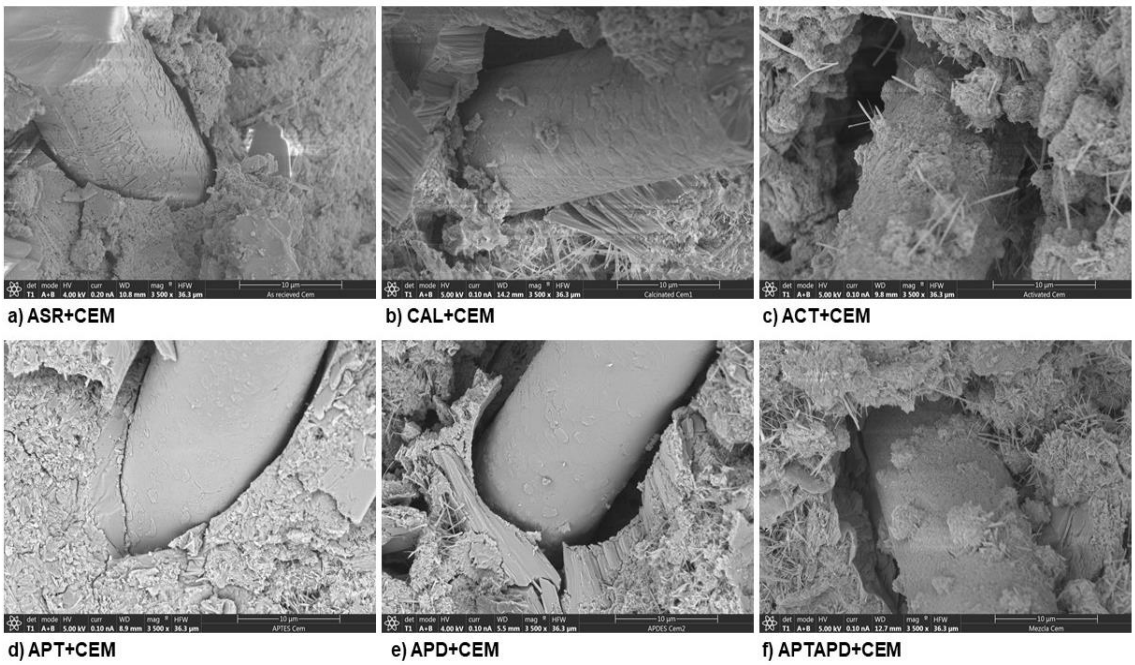

Figure 25. SEM images for all fiber reinforced mortar samples at 3500× magnification.

The SEM image at 2000× and 3500× of magnification (Figures 24 and 25) provided information about the type of failure at the fiber-matrix interface. When using as-received fibers and calcinated fibers (Figures 24 a and b, figures 25 a and b) smooth fibers surfaces can be observed in general indicating an adhesive failure at the interface. However, when activated or silanized fibers were used part of the cement matrix remained adhered to the

fibers surfaces which suggests a higher contribution of cohesive matrix failure. These results point out that silanized fibers or simply activated fibers enhance adhesion between the reinforcement and the matrix as expected attending the mechanical behavior already discussed. In fact, the samples, which present more cementitious material remaining on the fibers after the failure, are ACT+CEM and APTAPD+CEM also present the highest mechanical properties in terms of mechanical strength and toughness.

6.3.3.2. Surface Profilometry Measurements

- Laser Profilometry

To better understand the failure mechanism in the neat and fiber-reinforced cement-based mortars, 3D topographic images and the corresponding surface parameters (P_a and P_q) were evaluated. With this technique, information at a higher scale than that given by the SEM was obtained. Fractographic analysis was performed on the fracture surface of the materials resulting from the three-point flexural tests. A representative 3D topographic image for each sample is shown in Figure 26. In addition, linear profiles were extracted from the surfaces recorded. As an example, in Figure 27 the linear profile extracted from the fracture surface of the REF CEM sample is shown (blue line represents the mean profile).

The mean values of the profile parameters P_a and P_q for each sample are gathered in Table 7 and the corresponding trends are shown in Figure 28.

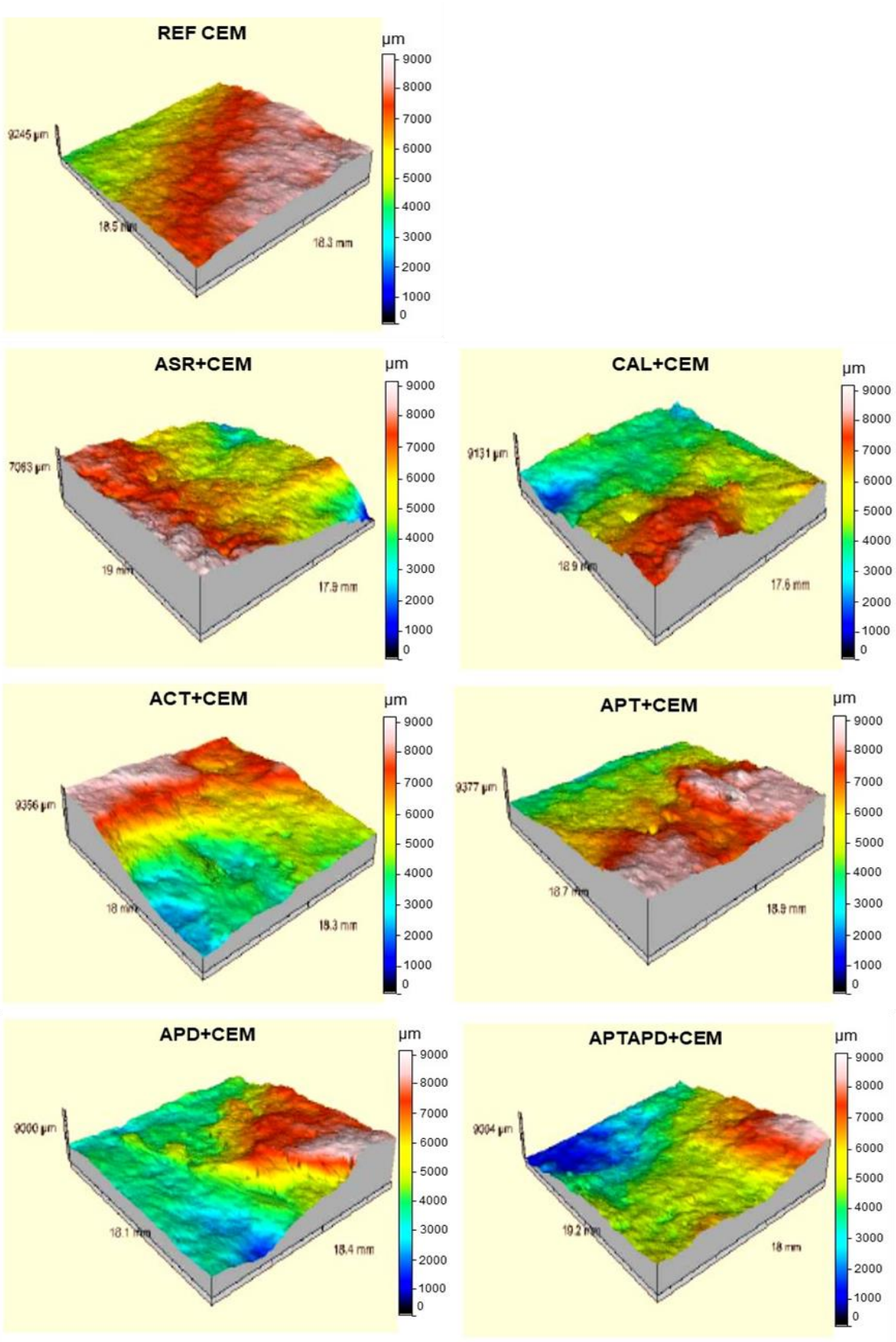

Figure 26. Representative 3D topographic images of fracture surfaces of the cement-based mortars under study.

3D profile images (Fig.26) point out that the RER CEM sample shows a smoother fracture surface than the other samples with fibers. Indeed, more tortuous fracture surfaces are evident for the mortars containing fibers. Studies about the influence of aggregates size indicate that, in general, tortuous fracture surfaces denote a less brittle behavior in concrete and mortars [41]. Consequently, and being in accordance with the mechanical studies, the results obtained point out that the presence of the fibers should lead to less brittle behavior since more topographic heterogeneity was obtained.

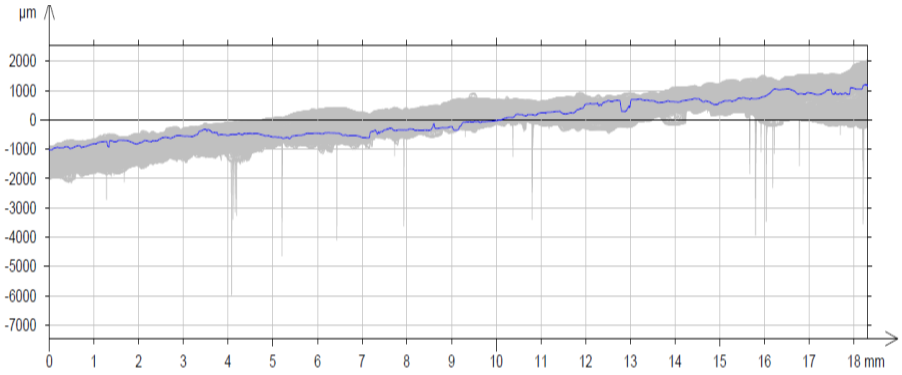

Figure 27. Example of linear profile extracted from a 3D image of a fracture surface of the REF CEM sample.

Table 7. Profile parameters obtained by laser profilometry.

	P_a (µm)	P_q (µm)
REF CEM	556 ± 233	643 ± 251
ASR+CEM	942 ± 316	1108 ± 345
CAL+CEM	613 ± 145	736 ± 162
ACT+CEM	868 ± 393	1052 ± 540
APT+CEM	678 ± 416	864 ± 396
APD+CEM	1180 ± 354	1376 ± 426
APTAPD+CEM	817 ± 386	956 ± 452

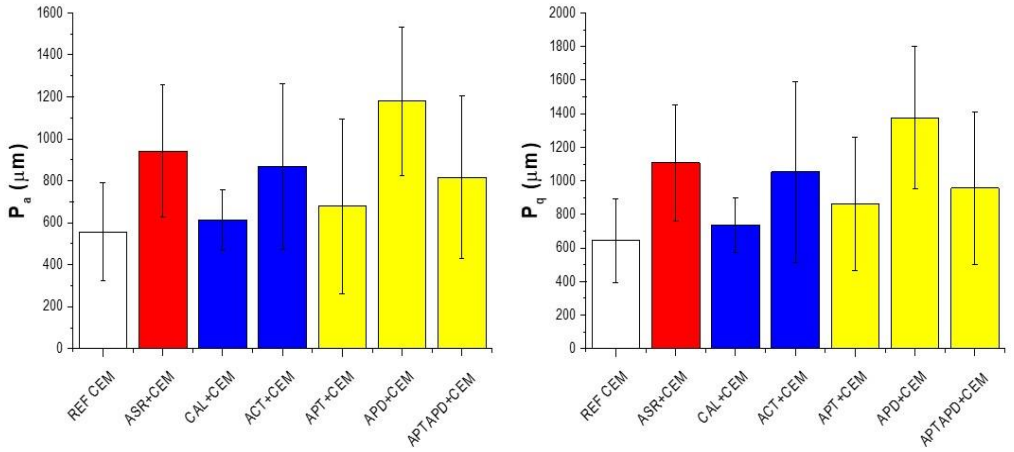

Figure 28. P_a (µm) and P_q (µm) profile parameters trend by laser profilometry for cement-based mortars.

On the other hand, P_a and P_q increase for the fiber reinforced samples compared to the neat sample. Considering the high standard deviation obtained due to the great heterogeneity of these materials in terms of defects, only qualitative consideration can be made. The presence of the fibers and the nature of their surface seems to slightly affect the interface adhesion and the meso and microstructure of the matrix and, as a consequence, the fracture mechanism that will be reflected in the final fracture surface of the whole materials.

- Optical Profilometry

In order to evaluate possible change on the failure mechanism at higher magnification, 3D profile images and the primary profile parameters (P_a and P_q) were collected by optical profilometry.

As an example, representative 3D images of all groups of investigated samples is shown in the Figure 29.

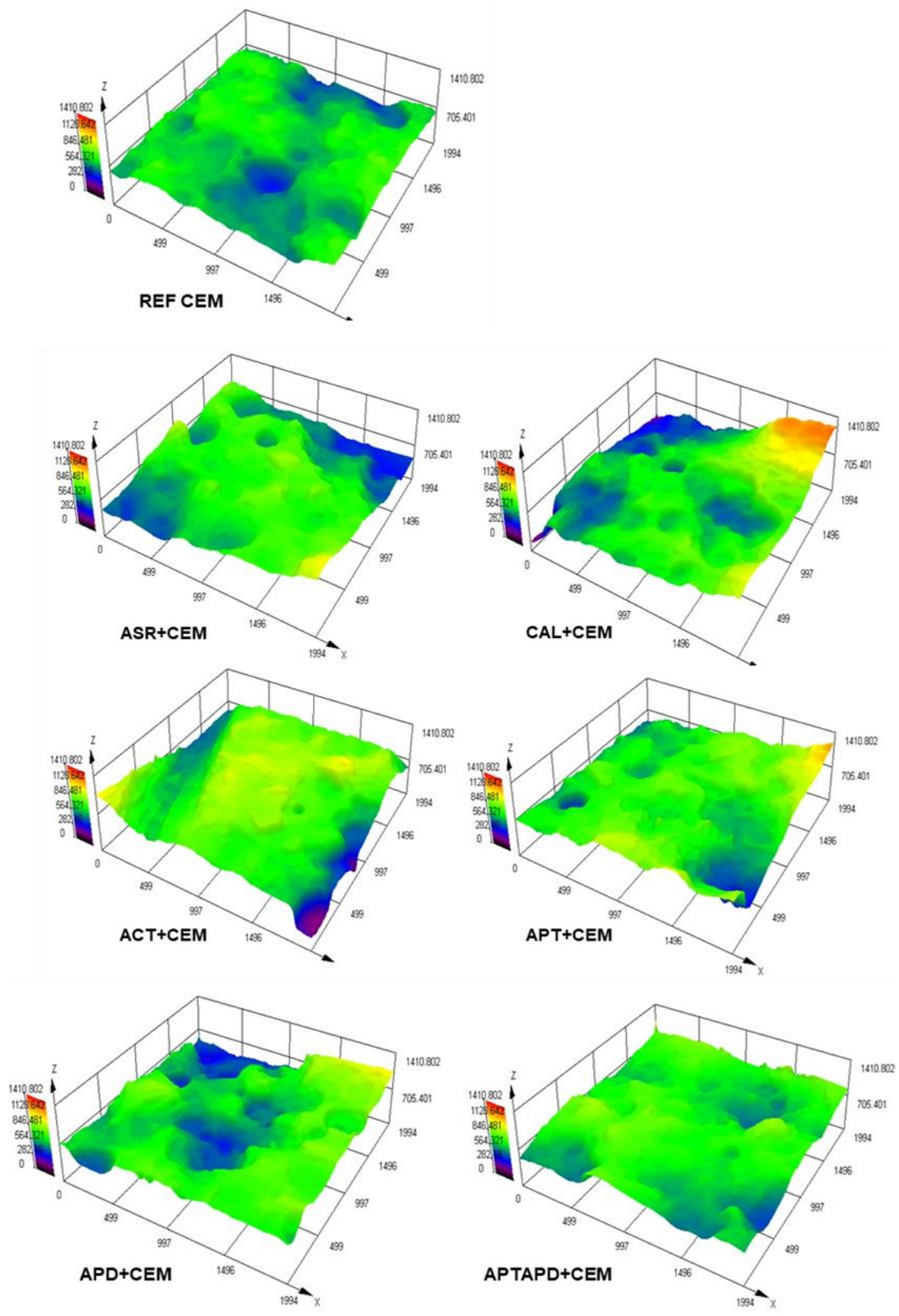

Figure 29. Representative 3D topographic images of fracture surfaces of the cement-based mortars under study.

In this case, the topographic characteristics (such as the presence of pores) of the fracture surfaces are more pronounced than the 3D profile images obtained with Laser Profilometry. However, the differences in surface irregularities between neat and reinforced samples are more clearly observed when lager regions of observations are taken into account as it happens using laser profilometer which allows inspecting the whole fracture surface of the speciments. The average of the profile parameters is given in Table 8 and plotted in Fig. 30.

Table 8. Profile parameters obtained by optical profilometry.

	P_a (µm)	**P_q (µm)**
REF CEM	56 ± 11	68 ± 13
ASR+CEM	74 ± 15	89 ± 17
CAL+CEM	76 ± 22	92 ± 26
ACT+CEM	70 ± 13	84 ± 15
APT+CEM	64± 16	77 ± 18
APD+CEM	72 ± 16	87 ± 20
APTAPD+CEM	61 ± 12	74± 13

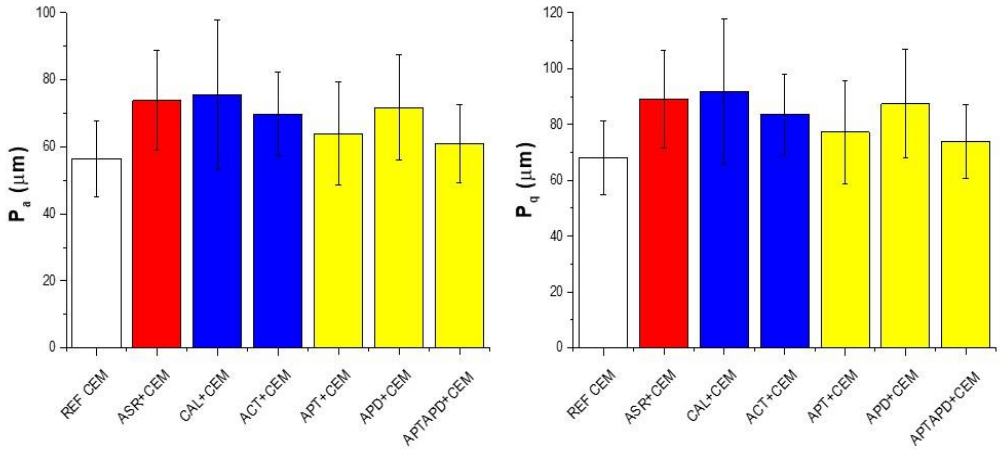

Figure 30. P_a (µm) e P_q (µm) profile parameters obtained by optical profilometry as a function of type of sample.

Results given in Table 8 and Figure 30 show similar tendencies to those obtained by laser profilometry. In fact, again, there was an increase in the P_a and P_q values for all the fiber reinforced mortar samples respect to the reference material. On the other hand, in general, the trends observed for the samples containing fibers with different surface treatment was the same to that observed in Figure 28.

6.3.4. Atomic Force Microscopy (AFM)

AFM characterization of the as-received and modified fibers surfaces was done. An estimation of surface roughness at nanoscopic scale is interesting to evaluate possible influences on the final interactions with the matrix. From AFM topographic images, the roughness parameters R_a and R_q of each kind of fiber were extracted (Table 9 and Figure 31).

Table 9. Roughness parameters (R_a and R_q) obtained for as-received and modified basalt fibers.

	R_a (nm)	**R_q (nm)**
AS-RECEIVED	2.2 ± 1.0	2.7 ± 1.0
CALCINATED	1.7 ± 0.7	2.3 ± 1.0
ACTIVATED	1.1 ± 0.7	2.1 ± 1.7
APTES	2.4 ± 1.3	3.2 ± 1.7
APDES	2.1 ± 0.2	2.6 ± 0.3
APTES+APDES	2 ± 1.5	2.7 ± 2.1

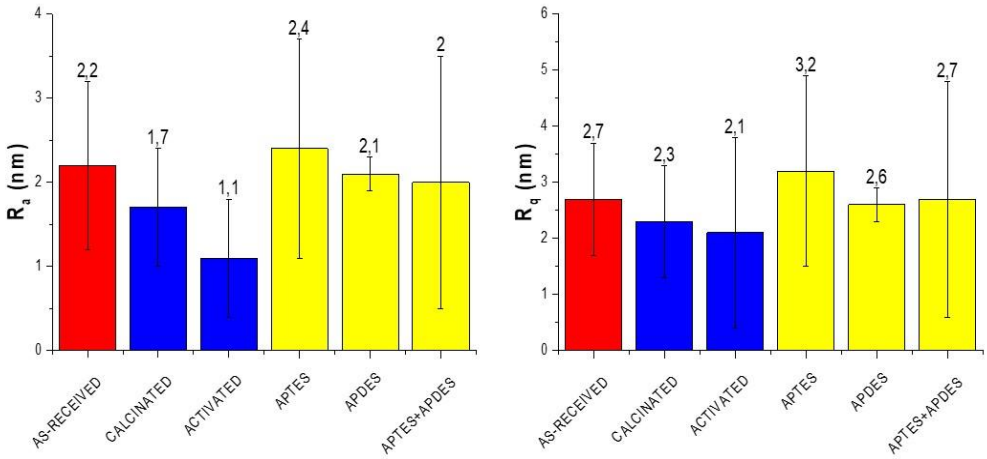

Figure 31. Roughness parameters as a function of the type of fibers (as-received and modified basalt fibers).

Observing the results and the high standard deviations obtained, only a few qualitative considerations can be taken into account. It is observed a decrease in R_a and R_q from the as-received fibers the calcinated and activated ones. When commercial sizing is removed by the calcination process and subsequent activation process (calcinated fibers subjected to an acid process for hydroxyl regeneration) smoother surfaces were obtained. On the other hand, when aminosilane are applied on the fibers surfaces an increase in R_a and R_q is shown. The highest values of the roughness parameters obtained for APTES coating is due

to the high amount of organic matter deposited on the fibers surfaces. These results are in accordance with morphologic and topographic observations carried out by SEM and AFM (Chapter 4). The higher surface roughness observed for fibers treated with the trifunctional silane might contribute to improve the adhesion between the fiber and the matrix. However, in this sense there is not any correspondence with SEM fractographic analysis nor the mechanical behavior of the samples. Therefore, the roughness differences at nanoscale of the surfaces of the reinforcement do not seem to influence the final adhesion and mechanical performance of the cement-based composites.

6.4. Conclusions

The study about interactions and therefore compatibility between as-received and modified basalt fibers with cement matrix allows to draw some interesting conclusions.

- The results obtained from mechanical tests shown that the presence of the fibers so as their surface treatment is a potential way to improve performance in cement-based mortars:
  - Results from three-point flexural test suggests that better performance are achieved for samples containing activated (ACT+CEM) and APTES+APDES basalt fibers (APTAPD+CEM). Probably, the presence of high number of OH groups and/or easier accessibility to those OH on the fibers, might be responsible of better interaction with the cement matrix. However, as a main conclusion extracted from the flexural results it seems that a better compatibility exists between the APTES+APDES basalt fibers and cement matrix. The latter, in fact, showed a lesser brittle behavior with an increase in the flexural strength and toughness values.
  - In the case of compressive behavior, it was observed that, although not relevant changes compared to the neat mortar were observed slightly higher compressive strength values were obtained for samples containing activated (ACT+CEM) and silanized APTES (APT+CEM) and APTES+APDES (APTAPD+CEM) basalt fibers. Here again it might be said that the higher accessibility to the OH groups generated by the activation process seems to induce a better compatibility with the cement matrix. However, here it is expected to be less effective the reinforcement due to the load transmission form the matrix to the

fibers and therefore only a small contribution due to the modulus increase for all samples containing fibers (except for ASR+CEM) associated to the incorporation of fibers was observed.

- The small differences in the results obtained by BET-BJH analysis, point out that the presence of the fibers and the surface treatments does not significantly change the micro and meso structure of the neat mortar.
- SEM images highlight a more cohesive failure mechanism for the samples containing activated (ACT+CEM) and APTES+APDES (APTAPD+CEM) basalt fibers. These results point out that silanized fibers or simply activated fibers enhance adhesion between the reinforcement and the matrix according to the mechanical behavior.
- Profilometry measurements have demonstrated that a more tortuous fracture surfaces are evident for the mortars containing fibers. Consequently, and being in accordance with the mechanical studies, the results obtained point out that the presence of the fiber confer a less brittle behavior.
- AFM results shown that the roughness differences at nanoscale of the surfaces of the reinforcement do not seem to influence the final adhesion and mechanical performance of the cement-based composites.

References

[1] D.W. Fowler, Repair materials for concrete structures, in: N. Delatte (Ed.), Fail. Distress Repair Concr. Struct., Woodhead Publishing Limited, 2009: pp. 194–207. doi:10.1533/9781845697037.2.194.

[2] A.M. Brandt, Fibre reinforced cement-based (FRC) composites after over 40 years of development in building and civil engineering, Compos. Struct. 86 (2008) 3–9. doi:10.1016/j.compstruct.2008.03.006.

[3] K. Raoufi, J. Weiss, The role of fiber reinforcement in mitigating shrinkage cracks in concrete, in: R. Fangueiro (Ed.), Fibrous Compos. Mater. Civ. Eng. Appl., Woodhead Publishing Limited, 2011: pp. 168–188. doi:10.1016/B978-1-84569-558-3.50006-5.

[4] M.E. Arslan, Effects of basalt and glass chopped fibers addition on fracture energy and mechanical properties of ordinary concrete: CMOD measurement, Constr. Build. Mater. (2016). doi:10.1016/j.conbuildmat.2016.03.176.

[5] S.P. Shah, C. Ouyang, Mechanical behavior of fiber- reinforced cement-based composites, J. Am. Ceram. Soc. 74 (1991) 2947–2953. doi:https://doi.org/10.1111/j.1151-2916.1991.tb06836.x.

[6] C.D. Johnston, Fiber-Reinforced Cements and Concretes, in: Adv. Concr. Technol., Taylor & F, Taylor & Francis Group, 2001: p. Volume 3.

[7] V. Fiore, T. Scalici, G. Di Bella, A. Valenza, A review on basalt fibre and its composites, Compos. Part B Eng. 74 (2015) 74–94. doi:10.1016/j.compositesb.2014.12.034.

[8] L.R. Betterman, C. Ouyang, S.P. Shah, Fiber-matrix interaction in microfiber-reinforced mortar, Adv. Cem. Based Mater. 2 (1995) 53–61. doi:10.1016/1065-7355(95)90025-X.

[9] L. Li, Z. Xia, Role of interfaces in mechanical properties of ceramic matrix composites, Adv. Ceram. Matrix Compos. Second Ed. (2018) 355–374. doi:10.1016/B978-0-08-102166-8.00015-3.

[10] V.A. Rybin, A. V. Utkin, N.I. Baklanova, Alkali resistance, microstructural and mechanical performance of zirconia-coated basalt fibers, Cem. Concr. Res. 53 (2013) 1–8. doi:10.1016/j.cemconres.2013.06.002.

[11] Y.M. Abbas, M. Iqbal Khan, Fiber–Matrix Interactions in Fiber-Reinforced Concrete: A Review, Arab. J. Sci. Eng. 41 (2016) 1183–1198. doi:10.1007/s13369-016-2099-1.

[12] M. Iorio, M.L. Santarelli, G. González-Gaitano, J. González-Benito, Surface

modification and characterization of basalt fibers as potential reinforcement of concretes, Appl. Surf. Sci. 427 (2018) 1248–1256. doi:10.1016/j.apsusc.2017.08.196.

[13] R.D. Tolêdo Filho, K. Ghavami, G.L. England, K. Scrivener, Development of vegetable fibre-mortar composites of improved durability, Cem. Concr. Compos. 25 (2003) 185–196. doi:10.1016/S0958-9465(02)00018-5.

[14] R. Ralegaonkar, H. Gavali, P. Aswath, S. Abolmaali, Application of chopped basalt fibers in reinforced mortar: A review, Constr. Build. Mater. 164 (2018) 589–602. doi:10.1016/j.conbuildmat.2017.12.245.

[15] J. Branston, S. Das, S.Y. Kenno, C. Taylor, Mechanical behaviour of basalt fibre reinforced concrete, Constr. Build. Mater. 124 (2016) 878–886. doi:10.1016/j.conbuildmat.2016.08.009.

[16] C. Jiang, K. Fan, F. Wu, D. Chen, Experimental study on the mechanical properties and microstructure of chopped basalt fibre reinforced concrete, Mater. Des. 58 (2014) 187–193. doi:10.1016/j.matdes.2014.01.056.

[17] C. High, H.M. Seliem, A. El-Safty, S.H. Rizkalla, Use of basalt fibers for concrete structures, Constr. Build. Mater. (2015). doi:10.1016/j.conbuildmat.2015.07.138.

[18] M.L. Santarelli, F. Sbardella, M. Zuena, M. Albé, G. Quattrociocchi, J. Tirilló, M. Valente, F. Sarasini, Malte più performanti con le fibre di basalto, Compos. Mag. 33 (2014) 7–16. http://hdl.handle.net/10278/44412.

[19] Z.C. Girgin, M.T. Yıldırım, Usability of basalt fibres in fibre reinforced cement composites, Mater. Struct. Constr. 49 (2016) 3309–3319. doi:10.1617/s11527-015-0721-4.

[20] J. Kaufmann, R. Loser, A. Leemann, Analysis of cement-bonded materials by multi-cycle mercury intrusion and nitrogen sorption, J. Colloid Interface Sci. 336 (2009) 730–737. doi:10.1016/j.jcis.2009.05.029.

[21] B. Zhang, Relationship between pore structure and mechanical properties of ordinary concrete under bending fatigue, Cem. Concr. Res. 28 (1998) 699–711. doi:10.1016/S0008-8846(98)00037-4.

[22] M. Lawrence, Y. Jiang, Porosity, Pore Size Distribution, Micro-structure, in: Bio-Aggregates Based Build. Mater., 2017. doi:10.1007/978-94-024-1031-0.

[23] E. Standard, EN 197-1 Cement. Part 1: Composition, specifications and conformity criteria for common cements, (2011).

[24] E. Standard, EN 196-1 Methods of testing cement. Part 1: Determination of strength, (2005) 1–33.

[25] E. Standard, EN 1015-11 Methods of test for mortar for masonry. Part 11: Determination of flexural and compressive strength of hardened mortar, (2000).

[26] M. Tiryakioğlu, D. Hudak, G. Ökten, On evaluating Weibull fits to mechanical testing data, Mater. Sci. Eng. A. 527 (2009) 397–399. doi:10.1016/j.msea.2009.08.014.

[27] A. Saghafi, A.R. Mirhabibi, G.H. Yari, Improved linear regression method for estimating Weibull parameters, Theor. Appl. Fract. Mech. 52 (2009) 180–182. doi:10.1016/j.tafmec.2009.09.007.

[28] J. Gonzalez-Benito, J. Martinez-Tarifa, M.E. Sepúlveda-García, R.A. Portillo, G. Gonzalez-Gaitano, Composites based on HDPE filled with $BaTiO_3$ submicrometric particles. Morphology, structure and dielectric properties, Polym. Test. 32 (2013) 1342–1349. doi:10.1016/j.polymertesting.2013.08.012.

[29] A. Nevarez-Rascon, A. Aguilar-Elguezabal, E. Orrantia, M.H. Bocanegra-Bernal, Compressive strength, hardness and fracture toughness of Al_2O_3 whiskers reinforced ZTA and ATZ nanocomposites: Weibull analysis, Int. J. Refract. Met. Hard Mater. 29 (2011) 333–340. doi:10.1016/j.ijrmhm.2010.12.008.

[30] J.B. Quinn, G.D. Quinn, A practical and systematic review of Weibull statistics for reporting strengths of dental materials, Dent. Mater. 26 (2010) 135–147. doi:10.1016/j.dental.2009.09.006.

[31] L. Chronopoulou, C. Palocci, F. Valentino, I. Pettiti, S. Wacławek, M. Černík, M. Petrangeli Papini, Stabilization of Iron (Micro)Particles with Polyhydroxybutyrate for In Situ Remediation Applications, Appl. Sci. 6 (2016) 417. doi:10.3390/app6120417.

[32] A. Pacella, C. Cremisini, E. Nardi, M.R. Montereali, I. Pettiti, M. Giordani, M. Mattioli, P. Ballirano, Different erionite species bind iron into the structure: A potential explanation for fibrous erionite toxicity, Minerals. 8 (2018) 1–16. doi:10.3390/min8020036.

[33] E.P. Barrett, L.G. Joyner, P.P. Halenda, The Determination of Pore Volume and Area Distributions in Porous Substances. I. Computations from Nitrogen Isotherms, J. Am. Chem. Soc. 73 (1951) 373–380. doi:10.1021/ja01145a126.

[34] J.N. Miller, J.C. Miller, Statistics and Chemometrics for Analytical Chemistry, Sixth Edit, Pearson Education Limited, 2010.

[35] K.S.W. Sing, International Union of Pure And Applied Chemistry, Reporting Physisorption data for Gas / Solid Systems with Special Reference to the Determination of Surface Area and Porosity, Pure Appl. Chem. 54 (1982) 2201–2218. doi:10.1351/pac198557040603.

[36] W.-H. Huang, C.-C. Tseng, Improving the Properties of Cement Grout using Organic Fibre and Superplasticizer, Spec. Tech. Mater. Concr. Constr. 31 (1999) 57–67. doi:10.1680/stamfcc.28258.0006.

[37] S. Maria, Methods for porosity measurement in lime-based mortars, Constr. Build. Mater. 24 (2010) 2572–2578. doi:10.1016/j.conbuildmat.2010.05.019.

[38] E.B. Bermejo Núñez, A. Moragues Terrades, M. Gálvez Ruiz , J. C. Fernández Cánovas, Permeabilidad Y Porosidad En Hormigones Autocompactantes, An. Mecánica La Fract. 2 (2008) 581–586.

[39] F. Rouquerol, J. Rouquerol, K. Sing, Adsorption by Powders & Porous Solids. Principles, Methodology and Applications, Academic Press, 1999. doi:https://doi.org/10.1016/B978-0-12-598920-6.X5000-3.

[40] R.S. Mikhail, L.E. Copeland, S. Brunauer, Pore structures and surface Areas of hardened Portland Cement Pastes By Nitrogen Adsorption, Can. J. Chemisrty. 42 (1964) 426–438. doi:https://doi.org/10.1139/v64-060.

[41] M.A. Issa, M.A. Issa, M.S. Islam, A. Chudnovsky, Fractal dimension-a measure of fracture roughness and toughness of concrete, Eng. Fract. Mech. 70 (2003) 125–137. doi:10.1016/S0013-7944(02)00019-X.

APPENDIX A. Weibull probability plot preparation

The Weibull strength distribution graphs for each group of samples were prepared as follow:

- The data were ordered from lowest to highest mechanical strength values, σ. When a certain value was repeated several times, it was eliminated and consequently only one value it was considered.
- The natural logarithms of the mechanical strength, ln(σ) were computed.
- The probability of fracture, P_f, was estimated and assigned to each datum. A common way to estimate P_f with low bias when used with linear regression analyses is $P_f = (i-0.5)/n$, where i is the i-th datum and n is the total number of data points (for this study n=6).
- The double natural logarithm of $[1/(1-P_f)]$ was calculated.
- A graph is prepared by representing $\ln\ln[1/(1-P_f)]$ as a function of ln(σ).
- The Weibull modulus was obtained from the slope of the straight line arising from the linear fit of the later plot.

APPENDIX B. Method used to obtain the final *stress-strain* curves

In the *load-displacement* original curves as those shown in the Figure 1 a) it is possible to observe some artifacts in the initial part of them arising from certain adjustments of the universal testing machine during the tests.

Therefore, to obtain the real *stress-strain* curves that finally were used to evaluate the parameters use to describe the mechanical behavior of these materials, a simple modification of the *load-displacement* original data was done.

The point considered as the beginning of the elastic part of the curve was estimated by extrapolation from a linear regression of the elastic region of the original plots. Therefore, in the initial part of the original plots, some intervals of clamps displacement for which values of stress remained constant (considered artifacts) were eliminated (Figure 1 b).

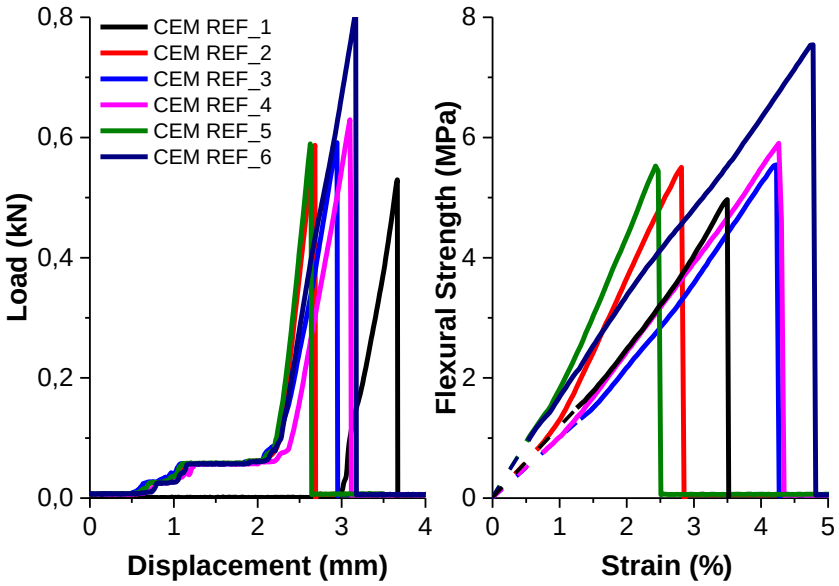

Figure 1. *Load-displacement* original curves a) and *stress-strain* curves b) for cement-based mortar sample

CHAPTER 7

STUDY OF THE INTERACTIONS BETWEEN BASALT FIBERS AND NATURAL HYDRAULIC LIME MATRIX

CHAPTER 7
STUDY OF THE INTERACTIONS BETWEEN BASALT FIBERS AND NATURAL HYDRAULIC LIME MATRIX

Abstract

In order to contribute to the development of sustainable materials in the building industry and to increase their use for restoration and conservation of Cultural Heritage, fiber-reinforced natural hydraulic lime-based mortars were prepared. A study on the compatibility in terms of interactions between basalt fibers and natural hydraulic lime, NHL, is proposed. Different characteristics of the reinforcement surface were studied looking for the best interphase respect to the final performance of the composite materials. As-received, calcinated, activated and silanized (by three different silane aqueous solutions: i)γ-aminopropyltriethoxysilane, APTES; ii) γ-aminopropylmethyldiethoxysilane, APDES and iii) a mixture APTES+APDES 50 % by weight) basalt fibers were dispersed in natural hydraulic lime (NHL 5) matrix. Performances of the resulting composites materials were evaluated by mechanical tests (three-point flexural test and compressive strength test). The mechanical performances were interpreted taking into account possible interactions between the fiber surface characteristics and the matrix that could be responsible of microstructural changes in the material. Aimed to study this, porosity measurements by BET-BJH textural analysis were carried out. On the other hand, the adhesion at the fiber-matrix interface was also studied with a fractographic analysis by SEM analysis and laser and optical profilometry.

The results obtained indicate that the presence of basalt fibers so as a surface treatment can improve mechanical performance in natural hydraulic lime-based mortar. In general, results from the analysis performed suggest that better behavior is achieved when APTES+APDES silanized basalt fibers are dispersed in natural hydraulic lime matrix (APTAPD+NHL sample).

7.1. Introduction

The use of materials non-compatible with the original structures for recovering and restoring ancient buildings and monuments represents one of the most risk for the preservation of the historic-architectural Cultural Heritage. Indeed, the use of improper binders, such as cement-based mortars represents one of the main problems to be faced in the restoration field. Although the modern architecture and the most of modern buildings could not exist without the presence of Portland cement, is nowadays recognized that it should never be used in the restoration of historical-artistic heritage because of its different physical, chemical and mechanical properties.

Sometimes cement-based mortars have been used in several restoration interventions causing failure and acceleration of damage to the monuments [1–8]. Occasionally, also polymer-based materials have been used to restoration interventions showing several incompatibilities with ancient materials due to the different behaviours in the environmental conditions [9].

In the Figure 1 an example of a restoration intervention is shown where the use of improper materials caused a great damage to the ancient structure. Indeed, an ancient mosaic of the Roman Villa of Silin (Leptis Magna-Libya) was damaged from the corrosion of the metallic bars (indicated by the red arrows) of the reinforced concrete. The latter was the material chosen in the 70s to restore the mosaic pavement. The oxidation of the bars has caused the detachment of tesserae [10].

Figure 1. Intervention restoration of the mosaic pavement of the Roman Villa of Silin (Lepcis Magna- Libya) (photos ISCR-Istituto Superiore per la Conservazione e il Restauro).

In addition to the improper use of materials for restoration interventions, climatic conditions and catastrophic events (such as floods and earthquakes) could contribute to damage ancient masonries and buildings. In the Figure 2, as an example, the historical Library of the University of L'Aquila (Italy) damaged for the earthquake can be observed.

Figure 2. Historical Library of the University of L'Aquila (Italy) damaged for the earthquake (photo Prof. F.Bontempi).

During a restoration, the compatibility between the new mortars and the original materials is requested and natural hydraulic lime-based mortars are normally used, especially to recover plasters.

As discussed in the Chapter 2 (section 2.1.2), hydraulic lime mortars have been used as construction materials since ancient times and they characterized the most of building of great cultural interest.
Therefore, this material fulfils the compatibility conditions required in the restoration intervention. Among them, i) chemical compatibility, ii) physical compatibility, iii) structural and mechanical compatibility [2–4].

Generally, the lime-based mortars are characterized by good breathability due to its high porosity and permeability. Usually, mortar permeability is desirable since vapor transport have to be maintained in a masonries to avoid salt crystallization (efflorescence and subflorescence) and mold [11,12]. In a restoration mortar, moreover, the strength is an important parameter to be considered. In fact, usually, masonry structures could be subjected to movements arising from creep or thermal effects. Consequently, a mortar

should be considerably weaker than original materials for supporting the slight movements occurring in the building. Despite, if the restoration mortar is too strong, stress development is possible causing failure in the original masonry. In this way, lime-based mortars have to show structural and mechanical properties compatible with ancient structure [2,4,11,13].

In contrast a cement-based mortar is too hard and rigid and lesser flexible to accommodate the building movements. In addition, they are lesser permeable and contains more soluble salts, which can be harmful for the historic building. These salts not only produce unaesthetic layers owing to efflorescence phenomena on the buildings, but can also develop large crystallization pressures, damaging the building materials [1–4,11,14,15]. For these reasons cement-based mortars have caused several damages to the ancient structures and it is important to avoid their use in the restoration field.

Nevertheless, often cement was used as repair material since lime based-mortars present some disadvantages such as: i) slow setting that could delay the restoration works, ii) lower strength than cement mortars, iii) take long time to harden and consequently to reach strength.
In fact, in cement, the setting is a consequence of the hydration of calcium silicates, which starts quickly owing to the hydration of the C_3S and continues more slowly because of the hydration of the C_2S. The hydration of both compounds gives strength to the mortar [2,4,11]. As described in Chapter 2 (section 2.1.2), natural hydraulic lime only contains C_2S phase with some trace of C_3S, therefore its final mechanical properties are lower. Another aspect that has increased the use of cement compared to the lime has been the lack of studies about the latter in contrast with a largely standardization of cement products [1,2,4].

Currently, the interest in the use of natural hydraulic lime is growing also in the modern building industry were the use of eco-friendly materials is rising. In this green approach, the natural hydraulic lime is responsible of a reduction of CO_2 emission in comparison with the common Portland Cement for different reasons: i) lesser energy is required in the NHL production process ii) the most of setting and hardening process in NHL occurs for carbonation process (section 2.1.2 of Chapter 2). Therefore, considering the life cycle of

the lime, most of the CO_2 produced during production process is reabsorbed during carbonation process [5,11,16–18].

However, as mentioned above, the main problem of NHL is due to its lower mechanical properties than Portland cement. In order to increase their mechanical performances, different types of natural and synthetic fibers have been used as reinforcements of lime based-mortar [11,19,20]. In addition, the presence of fibers, especially short fibers, could contribute to reduce the shrinkage cracking phenomena affecting mortars as for cement based-mortars (see section 6.1 of chapter 6). The presence of short fibers is limiting crack opening and distributing the stress to the nearby matrix, moreover, they are able to suppress strain localization and to prevent therefore microcracks from developing into macrocracks [5,21].

However, studies focused on the study of fibers reinforced natural hydraulic lime-based mortars are very not widespread today. Less widespread are the studies about the use of basalt fibers in this type of matrix. Recently, Iucolano et al. [5] studied the effect of basalt and glass fibers on natural hydraulic lime (NHL 3.5) mortars. They found that the presence of the fibers modified the mechanical behavior of the hydraulic lime based-mortars. A significant improvement of toughness and flexural post-cracking behavior have been observed in reinforced mortars. In contrast, a decrease in compressive strength value compared to the neat mortar was found. Santarelli et al. [6,7] investigated on the use of chopped basalt fibers in natural hydraulic lime (NHL 3.5) mortars. They refer that basalt fibers can affect the mechanical behavior of the mortars. However, they pointed out the need to investigate on the role of fiber-matrix interface and the need to improve it through surface treatments of the fibers to balance two opposing needs, strength and toughness.

In order to increase the scientific research in this sector, in this work a study about the compatibility in terms of interactions between as-received and modified chopped basalt fibers in natural hydraulic lime matrix is proposed. For improving fiber-matrix performance in this type of materials, surface treatments of the fibers surface are proposed (for the methods used to modify commercial basalt fibers surface see section 4.2.2 of Chapter 4). Despite this, it seems that until now there is not previous research about the effect of modified basalt fibers incorporated in this type of matrix.

The performances of the resulting mortars samples prepared were evaluated by mechanical tests (three-point flexural test and compressive strength tests). Porosity measurements by

BET-BJH textural analysis were performed to study possible microstructural changes in the material. A fractographic analysis by SEM and laser and optical profilometry was carried out to study failure mechanism and the adhesion at the fiber-matrix interface.

7.2. Experimental

7.2.1. Materials

In this study, a commercial natural hydraulic lime (NHL) provided by St.Astier (C.T.S., Madrid, Spain) was used as binder to prepare mortar samples. In particular the NHL used in this work is designed as NHL 5 according to European Standard UNI EN 459-1 [22].
As aggregate, a siliceous sand, with a grain size between 0.2-0.5 mm, provided by Arenas Silíceas Gómez Vallejo (Segovia, Spain) was used. Basalt continuous filament (mean diameter 17 μm) chopped to a length of about 6.4 mm with a sizing compatible with cement matrix was supplied by Incothelogy GmbH. A chlorhydric acid aqueous solution (37% wt), Sharlab, and two silanes, γ-aminopropiltriethoxysilane (APTES) and γ-aminopropilmethyldiethoxysilane (APDES), supplied by ABCR GmbH & Co.KG, were used to prepare pretreated and silanes coated basalt fibers. A commercial silicone (Silastic 3481 Base +Curing Agent S81, Feroca, S.A.) was used to prepare the molds for the mortar samples.

7.2.2. Samples Preparation

Mortar samples were prepared with a binder/aggregate ratio of 1:2. Distilled and deionized water was used in a water/binder ratio of 0.88. Compared to the mixtures prepared with cement matrix (see section 6.2.2 of Chapter 6), higher amount of water is necessary to allow the workability of the mixtures when lime is used. As-received and modified basalt fibers were added to the mixture at 1% by weight. The preparation methods of the modified basalt fibers are described in Chapter 4. The mixtures preparation and curing (Figure 3) were done in accordance to the standard UNI EN 196-1:2005 and UNI EN 1015-11:2007 as for cement-based mortars (section 6.2.2 of Chapter 6) [23,24]. In the Table 1 the samples codes and the components of the corresponding mixtures (six specimens for each mixture were prepared) are shown.

Table 1. Sample codes of the natural hydraulic lime-based mortars prepared and components of the mixtures.

Code	Components of Mixtures
REF NHL	NHL + sand
ASR + NHL	NHL + sand + as-received basalt fibers
CAL + NHL	NHL + sand + calcinated basalt fibers
ACT + NHL	NHL + sand + activated basalt fibers
APT + NHL	NHL + sand + silanized APTES basalt fibers
APD + NHL	NHL + sand + silanized APDES basalt fibers
APTAPD + NHL	NHL + sand + silanized APTES+APDES basalt fibers

Figure 3. Mixing (a) and curing (b-c) of natural hydraulic lime-based mortars.

7.2.3. Instrumental Techniques

The experimental techniques and methods, as well as the conditions, used to test and investigate natural hydraulic lime-based mortars, were the same used for cement based-mortars and described previously in the chapter 6 (see section 6.2.3). In particular, mechanical tests (*three-point flexural test* and *compressive test)*, BET-BJH textural analysis, fractographic analysis by scanning electron microscopy (SEM) and surface profilometry measurements (*laser and optical profilometry*) were carried out. Therefore, to avoid repetitive information, in this Chapter will proceed directly the discussion of the results obtained.

7.3. Results and Discussion

7.3.1. Mechanical Tests

➢ *Three-point flexural strength test*

The fracture and mechanical behavior of the mortar samples can be studied by the *stress-strain* curves and representative images of the fractured specimens (Figure 4-10).

Sometimes, the flexural curves obtained for each group of samples investigated showed irregular behavior. Therefore, and attending the complexity to analyze and interpret them, the method described in the Appendix B of Chapter 6 was used to eliminate artifacts arising from the testing machine.

Only some representative curves of the flexural behavior of these materials are given in Figures 4-10.

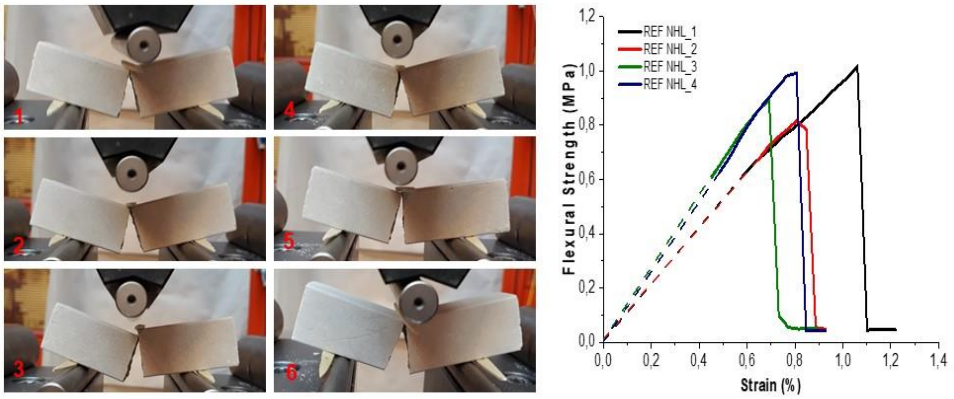

Figure 4. *Stress-strain* curves and representative images of fractured specimens of REF NHL samples.

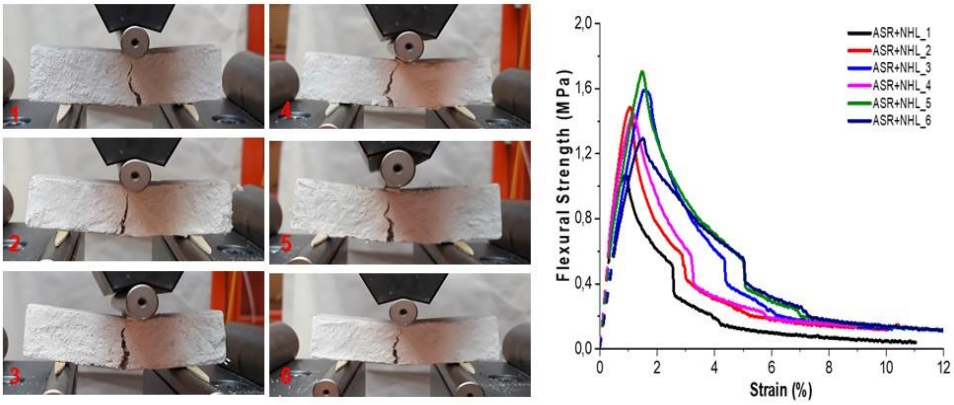

Figure 5. *Stress-strain* curves and representative images of fractured specimens of the ASR+NHL samples.

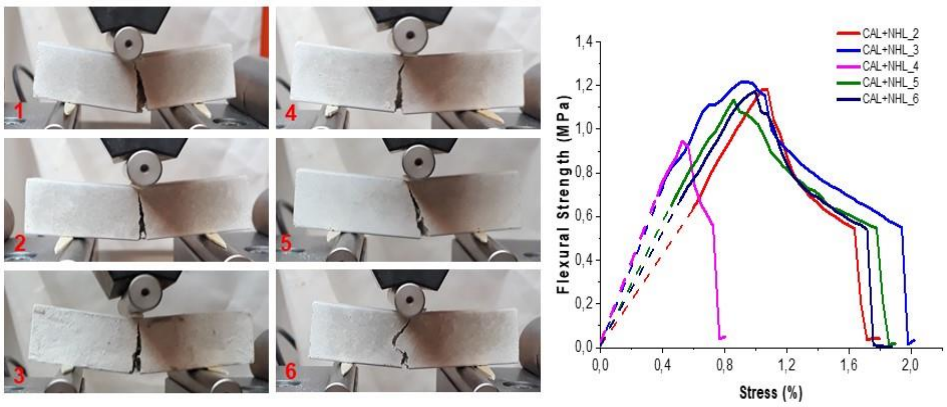

Figure 6. *Stress-strain* curves and representative images of fractured specimens of the CAL+NHL samples.

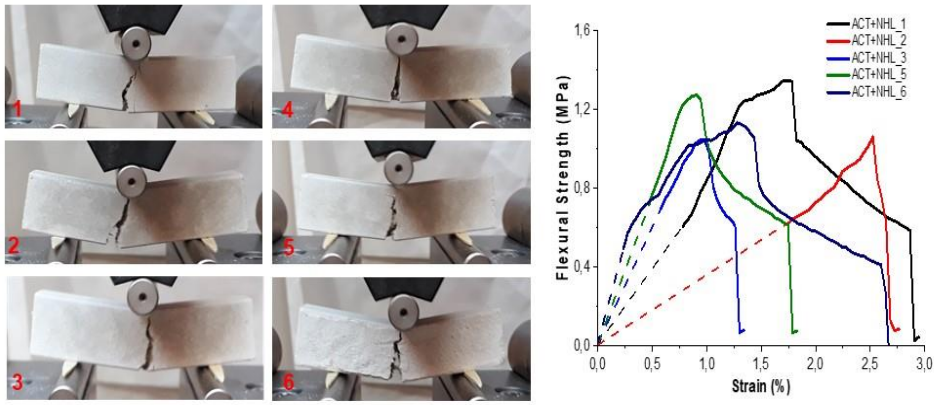

Figure 7. *Stress-strain* curves and representative images of fractured specimens of the ACT+NHL samples.

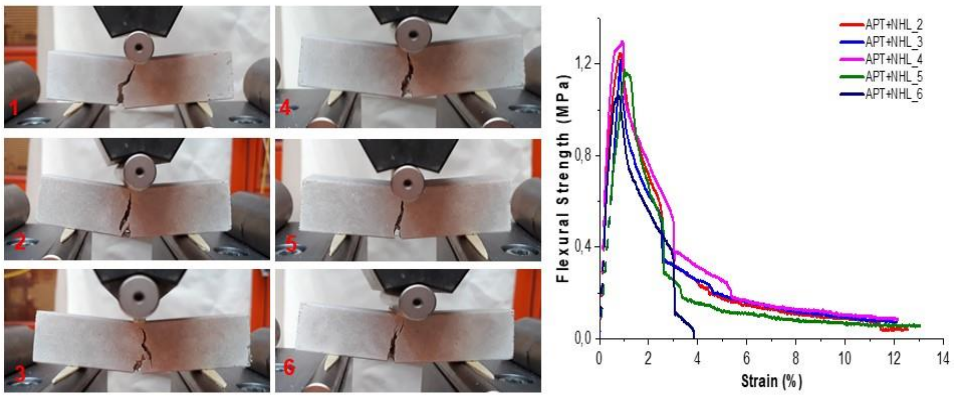

Figure 8. *Stress-strain* curves and representative images of fractured specimens of the APT+NHL samples.

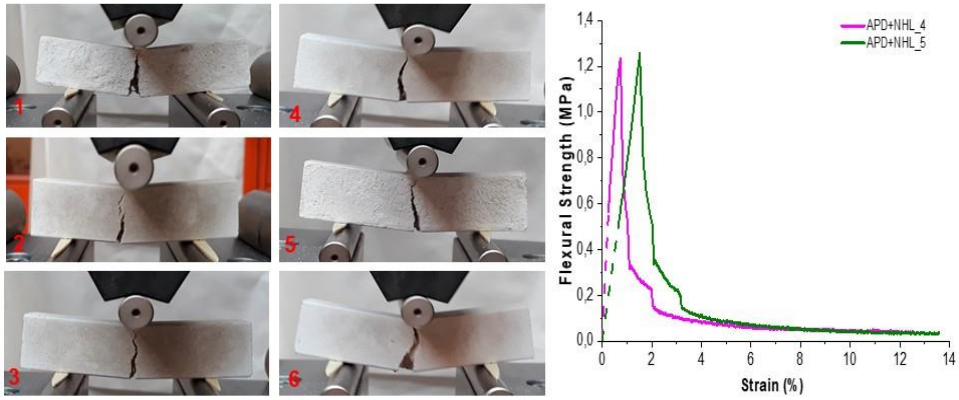

Figure 9. *Stress-strain* curves and representative images of fractured specimens of the APD+NHL samples.

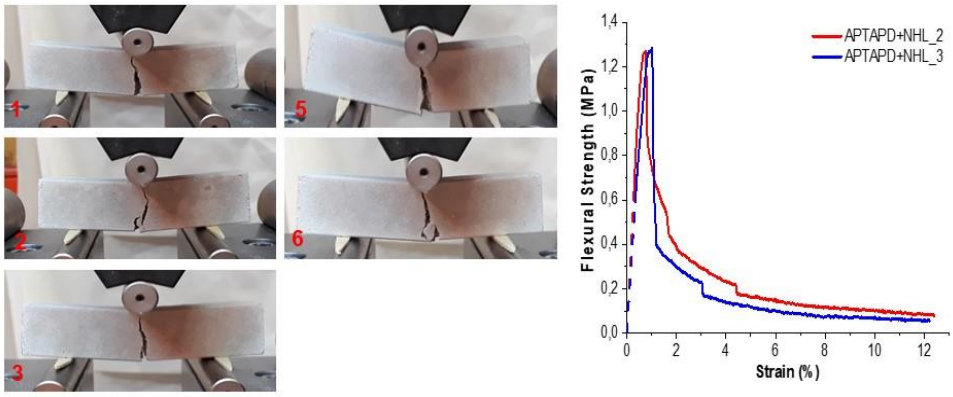

Figure 10. *Stress-strain* curves and representative images of fractured specimens of the APTAPD+NHL samples.

Observing the fracture behavior of neat and fiber-reinforced mortar samples in the photos of Figures 4-10, some differences can be noted. The neat mortar specimens (Figure 4) shown more homogeneous fracture leading to complete separation between the two pieces resulting from the fracture. Whereas, the samples reinforced with fibers (Figures 5-10) present more tortuous fracture development and the two pieces resulting from the fracture are not completely separated each other.

In addition, observing the *stress-strain* curves of Figures 4-10, the fiber-reinforced samples failed in a different way compared to the reference mortars (REF NHL). A brittle behavior is observed for the neat mortars (Figure 4). In fact, a toughness enhancement in the post-cracking behavior is apparently observed when fibers are added to the mixtures especially when as-received and aminosilanes treated basalt fibers are present (Figure 2, 7-10). In

fact, these samples failed in a more gradual way where it is possible to appreciate more signals of different points of mechanical failure. Probably, this behavior is due to a better interaction between the fibers and the natural hydraulic lime matrix conferring a lesser brittle behavior with an increase in toughness effect.

In contrast, when samples are prepared with activated and calcinated fibers (Figure 6-7), less brittle behavior is observed, showing a little improvement in post-peak toughness effect to finally fail catastrophically. In this case signals of different points of failure are not observed.

In order to better understand the flexural behavior of the samples prepared, a deeper analysis of the data obtained was done. The flexural strength (σ_f) values obtained for each sample were statistically analyzed by the Weibull distribution function (see section 6.2.3.1 of Chapter 6). In Figure 11 the Weibull probability plots for the flexural strength for all samples studied are shown.

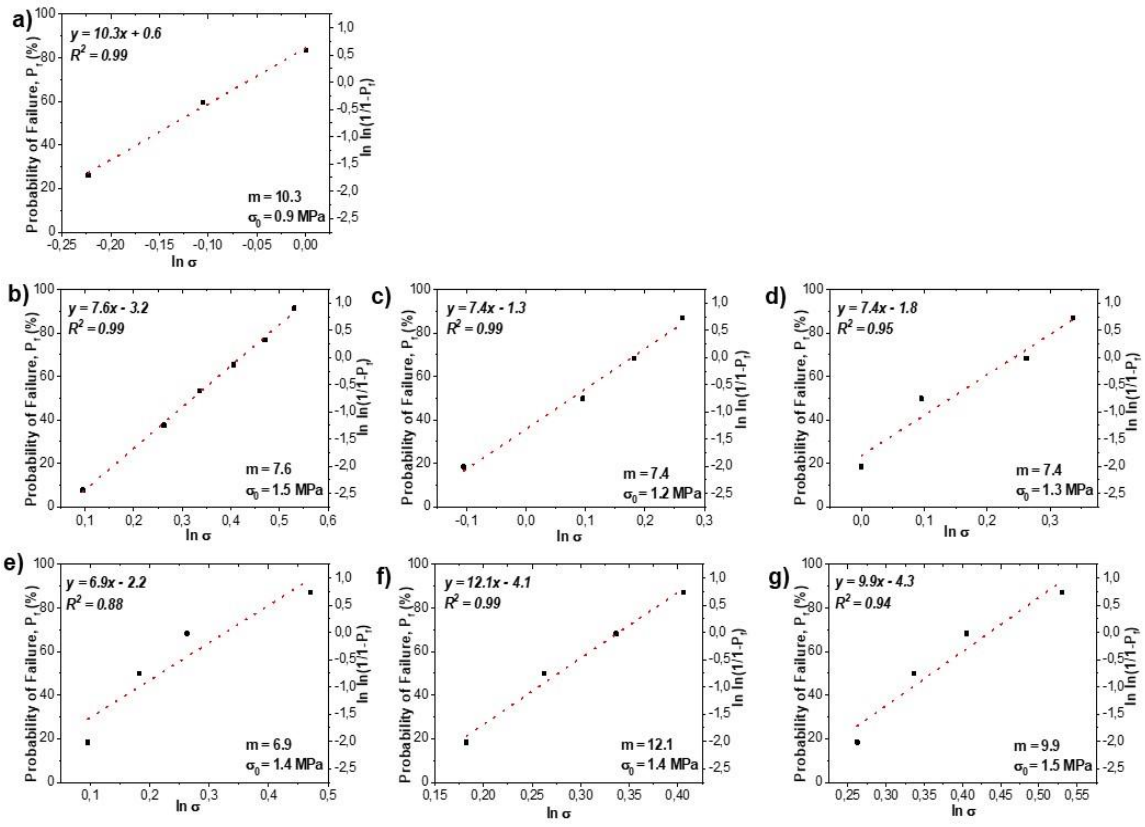

Figure 11. Weibull probability plots for the flexural strength of every sample under study: a) REF NHL, b) ASR+NHL, c) CAL+NHL, d) ACT+NHL, e) APT+NHL, f) APD+NHL and g) APTAPD+NHL.

The statistical properties of the averaged flexural strength values for the natural hydraulic lime-based mortars applying Weibull statistics are summarized in Table 2.

Table 2. Parameters obtained after the Weibull fitting of the data obtained from the three-point flexural tests.

Samples	Averaged Flexural Strength, σ_f (MPa)	Weibull Characteristic Strength, σ_0 (MPa)	Weibull Modulus, m	Correlation, (r)
REF NHL	0.9 ± 0.1	0.9	10.3	0.99
ASR+ NHL	1.4 ± 0.2	1.5	7.6	0.99
CAL+NHL	1.2 ± 0.1	1.2	7.4	0.99
ACT+ NHL	1.2 ± 0.2	1.3	7.4	0.95
APT+ NHL	1.3 ± 0.2	1.4	6.9	0.88
APD+ NHL	1.4 ± 0.1	1.4	12.1	0.99
APTAPD+ NHL	1.5 ± 0.2	1.5	9.9	0.94

Paying attention to the plots of Figure 11, a good linear relationship between lnln [1/(1−P)] and lnσ is observed. Moreover, being the correlation coefficient, *r*, a measure of the goodness of fit and observing the values in Table 2, it could be assumed that the experimental data obtained can be well described with the Weibull distribution.

Furthermore, observing the obtained results in Table 2 the Weibull characteristic strength σ_0, values are very similar to the mean flexural strength σ_f, values obtained experimentally. In addition, high Weibull moduli were obtained. This is very important since, as previously discussed in Chapter 6 with cement materials, a material with high Weibull modulus is more predictable in terms of its mechanical failure and less likely to break at a stress much lower than the mean value [25–27].

To better understand the flexural behavior of the materials tested, other mechanical parameters were considered. Toughness was evaluated in terms of fracture energy considering the total integrated area under the *stress-strain* curves to evaluate the effect of the basalt fibers. In this work, the post-cracking behavior was also considered for the toughness determination. Flexural modulus, *E* (calculated considering the elastic part of the curve and Equation (3) of Chapter 3) and the elongation at break, ε (deflection at the maximum stress) were calculated.

However, the toughness, flexural modulus and elongation at break values were estimated only for the curves shown in Figure 4-10. Therefore, the values gathered in Table 3 and plotted in Figure 12 are averaged values of the most representative curves.

Table 3. Flexural parameters of the studied natural hydraulic lime-based mortar samples.

Samples	Flexural Strength, σ_f (MPa)	Flexural Modulus, E (MPa)	Toughness (MPa)	Elongation at Break, ε (%)
REF NHL	0.9 ± 0.1	102± 20	69 ± 22	0.8 ± 0.2
ASR+NHL	1.4 ± 0.2	104 ± 19	463 ± 124	1.3 ± 0.3
CAL+NHL	1.2 ± 0.1	125 ± 42	142 ± 36	0.9 ± 0.2
ACT+NHL	1.2 ± 0.2	110 ± 42	193 ± 41	1.5 ± 0.7
APT+NHL	1.3 ± 0.2	153 ± 39	329 ± 103	0.9 ± 0.1
APD+NHL	1.4 ± 0.1	121 ± 49	193 ± 40	1.1 ± 0.6
APTAPD+NHL	1.5 ± 0.2	160 ± 37	264 ± 52	0.9 ± 0.2

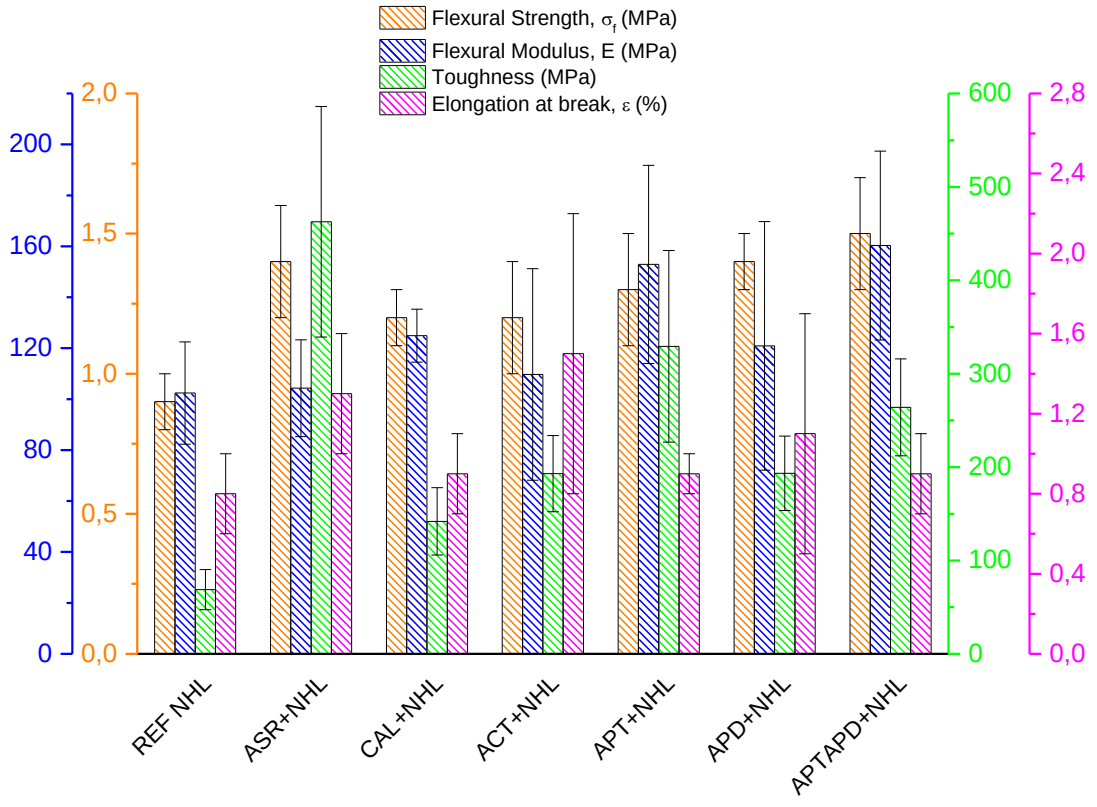

Figure 12. Comparison of flexural behavior from the values of different parameters for all the samples under study.

As previously observed for cement materials in Chapter 6 (section 6.3.1), also in this case high standard deviations in every parameter were obtained due to the great heterogeneity of these materials in terms of defects. Nevertheless, some considerations can be made.

The mechanical properties summarized in Table 3 and in Figure 12, highlighted differences between the neat mortars (REF NHL) and the samples containing fibers. In fact, an increase in flexural strength, σ_f values is observed for all samples compared to the neat mortar (REF NHL) with higher values for specimens containing as-received (ASR+NHL) and aminosilanes treated basalt fibers (APT+NHL, APD+NHL and APTAPD+NHL samples). However, the highest value is shown for samples containing APTES+APDES silanized basalt fibers (APTAPD+NHL sample).

Furthermore, observing the flexural modulus, *E* values, an increase for the fiber-reinforced samples in comparison with the REF NHL mortar is observed. ASR+NHL show a value comparable with the neat mortar while higher values are obtained for APT+NHL and APTAPD+NHL samples.

Toughness increases for all samples containing fibers compared to the neat mortar. However, a high increase in toughness values is shown for ASR+NHL sample and when APTES silanized fibers (APT+NHL sample) and APTES+APDES silanized fibers (APTAPD+NHL sample) are dispersed in natural hydraulic lime matrix. On the other hand, as received fibers (ASR+NHL sample) seems to confer a good toughness effect but low flexural modulus, *E* value very similar to the REF NHL sample which suggests a lower resistance for these materials, compared to APT+NHL and APTAPD+NHL samples.

Elongation at break, ε increases for all samples containing fibers compared to the neat mortar (REF NHL) suggesting that the presence of fibers confers less brittle behavior in all cases.

The flexural results obtained suggest that the presence of the fibers and the presence of a surface treatments enhance the mechanical performance of the final materials. Better trend in terms of strength and toughness is observed when a trifunctional silane and a mixture of the two silanes are used as the basalt fibers coating (APT+NHL and APTAPD+NHL samples).

In addition, it should be highlighted that APDES silanized basalt fibers seem to show better compatibility when dispersed in natural hydraulic lime matrix and consequently better flexural behavior in contrast with the results observed for cement-based mortars in Chapter 6 (see section 6.3.1). Probably this different behavior could be ascribed to a different reactivity between the fibers and the corresponding matrices (cement and natural hydraulic lime).

➢ *Compressive strength test*

The typical compressive behavior of natural hydraulic lime-based mortars is shown in Figure 13. In spite of the irregular curves obtained from the three-point flexural test, the compression *stress-strain* curves showed a homogenous trend. The compressive curves were also modified to eliminate possible artifacts using the method described in the Appendix B of Chapter 6.

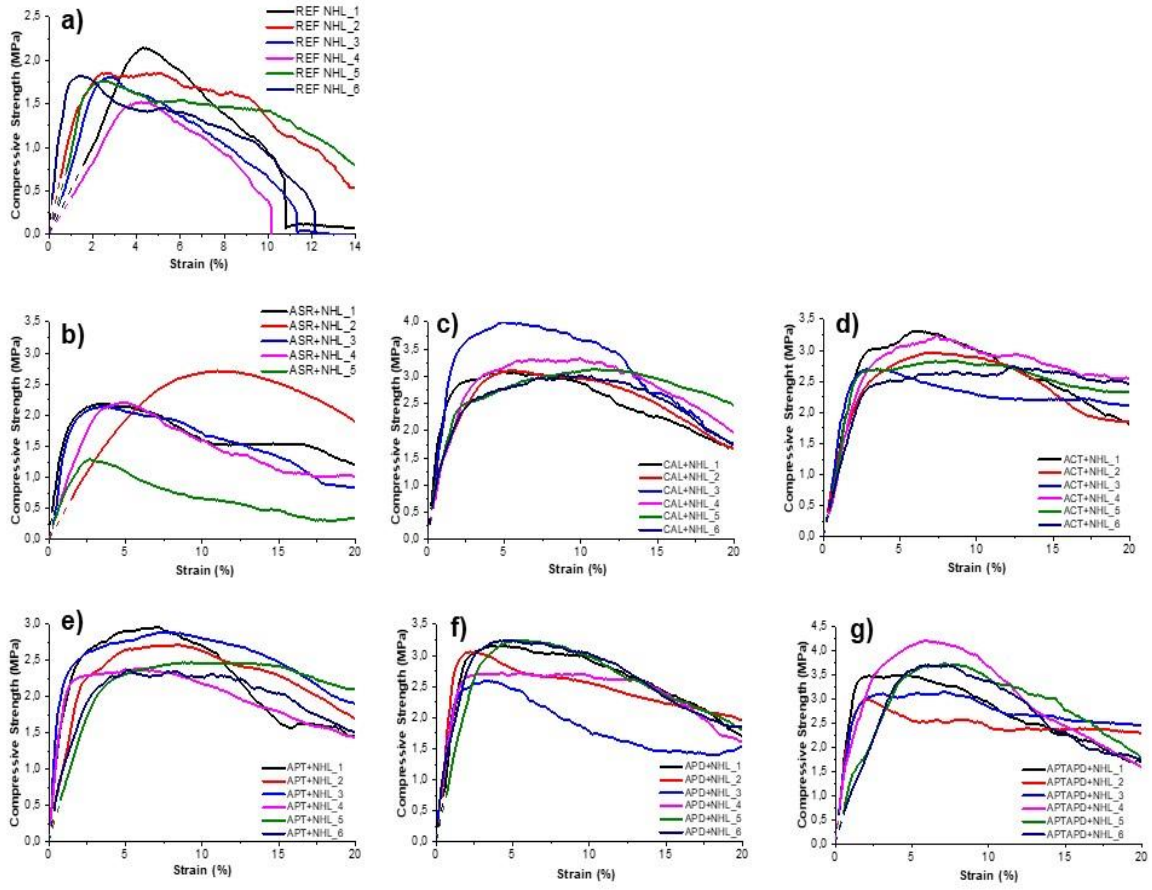

Figure 13. *Stress-strain* curves for all the samples under study: a) REF NHL, b) ASR+NHL, c) CAL+NHL, d) ACT+NHL, e) APT+NHL, f) APD+NHL and g) APTAPD+NHL.

Compressive strength, σ_c, values were statistically treated using Weibull distribution. The results are shown in Figure 14 and Table 4.

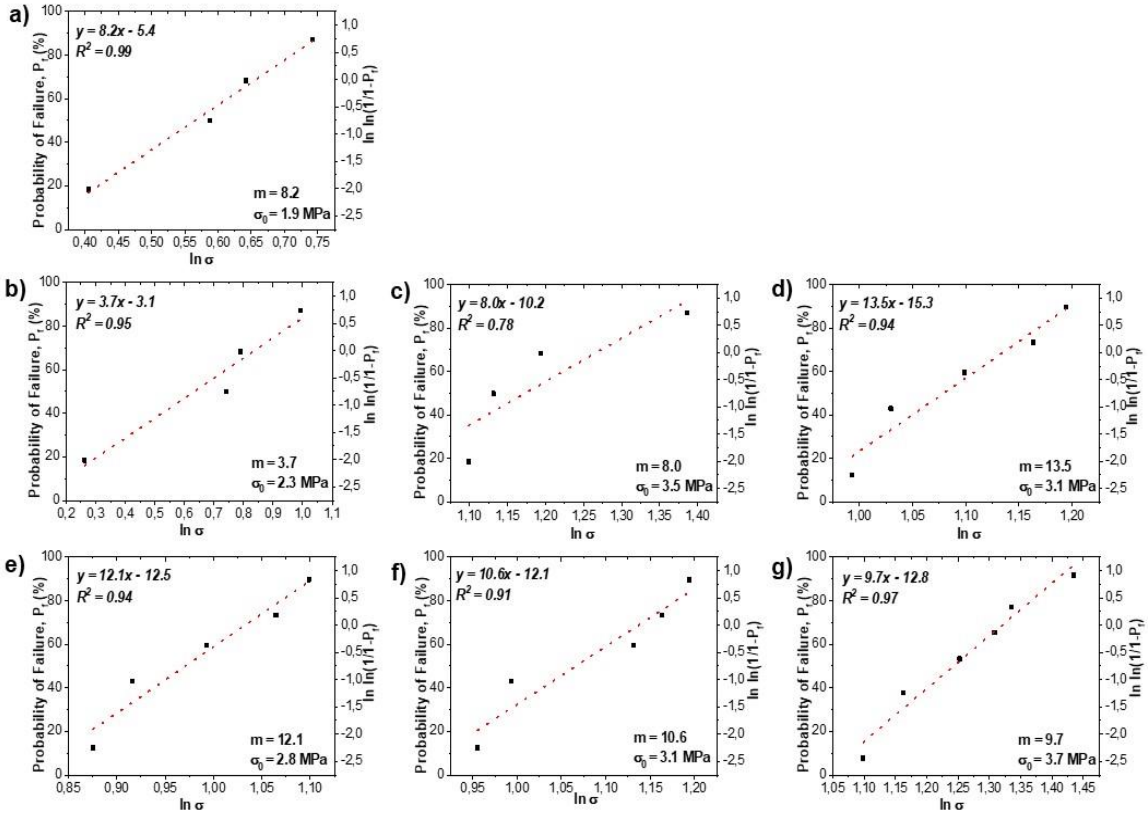

Figure 14. Weibull probability plots for the compressive strength of every sample under study: a) REF NHL, b) ASR+NHL, c) CAL+NHL, d) ACT+NHL, e) APT+NHL, f) APD+NHL and g) APTAPD+NHL.

Table 4. Parameters obtained after the Weibull fitting of the compressive strength tests data.

Samples	Averaged Compressive Strength, σ_c (MPa)	Weibull Characteristic Strength, σ_0 (MPa)	Weibull modulus, m	Correlation (r)
REF NHL	1.8 ± 0.2	1.9	8.2	0.99
ASR+ NHL	2.2 ± 0.5	2.3	3.7	0.95
CAL+NHL	3.3 ± 0.4	3.5	8.0	0.78
ACT+NHL	3.0 ± 0.3	3.1	13.5	0.94
APT+NHL	2.6 ± 0.3	2.8	12.1	0.94
APD+NHL	3.0 ± 0.3	3.1	10.6	0.91
APTAPD+NHL	3.6 ± 0.4	3.7	9.7	0.97

The obtained results showed, could be well fitted by a straight line function. Therefore, it can be considered that compressive strength, σ_c, values are statistically significant showing

high Weibull moduli, *m*, values. Besides, the characteristic strength, σ_0, values are very similar to the mean compressive strength, σ_c associated to each sample.

The compressive behavior of the mortars was studied considering other mechanical parameters such as toughness, compressive modulus, *E* and elongation at break, *ε*. In this case, toughness values were estimated considering the area under the *stress-strain* curves until the maximum compressive strength value. Elongation at break, ***ε***, was estimated as well. Compressive Modulus, *E*, was estimated by the slope of the elastic part of the *stress-strain* curves.

The results are gathered in Table 5 and the corresponding trend is shown in Figure 15.

Table 5. Compressive behavior of the natural hydraulic lime-based mortar samples under study.

Samples	**Compressive Strength, σ_c (MPa)**	**Compressive Modulus, E (MPa)**	**Toughness (MPa)**	**Elongation at Break, ε (%)**
REF NHL	1.8 ± 0.2	100 ± 50	421 ± 231	3.4 ± 1.4
ASR+NHL	2.2 ± 0.5	101 ± 66	829 ± 680	5.1 ± 3.4
CAL+NHL	3.3 ± 0.4	145 ± 71	1986 ± 721	7.5 ± 2.7
ACT+NHL	3.0 ± 0.3	141 ± 31	1748 ± 731	7.4 ± 3.1
APT+NHL	2.6 ± 0.3	150 ± 78	1584 ± 414	7.2 ± 1.5
APD+NHL	3.0 ± 0.3	190 ± 63	948 ± 328	4.3 ± 1.3
APTAPD+NHL	3.6 ± 0.4	207 ± 105	1575 ± 634	5.6 ± 2.2

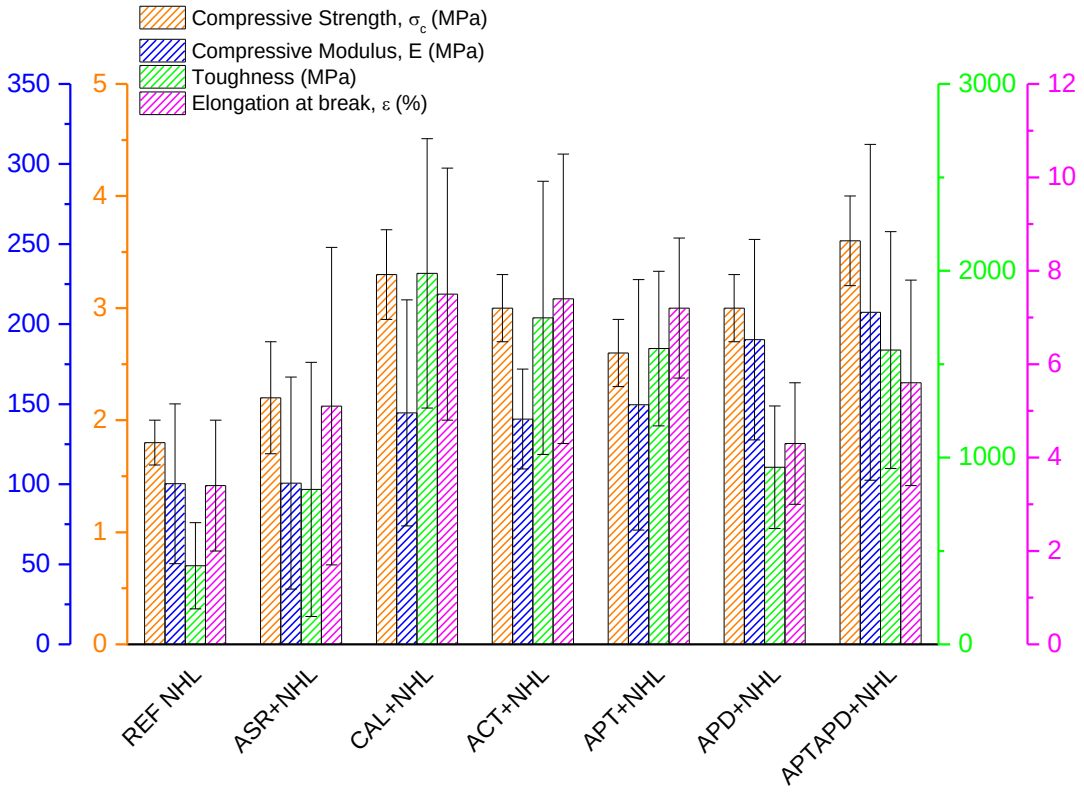

Figure 15. Comparison of compressive behavior from the values of different parameters for all the samples under study.

Evaluating the compressive behavior for all sample studied (Table 5 and Figure 15) and considering that, also in this case, high standard deviations values were obtained, some observations can be drawn.

When basalt fibers are added, compressive strength σ_c, values increase with respect to that obtained for the neat mortar (REF NHL). However, the sample ASR+NHL showed similar value to that obtained for REF NHL, whereas the highest value was obtained for APTAPD+NHL sample, which, in addition, showed the higher flexural strength, σ_f, value.

Toughness values increase with the presence of fibers and their corresponding surface treatment, conferring to the mortar a less brittle behavior.

Attending the elongation at break, ε, it is observed that there is an increase in the values when basalt fibers are present in the samples.

Considering the compressive modulus, *E*, it increased respect to the reference mortar (REF NHL) due to the addition of the fibers and the corresponding surface treatment. The highest value was obtained for APTAPD+CEM sample.
Moreover, as was previously observed for the flexural behavior, the mortars containing commercial fibers (ASR+NHL) showed a value similar to the neat mortar. As discussed in the Chapter 6, this unexpected result could be attributed to a different disposition of the fibers when dispersed in the reactive mixture. Probably, the sizing of the commercial basalt fibers makes them flexible which might cause their collapse in the form of random coil that could not confer the opportune resistance in terms of rigidity to the whole material. On the contrary, the surface treatments proposed in the present work make the fibers less flexible. Therefore, it is reasonable to think that when they are mixed with the components of the reactive mortar, they remain in their more extended form, being more separated each other and consequently, leading to more effective reinforcement.

Therefore, in agreement with the obtained results for cement materials (Chapter 6) and previous results found in bibliography [28,29], when natural hydraulic lime is used, the presence of the commercial basalt fibers do not increase significantly the compressive behavior of the composites showing a behavior quite similar to the neat mortar. Iucolano et. al [5], studying the behavior of commercial basalt fiber in natural hydraulic lime-based mortar (NHL 3.5 was used as matrix) observed a decrease in compressive strength values respect to the reference (without fibers). In contrast, Santarelli et al. [6,7] found that for most of neat mortars compressive strength (a NHL 3.5 was used as matrix) increased with the addition of commercial basalt fibers.

As main conclusions extracted from the results obtained, it is found that the presence of fibers and the surface treatments affect the final performance of the material. In general, a better compressive behavior is shown for samples containing APTES+APDES (APTAPD+NHL) basalt fibers.

7.3.2. BET-BJH Textural Analysis

The N_2 adsorption-desorption isotherms for all the samples prepared are shown in Figure 16. *Type IV* adsorption curves and *Type H3* hysteresis loops according to IUPAC classification are observed (see section 3.2.3 of Chapter 3). As previously described for

cement based-mortars (section 6.3.2 of chapter 6) the *Type H3* shape hysteresis loops, refers to aggregates giving rise to slit-shaped pores due to the presence of C-S-H gel [30–32].

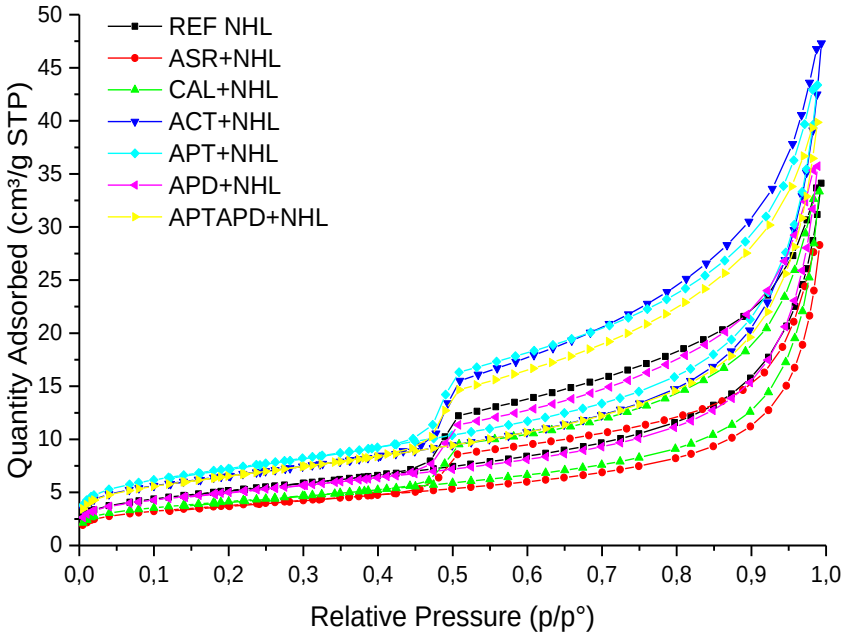

Figure 16. Nitrogen adsorption-desorption isotherms of natural hydraulic lime-based mortars.

BET specific surface area (SA) and total pore volume values obtained are given in Table 6. The standard deviations assigned to SA (BET) values are associated to the instrumental error.

Table 6. SA and Pore Volume results of natural hydraulic lime-based mortars.

	SA (BET) (m^2*g^{-1})	**Total Pore Volume (cm^3*g^{-1})**
REF NHL	18.3 ± 0.5	0.0529
ASR+ NHL	13.2 ± 0.5	0.0438
CAL+ NHL	14.5 ± 0.5	0.0517
ACT+ NHL	23.2 ± 0.5	0.0733
APT+ NHL	25.7 ± 0.5	0.0672
APD+ NHL	17.7 ± 0.5	0.0554
APTAPD+ NHL	23.2 ± 0.5	0.0618

From results of Table 6, it is observed that higher SA (BET) and total pore volume values are obtained for samples prepared with fibers treated with a trifunctional silane (APT+NHL), with a mixture of the two silanes used (APTAPD+NHL) and with activated

fibers (fiber subjected to activation process through chlorhydric acid) compared to the reference mortar (REF NHL).

An estimation of the distributions of pore diameters of the samples investigated was carried out. The results are plotted in Figure 17.

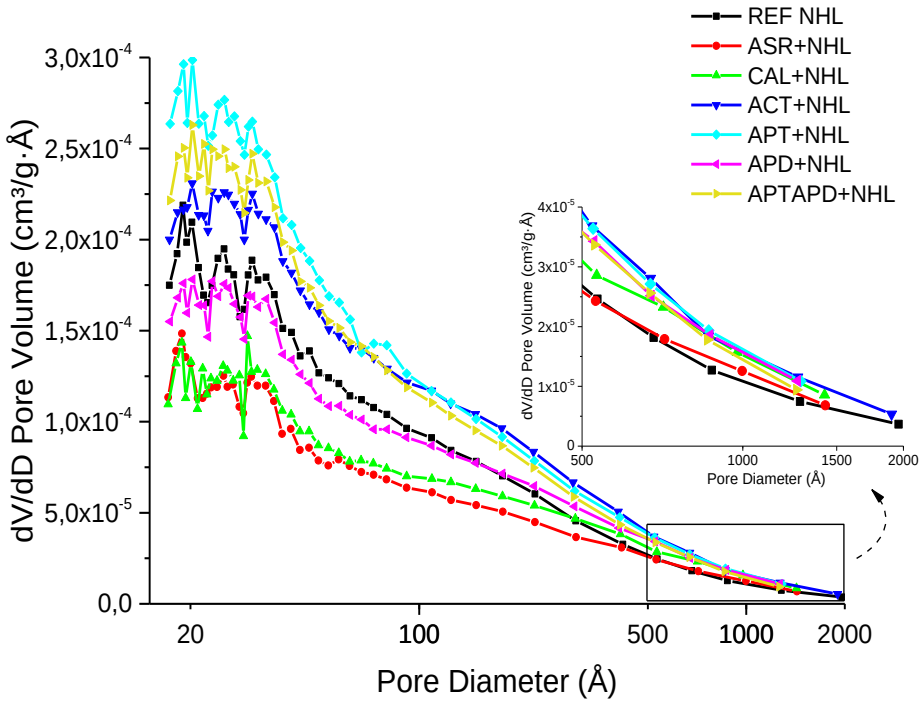

Figure 17. Pore diameter distributions of natural hydraulic lime-based mortars.

Figure 17 shows that the mortar samples investigated are mainly characterized by mesopores (with a diameter between 20-500 Å) and macropores (with a diameter greater than 500 Å). For all the samples, the pore distribution curves shown maxima at around 20 Å of pore diameter.

Comparing the porosity of the samples, there is an increase of porosity in the whole range investigated (~17-2000 Å) for the samples containing activated (ACT+NHL), APTES+APDES (APTAPD+NHL) and APTES (APT+NHL) treated basalt fibers respect to the reference (black curve) sample.

On the other hand, observing the range of macropores (500-2000 Å), an increase in the porosity compared to the reference (REF NHL) is shown for all samples containing fibers.

Furthermore, the order in terms of porosity is APTES > APTES+APDES > APDES suggesting that the higher the crosslinking degree of the fiber coating the higher the porosity in the whole composite material. This observation agrees the results obtained when cement is used as a matrix (see section 6.3.2 of Chapter 6).

However, slight differences in the obtained results indicates that, as was also found for cement materials (see section 6.3.2 of Chapter 6) the presence of fibers so as their surface treatments do not seem to change significantly the meso and microstructure of the neat mortar.

7.3.3. Fractographic Analysis

7.3.3.1. Scanning Electron Microscopy (SEM)

The failure mechanisms of the mortar samples were studied by scanning electron microscopy (SEM). Especially, the fracture surfaces of samples arising from three-point flexural test were observed at different magnifications to obtain information about the dispersion of the fibers in the matrix (Figure 18), the adhesion of the matrix to the fiber surface and to study the fiber-matrix interface (Figures 19 and 20).

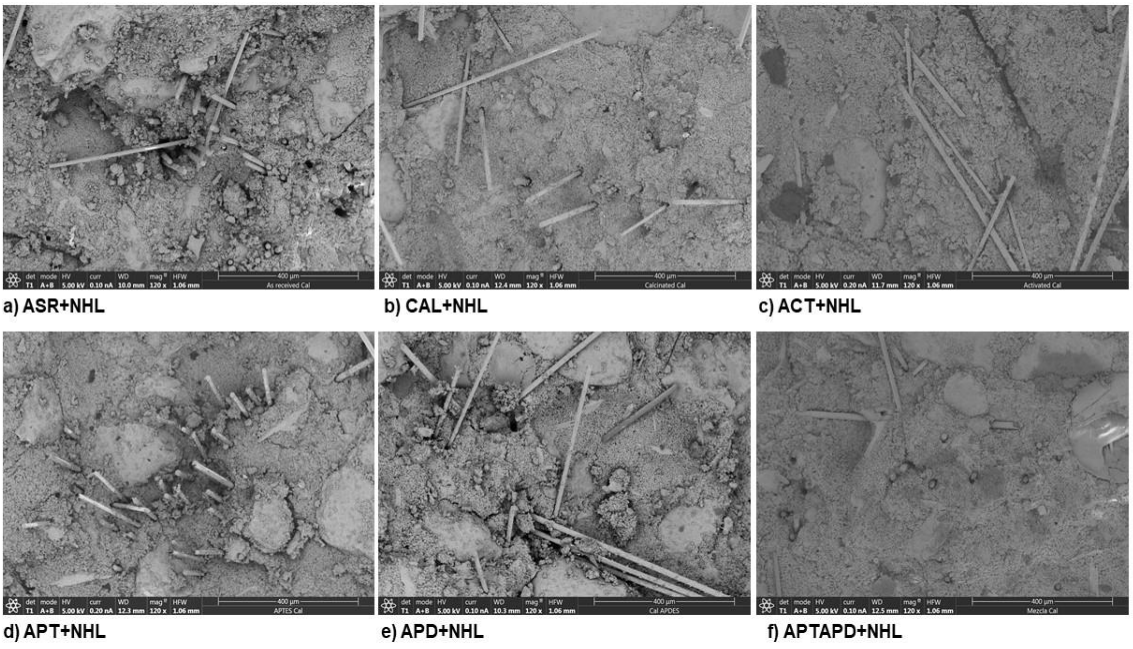

Figure 18. SEM images for all fiber-reinforced mortar samples at 120× magnification

The SEM images at 120× magnification (Figure 18), show that basalt fibers are heterogeneously dispersed in the matrix and pull-out phenomena are evident for all samples. Some voids due to the fiber pull-out are visible. As previously discussed in Chapter 6 for cement-based mortars, this non-uniform dispersion of the fibers in the matrix could be attributed to the process of mixing that does not allow separating fibers each others.

However, observing APTAPD+NHL micrograph (Figure 18 f) it seems that the fibers were less pulled-out from the matrix. This observation suggests a better compatibility between the fibers and the matrix through higher attractive interactions between the modified surface (mixture of the two silanes used) and the natural hydraulic lime matrix.

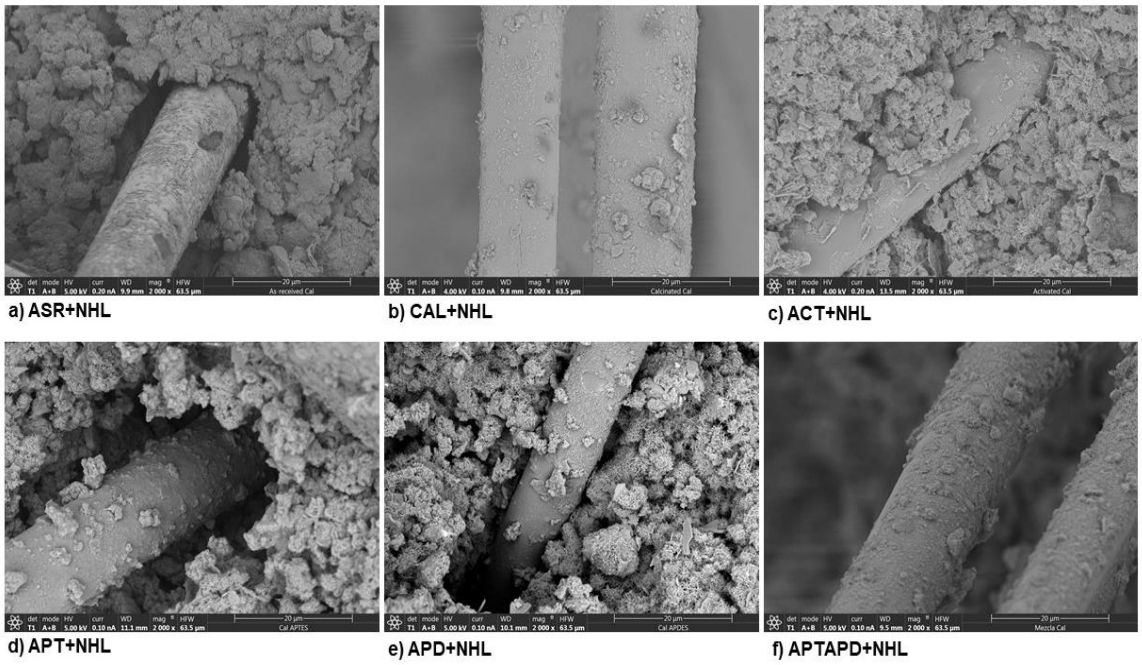

Figure 19. SEM images for all fiber reinforced mortar samples at 2000× magnification.

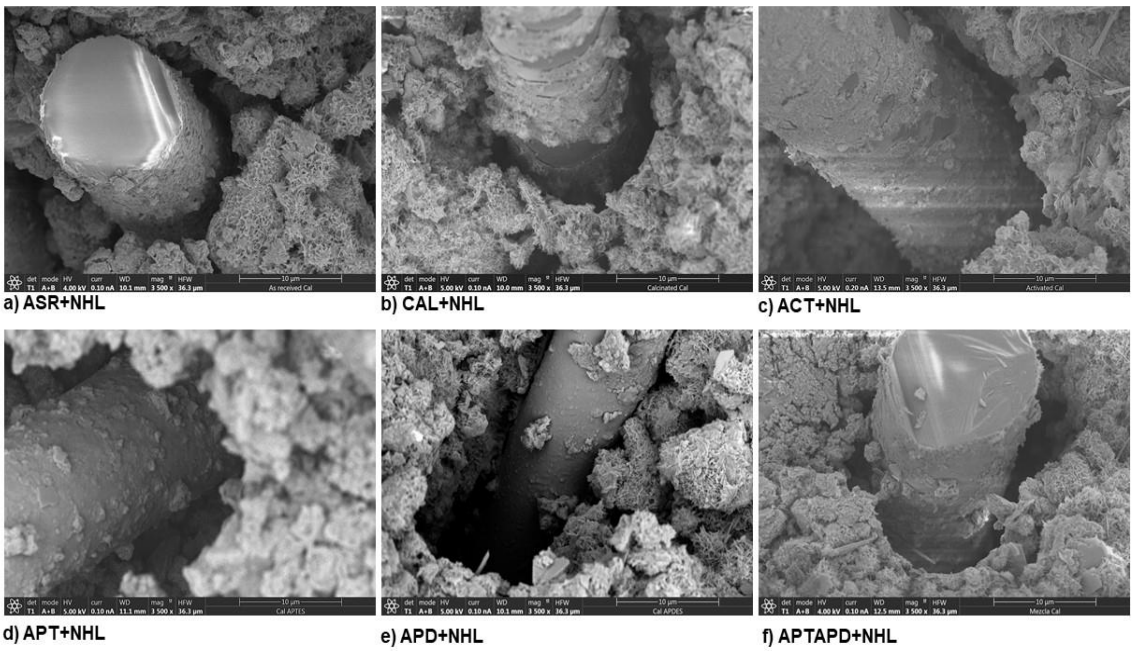

Figure 20. SEM images for all fiber reinforced mortar samples at 3500× magnification.

SEM images in Figures 19 and 20 provide information about the adhesion of the matrix to the fiber surface in terms of interfaces. In general, when using as-received, calcinated and activated basalt fibers (Figures 19 a-c, Figures 20 a-c) smooth surfaces with some matrix fragments adhered to the fiber surface are observed. This suggest that an adhesive failure at the interface take place for this sample. Instead, a more cohesive failure mechanism for the mortar samples prepared with fibers treated with aminosilane coupling agents (images d-f of Figures 19 and 20) is observed. In fact, several matrix fragments are present on the fiber's surfaces. In particular, better compatibility in terms of fiber-matrix adhesion is observed for samples containing fibers modified with the trifunctional silane and with the mixture of the two silanes used (Figures 19 d and f, Figures 20 d and f). For these last two samples, especially for the APTAPD+CEM sample, also better mechanical performance was observed.

In addition, an irregular and non-homogenous microstructure is observed. Two possible explanations of this behavior could be made: i) necessity of more time of mixing, ii) slower hydration and hardening processes when natural hydraulic lime is used could make the matrix not enough compact after 28 days of curing.

7.3.3.2. Surface Profilometry Measurements

- *Laser Profilometry*

Laser profilometry was performed to obtain information at higher scale than that given by SEM about the failure mechanism of the natural hydraulic lime-based mortars. Three fracture surfaces resulting from three-point flexural tests. A representative 3D topographic image for each sample is shown in Figure 21.

Furthermore, the profile parameters P_a and P_q were also evaluated (Table 7, Figure 22).

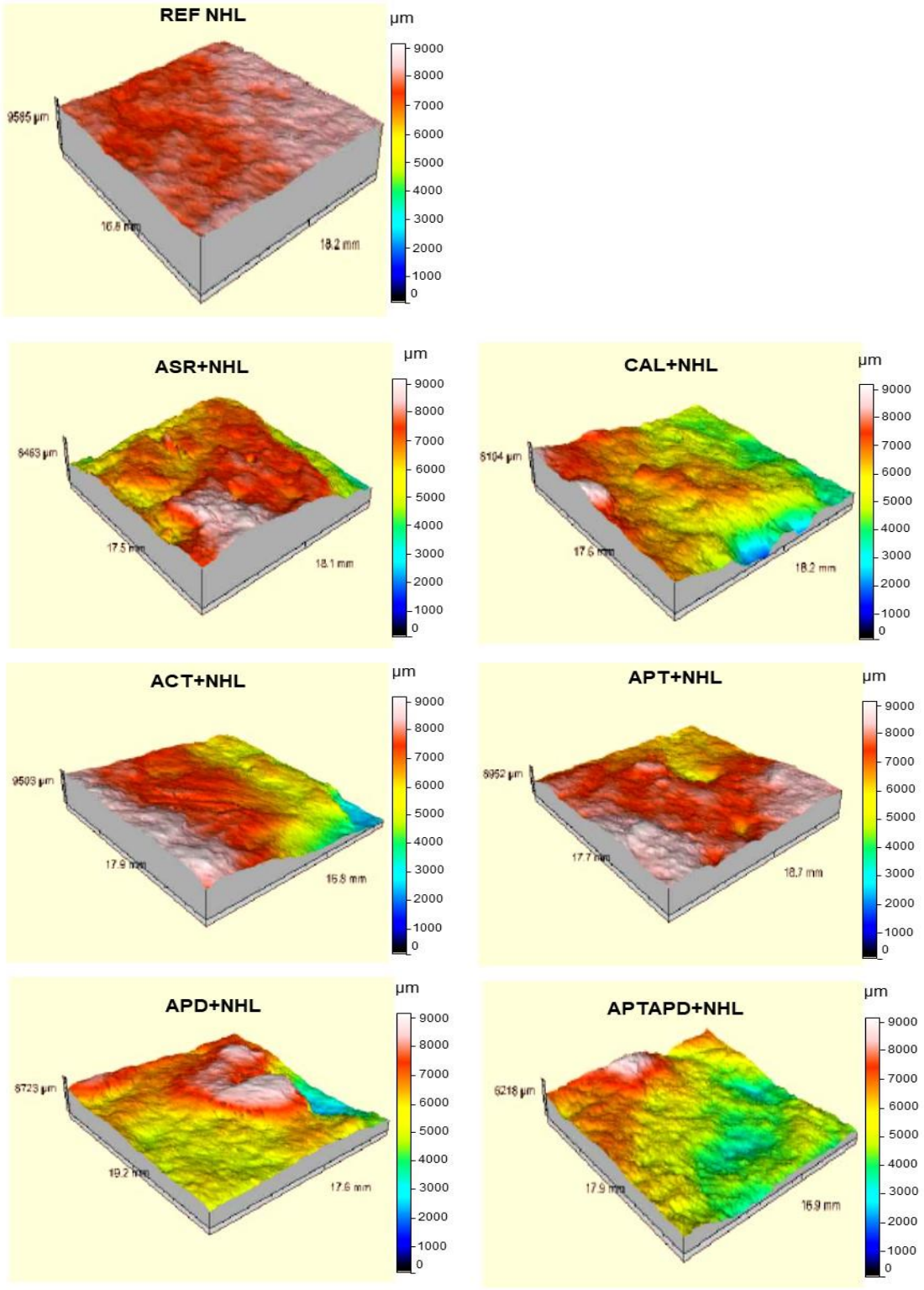

Figure 21. Representative 3D topographic images of fracture surfaces of the natural hydraulic lime-based mortars under study.

As previously observed for cement-based mortars in Chapter 6 (section 6.3.3.2), in this case a smoother fracture surface is observed for the neat mortar (REF NHL) compared to the fiber-reinforced mortar samples. As for cement-based mortars, the presence of fibers in natural hydraulic lime matrix is responsible of more tortuous fracture surfaces and consequently of a less brittle behavior [33].

Table 7. Profile parameters obtained by laser profilometry.

	P_a (µm)	**P_q (µm)**
REF NHL	267± 24	325 ± 36
ASR+NHL	824 ± 215	999 ± 234
CAL+ NHL	683 ± 272	855 ± 244
ACT+ NHL	1259 ± 604	1454 ± 638
APT+ NHL	584 ± 65	717 ± 122
APD+ NHL	877 ± 389	1049 ± 462
APTAPD+ NHL	482 ± 90	592 ± 120

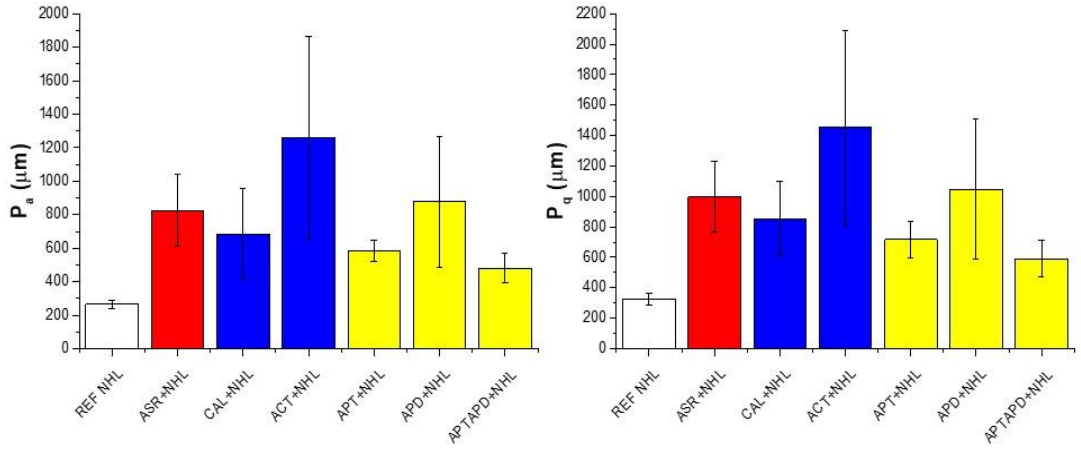

Figure 22. P_a (µm) and P_q (µm) profile parameters trend by laser profilometry for natural hydraulic-based mortars.

The values in the Table 7 and their trends (Figure 22) point out that P_a and P_q increase for the samples containing as-received and modified basalt fibers compared to the neat mortar (REF NHL). However, due to the high standard deviations only few qualitative considerations can be done. It seems that the presence of the fibers and their treatments affects the interface adhesion and the meso and microstructure of the natural hydraulic

lime matrix. Consequently, the fibers affect the failure mechanism of the mortars conferring a lesser brittle behavior.

- *Optical Profilometry*

An evaluation at higher magnification (10x) of the failure mechanism of the mortar samples were carried out also by optical profilometry. After performing the three-point flexural tests, the corresponding fracture surfaces were studied. Three specimens for each sample and five different regions (see section 6.2.3.4 of Chapter 6) were investigated. Representative 3D topographic images of the fracture surface for each sample are shown in Figure 23. Here, the profile parameters, Pa and P_q were also evaluated. The mean value of the profile parameters collected for each sample are shown in Table 8 and plotted in Figure 24.

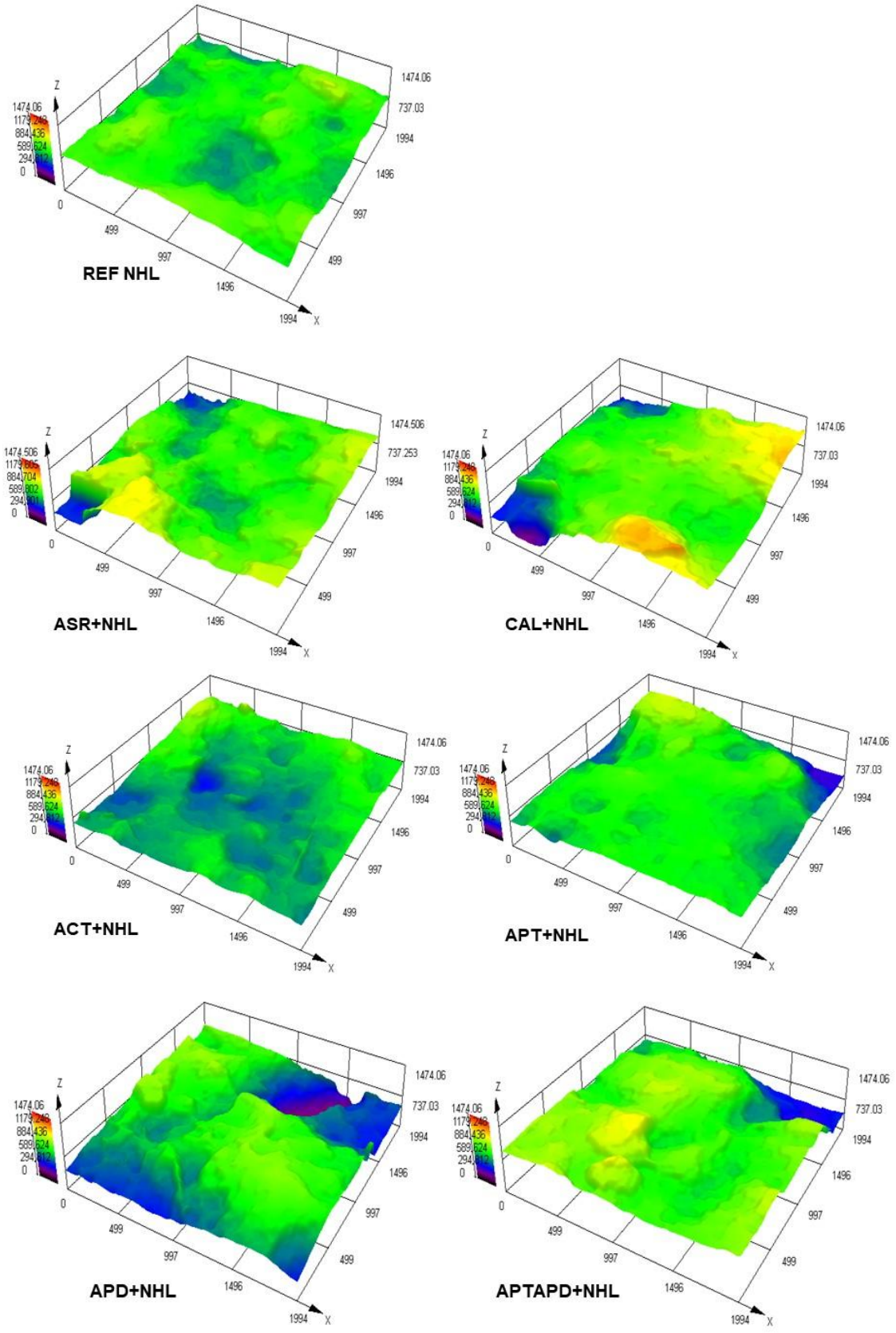

Figure 23. Representative 3D topographic images of the fracture surfaces of the natural hydraulic lime-based mortars under study.

As was already observed in Chapter 6 (section 6.3.3.2), in the 3D topographic images obtained using optical profilometry (in Figure 23), the surface characteristics are sharper compared to 3D images obtained with laser profilometer. However, differences in surface irregularities between the samples, are more clearly observed when larger regions of the fracture surfaces are considered. Nevertheless, in agreement with the observation by laser profilometry, more irregular and tortuous topography is observed when fibers are dispersed in the natural hydraulic lime matrix.

Table 8. Profile parameters obtained by optical profilometry.

	P_a (µm)	**P_q (µm)**
REF NHL	56 ± 8	67 ± 10
ASR+NHL	79 ± 21	95 ± 24
CAL+ NHL	69 ± 8	82 ± 9
ACT+ NHL	59 ± 23	72 ± 27
APT+ NHL	59 ± 11	72 ± 12
APD+ NHL	66 ± 15	80 ± 18
APTAPD+ NHL	64 ± 12	77 ± 14

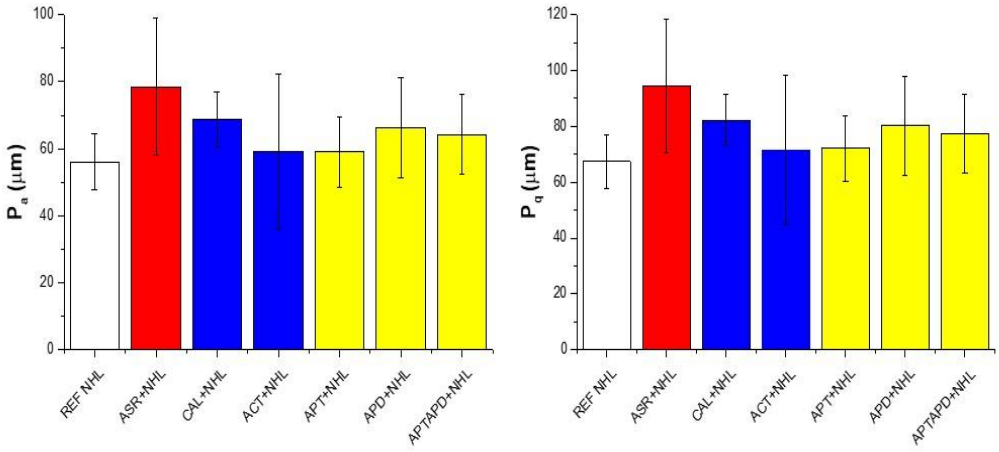

Figure 24. P_a (µm) e P_q (µm) profile parameters obtained by optical profilometry as a function of type of sample.

Observing the profile parameters values in Table 8 and Figure 24, it can be said that there is the same tendencies found from the results obtained by laser profilometry. In fact, again an increase in P_a and P_q values of the reinforced mortar compared to the REF NHL sample is found.

7.4. Conclusions

The study about interactions and therefore compatibility between basalt fibers (as-received and modified) and natural hydraulic lime matrix allows to draw some conclusions that opens a new scientific research field.

- The obtained results confirm that the presence of basalt fibers so as their surface treatment is revealed as potential ways of improving mechanical performance in natural hydraulic lime-based mortar:
  - The incorporation of commercial basalt fiber to the matrix shown high flexural strength and toughness values but a slower flexural modulus values compared to the other samples containing modified fibers that could be responsible of a lower resistance of the resulting material. On the other hand, higher strength and toughness was observed when a trifunctional silane and a mixture of the two silanes used interact with the matrix (APT+NHL and APTAPD+NHL samples). Besides, the APTAPD+NHL sample showed the highest flexural strength value.
  - It was evidenced the positive role played by the basalt fibers in improving the compressive behavior. However, the compressive behavior of the sample with commercial basalt fibers (ASR+NHL) did not show significant enhancement of compressive resistance compared to the rest of samples. The best compressive behavior was obtained when the basalt fibers are modified with a mixture of APTES and APDES silanes (APTAPD+NHL).
- The small differences shown by the BET-BJH results point out that the presence of fibers does not change significantly the micro and meso structure of the neat mortar.
- The investigation of fracture surface by SEM analysis points out more adhesive failure for mortar samples containing as-received, calcinated and activated basalt fibers. On the contrary, a more cohesive failure is observed when fibers treated with aminosilanes are used to reinforce the natural hydraulic lime matrix. However, better compatibility in terms of fiber-matrix adhesion is observed for samples containing fibers modified with the trifunctional silane (APT+NHL) and with the mixture of the two silanes used (APTAPD+NHL). For these samples, especially for the APTAPD+CEM sample, a better mechanical performance was also observed. SEM analysis revealed a non-homogenous microstructure, explained as follow: i) necessity of more time of mixing,

ii) slower hydration and hardening processes when natural hydraulic lime is used could make the matrix not enough compact after 28 days of curing.

- The fractographic study by laser and optical profilometry shows more tortuous fracture surface for samples containing fibers. Consequently, and being in accordance with the mechanical studies, the presence of the fibers confers a less brittle behavior.

References

[1] K. Callebaut, J. Elsen, K. Van Balen, W. Viaene, Nineteenth century hydraulic restoration mortars in the Saint Michael's Church (Leuven, Belgium): Natural hydraulic lime or cement?, Cem. Concr. Res. 31 (2001) 397–403. doi:10.1016/S0008-8846(00)00499-3.

[2] J. Lanas, J.I. Alvarez, Masonry repair lime-based mortars: Factors affecting the mechanical behavior, Cem. Concr. Res. 33 (2003) 1867–1876. doi:10.1016/S0008-8846(03)00210-2.

[3] J. Lanas, J.L. Perez Bernal, M.A. Bello, J.I. Alvarez Galindo, Mechanical properties of natural hydraulic lime-based mortars, Cem. Concr. Res. 34 (2004) 2191–2201. doi:10.1016/j.cemconres.2004.02.005.

[4] M. Arandigoyen, J.I. Alvarez, Pore structure and mechanical properties of cement-lime mortars, Cem. Concr. Res. 37 (2007) 767–775. doi:10.1016/j.cemconres.2007.02.023.

[5] F. Iucolano, B. Liguori, C. Colella, Fibre-reinforced lime-based mortars: A possible resource for ancient masonry restoration, Constr. Build. Mater. 38 (2013) 785–789. doi:10.1016/j.conbuildmat.2012.09.050.

[6] M.L. Santarelli, F. Sbardella, M. Zuena, J. Tirillò, F. Sarasini, Basalt fiber reinforced natural hydraulic lime mortars: A potential bio-based material for restoration, Mater. Des. 63 (2014) 398–406. doi:10.1016/j.matdes.2014.06.041.

[7] M.L. Santarelli, F. Sbardella, M. Zuena, M. Albé, G. Quattrociocchi, J. Tirilló, M. Valente, F. Sarasini, Malte più performanti con le fibre di basalto, Compos. Mag. 33 (2014) 7–16. http://hdl.handle.net/10278/44412.

[8] M. Iorio, M.L. Santarelli, G. González-Gaitano, J. González-Benito, Surface modification and characterization of basalt fibers as potential reinforcement of concretes, Appl. Surf. Sci. 427 (2018) 1248–1256. doi:10.1016/j.apsusc.2017.08.196.

[9] P. Maravelaki-Kalaitzaki, A. Bakolas, I. Karatasios, V. Kilikoglou, Hydraulic lime mortars for the restoration of historic masonry in Crete, Cem. Concr. Res. 35 (2005) 1577–1586. doi:10.1016/j.cemconres.2004.09.001.

[10] B.. Petriaggi et.al., Innovative materials to restore mosaic pavements of the Roman villa of Silin (Lepcis Magna-Lybia), Conf. Pap. (2014).

[11] R. Ds, A Review on Modified Lime based Mortars - an Alternative to Cement Mortar, IJIRST-International J. Innov. Res. Sci. Technol. 2 (2016) 350–356.

[12] A.J. Edwards, Properties of Hydraulic and Non- Hydraulic Limes for Use in Construction, Napier University, School of the built environment, 2005. doi:10.1007/bf00391402.

[13] M.J. Mosquera, D. Benítez, S.H. Perry, Pore structure in mortars applied on restoration: Effect on properties relevant to decay of granite buildings, Cem. Concr.

Res. 32 (2002) 1883–1888. doi:10.1016/S0008-8846(02)00887-6.

[14] P.R. Rossi-Doria, Mortars for restoration: Basic requirements and quality control, Mater. Struct. 19 (1986) 445–448. doi:10.1007/BF02472148.

[15] A. Battaglia, A. Rattazzi, V. Kafetsi, Terra, Fuoco, Acqua, Aria: LA CALCE, ERMES, 2011.

[16] S. Amziane, L. Arnaud, Bio-aggregate-based Building Materials: Applications to Hemp Concretes, John Wiley & Sons, Inc, 2013. doi:DOI: 10.1002/9781118576809.

[17] R. Maddalena, J.J. Roberts, A. Hamilton, Can Portland cement be replaced by low-carbon alternative materials? A study on the thermal properties and carbon emissions of innovative cements, J. Clean. Prod. 186 (2018) 933–942. doi:10.1016/j.jclepro.2018.02.138.

[18] R.M. Andrew, Global CO_2 emissions from cement production, Earth Syst. Sci. Data. 10 (2018) 195–217. doi:10.5194/essd-10-195-2018.

[19] G. Di Bella, V. Fiore, G. Galtieri, C. Borsellino, A. Valenza, Effects of natural fibres reinforcement in lime plasters (kenaf and sisal vs. Polypropylene), Constr. Build. Mater. 58 (2014) 159–165. doi:10.1016/j.conbuildmat.2014.02.026.

[20] R. Codispoti, D. V. Oliveira, R.S. Olivito, P.B. Lourenço, R. Fangueiro, Mechanical performance of natural fiber-reinforced composites for the strengthening of masonry, Compos. Part B Eng. 77 (2015) 74–83. doi:10.1016/j.compositesb.2015.03.021.

[21] A. Izaguirre, J. Lanas, J.I. Alvarez, Effect of a polypropylene fibre on the behaviour of aerial lime-based mortars, Constr. Build. Mater. 25 (2011) 992–1000. doi:10.1016/j.conbuildmat.2010.06.080.

[22] E. Standard, EN 459-1 Building lime. Part 1: Definitions, specifications and conformity criteria, (2011).

[23] E. Standard, EN 196-1 Methods of testing cement. Part 1: Determination of strength, (2005) 1–33.

[24] E. Standard, EN 1015-11 Methods of test for mortar for masonry. Part 11: Determination of flexural and compressive strength of hardened mortar, (2000).

[25] J.B. Quinn, G.D. Quinn, A practical and systematic review of Weibull statistics for reporting strengths of dental materials, Dent. Mater. 26 (2010) 135–147. doi:10.1016/j.dental.2009.09.006.

[26] A. Nevarez-Rascon, A. Aguilar-Elguezabal, E. Orrantia, M.H. Bocanegra-Bernal, Compressive strength, hardness and fracture toughness of Al2O3 whiskers reinforced ZTA and ATZ nanocomposites: Weibull analysis, Int. J. Refract. Met. Hard Mater. 29 (2011) 333–340. doi:10.1016/j.ijrmhm.2010.12.008.

[27] J. Gonzalez-Benito, J. Martinez-Tarifa, M.E. Sepúlveda-García, R.A. Portillo, G. Gonzalez-Gaitano, Composites based on HDPE filled with BaTiO3 submicrometric

particles. Morphology, structure and dielectric properties, Polym. Test. 32 (2013) 1342–1349. doi:10.1016/j.polymertesting.2013.08.012.

[28] C. Jiang, K. Fan, F. Wu, D. Chen, Experimental study on the mechanical properties and microstructure of chopped basalt fibre reinforced concrete, Mater. Des. 58 (2014) 187–193. doi:10.1016/j.matdes.2014.01.056.

[29] C. High, H.M. Seliem, A. El-Safty, S.H. Rizkalla, Use of basalt fibers for concrete structures, Constr. Build. Mater. (2015). doi:10.1016/j.conbuildmat.2015.07.138.

[30] F. Rouquerol, J. Rouquerol, K. Sing, Adsorption by Powders & Porous Solids. Principles, Methodology and Applications, Academic Press, 1999. doi:https://doi.org/10.1016/B978-0-12-598920-6.X5000-3.

[31] K.S.W. Sing, International Union of Pure And Applied Chemistry, Reporting Physisorption data for Gas / Solid Systems with Special Reference to the Determination of Surface Area and Porosity, Pure Appl. Chem. 54 (1982) 2201–2218. doi:10.1351/pac198557040603.

[32] R.S. Mikhail, L.E. Copeland, S. Brunauer, Pore structures and surface Areas of hardened Portland Cement Pastes By Nitrogen Adsorption, Can. J. Chemisrty. 42 (1964) 426–438. doi:https://doi.org/10.1139/v64-060.

[33] M.A. Issa, M.A. Issa, M.S. Islam, A. Chudnovsky, Fractal dimension-a measure of fracture roughness and toughness of concrete, Eng. Fract. Mech. 70 (2003) 125–137. doi:10.1016/S0013-7944(02)00019-X.

CHAPTER 8

CONCLUSIONS AND FUTURE WORKS

CHAPTER 8
CONCLUSIONS AND FUTURE WORKS

8.1. Conclusions and Future Works

In the present PhD thesis, cement-based composites reinforced with basalt fibers were studied. In particular, the study was focused on the optimization of the fiber-matrix interface through specific surface treatments of the natural basalt fibers. Therefore, the compatibility between chopped basalt fibers (commercial and modified) and the selected matrices (Portland cement and natural hydraulic lime) was studied to understand and define possible improvements of the final composite materials.

Different surface treatments were designed and characterized, the hydrolytic degradation phenomena of the surface treatments based on silane coupling agents were studied and finally, fiber-reinforced composite materials were designed and characterized.

The most relevant conclusions that can be drawn from this research project are the following:

- It was found that the study on the design and characterization of **surface treatments** of basalt fibers is crucial to understand possible interactions in terms of better adhesion between basalt fibers and cement matrices and/or natural hydraulic lime. The detailed characterization of commercial and modified fiber surfaces carried out by several analytical techniques (XRD, FT-IR, TGA, SEM and AFM) showed that, depending on the treatment given, changes in the structure, composition and morphology were observed.

  In particular, it was observed that calcination process (elimination of the sizing applied during the production process on the commercial fiber) and the subsequent activation process (process with chlorhydric acid to regenerate silanol groups on the fiber surface) removed the sizing present on the commercial fiber surface making the surface smooth.

In addition, the activation process regenerated silanol groups allowing the grafting of aminosilanes (silane coupling agents) on the fibers surface.

The morphological analysis of the fibers chemically coated with aminosilanes (APTES, APDES, APTES+APDES), revealed surface heterogeneity due to the presence of the organic matter deposited on the fibers. These heterogeneities made the surface rough. It was observed that the higher the amount of triethoxysilane in the composition of the solution used to perform the coating, the higher the surface heterogeneity (topographical). These surface heterogeneities were subsequently confirmed by the surface roughness results obtained by AFM.

These superficial heterogeneities suggest that they could be responsible of a better adhesion between the fibers and the matrix. However, the fractographic analysis carried out on the images obtained by SEM and the results of mechanical tests, pointed out that a good or poor interfacial adhesion could be attributed to other causes. Therefore, it can be concluded that the roughness at the nanoscale does not seem influence the adhesion between the fibers and the matrix and, consequently, the mechanical performance of the cement-based composite materials.

- The study of **hydrolytic degradation** of the polysiloxane coatings seems to be crucial to understand the behavior of these coatings in the cement-based composite materials.

  A kinetic study of the hydrolytic degradation process was carried out. It allowed to obtain information about the activation energy depending on the considered type of coating (APTES, APTES+APDES, APDES) and to evaluate the equilibrium degradation times. The results obtained with different measurements, indicated that the hydrolytic rate of the three coatings increased according to the order in which the crosslinking degree increases: APDES < APTES+APDES < APTES. It was found that the mechanism of the hydrolytic process is the same for the three studied systems; therefore, it was concluded that the rate of the hydrolytic degradation process is related to the initial concentration of siloxane bonds (-Si-O-Si-) able to be hydrolyzed.

Consequently, this study demonstrated that, in fiber-reinforced cement-based composites, the use of a polyorganosiloxane with a lower crosslinking degree, such as the APDES coating, could be the most effective strategy to resist a possible attack of water, especially in the alkaline environment characteristic of the cement matrix.

It should be highlighted that the results obtained could be interesting not only in the sector of ceramic matrix composites but also to understand the behavior of these coatings in other applications in the field of engineering and materials science.

- The study of **fiber-reinforced composite materials** allowed to obtain information about the effect of chopped basalt fibers and their coatings in cement and natural hydraulic lime matrices respectively.

  In particular, the results indicated that, in general, the presence of basalt fibers and the surface treatments, enhance the mechanical performance of the materials compared to the reference mortar (without fibers). Independently of the matrix used, the best results in terms of fiber-matrix adhesion and consequently better mechanical performance, were obtained for the mortars reinforced with basalt fibers treated with the mixture of the two silanes (APTES + APDES).

  From the results obtained for the system corresponding to the cement matrix, it was possible to have an idea of the cause responsible of the best interactions at the fiber-matrix interface. For example, the good compatibility shown between the activated fibers and the cement matrix suggested that the OH groups generated during the activation process were probably responsible for the best adhesion.
  In addition, the presence of a surface coating based on aminosilanes could contribute further to improve this adhesion due to interactions by hydrogen bonds between the amino groups ($-NH_2$) and the cement matrices.

  In addition, the molecular structure with an intermediate crosslinking degree that could be generated at the fiber-matrix interface (cement and natural hydraulic lime) when using the mixture of the two silanes (APTES + APDES), could be responsible for higher accessibility to the OH groups on the fiber surface and, in addition, to the

amino groups. This could help to increase the favorable interactions between the reinforcement and the matrix.

The variations found in the obtained results (especially in the activated fibers) for the second studied system (natural hydraulic lime mortars) compared to the results found for cement mortars, could be attributed to a different reactivity between the fibers and the matrix with a different chemical composition.

For example, the lower number of hydration products (hydrated calcium silicate, C-S-H) in natural hydraulic lime mortars could be responsible for the lower interactions between the matrix and the OH groups of the fibers.

In order to better understand this type of interactions, it would be necessary to further investigate about this topic with more specific studies, for example through research proposals associated to future works.

In addition, it should be noted that the materials studied in this work, may be possible candidates for applications within the framework of the construction industry and the sector of restoration and conservation of Cultural Heritage. However, for both areas it would be necessary to further optimize the materials.

For this reason, as future works, it is proposed, to optimize the surface treatments of the fibers in terms of morphological and chemical nature. Options as future works could include adding nanoparticles that could confer higher surface roughness enhancing mechanical joint that could contribute to the physico-chemical interactions generated between the aminosilanes treated fibers and the matrix. In addition, it is proposed to use a method of application of the coatings by "spray" that would help in the corresponding production systems.

Finally, it is proposed, to optimize the preparation and consequently the final performance of the composite materials improving the dispersion process of the fibers and adding higher percentage of fibers in the matrix. In addition, the use of fibers with different morphologies (short and large) could also contribute to improve the mechanical behavior of the final materials.

8.2. Conclusiones y Trabajos Futuros

En esta tesis doctoral se han estudiado materiales compuestos de matriz cerámica reforzados con fibras de basalto. En particular, el estudio se ha centrado en la optimización de la interfase fibra-matriz a través de tratamientos superficiales de las fibras naturales de basalto. Para ello, estudió la compatibilidad existente entre las fibras cortas de basalto (comerciales y modificadas) y las matrices seleccionadas (un cemento Portland y una cal hidráulica natural) con el fin de comprender y definir posibles mejoras futuras en el rendimiento final del material compuesto.

Se diseñaron y caracterizaron diferentes tratamientos superficiales, se estudiaron los fenómenos de degradación hidrolítica de los tratamientos superficiales con agentes de acoplamiento propuestos y finalmente se diseñaron y caracterizaron los materiales compuestos reforzados con fibras.

Las conclusiones más relevantes que se pueden extraer de este proyecto de investigación son las siguientes:

- Se ha demostrado que el estudio sobre el diseño y caracterización de **tratamientos superficiales** de fibras de basalto es fundamental para poder comprender posibles interacciones en términos de mejor adhesión entre las fibras de basalto y las matrices de cemento y/o cal hidráulica natural. La detallada caracterización realizada, a través de la utilización de diferentes técnicas analíticas (DRX, FT-IR, TGA, SEM y AFM), de las superficies de las fibras comerciales y modificadas ha mostrado que dependiendo del tratamiento realizado se han generado cambios en la estructura, composición y morfología.

  En particular, se observó que el proceso de calcinación (eliminación del ensimaje superficial aplicado durante la fase producción, fibras comerciales) y el siguiente proceso de activación (proceso con ácido clorhídrico para promover la regeneración de los grupos silanoles de superficie) eliminaban el recubriemiento presente en la fibra comercial y suavizaban la superficie.

Además, el proceso de activación ha favorecido la regeneración de grupos silanol que fueron fundamentales para el injerto de los aminosilanos (agentes de acoplamiento) en la superficie de las fibras.

A través del análisis morfológico sobre las fibras recubiertas químicamente con aminosilanos (APTES, APDES, APTES+APDES) se encontraron heterogeneidades superficiales debidas a la presencia de la sustancia orgánica depositada sobra las fibras que hacía que sus superficies fueran más rugosas. Se encontró que cuanto mayor era la cantidad de trietoxisilano en la composición de la disolución empleada para realizar el recubrimiento, mayor era la heterogenidad superficial (topográfica). Estas observaciónes morfologícas se confirmaron a partir de los resultados de rugosidad superficial obtenidos del análisis de imágenes obtenidas por AFM.

Estas heterogeneidades superficiales hacen pensar que podrían ser las responsables de una mejor adhesión entre las fibra y la matriz. Sin embargo, el análisis fractográfico realizado sobre las imágenes obtenidas por SEM y resultados de pruebas mecánicas apuntan a que parecen ser otras las causas fundamentales de la mejor o peor adhesión interfacial. Por lo tanto, se puede concluir que la rugosidad a escala nanoscópica no parece ser determinante en la mejor adhesión entre las fibras y la matriz y, en consecuencia, en las posteriores prestaciones mecánicas de los materiales compuestos de matriz de cemento.

- El estudio de **degradación hidrolítica** de los recubrimientos polisiloxánicos parece ser de vital importancia para poder comprender el comportamiento de dichos recubriementos en materiales compuestos de matriz de cemento.

  Se realizó un estudio cinético de dicho proceso de degradación que permitió obtener información sobre la energía de activación en función del tipo de recubrimiento considerado (APTES, APTES+APDES, APDES) así como estimar los tiempos de degradación hidrolítica en el equilibrio. Los resultados obtenidos con diferentes mediciónes indicaron que la velocidas de degradación de los tres recubrimientos aumentaba según el orden en el que el grado de reticulación aumenta: APDES < APTES+APDES < APTES.

Se ha encontrado que el mecanismo del proceso de degradación hidrolítica es el mismo para los tres sistemas estudiados, por lo que se ha podido concluir que la velocidad de hydrolysis depende de la concentración inicial de los enlaces de siloxano (-Si-O-Si-) susceptibles de ser hidrolizados.

Por lo tanto, este estudio demonstró que, en compuestos a base de cemento reforzado con fibras, el uso de un poliorganosiloxano con un bajo grado de reticulación, como el recubrimiento APDES, podría ser la estrategia más eficaz para resistir un posible ataque de agua, especialmente en el ambiente alcalino característico de la matriz de cemento.

Cabe destacar, además, que los resultados obtenidos podrían ser interesantes no solo en el sector de los materiales compuestos de matriz cerámica si no también para comprender el comportamiento de estos recubriementos en otras aplicaciones en el sector de la ingeniería y ciencia de materiales.

- En cuanto al estudio de los **materiales compuestos renforzados con fibras**, se ha podido tener una idea del efecto de las fibras cortas de basalto y de sus recubrimientos en matriz de cemento y cal hydraulica natural respectivamente. Concretamente, los resultados indicaron que, en general, la presencia de las fibras de basalto y los tratamientos superficiales mejoran las prestaciones mecánicas de los materiales en comparación con el mortero de referencia (sin fibras).
  Independientemente de la matriz utilizada, se obtuvieron mejores resultados en términos de adhesión fibra-matriz y, en consecuencia, mayores prestaciones mecánicas, para los materiales contituidos por mortero reforzado con fibras de basalto modificadas con la mezcla de los dos silanos (APTES+APDES).

  A partir de los resultados obtenidos para el sistema correspondiente a matriz de cemento se ha podido tener una idea de la causa responsable de la mejores interacciones en la interfase fibra-matriz. Por ejemplo, la buena compatibilidad mostrada entre la fibras activadas y la matriz de cemento, hizo pensar que probablemente los grupos OH generados durante el proceso de activación eran los responsables de la mejor adhesión. La presencia de un recubrimiento superficial basado en aminosilanos además parece contribuir a mejorar aun más esta adhesión

debido entre otras cosas a interaciones por enlaces de hidrogeno entre los grupos aminos ($-NH_2$) y las matrices de cementos.

Además, la estructura molecular con una reticulación intermedia que se podría generar en la interfase fibra-matriz (cemento y cal hidráulica natural) cuando se utiliza la mezcla de los dos silanos (APTES+APDES), podría ser responsable de mayor accesibilidad a los grupos OH sobre la superficie de la fibra y, además, a los grupos aminos. Esto podría ayudar a aumentar las interacciones favorables entre el refuerzo y la matriz.

Las variaciones encontradas en los resultados obtenidos (especialmente en las fibras activadas) del segundo sistema estudiado (morteros de cal hidráulica natural) respecto de los resultados encontrados para los morteros de cemento, podrían ser atribuidas a una diferente reactividad entre las fibras y la matriz con diferente composición química.
Por ejemplo, el menor numero de productos de hydrataciòn (silicato de calcio hidratado, C-S-H) en los morteros de cal hidráulica natural, podría ser responsable de las menores interaciones entre la matriz y los grupos OH de las fibras.

Para comprender mejor este tipo de interacciones específicas se requeriría profundizar más sobre este tema con estudios más concretos, por ejemplo mediantes propuestas de investigación asociadas a líneas de trabajo futuras.

Además, cabe destacar que los materiales estudiados a lo largo de este trabajo, pueden ser posibles candidatos en aplicaciones dentro el marco de la industria de la construcción y del sector de la restauración y conservación del Patrimonio Cultural. No obstante, para ambas áreas se requeriría optimizar aún más los materiales.

Por ello, como líneas futuras se puede plantear, optimizar los tratamientos superficiales de las fibras tanto en términos morfológicos como en términos de naturaleza química. Se podría pensar en añadir nanopartículas que podrían conferir mayor rugosidad superficial y favorecer un anclaje mecáanico más efectivo que se sumaría a la contribución debida a las interacciones fisico-químicas generadas entre las fibras tratadas con aminosilanos y la

matriz. Además, se podría pensar en utilizar un método de aplicación de los recubrimientos mediante "spray" que ayudaría en los correspondientes sistemas de producción.

Por ultimo, se puede plantear optimizar la preparación y por tanto las prestaciones finales de los materiales compuestos mejorando el proceso de dispersión de las fibras y añadiendo mayor porcentaje de fibras en la matriz. Además, el uso de fibras de diferentes morfologías (cortas y largas) podría contribuir también a mejorar el comportamiento mecánico de los materiales finales.

8.3. Conclusioni e Sviluppi Futuri

Nella presente tesi di dottorato di ricerca, sono stati studiati materiali compositi a matrice cementizia rinforzati con fibre di basalto. In particolare, lo studio si è incentrato sull'ottimizzazione dell'interfase fibra-matrice attraverso trattamenti superficiali delle fibre naturali di basalto. E' stata studiata la compatibilità esistente tra le fibre corte di basalto (commerciali e modificate) e le matrici selezionate (un cemento Portland e una calce idraulica naturale) per comprendere e definire possibili miglioramenti nelle prestazioni finali del materiale composito.

Sono stati preparati e caratterizzati diversi trattamenti superficiali, sono stati studiati i fenomeni di degradazione idrolitica dei trattamenti superficiali a base degli agenti di accoppiamento silano proposti e infine, sono stati preparati e caratterizzati i materiali compositi fibrorinforzati.

Le conclusioni più rilevanti che possono essere tratte da questo progetto di ricerca sono le seguenti:

- È stato dimostrato che lo studio relativo alla preparazione e caratterizzazione dei **trattamenti superficiali** delle fibre di basalto è fondamentale per poter comprendere possibili interazioni in termini di migliore adesione tra le fibre di basalto e la matrice di cemento e/o di calce idraulica naturale. La dettagliata caratterizzazione realizzata attraverso diverse tecniche analitiche (XRD, FT-IR, TGA, SEM e AFM) delle superfici delle fibre commerciali e modificate, ha

mostrato che, in base ai diversi trattamenti realizzati, sono stati evidenziati cambi nella struttura, composizione e morfologia.

In particolare, è stato osservato che il processo di calcinazione (eliminazione del rivestimento superficiale applicato durante il processo di produzione delle fibre commerciali) e il successivo processo di attivazione (trattamento con acido cloridrico per promuovere la rigenerazione dei gruppi silanoli superficiali) eliminavano il rivestimento superficiale presente sulla fibra commerciale, rendendo la superficie liscia.

Inoltre, il processo di attivazione ha permesso la rigenerazione dei gruppi silanoli, fondamentali per l'innesto degli amminosilani (agenti di accoppiamento) sulla superficie della fibra.

Attraverso l'analisi morfologica effettuata sulle fibre trattate chimicamente con amminosilani (APTES, APDES, APTES+APDES), sono state rilevate eterogeneità superficiali dovute alla presenza della sostanza organica depositata sulla superficie della fibra che rendeva la superficie della fibra più rugosa. È stato osservato che quanto maggiore era la quantità del trietossisilano nella dissoluzione utilizzata per la realizzazione del rivestimento, tanto maggiore era l'eterogeneità superficiale (topografica). Queste eterogeneità superficiali sono state successivamente confermate dai risultati di rugosità superficiale ottenuti mediante AFM.

Queste eterogeneità superficiali, fanno pensare che potrebbero essere la causa responsabile di una migliore adesione tra fibra e matrice. Ad ogni modo, dall'analisi frattografica realizzata attraverso il SEM e dai risultati delle prove meccaniche si è potuto constatare che sembrerebbero essere altre le cause responsabili di una migliore o peggiore adesione all'interfaccia fibra-matrice. Pertanto, si può concludere che la rugosità a scala nanoscopica non sembra essere determinante della migliore adesione tra fibra e matrice, e di conseguenza, delle prestazioni meccaniche dei materiali compositi a matrice cementizia.

- Lo studio di **degradazione idrolitica** dei rivestimenti polissilossanici sembra essere di fondamentale importanza per poter comprendere il comportamento dei presenti rivestimenti nei materiali compositi a matrice cementizia.

  È stato realizzato uno studio cinetico del processo di degradazione idrolitica che ha permesso di ottenere informazioni sull'energia di attivazione in funzione del tipo di rivestimento considerato (APTES, APDES, APTES+APDES) e di stimare i tempi di degradazione idrolitica all'equilibrio. I risultati ottenuti con diversi metodi di misurazione, hanno indicato che la velocità di degradazione dei tre rivestimenti aumentava secondo l'ordine in cui aumenta il grado di reticolazione: APDES < APTES+APDES < APTES.
  Il seguente studio ha rilevato che il meccanismo del processo di degradazione idrolitico è lo stesso per i tre sistemi studiati; pertanto, è stato possibile concludere che la velocità di idrolisi dipende dalla concentrazione iniziale dei legami silossanici (-Si-O-Si-) in grado di essere idrolizzati.

  Pertanto, questo studio ha dimostrato che nel caso di materiali compositi fibrorinforzati a matrice cementizia, l'uso di un poliorganosilossano con un basso grado di reticolazione, come il rivestimento APDES, potrebbe essere la soluzione più efficace per resistere ad un possibile attacco dell'acqua, specialmente nell'ambiente alcalino della matrice cementizia.

  Bisogna sottolineare, inoltre, che i risultati ottenuti potrebbero essere interessanti non solo nel settore dei materiali compositi a matrice ceramica ma potrebbero essere utili anche per comprendere il comportamento di questi rivestimenti in altre applicazioni nel settore dell'ingegneria e scienza dei materiali.

- Per quanto riguarda lo studio dei **materiali compositi fibrorinforzati**, è stato possibile ottenere informazioni sull'effetto delle fibre corte di basalto e dei loro rivestimenti rispettivamente sulla matrice cementizia e sulla calce idraulica naturale. Nello specifico, i risultati hanno indicato che, in generale, la presenza di fibre di basalto e trattamenti superficiali migliorano le prestazioni meccaniche dei materiali rispetto alla malta di riferimento (senza fibre).

Indipendentemente dalla matrice utilizzata, sono stati ottenuti risultati migliori in termini di adesione fibra-matrice e, di conseguenza, maggiori prestazioni meccaniche, per la malta rinforzata con fibre di basalto modificata con la miscela dei due silani (APTES + APDES).

Dai risultati ottenuti per il sistema corrispondente alla matrice cementizia, è stato possibile ottenere informazioni sulla possibile causa responsabile delle migliori interazioni all'interfaccia fibra-matrice. Ad esempio, la buona compatibilità mostrata tra le fibre attivate e la matrice di cemento ha suggerito che i gruppi OH generati durante il processo di attivazione erano probabilmente responsabili della migliore adesione. Inoltre, la presenza di un rivestimento superficiale a base di amminosilani sembra, contribuire a migliorare ulteriormente questa adesione a causa di interazioni da legami idrogeno tra i gruppi amminici (-NH_2) e le matrici cementizie.

Inoltre, la struttura molecolare con una reticolazione intermedia che potrebbe essere generata all'interfaccia fibra-matrice (cemento e calce idraulica naturale) quando si utilizza la miscela dei due silani (APTES + APDES), potrebbe essere responsabile di una maggiore accessibilità ai gruppi OH sulla superficie della fibra e, inoltre, anche ai gruppi amminici. Ciò potrebbe aiutare ad aumentare le favorevoli interazioni tra il rinforzo e la matrice.

Le variazioni riscontrate nei risultati ottenuti (specialmente nel caso delle fibre attivate) per il secondo sistema studiato (malte di calce idraulica naturale) rispetto ai risultati ottenuti per le malte cementizie, potrebbero essere attribuite a una differente reattività tra le fibre e la matrice con composizione chimica diversa.
Ad esempio, il minor numero di prodotti di idratazione (silicato di calcio idrato, C-S-H) nelle malte di calce idrauliche naturali, potrebbe essere responsabile delle minori interazioni tra la matrice e i gruppi OH delle fibre.

Per poter comprendere meglio questo tipo di interazioni, sarebbe necessario approfondire questo argomento con studi più specifici, ad esempio attraverso proposte di ricerca associate a linee di sviluppi futuri.

Inoltre, è importante sottolineare che i materiali studiati durante questo progetto, potrebbero essere utilizzati per applicazioni nell'ambito del settore delle costruzioni e del restauro e conservazione dei Beni Culturali. Tuttavia, per entrambe le aree sarebbe necessario ottimizzare ulteriormente i materiali.

Per questo motivo, come sviluppi futuri, si propone di ottimizzare i trattamenti superficiali delle fibre sia in termini morfologici che in termini di natura chimica. Si potrebbe pensare di aggiungere nanoparticelle che potrebbero conferire maggiore rugosità superficiale e favorire un ancoraggio meccanico più efficace che si aggiungerebbe al contributo dovuto alle interazioni fisico-chimiche generate tra le fibre trattate con amminosilani e le matrici cementizie. Inoltre, si potrebbe pensare di utilizzare un metodo di applicazione dei rivestimenti mediante "spray" che aiuterebbe nei corrispondenti sistemi di produzione.

Infine, si propone di ottimizzare la preparazione e di conseguenza le prestazioni finali dei materiali compositi, migliorando il processo di dispersione delle fibre e aggiungendo una percentuale maggiore di fibre alla matrice. Inoltre, l'uso di fibre di morfologie diverse (corte e lunghe) potrebbe contribuire ulteriormente a migliorare il comportamento meccanico dei materiali finali.